

EVALUATION OF GAMMA RAY SPECTROMETRIC DATA PROCESSING TECHNIQUES

BY

PETER USIKARORE KRAGHA, B.Sc., M.Sc.

A Thesis submitted to the University of London for the degree of
DOCTOR OF PHILOSOPHY

Department of Geology

Geophysics Section

Imperial College of Science and Technology

London

January, 1984

TO MR. MOSES OVIGHO KRAGHA - a kind and caring brother

ABSTRACT

Gamma ray spectrometric surveys for geological applications are aimed at detecting three elements - potassium, uranium and thorium. The data are thus mostly conventionally processed using three windows, a window being assigned to each element. Even with the advent of multichannel analyzers which produce full spectral output, processing of the data is still often restricted to the three window case.

This project is aimed at comparing the results from the conventional three window analysis with those from multichannel analysis. Also the performances of a NaI(Tl) detector and a Ge(Li) detector are experimentally compared. Because both laboratory and field data are available, their results are compared.

The least squares' method is used in the analysis of the data and its theory is discussed with respect to a spectrometer having an arbitrary number of channels.

It is observed from the results that the accuracy of results is better when multichannel analysis method is used. It is also seen that in the three window case, potassium may be overestimated. While a Ge(Li) detector is preferable to a NaI(Tl) detector in a survey where identification of isotopes is the objective, a Ge(Li) detector has poor performance as compared to a NaI(Tl) detector in the determination of the concentrations of potassium, uranium and thorium.

The problem of handling large matrices in multichannel analysis can be minimized by spectral partitioning.

The thesis consists of eight chapters. Chapter One contains an introduction in which the need for gamma ray survey and the objective

of this project are mentioned. In chapter Two, the principles of gamma ray spectrometry are presented, while in chapter Three, the geological importance of gamma radiation measurement is stated. Survey procedures and corrections are treated in chapter Four. Chapter Five deals with instrumentation for detection and measurement of gamma radiation. In chapter Six, the theory and application of least squares' method to radiometrics are dealt with. Data acquisition, analysis, comparison and interpretation of results are presented in chapter Seven. Finally, the findings of the project, limitations and recommendations are stated in chapter Eight.

ACKNOWLEDGMENTS

I wish to express my profound gratitude to Dr. D. Cowan of the Geophysics Section for his supervision of this work. I am thankful to him for providing all the data (the laboratory samples, airborne data, the ground radiometric and chemical results) used in this project. His assistance in reading and correcting the manuscripts is highly appreciated.

I am also thankful to Dr. T. D. MacMahon of the University of London Reactor Centre, for his assistance during the laboratory work at Silwood Park.

My thanks and appreciation to Mr. M. O. Kragha and his wife, Stella, for their financial support, encouragement and care throughout the period of this work. To my wife, Yetunde and my children, Efemuaye, Edirin and Okemute, I say a big thank you for your steadfastness, understanding, moral support, patience and love.

My regards to all my friends and colleagues for their encouragement.

Lastly, my thanks to the Federal Government of Nigeria for financing this course.

TABLE OF CONTENTS

	PAGE
Abstract	i
Acknowledgements	iii
Table of Contents	iv
List of Figures	ix
List of Tables	xiv
CHAPTER ONE: INTRODUCTION	1
CHAPTER TWO: PRINCIPLES OF GAMMA RAY SPECTROMETRY	10
2.1. Composition of an atom	10
2.2. Radioactive decay	14
2.3. Interaction of gamma ray with matter	19
Absorption of gamma rays	20
Photoelectric absorption	26
Compton scattering	28
Pair production	36
2.4. Decay process	39
CHAPTER THREE: GEOLOGICAL IMPORTANCE OF GAMMA RADIATION	55
3.1. Dating	57
3.2. Heat flow studies	58
3.3. Geological mapping	59
3.4. Exploration work	62
CHAPTER FOUR: SURVEY PROCEDURES AND CORRECTIONS	66
4.1. Laboratory measurement	67
4.2. Field measurements	67
4.2.1. Surface survey	67

4.2.2. Airborne survey	68
4.2.3. Factors influencing field survey	69
4.2.4. Design parameters for airborne survey	74
4.3. Corrections	81
4.3.1. Background and its correction	83
4.3.1.1. Determination of background	83
4.3.1.1.1. Surface measurement	83
4.3.1.1.2. Airborne measurement	84
Overwater	85
Upward looking crystal	86
High altitude	92
4.3.2. Compton scattering correction	92
4.3.3. Height correction	94
4.4. Survey statistics	100
4.4.1. Propagation of errors	101
4.4.1.1. Application of error propagation formula in radiometrics	102
4.5. Calibration of measuring system	109
4.5.1. Energy calibration	112
4.5.2. Sensitivity calibration	116
4.5.2.1. Calibration of surface systems	116
4.5.2.2. Calibration of airborne systems	118
4.6. Data presentation	119
CHAPTER FIVE: RADIATION DETECTION AND MEASUREMENT	138
5.1. Detectors	138
5.1.1. Gas-filled detectors	138

5.1.2. Scintillation counter	144
5.1.2.1. Photomultiplier Tube	155
5.1.3. Semiconductor detectors	158
5.1.4. Coincidence and anticoincidence spectrometry	172
5.2. Amplifying section	178
5.2.1. Preamplifiers	179
5.2.1.1. Voltage-sensitive preamplifier	180
5.2.1.2. Charge-sensitive preamplifier	181
5.2.2. Amplifiers	183
5.2.2.1. Shaping of pulse	184
5.2.2.2. Pole-zero cancellation	185
5.2.2.3. Baseline shift	186
5.3. Counting Section	188
(a) Wilkinson Ramp principle	193
(b) Successive approximation method	195
5.3.1. Choice of window width for 3-window spectrometer	196
5.4. Distortion of signal	197
CHAPTER SIX: DATA ANALYSIS TECHNIQUES	212
6.1. Graphical method	212
6.2. Peak area method	213
6.3. Least squares' method	218
6.4. Theory of data analysis	220
6.5. Calibration of spectrometer (isotopic)	229
6.5.1. Calibration of 3-window spectrometer	231
6.5.2. Calibration of multichannel spectrometer	234
6.6. Sample spectrum	237

6.6.1. Instrumental drift and its correction	238
CHAPTER SEVEN: DATA ACQUISITION, ANALYSIS AND INTERPRETATION OF RESULTS	245
7.1. Data analysis	247
7.1.1. Laboratory	247
7.1.2. Field (airborne)	250
7.2. Calibration of instruments and analysis of samples	251
7.2.1. Laboratory	251
7.2.1.1. Multichannel analysis	256
7.2.1.1.1. Statistical adequacy test on results	263
7.2.1.2. Window analysis	267
7.2.2. Field (airborne)	268
7.3. Spectra partitioning	285
7.4. Analysis program	290
7.5. Comparison of results	293
7.5.1. Experimental comparison of NaI(Tl) and Ge(Li) detectors' performances	293
7.5.2. Conventional three window versus multichannel analysis	299
7.5.2.1. Laboratory results	300
7.5.2.2. Airborne results	303
7.5.3. Laboratory versus field results	304
7.6. Interpretation of results	306
CHAPTER EIGHT: CONCLUSION	318
8.1. Summary	318

8.2. Limitations and Recommendations	321
BIBLIOGRAPHY	323
APPENDICES	338
A. Weighting and Normalizing coefficients for least squares' fit	338
B. Spectra	344
B1. Laboratory sample spectra	345
B2. Calibration spectra at various heights	363
B3. Survey and background spectra	371
C. Analysis program - ANASPEC (in folder)	

LIST OF FIGURES

FIGURE		Page
1.1	Estimated demand for uranium	3
1.2	Elemental windows	6
2.1	Structure of an atom	13
2.2	Chart of isotopes	18
2.3	Photoelectric absorption events	27
2.4	Compton scattering of a photon	28
2.5	Compton continuum for any one specific gamma ray energy	35
2.6	Observed shape of compton continuum	36
2.7	Location of electron-positron pair	37
2.8	Relative importance of the three major types of gamma ray interaction	38
2.9	Uranium and Thorium radioactive decay series	49
3.1	Contoured total counts and geology map	61
3.2	Gamma ray logs	64
4.1	Collimated and uncollimated detector	68
4.2	Source-detector geometries encountered in surface survey	70
4.3	Effect of source geometry on airborne survey	70
4.4	Absorption curves for overburden material	72
4.5	Ground resolution as a function of detector altitude	77
4.6	Radius of circle of investigation versus altitude	77
4.7	Ground coverage as a function of flight line spacing	77
4.8	Peak yield as a function of detector velocity	79
4.9	Area under the curve as a function of detector velocity	79
4.10	Count rate as a function of detector altitude	82

4.11	Shape of cosmic spectral curve	87
4.12	Correlation of the uranium window with the lead-214 peak area	91
4.13	Representation of the interaction between potassium, uranium and thorium energy windows	93
4.14	Height correction factors	97
4.15	Effect of altitude on countrates	98
4.16	Relationship between primary and secondary calibration facilities	110
4.17	Calibration of a pulse height spectrum	114
4.18	Correction factors for calibrating portable gamma ray spectrometers on pads of less than infinite diameter	117
4.19	Presentation of data using symbols superimposed on a flight line map	121
4.20	Presentation showing peak values of elements and their background values	122
4.21	Contour map of concentration values of elements	124
4.22	Offset profiles	125
4.23	Comparison of geology and anomaly maps	126
4.24	Uranium countrate contour map	127
4.25	Significance factor contour map	127
4.26	Three-component radiation map	128
4.27	Zoning technique	131
4.28	The Zoned map	131
4.29	A printer-plot anomaly description	132
4.30	Ternary diagram	134

4.31	Frequency distribution of geology unit	136
5.1	Typical gas-filled detector	140
5.2	Counting characteristics of gas-filled detectors	140
5.3	Geiger-Muller counter circuit	143
5.4	Energy band in ideal insulating crystal	145
5.5	Potential energy diagram of luminescence centre	146
5.6	Energy band structure of activated crystal	148
5.7	Typical array of six NaI detectors	153
5.8	PHOSWICH detector	154
5.9	Basic elements of photomultiplier tube	156
5.10	Different photomultiplier tube geometries	157
5.11	Band structure of a semiconductor material containing impurities	160
5.12	Charge collection in an ideal homogeneous crystal	161
5.13	Effects of trapping	166
5.14	Basic configuration of a lithium drifted p-i-n junction detector	168
5.15	Drifted detector configurations	171
5.16	Effect of large detectors	172
5.17	Effect of small detectors	173
5.18	Effect of shielding	174
5.19	Anticoincidence spectrometer	175
5.20	Compton spectrometer	176
5.21	Pair spectrometer	177
5.22	Response function of a pair spectrometer	178
5.23	Typical preamplifier block diagram	179

5.24	Simplified voltage-sensitive preamplifier	181
5.25	Simplified charge-sensitive preamplifier	182
5.26	Effect of pulse shaping	184
5.27	Application of pole-zero cancellation	186
5.28	Illustration of baseline shift	187
5.29	Measurement of pulse spectrum	189
5.30	Channel arrangement in a spectrometer	191
5.31	Principle of multichannel analyzer	192
5.32	Principle of the Wilkinson Ramp method	194
5.33	Principle of Successive Approximation method	195
5.34	Comparison of output pulse shapes	199
5.35	Effect of noise on pulses	200
5.36	Pulse shape functions	201
5.37	Principle of spectrum stabilizer with a reference peak	209
5.38	Stabilization without a reference peak	210
6.1	Determination of peak area	215
6.2	Change in peak position due to gain and threshold changes	239
6.3	Energy calibration under different gain and threshold	239
6.4	Illustration of channel boundary changes due to gain and/or threshold changes	241
6.5	Smoothing functions	244
7.1	External features of the NS-700 Series pulse height analyzer	248
7.2	System interconnection	249
7.3	Sample spectra	255

7.4	Flow chart for laboratory data analysis	256
7.5	Spectrum condensation	258
7.6	Energy calibration for Ge(Li) detector	259
7.7	Energy calibration for NaI(Tl) detector	259
7.8	Information vector for laboratory systems	261
7.9	Flow chart for airborne data analysis	272
7.10	Calibration spectra at various heights	277
7.11	Information vector for airborne system at various heights	279
7.12	Variation of stripping ratios with height	282
7.13	Determination of attenuation coefficients	283
7.14	NaI(Tl) versus Ge(Li) results	298
7.15	NaI(Tl) multichannel versus three window results	302
7.16	Concentration of elements along survey line (laboratory)	309
7.17	Correlation between potassium, uranium and thorium (laboratory)	310
7.18	Concentration of elements along survey line (ground)	312
7.19	Correlation between potassium, uranium, and thorium (ground)	313
7.20	Concentration of elements along survey line (chemical)	314
7.21	Histograms of ground radiometric results	315
7.22	Histograms of chemical results	317

LIST OF TABLES

TABLE		Page
1.1	The radioactive rays	1
2.1	Commonly encountered nuclear radiation	11
2.2	Approximate frequency and wavelength of electromagnetic radiations	11
2.3	Number of electrons in a shell	13
2.4	Natural radioactive series of uranium and thorium	50
3.1	Radioactive minerals	56
3.2	Radioactive contents	56
3.3	Half-lives and heat production values	59
3.4	Application of radiometric methods in exploration work	63
4.1	Count-rates showing estimated errors for three detector volumes	80
4.2	Some energy calibration standards	113
4.3	Example of classification of anomalies using Ternary diagram	134
5.1	Some characteristics of gas-filled detectors	143
5.2	Some properties of the main gamma ray scintillators	151
5.3	Some properties of silicon and germanium	170
5.4	NIM standards	193
6.1	Methods of peak detection	217
6.2	Methods of peak-position determination	217
6.3	Methods of peak-area estimation	2.17
6.4	Methods for the evaluation of double peaks	219

6.5	Values of the score for the determination of the separation of double peaks	219
6.6	Values of the score for the determination of the ratio of areas of double peaks	219
7.1	Relative information importance of isotopes (laboratory systems)	262
7.2	Results obtained from Ge(Li) and NaI(Tl) detectors (multichannel)	264
7.3	Critical detection limits for laboratory systems	267
7.4	Laboratory results from window analysis of NaI(Tl) detector	269
7.5	Window widths used	272
7.6	Relative information importance of isotopes (airborne system)	280
7.7	Attenuation coefficients	284
7.8	Results of multichannel analysis of airborne data	286
7.9	Results of window analysis of airborne data	287
7.10	Average results obtained by partitioning	289
7.11	Ge(Li) results for energies from 0 - 1.61MeV	296
7.12	Laboratory results with relative errors expressed as percentages	301
7.13	Average values from airborne survey	304
7.14	Comparison of laboratory and field results	305
7.15	Results from different survey methods	307

CHAPTER ONE

INTRODUCTION

Gamma ray spectrometry in geological application is a method used to determine the amount of potassium, uranium and thorium contained in rocks. The method relies on the principles of radioactivity which was first discovered by Henry Becquerel in 1896, shortly after Wilhelm Roentgen in 1895 discovered X-rays. Becquerel found that minerals containing uranium as well as salts of uranium, emitted radiations which passed through materials opaque to ordinary light and which affected photographic emulsions in a manner similar to X-rays. He also found that the radiation was characteristic of the particular uranium compound and that it would ionize a gas. This was soon followed by the discovery of other radioactive elements.

Radioactivity is the spontaneous decay of the nuclei of unstable atoms through the emission of alpha particles, beta particles and gamma rays. The properties of these rays are listed in Table 1.1.

Name	Charge	Approx.Mass	Penetrating Power
Alpha (α)	2+	4	weak but induces many ions
Beta (β)	-	1/1857	about 1000 times that of α -rays, but induces fewer ions
Gamma (γ)	none	0	very penetrating, but able to induce only a few ions

Table 1.1: The Radioactive Rays (after Slabaugh and Parsons, (1976))

From these properties it is deduced that alpha particles are streams of helium nuclei, beta particles are streams of electrons, and gamma rays are electromagnetic radiation whose frequency is even greater than that of X-rays. Hence the emanation from radioactivity decay, which may be composed of alpha and/or beta particles, but almost always includes gamma rays, is highly penetrating.

The detection and measurement of the radioactive emission of alpha, beta and gamma rays are based on their ability to induce ionization in the medium through which they pass. These have led to the detection of the amount of radioactive materials, e.g. uranium.

Because all nuclear reactions are accompanied by the release of large amount of energy (see equation 2.1), it is expected that much effort has to be made to capitalize on this form of energy to generate electrical energy (nuclear fission). Thus the use of the gamma ray spectrometry in the detection and measurement of radioactive materials can not be overemphasized. For some time there was not much interest in this method but between 1945 and 1957, it was revived when there was demand for uranium to generate nuclear power. So with the progressive decline in the world's hydrocarbon reserves and with the increasing demand for nuclear power, the demand for uranium and other radioactive minerals is bound to grow (see Fig 1.1) and this will consequently lead to greater exploration activity. It may be required to locate, apart from the large ore deposits, very small and shallow targets and at the same time being very discriminating so that large

sums of money will not be wasted on subsequent follow-up of uneconomic targets. One of the ways of meeting this requirement could be the use

Fig. 1.1a : Estimated annual requirements for uranium
(after Davis, 1972)

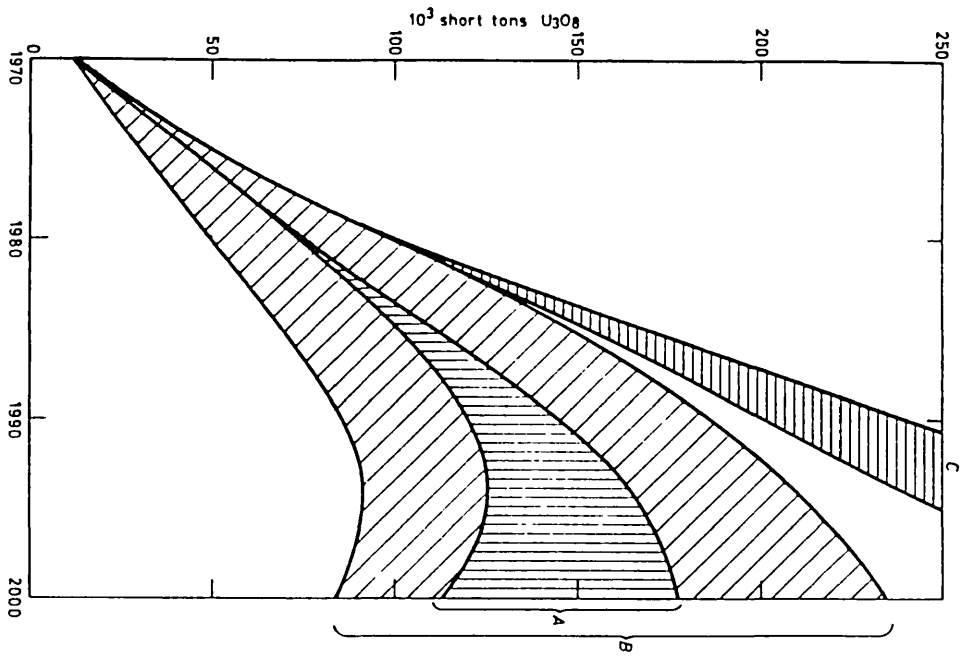
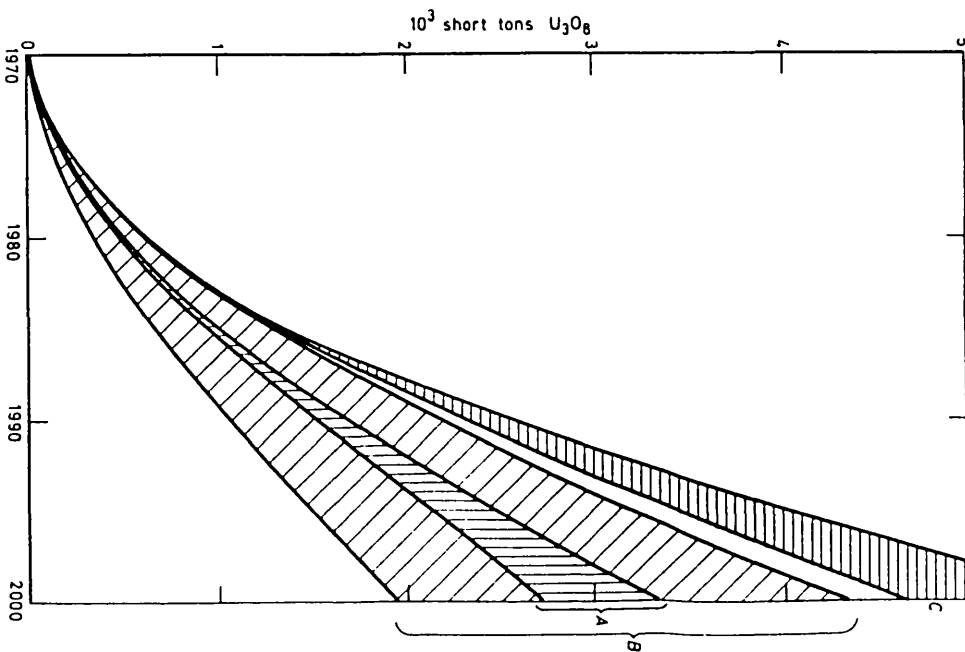


Fig. 1.1b : Estimated cumulative requirements for uranium
(after Davis, 1972)



of gamma ray spectrometry. High resolution gamma ray spectra could provide the sort of information required for detailed interpretation. From these spectra it may be possible to assess whether or not an anomalous activity is caused by an ore body in equilibrium or by its daughter product through the identification of all the elements making up the series. It will also be possible to obtain an idea of the concentration of the mineral in the ground after the calibration of the spectrometer. It will be required that a decision based on the spectrometric data have a high degree of confidence. This degree of confidence can be achieved by using a high resolution, low background detectors and sophisticated data processing techniques.

The objective of gamma ray spectrometry for uranium evaluation should be to provide quantitative information capable of being used in ore reserve calculation. However, the method is not restricted to the search for the ores of radioactive metals or minerals associated with them, but can be used in geological and structural investigations as well (see chapter Three).

Gamma ray spectrometric survey can be carried out in the laboratory and/or in the field. While the laboratory survey involves the analysis of rock samples collected from the survey area, the field survey is an in-situ measurement which can be done either on the surface, subsurface or by means of airborne measurement. Although there are significant differences in the methods, instrumentations and corrections in different survey environments, the end results are expected to complement each other. The airborne survey is particularly useful because it can provide geologic information on

large, often relatively inaccessible areas in a short period of time.

Although many occurring elements are known to be radioactive, only uranium, thorium and an isotope of potassium (potassium-40) are of significant importance in radiometric survey for geological purpose. Hence gamma ray spectrometric surveys are aimed at detecting three elements—potassium, uranium and thorium. These surveys are mostly conventionally carried out using three-channel (window) spectrometers, a window, centred on a prominent gamma ray peak, being assigned to each of the three elements. Because potassium emits only one gamma ray of energy 1.46MeV, this is the energy peak used for its determination. Uranium and thorium on the other hand, have wide range of energies (see Table 2.4) but the energies 1.76MeV and 2.62MeV have generally been accepted as being most suitable for the measurements of uranium and thorium respectively. This is because these energies are relatively abundant, high and consequently are not appreciably absorbed in air. They can also be easily discriminated from the other gamma rays in a spectrum. Thus whereas potassium is measured directly from the 1.46MeV gamma rays emitted by the radioactive isotope, potassium-40, uranium and thorium are respectively measured indirectly from the daughter products, bismuth-214 of energy 1.76MeV in the uranium decay series and thallium-208 of energy 2.62MeV in the thorium decay series. Hence the measurements of uranium and thorium by gamma ray analysis are only valid if the respective decay series is in the state of secular equilibrium. Sometimes a non-discriminatory (total or gross count) survey is required. While the spectrometric survey enables the determination of the relative concentrations of potassium,

uranium and thorium, the total count survey only permits the determination of the effective concentration of radioactive materials present. Hence in a total count survey, an energy window is set to include the photopeaks for potassium, uranium and thorium (see Fig 1.2).

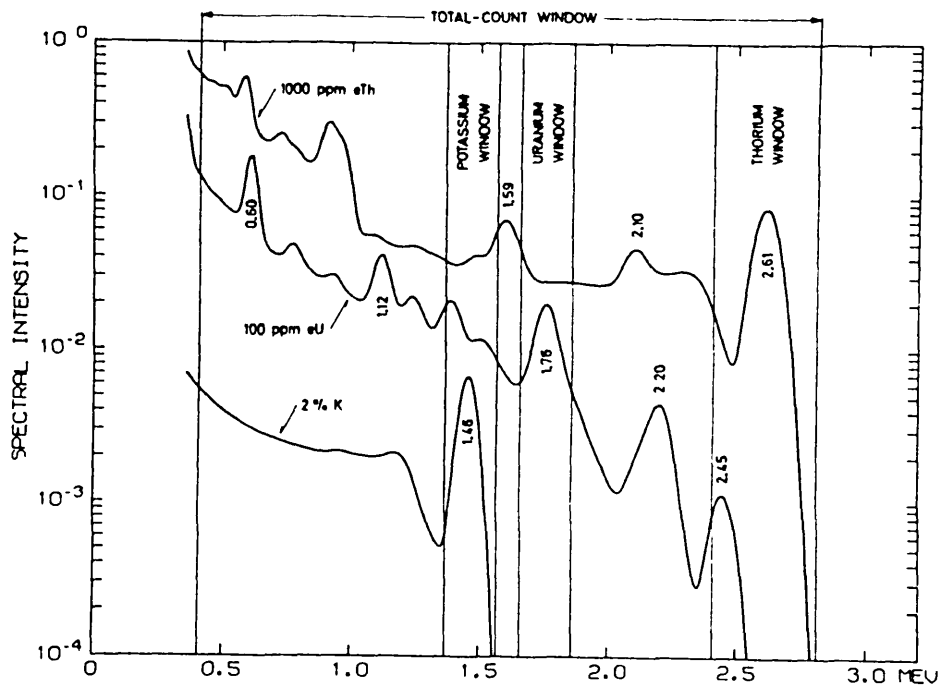


Fig.1.2 : Elemental windows (after IAEA, 1979)

Several gamma ray detectors have been used but the NaI(Tl) detector is the most widely used because of its sensitivity. Its availability in large volumes also favours its use in airborne surveys. But owing to its limited resolution, energy windows are selected to

register the gamma rays for potassium, uranium and thorium (see Fig 1.2 and Table 7.5). Due to the high resolution of semiconductor detectors, Ge(Li) detector appears to be an alternative to NaI(Tl) detector. But its small sizes and its operational disadvantage of requiring continuous cooling by liquid nitrogen limit its use in the field, especially in an airborne survey. It is however very useful in boreholes.

Even with the advent of multi-channel analyzers which produce full spectral output, processing of the spectrum is still often restricted to the three-window case. While it is an advantage to be able to stabilize the spectrum before summing the window counts, a large part of the spectrum which does not fall within any of these windows, is neglected, resulting in loss of some of the information contained in the spectrum. It is intended in this project to use all the data contained in a spectrum (multichannel analysis) and not being restricted to those in the region of photopeaks (windows). An advantage of the multichannel analysis is that the method will be free from subjective errors which might be involved in the definition of the window widths.

The main objectives of this project may be stated as follows:

- (1) experimental comparison of the performances of NaI(Tl) and Ge(Li) detectors in geological/mineral exploration application. Since it is known that a NaI(Tl) detector has better efficiency than a comparative Ge(Li) detector while the later has better resolution than the former, this comparison will give an idea whether or not in geological

application of gamma ray spectrometry, high efficiency or high resolution data are preferred.

- (ii) comparison of the results from multichannel and conventional three window analyses.
- (iii) comparison of results obtained from laboratory and field surveys. This will enable us see how these surveys complement each other.

To achieve these objectives, the same set of samples from the surveyed area (field) will be analyzed in the laboratory using both a NaI(Tl) detector and a Ge(Li) detector. Both the laboratory and field data will then be processed using:

- (a) the conventionally defined three windows,
- (b) all the data in the spectrum, and
- (c) comparing the results from (a) and (b)

The determination of the amount of potassium, uranium and thorium in a sample is generally done by comparative method, that is, the count rate from the sample is compared with the count rates from pure potassium, uranium and thorium standards of known concentrations. Often this is done by graphical method, peak area method or least squares method (see chapter Six). In this work however, the least squares method is preferred because, apart from it not being subjective, it can make use of all the data in a spectrum as well as photopeak (window) areas. Its main disadvantage is that it leads to handling of very large matrices. A review of the least squares method has been made by several authors including Trombka (1963), Eckhoff

(1969), Richards (1977) and Crossley and Reid (1982).

For the understanding of gamma ray spectrometry, the principles of radioactivity is reviewed in chapter Two. In chapter Three, the usefulness of gamma ray spectrometry is presented in relation to geological/mineral exploration application. While chapter Four deals with survey procedures and corrections, chapter Five contains an account of instrumentation for the detection and measurement of gamma radiation. In chapter Six, the theory and application of least squares' method in radiometrics are given. The comparison and interpretation of results are presented in chapter Seven. Also contained in chapter Seven is the description of the acquisition of data. In conclusion, the project is reviewed and recommendations on the problems arising are suggested in chapter Eight.

CHAPTER TWO

PRINCIPLES OF GAMMA RAY SPECTROMETRY

Geophysical prospecting for radioactive elements is based on physical detection of the radiation emitted by the disintegration of an atomic nucleus. Although the term 'radiation' is applied to all forms of energy emission from nuclear events, there are in fact significant and characteristic differences between the various types of radiation that are emitted under various circumstances of nuclear excitation. Table 2.1 lists the characteristics of the radiations commonly encountered in nuclear radiation applications.

Of interest to us here are the gamma rays which are highly penetrating electromagnetic radiations originating within the atom's nucleus. They are characterized by wavelengths in the range of 10^{-9} to 10^{-11} cm and, consequently, by frequencies ranging from 3×10^{19} to 3×10^{21} sec^{-1} (see Table 2.2). They are unaffected by electrical or magnetic fields.

Energies of radiation are usually expressed in electron volt (eV) which is defined as the energy acquired by a charged particle carrying a unit electronic charge when it is accelerated through a potential difference of one volt. Bigger units are kilo-electron volts (1KeV = 10^3 eV) and mega-electron volts (1MeV = 10^6 eV).

2.1. Composition Of An Atom

An atom is the smallest particle of a chemical element which can exist by itself while conserving all its chemical properties (Velimirovich,

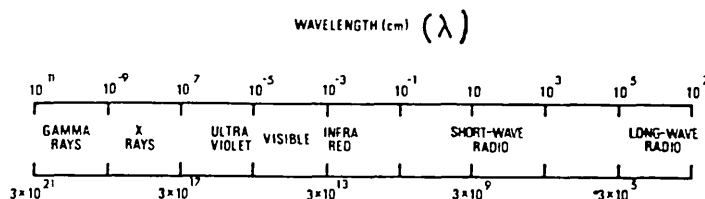
1974). It is made up of a nucleus having positive charges, and electrons having negative charges.

Radiation	Energy Range	Path Length		Comments
		Air	Solid	
Alpha (α)	4 - 10MeV	5 - 10cm	25 - 40cm	Identical to ionized He nucleus
Beta (β^-)	0 - 4MeV	0 - 1m	0 - 1cm	Identical to electron
Positron (β^+)	0 - 4MeV	0 - 1m	0 - 1cm	Identical to electron except for charge
Proton	0 - 100MeV	-	short	Identical to H ¹ nucleus
Neutron	0 - 15MeV	0 - 100m	0 - 100cm	Free, Half-life 16min
X (Em photon)	eV - 100KeV	0.1 - 10m ^a	0 - 1m ^a	photons from transitions
γ (Em photon)	0.01 - 3MeV	0.1 - 10m ^a	0.001 - 1m	Photons from nuclear transitions
Neutrino	-	>> 1Km		Very little interaction with matter

(a) - exponential attenuation in case of electromagnetic radiation

Table 2.1: Commonly encountered nuclear radiations

(after Eichholz and Poston, 1979).



$f = C/\lambda$, where C is the velocity of light (3×10^{10} cm/sec)

Table 2.2 : Approximate frequency and wave length of electromagnetic radiations (after Adams and Gasparini, 1970)

The nucleus is composed of protons and neutrons. While a proton has a unit positive charge and a unit mass, a neutron has no charge but does possess a unit mass. The total sum of the masses of the protons and neutrons in a nucleus is referred to as the atomic mass, while the atomic number is simply the number of protons alone and hence is the total (positive) nuclear charge. The atomic mass and the atomic number are generally represented by A and Z respectively.

The nucleus is surrounded by electrons which rotate in different orbits at different distances from the nucleus. Each of these orbits corresponds to a fixed quantity of energy and on the basis of these energy levels, the electrons are divided into shells denoted by K, L, M, N, O, P, and Q (see Fig 2.1); each of these shells has a definite number of electrons which it can hold. These numbers are indicated in Table 2.3. The binding energy between electrons and the nucleus decreases as the distance of the shell the electrons belong increases from the nucleus. Thus the binding energy decreases from the innermost (K-) shell to the outermost shell.

Since atoms are electrically neutral, they always contain equal number of protons and electrons. Hence the atomic number of an element also indicates how many electrons it contains.

An atom may release or accept an electron if enough energy, called the ionization energy or potential, is provided; and the easiest electron to be removed from an atom is that in the outermost shell since this has the weakest bond energy. If an electron is removed (atom releases an electron), the remaining assembly would be positively charged, and if a proton is removed (atom accepts an

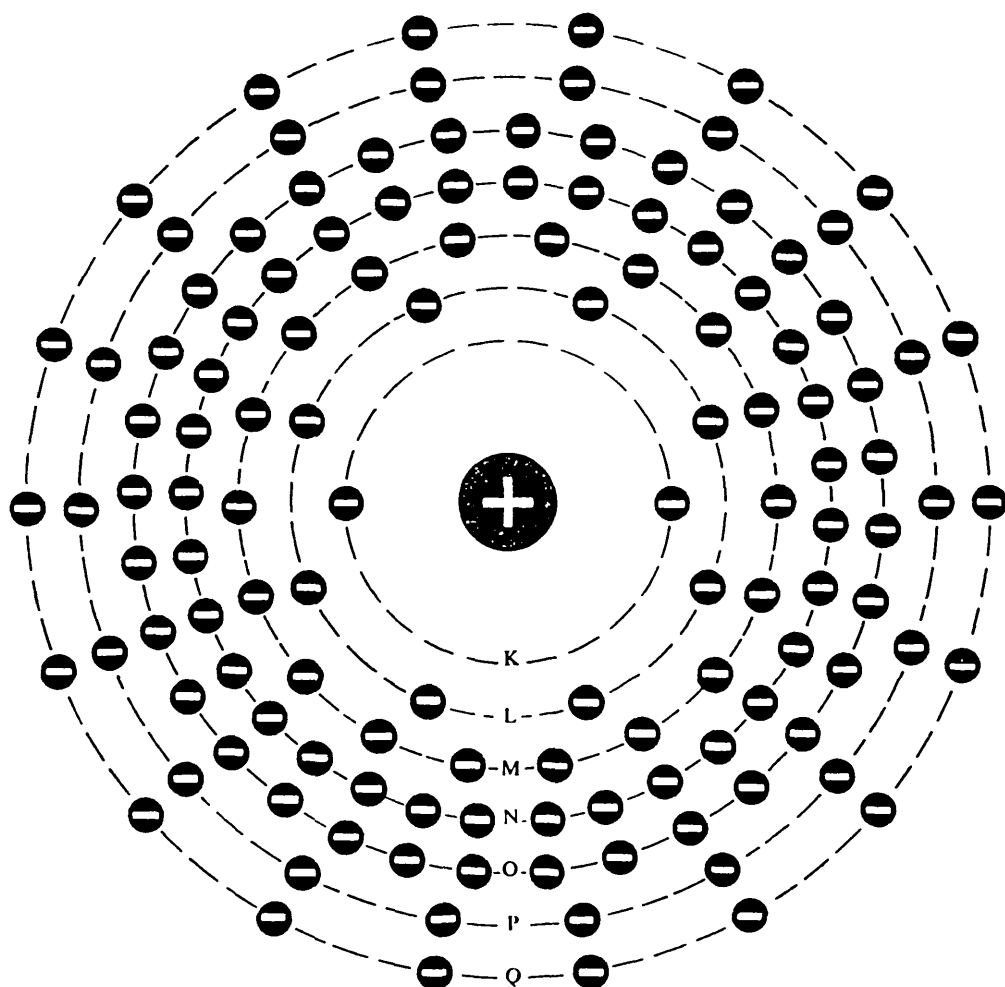


Fig.2.1: Structure of an atom (after Velimirovich, 1974)

Shell	Subgroup							Number of electrons
	s	p	d	f	g	h	i	
K	2	—	—	—	—	—	—	2
L	2	6	—	—	—	—	—	8
M	2	6	10	—	—	—	—	18
N	2	6	10	14	—	—	—	32
O	2	6	10	14	18	—	—	50
P	2	6	10	14	18	22	—	72
Q	2	6	10	14	18	22	26	98

Around the positively charged atomic nucleus rotate the negatively charged electrons, which form the electron cloud (the symbols K, L, M, N, O, P and Q represent the electron shells which correspond to the values of the principle quantum number $n = 1, 2, 3, 4, 5, 6, 7$, while the symbols s, p, d, f, g, h, i, designate the subgroups of energy levels in the electrons, which correspond to the values of the orbital quantum number $l = 0, 1, 2, 3, 4, 5, 6$).



Nucleus of the atom



Electrons

Table 2.3: Number of electrons in a shell (after Velimirovich, 1974)

electron), the remaining assembly would be negatively charged. This assembly is called a positive or a negative ion depending on whether an electron or proton is removed.

2.2. Radioactive Decay

After the discovery of radioactivity by Becquerel in 1896, it was found that three kinds of radiations are emitted by radioactive substances (see Table 2.1). Sir Ernest Rutherford and his group showed that

- (i) the alpha particles are the most easily absorbed rays. They can be deflected by both electric and magnetic fields and the direction of deflections showed that the charges are positive. They also observed that the alpha particles are nuclei of helium of mass four units and that they can be stopped by a piece of paper.
- (ii) the beta particles required about 1000 times as much matter to bring them to rest. They are deflected more readily by magnetic fields than alpha particles but in the opposite direction. They therefore carry negative electrical charge.
- (iii) the gamma rays are even more penetrating than the beta particles. They can be stopped by several centimeters of lead. The gamma rays are not deflected by magnetic or electric fields and therefore they carry no charge.

The equivalent range of penetration in overburden or rock is

practically zero for alpha and beta particles and not more than a foot or two of rock for gamma rays (Telford et al, 1976)

It was realized that the emission of various types of radiations must be an atomic property rather than a molecular or bulk phenomenon because the rate of emission does not depend on the state of chemical composition of the radioactive element concerned. Also the appearance of helium nuclei among the emissions indicates that the phenomenon probably involves the atomic nucleus.

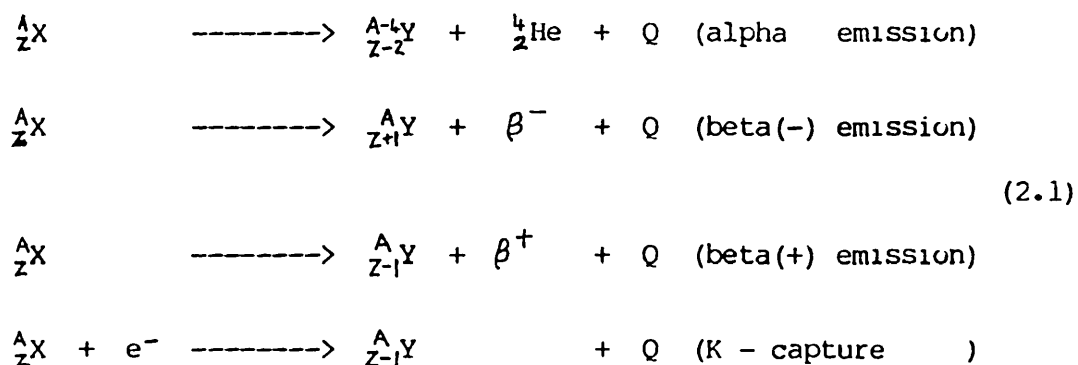
Each of the alpha, beta and gamma rays produces three different effects in varying degree.

- (i) They affect photographic emulsions in much the same way as light and X-rays
- (ii) They ionize gas, making it electrically conducting, and
- (iii) They produce scintillation or phosphorescence in certain minerals and chemical compounds.

All these three effects can be used in geophysical prospecting by radioactive methods.

Radioactive decay consists of the emission or capture of elementary or composite particles with consequent transformations into daughter nuclei having different atomic numbers and in some cases, different mass numbers. This process is accomplished by a nucleus having a neutron/proton ratio either too high or too low for stability. If the nucleus contains too many neutrons, that is, when the ratio of neutron/proton is too high, it takes steps to reduce the number of neutrons by emitting a β -particle, which transforms a

neutron into a proton. Thus if the initial nucleus has Z protons and mass number A , the neutron-proton ratio will be $(A - Z)/Z$, and after the emission of the β -particle, the ratio becomes $(A - Z - 1)/(Z + 1)$, which is smaller than the former for any values of A and Z . On the other hand, if the nucleus is deficient in neutrons, that is, when the neutron-proton ratio is too low, the number of excess protons can be decreased by one of three processes - alpha emission, beta emission, and orbital electron capture (K-capture). The alpha emission involves the expulsion of an He^{2+} nucleus from the parent nucleus. This emission is rare because of the high energy required. In the beta emission, a proton is transformed into a neutron, thus leaving the nucleus with one more neutron and loss of one positive charge. This is actually referred to as a positron or β^+ -emission. The orbital electron capture is the capture by the nucleus of an extra nuclear electron. This is often referred to as K-capture because the captured electron often belongs to the innermost shell (or K-shell) of the atom. The following equations thus represent the transition of an element X to element Y by alpha emission, beta emission and orbital electron capture.



where

Z is the number of protons (atomic number)

A is the atomic mass, and

Q is the energy released in the transformation

Note: It is usual to represent electrons emitted from the nuclei by the symbols β^- (electron) and β^+ (positron). β^- is of course exactly the same as the e, orbital atomic electron, but the different symbols are used to distinguish the origin of the electrons.

The stability of a nucleus is affected not only by the ratio of the neutron and proton numbers, but also by whether these numbers are even or odd (see Fig 2.2). The most stable nuclei are of the even-even type, while the least stable are the odd-odd types. The even-odd and odd-even nuclei are about equally stable and intermediate between the other two types. The even-odd and odd-even nuclei must have odd A, while the other two types, even-even and odd-odd types must have even A (Adams and Gasparini, 1970).

While the alpha emission decreases the atomic number by two and the atomic mass by four units, the beta emission and the K-capture have the same effects of changing the atomic number by unity without any significant change in mass of the nucleus.

Energy requirements set a lower limit for the occurrence of positron emission, that is, the atomic mass difference between parent and daughter must be higher than twice the rest energy (0.511MeV) of

the electron. Starting from this value, the relative probability of positron emission increases with increasing available decay energy (Adams and Gasparini, 1970).

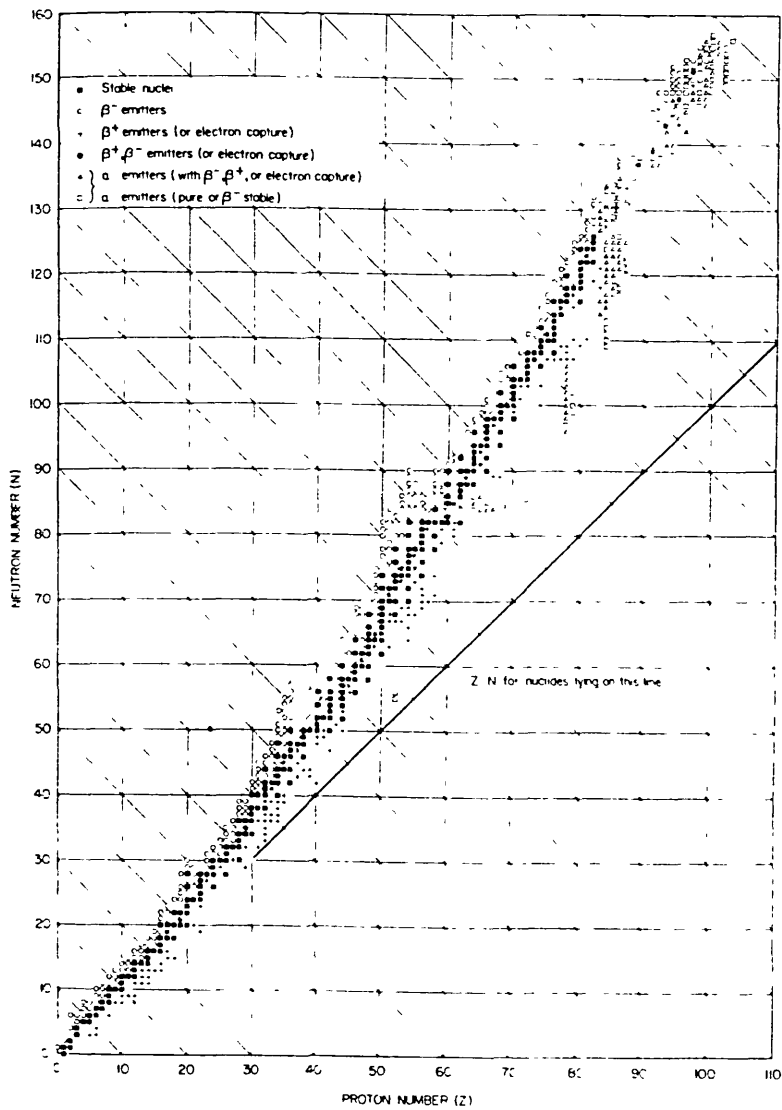


Fig.2.2 : Chart of isotopes (after Adams and Gasparini, 1970)

Following the initial decay, the residual nucleus is frequently left with excess energy which it subsequently emits as one or more gamma rays until it reaches its lowest energy level which is often called ground state.

Some nuclides can decay by two of these processes and when this happens, the nuclides are said to undergo 'branched decay'.

Nuclei decaying by any process may emit primary particles which often are not all of the same energy, but can be gathered into discrete groups. The nucleus may emit gamma rays in cascade in order to bring it to successively lower energy level. An energy decay scheme may be built up by matching each gamma ray to the energy differences between two nuclear energy levels. Thus it follows that if gamma rays arise from the excess nuclear energy from a primary decay, they are emitted from the excited daughter and not the parent.

2.3. Interaction Of Gamma Ray With Matter

The operation of any radiation detector basically depends on the manner in which the radiation to be detected interacts with the matter of the detector itself. An understanding of the response of a specific type of detector must therefore be based on a familiarity with the fundamental mechanisms by which radiations interact and lose their energy in matter. Also it is important to understand the interactions occurring between the source and the detecting instrument, e.g. source in ground and air.

Gamma rays being uncharged, are not subject to Coulomb force,

instead they undergo an interaction (often involving the nucleus of the constituent atoms) which radically alters the properties of the incident radiation in a single encounter. In all cases of practical interest, the interaction results in the full or partial transfer of energy of the incident radiation to electrons or nuclei of the constituent atoms or the charged particle products of nuclear reactions. If some interactions do not occur within the detector, these uncharged radiations can pass completely through the detector volume without being noticed (detected). Hence devices designed to detect gamma rays must be tailored to provide such interactions and to fully stop the resulting secondary electrons so that their energy may contribute to the output signal.

Absorption Of Gamma Rays

The absorption of gamma rays in matter occurs by mechanisms which are completely different from the absorption of charged particles. When a beam of alpha particles passes through an absorbing medium, each particle releases energy continuously until it captures two electrons and stops. The kinetic energy of the whole beam decreases continuously along the path, but the number of particles forming the beam remains practically constant until all of them are stopped. The length of this path (range) is a function of the nature and initial energy of the particles, and the nature of the absorber. Beta particles are also absorbed in a similar manner. But when a beam of gamma ray photons passes through an absorber, each photon either disappears after giving off all its energy in a single event or is

scattered away from the beam. Thus the number of photons in the beam decreases continuously with increasing range but there is no quantity corresponding to the range.

The intensity I , of the beam is defined as

$$I = \phi h\nu \quad (2.2)$$

where

ϕ is the photon flux (the number of photons crossing unit area in unit time), and

$h\nu$ is the energy of each photon, h and ν are Planck's constant and the frequency of radiation respectively.

If the beam of intensity I passes through an absorber of thickness dx , the amount of radiation dI , absorbed is proportional both to the thickness dx and to the intensity I . That is

$$dI \propto I dx$$

or
$$dI = -\mu I dx \quad (2.3)$$

where

μ is known as the linear absorption (attenuation) coefficient. This is a function of the energy of the gamma rays and the absorbing medium.

From equation 2.3,

$$dI/I = -\mu dx$$

Hence by integration,

$$\ln I = -\mu x + C$$

where

C is a constant of integration.

If $I = I_0$ when $x = 0$, then

$$\ln I_0 = C$$

Hence on substitution for C above gives

$$\ln I = -\mu x + \ln I_0$$

Therefore

$$I = I_0 e^{-\mu x} \tag{2.4}$$

The radiation intensity is generally measured in counts/second, counts/minute or in milliroentgens/hour (mR/h). The roentgen is the amount of gamma radiation which produces 2.083×10^9 ion pairs/cm³ of air at standard temperature and pressure.

The gamma ray photons can also be characterized by their mean free path X defined as the average distance travelled in the absorber before an interaction takes place. The value of X is given by

$$X = \frac{\int_0^{\infty} X e^{-\mu X} dX}{\int_0^{\infty} e^{-\mu X} dX} = \frac{1/\mu^2}{1/\mu}$$

That is

$$X = 1/\mu \quad (2.5)$$

Thus the mean free path X is simply the reciprocal of the linear absorption coefficient. For common gamma ray energies in solids, the values of X range from a few millimeters to tens of centimeters.

The thickness of the absorber required to absorb one half of the intensity is called half-thickness ($X_{1/2}$). This can be calculated using equation (2.4) by substituting $I_0/2$ for I and $X_{1/2}$ for x . Thus

$$I_0/2 = I_0 e^{-\mu X_{1/2}}$$

Therefore

$$1/2 = e^{-\mu X_{1/2}}$$

Hence

$$-\ln 2 = -\mu X_{1/2}$$

$$X_{1/2} = \frac{\ln 2}{\mu} = \frac{0.693}{\mu} \quad (2.6)$$

The use of the linear absorption coefficient is limited by the fact that it varies with the density of the absorber, even though the absorber material is the same. To circumvent this, mass attenuation coefficient is more widely used; and this is defined as

$$\text{Mass attenuation coefficient} = \frac{\text{linear attenuation coefficient}}{\text{density of absorber}}$$

That is,

Mass attenuation coefficient = μ/ρ

Hence for a given energy, the mass attenuation coefficient does not change with the physical state of a given absorber. For example, it is the same for water whether present in liquid or vapour form.

The mass attenuation coefficient of a compound or mixtures of elements can be calculated using the following equation:

$$\left(\frac{\mu}{\rho}\right)_c = \sum_{i=1}^n w_i \left(\frac{\mu}{\rho}\right)_i \quad (2.7)$$

where

w_i represents the weight function of element i in the compound or mixture.

In cgs units,

X is expressed in cm and

μ is expressed in cm^{-1}

Hence by definition the mass attenuation coefficient is expressed in cm^2/gm .

The thickness X of the absorber may be expressed in other ways as electron/ cm^2 and atoms/ cm^2 . When the thickness is expressed in this way, the absorption coefficient are then given in $\text{cm}^2/\text{electron}$ (μ_e) and cm^2/atom (μ_a). The relationship among such units are:

$$\mu_a = Z\mu_e$$

$$\mu_a/\rho = n(Z/A)\mu_e \quad (2.8)$$

$$= (N/A) \mu_a$$

where

Z and A are the atomic and mass numbers respectively and N is the Avogadro's number.

Although a large number of possible interaction mechanisms are known for gamma rays in matter, only three major types play an important role in radiation measurements. These are

- (i) photoelectric absorption
- (ii) Compton scattering and
- (iii) pair production

While photoelectric effect involves interaction with the whole atom, Compton scattering and pair production involve one electron in the atom. All these three processes lead to the partial or complete transfer of the gamma ray photon energy to electron energy. They result in sudden and abrupt changes in the gamma ray photon history, in that the photon either disappears entirely or is scattered through an angle.

As will be seen later, the atomic number of the absorber has a strong influence on the relative probabilities of these three interactions, and hence on the total absorption coefficient as this is the sum of the photoelectric absorption coefficient (μ_{ph}), the Compton absorption coefficient (μ_c) and the pair production absorption coefficient (μ_{pp}). That is

$$\mu = \mu_{ph} + \mu_c + \mu_{pp} \quad (2.9)$$

Photoelectric Absorption

The incident photon gives all its energy E_I , to a bound electron and disappears. The electron, usually from the innermost shell, is immediately emitted with a kinetic energy E_{e^-} , given by:

$$E_{e^-} = E_I - E_B \quad (2.10)$$

where

E_B is the binding energy of the ejected electron.

This equation shows that when the gamma ray energy E_I , is less than the binding energy E_B , of the electron in a particular shell, it cannot eject them from the atom, and so the electron will contribute nothing to the absorption of the photons.

The vacancy left by the ejected electron in the innermost shell is then filled through the capture of a free electron from the medium and/or rearrangement of electrons from the other shells of the atom. This results in the emission of characteristic X-rays or Auger electrons while momentum is conserved by the backward recoil of the residual atom. Although in most cases these X-rays are re-absorbed close to the original site through photoelectric absorption involving less tightly bound shells, their migration and possible escape from the radiation detectors, can influence their responses.

The effect of photoelectric absorption is thus the liberation of a photoelectron which carries off most of the gamma ray energy together with one or more low energy electrons corresponding to the absorption

of the original binding energy of the photoelectron. If nothing escapes from the detector then the sum of the kinetic energies of the electrons that are created, must equal the original energy of the gamma ray. The differential distribution of electron kinetic energy for a series of photoelectric absorption events is shown in Fig 2.3. The single peak appears at a total electron energy corresponding to the energy of the incident gamma ray photon.

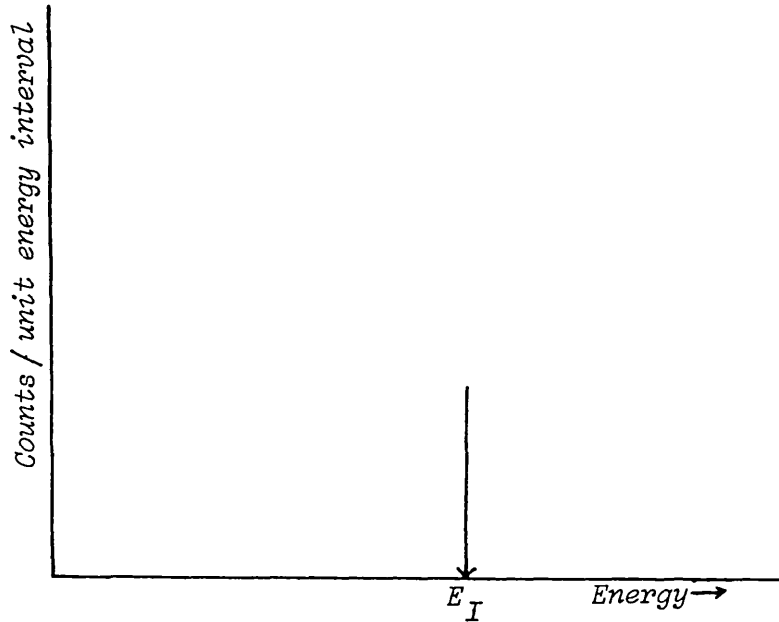


Fig.2.3: Photoelectric absorption events

The photoelectric effect is predominant at very low energies. It is also enhanced for absorber materials of high atomic number Z . The probability of photoelectric absorption follows, very roughly, the equation:

$$\text{Probability of photoelectric absorption} = \frac{Z^n}{E_\gamma^3} \quad (2.11)$$

where

E_γ is the gamma ray energy and

n varies between 4 and 5.

Compton Scattering

This involves the interaction of the incident photon with a free or loosely bound electron in the absorbing material, the incident photon transfers part of its energy to an electron, resulting in a photon of lower energy which is deflected at an angle Θ with respect to the original direction of the incident photon. The process can be described as an ordinary elastic collision as shown in Fig 2.4.

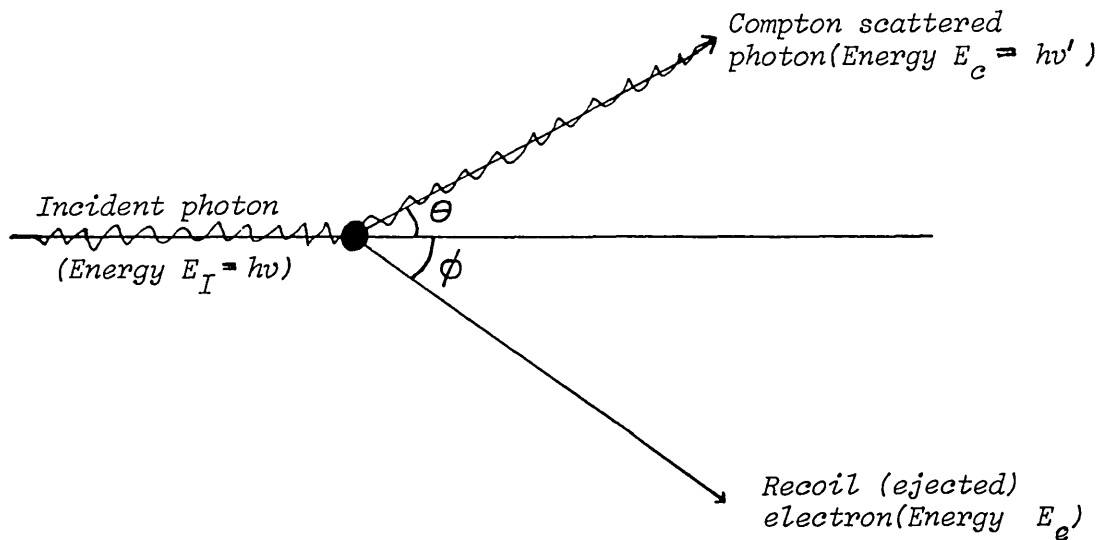


Fig.2.4: Compton scattering of a photon

The Compton scattered photon may undergo further Compton or photoelectric interactions. Since energy and momentum must be conserved,

$$E_I = E_C + E_e \quad (2.12a)$$

neglecting the binding energy of the electron. Also conservation of momentum in the direction of the incident photon gives

$$\frac{E_I}{c} = \frac{E_C \cos \theta}{c} + p \cos \phi \quad (2.12b)$$

where

p is the momentum of the electron, and

c is the speed of light

Also

$$\frac{E_C \sin \theta}{c} = p \sin \phi \quad (2.12c)$$

(conservation of momentum in the direction perpendicular to the direction of the incident photon).

The momentum of the electron is related to its kinetic energy E_e by the relativistic equation

$$p^2 = 1/c^2 \left[E_e (E_e + 2mc^2) \right] \quad (2.12d)$$

where

m is the mass of the electron at rest.

These equations (2.12(a-d)) may be solved for E_C and E_e in terms of E_I .

From equation 2.12c,

$$\sin^2 \phi = \frac{E_C^2 \sin^2 \theta}{c^2 p^2}$$

Hence

$$\cos^2 \phi = 1 - \frac{E_C^2 \sin^2 \theta}{c^2 p^2}$$

and

$$\cos \phi = \frac{(c^2 p^2 - E_C^2 \sin^2 \theta)^{1/2}}{cp}$$

Substitute for $\cos \phi$ in equation 2.12b

$$\frac{E_I}{c} = \frac{E_C \cos \theta}{c} + \frac{(c^2 p^2 - E_C^2 \sin^2 \theta)^{1/2}}{c}$$

Substitute for p^2 from equation 2.12d

$$E_I = E_C \cos \theta + \left\{ \left[E_e (E_e + 2mc^2) \right] - E_C^2 \sin^2 \theta \right\}^{1/2}$$

Therefore

$$E_I - E_C \cos \theta = \left\{ \left[E_e (E_e + 2mc^2) \right] - E_C^2 \sin^2 \theta \right\}^{1/2}$$

Square both sides

$$E_I^2 + E_C^2 \cos^2 \theta - 2E_I E_C \cos \theta = E_e(E_e + 2mC^2) - E_C^2 \sin^2 \theta$$

Therefore

$$E_I^2 + E_C^2 - 2E_I E_C \cos \theta = E_e(E_e + 2mC^2)$$

Sustitute for E_e from equation 2.12a

$$\begin{aligned} E_I^2 + E_C^2 - 2E_I E_C \cos \theta &= (E_I - E_C)^2 + 2mC^2(E_I - E_C) \\ &= E_I^2 + E_C^2 - 2E_I E_C + 2mC^2(E_I - E_C) \end{aligned}$$

Therefore

$$2E_I E_C (1 - \cos \theta) = 2mC^2(E_I - E_C) \quad (2.13a)$$

Therefore

$$\frac{E_I - E_C}{E_C} = \frac{E_I}{mC^2} (1 - \cos \theta) \quad (2.13b)$$

This shows that the fractional change in energy is proportional to the incident energy. Although the fractional energy loss is greater for

higher energy photons, the probability that a photon will be Compton scattered at all decreases about linearly with increasing energy. Therefore Compton scattering makes only a small contribution to the absorption of high energy photons. The probability also depends on the number of electrons available as scattering targets, and therefore increases linearly with the atomic number Z .

From 2.13a

$$E_I E_C (1 - \cos \theta) + mC^2 E_C = mC^2 E_I$$

Therefore

$$E_C \left[mC^2 + E_I (1 - \cos \theta) \right] = mC^2 E_I$$

Therefore

$$E_C = \frac{mC^2 E_I}{mC^2 + E_I (1 - \cos \theta)}$$

or

$$E_C = \frac{E_I}{1 + \frac{E_I}{mC^2} (1 - \cos \theta)} \quad (2.14a)$$

Also from equations 2.12a and 2.13b

$$E_e = \frac{E_c E_I}{mC^2} (1 - \cos\theta)$$

and substituting for E_c from equation 2.14a gives

$$E_e = \frac{E_I}{1 + \frac{E_I}{mC^2} (1 - \cos\theta)} \cdot \frac{E_I}{mC^2} (1 - \cos\theta)$$

or

$$E_e = E_I \left[\frac{\frac{E_I}{mC^2} (1 - \cos\theta)}{1 + \frac{E_I}{mC^2} (1 - \cos\theta)} \right] \quad (2.14b)$$

Two extreme cases can be identified.

(i) when $\theta \approx 0$

Then equation 2.14(a and b) becomes:

$$E_c \approx E_I \text{ (from equation 2.14a)}$$

and

$$E_e \approx 0 \text{ (from equation 2.14b)}$$

Thus in this case, the recoil compton electron has very little energy and the scattered gamma ray has nearly the same energy as the incident gamma ray.

(ii) when $\Theta \approx \pi (180^\circ)$

Then equation 2.14(a and b) become:

$$E_C = \frac{E_I}{1 + \frac{2E_I}{mC^2}} \quad (2.15a)$$

and

$$E_e = E_I \left[\frac{\frac{2E_I}{mC^2}}{1 + \frac{2E_I}{mC^2}} \right] \quad (2.15b)$$

In this case, there is a head-on collision in which the incident gamma ray is backscattered towards its direction of origin (compton interaction).

In normal circumstances, all scattering angles will occur in the detector. Therefore a continuum of energies can be transferred to the electron ranging from zero (minimum) up to the maximum (see equation 2.15b). The maximum energy which represents a sharp change in the distribution is called the compton edge. Fig 2.5 shows the general

shape of the electron energy distribution for any one specific gamma ray energy.

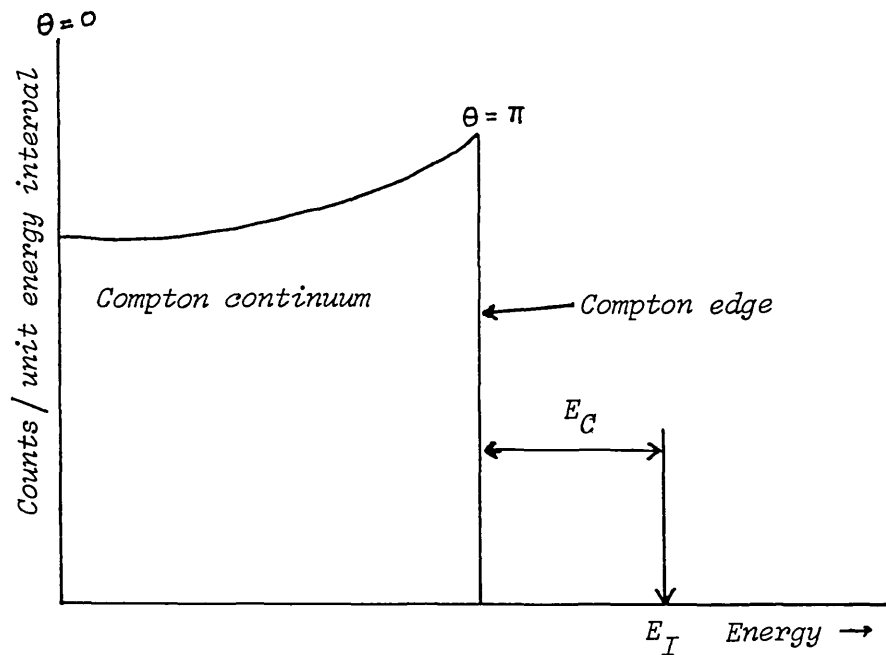


Fig 2.5. Compton Continuum For Any One Specific Gamma Ray Energy

We recall that in equation 2.12a, the binding energy E_b of the electron is neglected. In actual detector materials, the binding energy of the electron prior to the scattering process can have measurable effect on the shape of the Compton continuum. These effects are particularly more for low incident gamma ray energy. They involve a rounding off of the rise in the continuum near its upper extreme, and the introduction of a finite shape to the abrupt drop of the Compton edge. These effects are often masked by the finite energy resolution of the detector, but can be evident in a spectrum from detectors with high inherent resolution (see Fig 2.6).

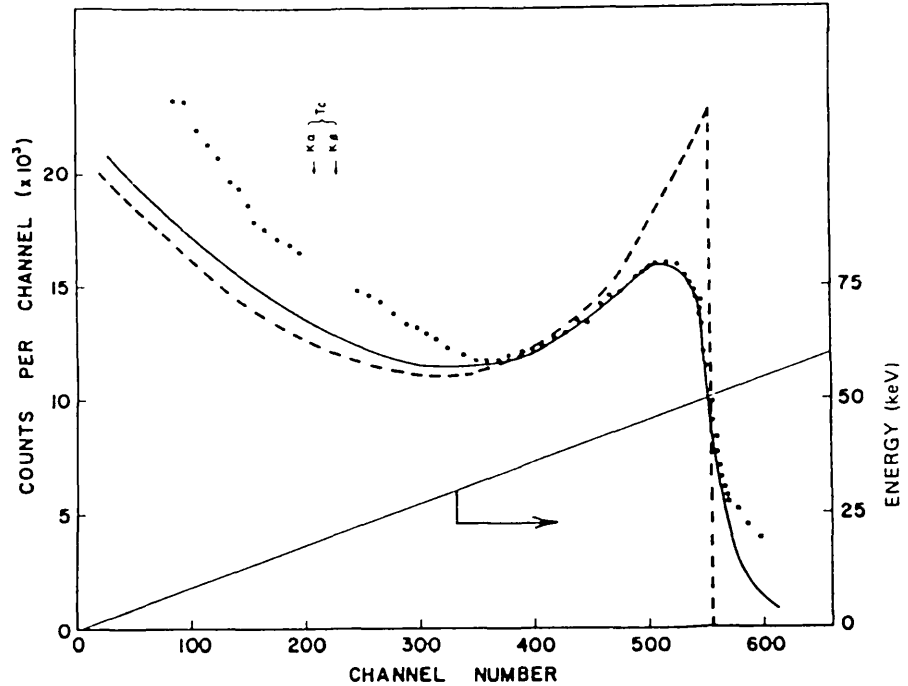


Fig. 2.6: Calculated and observed shape of the Compton continuum for a ^{99m}Tc source (140 keV). The dashed curve is predicted based on scattering of free electrons, whereas the solid curve is calculated taking into account the finite electron binding energy in silicon. The points are experimental data. (after knoll, 1979)

Pair Production

This process occurs in the field of a nucleus of the absorbing material, and corresponds to the creation of an electron-positron pair at the point of complete disappearance of the incident gamma ray photon. Because an energy of $2mC^2$ is required to create the electron-positron pair, a minimum gamma ray energy of 1.02MeV is required to make the process energetically possible. If the energy of the gamma ray photon exceeds $2mC^2$ (1.02MeV), the excess energy appears in the form of kinetic energy shared by the electron-positron pair. Thus the kinetic energies E_e and E_p , for electron and positron are

related to the incident photon energy E_I by the equation

$$E_I = E_e + E_p + 2mC^2 \quad (2.16)$$

The electron-positron pair disappears after losing all their kinetic energy to absorbing medium. The location of the total kinetic energy of the electron-positron pair is shown in Fig 2.7. The positron is not a stable particle and once its kinetic energy becomes very low, it annihilates (or combines) with a normal electron in the absorbing

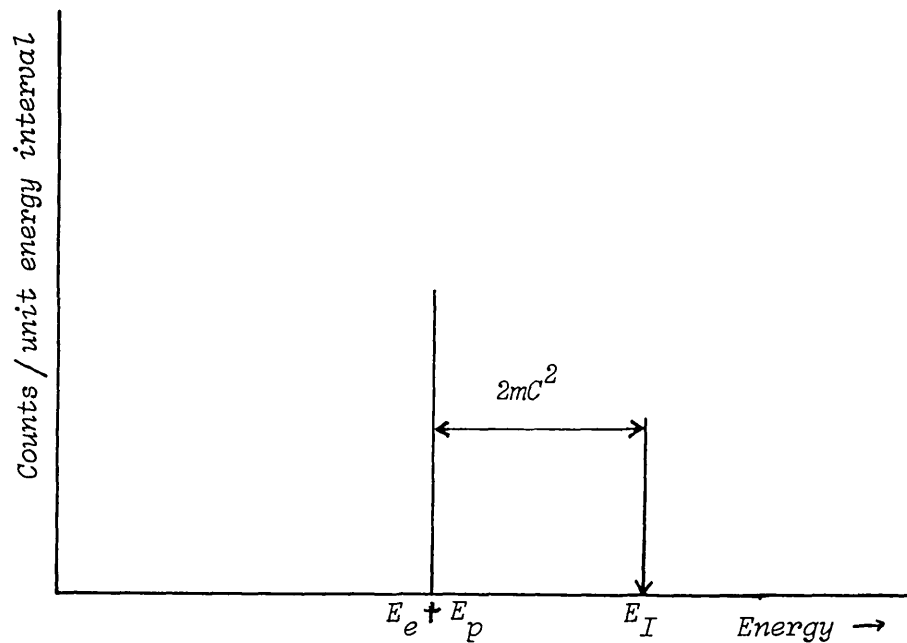


Fig.2.7: Location of electron-positron pair

medium, and they both disappear and replaced by two annihilation photons of energy mC^2 each, emitting in nearly opposite directions. The importance of pair production increases slowly for photon energies above 1.02MeV, and also approximately as the square of the atomic number Z of the absorbing material.

The relative importance of the three processes, viz, photoelectric, Compton scattering, and pair production is shown in Fig 2.8.

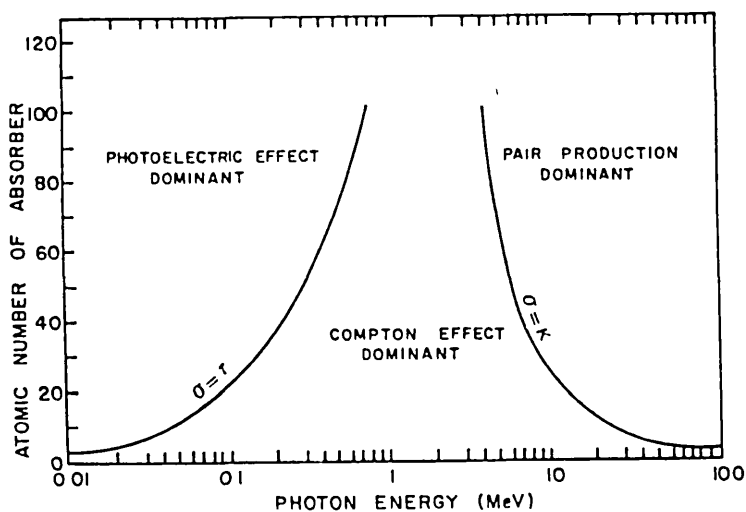


Fig. 2.8: Relative importance of the three major types of γ -ray interaction as a function of photon energy and atomic number. (after Lichholz and Poston, 1979)

While the line at the left represents the energy at which photoelectric absorption and Compton scattering are equally probable as a function of the absorption atomic number, the line at the right represents the energy at which Compton scattering and pair production are equally probable. Three areas are thus defined on the plot within which photoelectric absorption, Compton scattering, and pair production, each predominates.

In summary, gamma rays are usually detected by observing the electrons they produce. These have a fairly well-defined energy if

produced by Compton effects or pair production, though in the later case, the annihilation photon itself may again produce a photoelectron. Within the energy range of interest (0 to 3MeV) in gamma ray application in geology, pair production is less important absorption process than the photoelectric and Compton scattering processes. It however becomes comparatively important at higher energies and for heavy absorbers like lead.

2.4. Decay Process

In 1902 Rutherford and Soddy in their theory of radioactive transformation stated that when an element emits alpha and beta particles, it is transmuted into a new element, the rate of disintegration being a characteristic of each radioactive nucleus. They also showed that the rate of change is proportional to the number of atoms present and this is not affected by physical or chemical processes in the surrounding (Telford et al, 1976). Thus for any radioactive element, the rate of decay is given by

$$\frac{dN_1}{dt} = -\lambda_1 N_1 \quad (2.17)$$

where

N_1 is the number of atoms present at time t and

λ_1 is a decay constant which is characteristic of each element

From equation 2.17,

$$\frac{dN_1}{N_1} = -\lambda_1 dt$$

and on integration, this gives

$$\ln N_1 = -\lambda_1 t + C$$

where

C is a constant of integration

If $N_1 = N_0$ when $t = 0$, then

$$\ln N_0 = C$$

Hence

$$\ln N_1 = -\lambda_1 t + \ln N_0$$

or

$$N_1 = N_0 e^{-\lambda_1 t} \quad (2.18)$$

Half-life ($T_{1/2}$) is the time required for half of the nuclei to disintegrate. Thus from equation 2.18, substitution of $N_1 = N_0/2$ and $t = T_{1/2}$ gives

$$\frac{N_0}{2} = N_0 e^{-\lambda_1 T_{1/2}}$$

Therefore

$$-\ln 2 = -\lambda_1 T_{1/2}$$

Hence

$$T_{1/2} = \frac{\ln 2}{\lambda_1}$$

Or

$$T_{1/2} = \frac{0.693}{\lambda_1} \tag{2.19}$$

While a short half-life indicates a fast rate of disintegration, a long half-life may indicate stability of the atom. The mean or average life of the radioactive nuclei is given by

$$\tau_1 = \frac{1}{\lambda_1} \tag{2.19a}$$

Equation 2.17 shows the rate of decay of the parent atom and this is also the rate of formation of the daughter atoms. At the same time of

formation, the daughter atoms are also decaying at a rate $\lambda_2 N_2$ say, where N_2 is the number present at time t and λ_2 its decay constant. Thus the accumulation rate of the daughter atoms may be given by

$$\frac{dN_2}{dt} = \lambda_1 N_1 - \lambda_2 N_2 \quad (2.20)$$

This equation may be solved for N_2 , the number of daughter atoms present at any time t , given the number N_1 of the parent at time $t = 0$.

Let

$$N_2 = Ae^{-\lambda_1 t} + Be^{-\lambda_2 t} \quad (2.21)$$

where

A and B are constants

Therefore

$$\frac{dN_2}{dt} = -\lambda_1 Ae^{-\lambda_1 t} - \lambda_2 Be^{-\lambda_2 t}$$

Substituting in equation 2.20 gives

$$-\lambda_1 Ae^{-\lambda_1 t} - \lambda_2 Be^{-\lambda_2 t} = \lambda_1 N_0 e^{-\lambda_1 t} - \lambda_2 (Ae^{-\lambda_1 t} + Be^{-\lambda_2 t})$$

Therefore

$$(\lambda_2 - \lambda_1)Ae^{-\lambda_1 t} = \lambda_1 N_0 e^{-\lambda_1 t}$$

Therefore

$$A = \frac{\lambda_1 N_0}{\lambda_2 - \lambda_1}$$

Substituting for A in equation 2.21 gives

$$N_2 = \frac{\lambda_1 N_0}{\lambda_2 - \lambda_1} e^{-\lambda_1 t} + B e^{-\lambda_2 t}$$

If $N_2 = 0$ when $t = 0$, then

$$0 = \frac{\lambda_1 N_0}{\lambda_2 - \lambda_1} + B$$

and

$$B = - \frac{\lambda_1 N_0}{\lambda_2 - \lambda_1}$$

Hence

$$N_2 = \frac{\lambda_1 N_0}{\lambda_2 - \lambda_1} (e^{-\lambda_1 t} - e^{-\lambda_2 t}) \quad (2.22a)$$

Similar equations may be derived for the growth and decay of the third or later members of a decay series. The general solution for the number of atoms of the nth product, N_n , after time t , is given by

$$N_n = C_1 e^{-\lambda_1 t} + C_2 e^{-\lambda_2 t} + \dots + C_n e^{-\lambda_n t} \quad (2.22b)$$

where

$$\begin{aligned} C_1 &= \lambda_1 \lambda_2 \lambda_3 \dots \lambda_{n-1} N_0 / (\lambda_2 - \lambda_1) (\lambda_3 - \lambda_1) \dots (\lambda_n - \lambda_1) \\ C_2 &= \lambda_1 \lambda_2 \lambda_3 \dots \lambda_{n-1} N_0 / (\lambda_1 - \lambda_2) (\lambda_3 - \lambda_2) \dots (\lambda_n - \lambda_2) \\ &\dots \dots \dots \\ C_n &= \lambda_1 \lambda_2 \lambda_3 \dots \lambda_{n-1} N_0 / (\lambda_1 - \lambda_n) (\lambda_2 - \lambda_n) \dots (\lambda_{n-1} - \lambda_n) \end{aligned}$$

Radioactivity is measured in Curie (Ci) which is defined as the amount of radiation emitted by 1 gram of radium and is equivalent to 3.7×10^{10} disintegration/second.

Equilibrium

We recall that the accumulation rate of the daughter atoms is given by

$$\frac{dN_2}{dt} = \lambda_1 N_1 - \lambda_2 N_2 \quad (2.20)$$

When the rates of formation and decay of the daughter atoms are equal,

then dN_2/dt will be zero. That is

$$\lambda_1 N_1 - \lambda_2 N_2 = 0$$

Then

$$\lambda_1 N_1 = \lambda_2 N_2 \tag{2.23}$$

This condition is referred to as a state of secular equilibrium. Hence at equilibrium, the number of daughter atoms disintegrating per unit time is the same as the number being created by the disintegrations of the parent atoms.

From equations 2.23 and 2.19

$$\frac{N_2}{N_1} = \frac{\lambda_1}{\lambda_2} = \frac{T_2}{T_1} \tag{2.24}$$

where

T_1 and T_2 are the half-lives of the parent and daughter atoms respectively

The time taken by the parent atoms to achieve equilibrium with their daughter atoms may be calculated as follows:

From equations 2.22a and 2.18, we have

$$\frac{N_2}{N_1} = \frac{\lambda_1 N_0}{\lambda_2 - \lambda_1} \frac{[e^{-\lambda_1 t} - e^{-\lambda_2 t}]}{N_0 e^{-\lambda_1 t}}$$

$$= \frac{\lambda_1}{\lambda_2 - \lambda_1} \left[1 - e^{-(\lambda_2 - \lambda_1)t} \right]$$

But at equilibrium,

$$\frac{N_2}{N_1} = \frac{\lambda_1}{\lambda_2} \quad (\text{see equation 2.24})$$

Therefore

$$\frac{\lambda_1}{\lambda_2 - \lambda_1} \left[1 - e^{-(\lambda_2 - \lambda_1)t_{eq}} \right] = \frac{\lambda_1}{\lambda_2}$$

(t_{eq} = time at equilibrium)

Therefore

$$\begin{aligned} \frac{\lambda_1}{\lambda_1 - \lambda_2} e^{(\lambda_1 - \lambda_2)t_{eq}} &= \frac{\lambda_1}{\lambda_2 - \lambda_1} - \frac{\lambda_1}{\lambda_2} \\ &= \frac{\lambda_1 \lambda_2 - \lambda_1 \lambda_2 + \lambda_1^2}{\lambda_2 (\lambda_2 - \lambda_1)} \end{aligned}$$

Therefore

$$\begin{aligned} e^{(\lambda_1 - \lambda_2)t_{eq}} &= \frac{\lambda_1^2}{\lambda_2(\lambda_2 - \lambda_1)} \cdot \frac{\lambda_2 - \lambda_1}{\lambda_1} \\ &= \frac{\lambda_1}{\lambda_2} \end{aligned}$$

Therefore

$$(\lambda_1 - \lambda_2)t_{eq} = \ln\left(\frac{\lambda_1}{\lambda_2}\right)$$

Hence

$$t_{eq} = \frac{1}{\lambda_1 - \lambda_2} \ln\left(\frac{\lambda_1}{\lambda_2}\right) \quad (2.25a)$$

In the case of a series with n products, the time to reach equilibrium can be found, using equation 2.22b, and this is given as:

$$\frac{N}{N} = K \left[\frac{1}{\sigma_1} + \frac{e^{(\lambda_1 - \lambda_2)t_{eq}}}{\sigma_2} + \dots + \frac{e^{(\lambda_1 - \lambda_n)t_{eq}}}{\sigma_n} \right] \quad (2.25b)$$

where

$$\begin{aligned}
 K &= \lambda_1 \lambda_2 \lambda_3 \cdots \lambda_{n-1} \\
 \sigma_1 &= (\lambda_2 - \lambda_1)(\lambda_3 - \lambda_1) \cdots (\lambda_n - \lambda_1) \\
 \sigma_2 &= (\lambda_1 - \lambda_2)(\lambda_3 - \lambda_2) \cdots (\lambda_n - \lambda_2) \\
 &\dots\dots\dots \\
 &\dots\dots\dots \\
 \sigma_n &= (\lambda_1 - \lambda_n)(\lambda_2 - \lambda_n) \cdots (\lambda_{n-1} - \lambda_n)
 \end{aligned}$$

Fig 2.9 shows the decay series of Uranium-238, Uranium-235 and Thorium series; and Table 2.4 shows in detail the radioactive series for uranium and thorium series with principal radiation accompanying each disintegration. Also a wide spectrum of gamma rays accompanying both alpha and beta emissions are included in the table.

Within a chemically closed system, the process of radioactive decay will result in a state of equilibrium being reached, whereby each intermediate daughter product in the chain is being formed at the same rate as it decays. Once the decay system has achieved equilibrium, a measurement of the abundance of a daughter product will provide a reliable measurement of the abundance of the parent element. Hence a measurement of the intensity of the 1.76MeV gamma emission of Bismut-214 can provide a measure of the abundance of uranium; similarly the measurement of the 2.62MeV gamma emission of Thallium-208 can provide a measure of the abundance of thorium.

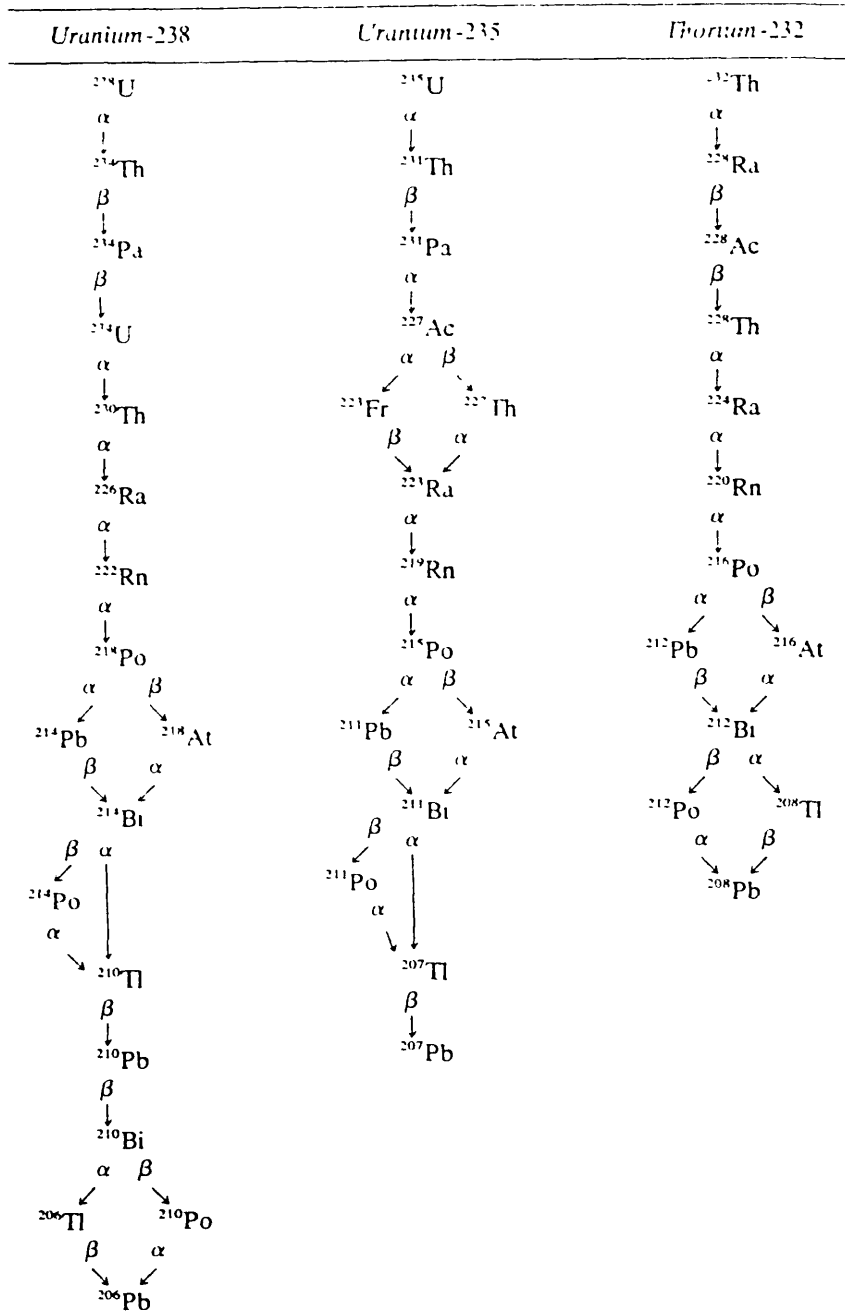


Fig.2.9: Uranium and Thorium radioactive decay series (after Reedman, 1979)

Element	Isotope	Half-life	Decay constant sec ⁻¹	Radiation	γ-ray energies (MeV)	No. of γ-rays
Thorium	⁹⁰ Th ²³²	1.4 × 10 ¹⁰ yr	1.58 × 10 ⁻¹⁸	α, SF*, γ	0.059	
Radium	⁸⁸ Ra ²²⁸	6.7 yr	3.3 × 10 ⁻⁹	β, γ	0.03	
Actinium	⁸⁹ Ac ²²⁸	6.1 hr	3.1 × 10 ⁻⁴	β, γ	0.06-0.97	>10
Thorium	⁹⁰ Th ²³⁰	1.91 yr	1.15 × 10 ⁻⁸	α, γ	0.085-0.214	5
Radium	⁸⁸ Ra ²²⁴	3.64 day	2.2 × 10 ⁻⁶	α, γ	0.24, 0.29	
Radon	⁸⁶ Rn ²²⁰	51 sec	1.3 × 10 ⁻²	α, γ	0.54	
Polonium	⁸⁴ Po ²¹⁶	0.16 sec	4.3	α		
Lead	⁸² Pb ²¹²	10.6 hr	1.8 × 10 ⁻⁵	β, γ	0.11-0.41	5
Bismuth	⁸³ Bi ²¹²	60.6 min	1.9 × 10 ⁻⁴	β, α, γ	0.04-2.2	>10
Polonium	⁸⁴ Po ²¹²	0.3 × 10 ⁻⁶ sec	2.3 × 10 ⁶	α		
Thallium	⁸¹ Tl ²⁰⁸	3.1 min	3.7 × 10 ⁻³	β, γ	0.28-2.62	5
Lead	⁸² Pb ²⁰⁸	Stable				
Uranium	⁹² U ²³⁵	7.1 × 10 ⁸ yr	3.1 × 10 ⁻¹⁷	α, SF*, γ	0.07-0.38	10
Thorium	⁹⁰ Th ²³¹	25.6 hr	7.4 × 10 ⁻⁶	β, γ	0.08-0.31	>10
Protact.	⁹¹ Pa ²³¹	3.4 × 10 ⁴ yr	6.5 × 10 ⁻¹³	α, γ	0.29-0.36	>10
Actinium	⁸⁹ Ac ²²⁷	21.6 yr	10 ⁻⁹	β, α, γ	0.09-0.19	9
Thorium	⁹⁰ Th ²²⁷	18.2 day	4.35 × 10 ⁻⁷	α, γ	0.05-0.33	>10
Francium	⁸⁷ Fr ²²³	22 min	5.2 × 10 ⁻⁴	β, α, γ	0.05-0.31	4
Radium	⁸⁸ Ra ²²³	11.7 day	6.76 × 10 ⁻⁷	α, γ	0.03-0.45	>10
Radon	⁸⁶ Rn ²¹⁹	4 sec	0.17	α, γ	0.27, 0.4	
Astatine	⁸⁵ At ²¹⁹	54 sec	1.28 × 10 ⁻²	α, β		
Polonium	⁸⁴ Po ²¹⁵	1.8 × 10 ⁻³ sec	3.8 × 10 ²	α, β		
Astatine	⁸⁵ At ²¹⁵	10 ⁻⁴ sec	6.9 × 10 ³	α		
Bismuth	⁸³ Bi ²¹⁵	8 min	1.44 × 10 ⁻³	β		
Bismuth	⁸³ Bi ²¹¹	2.15 min	5.35 × 10 ⁻³	α, β, γ	0.35	
Polonium	⁸⁴ Po ²¹¹	0.52 sec	1.32	α, γ	0.56, 0.88	
Lead	⁸² Pb ²¹¹	36 min	3.2 × 10 ⁻⁴	β, γ	0.065-0.83	4
Thallium	⁸¹ Tl ²⁰⁷	4.8 min	2.4 × 10 ⁻³	β, γ	0.89	
Lead	⁸² Pb ²⁰⁷	Stable				
Uranium	⁹² U ²³⁸	4.51 × 10 ⁹ yr	4.9 × 10 ⁻¹⁸	α, SF*, γ	0.048	
Thorium	⁹⁰ Th ²³⁴	24.1 day	3.3 × 10 ⁻⁷	β, γ	0.03-0.09	3
Protoact.	⁹¹ Pa ²³⁴	6.7 hr	2.84 × 10 ⁻⁵	β, γ	0.044-1.85	>10
Uranium	⁹² U ²³⁴	2.48 × 10 ⁵ yr	8.9 × 10 ⁻¹⁴	α, SF*, γ	0.053, 0.118	
Thorium	⁹⁰ Th ²³⁰	8 × 10 ⁴ yr	2.75 × 10 ⁻¹⁰	α, γ	0.068-0.25	7
Radium	⁸⁸ Ra ²²⁶	1622 yr	1.35 × 10 ⁻¹¹	α, γ	0.19-0.64	4
Radon	⁸⁶ Rn ²²²	3.82 day	2.07 × 10 ⁻⁶	α, γ	0.51	
Polonium	⁸⁴ Po ²¹⁸	3.05 min	3.8 × 10 ⁻³	α, β		
Astatine	⁸⁵ At ²¹⁸	1.35 sec	0.51	α		
Radon	⁸⁶ Rn ²¹⁸	0.03 sec		α	0.61	
Bismuth	⁸³ Bi ²¹⁴	19.7 min	5.85 × 10 ⁻⁴	β, α, γ	0.45-2.43	>10
Polonium	⁸⁴ Po ²¹⁴	1.64 × 10 ⁻⁴ sec	4.2 × 10 ³	α		
Lead	⁸² Pb ²¹⁴	26.8 min	4.3 × 10 ⁻⁴	β, γ	0.05-0.35	>10
Lead	⁸² Pb ²¹⁰	21 yr	1.05 × 10 ⁻⁹	β, γ	0.047	
Bismuth	⁸³ Bi ²¹⁰	5 day	1.58 × 10 ⁻⁶	β		
Polonium	⁸⁴ Po ²¹⁰	138.4 day	5.7 × 10 ⁻⁸	α, γ	0.79	
Thallium	⁸¹ Tl ²¹⁰	1.3 min	8.85 × 10 ⁻³	β, γ	0.3, 0.78, 1.1	
Thallium	⁸¹ Tl ²⁰⁶	4.2 min		β		
Lead	⁸² Pb ²⁰⁶	Stable				

SF* = spontaneous fission.

Table 2.4: Natural radioactive series of uranium and thorium (after Telford et al, 1976)

As can be seen from Table 2.4, the gamma ray from different sources will have a wide spectrum of energy and instruments which can distinguish these different energies are known as gamma ray spectrometers. Thus such instruments make it possible to identify the source of radiation. When a gamma ray interacts with the detector of the spectrometer, pulses are produced and these are monitored by an analyzer which is able to discriminate various energies through complicated electronic circuitry (see chapter Five). A common gamma ray spectrometer for a spectrometric survey will thus be capable of distinguishing energies within bands corresponding to potassium, uranium and thorium (see Fig 1.2). Although there are many photopeaks in the uranium and thorium decay series, as mentioned above, the photopeaks of energies 1.76MeV and 2.62MeV are used for uranium and thorium respectively. Also sometimes a gamma ray spectrometer is used to measure total radiation. But usually in this case, all photons above some energy threshold are counted.

Procedures and corrections of gamma ray spectrometric surveys are discussed in chapter Four.

Disequilibrium

When a radioactive decay series is at equilibrium, the rate of decay of the parent atom is the same as the rate of decay of the daughter isotope (see equation 2.23). It may simply thus be said that for radioactive disequilibrium, the rate of decay of the parent atom is unequal to the rate of disintegration of the daughter element. A state of non-equilibrium exists when all or part of one or more of the

daughters or parents is physically removed from the decay series. If a nuclide with a short half-life is removed, equilibrium can be rapidly regained, but if a nuclide with a long half-life is removed, it may take very long time before complete equilibrium is regained between all the members of the decay chain.

Under surface and near surface geological conditions, a closed chemical system may not exist. Weathering provides both the introduction and removal of material. Thus under weathering conditions, some chemical and physical dispersal of parent and daughter products will take place. This will cause disequilibrium in the decay series with the result that the intermediate end products may not be present at any one point in the proportions predicted by the law of radioactive decay (see equation 2.22). Under this condition a measurement of the abundance of a decay product will not necessarily provide a reliable measurement of the abundance of the parent element.

The degree of disequilibrium is dependent upon climate, topography and surface hydrology as these are the agents of weathering. The recognition of disequilibrium is also dependent on the sample size studied. A small hand specimen is much more likely to show extreme disequilibrium than will a large bulk sample or an in-situ measurement on a large volume of material; but unfortunately field measurements do not easily lead to the establishment of the degree of disequilibrium. However in the laboratory the degree of disequilibrium can be determined in a number of ways by either comparing chemical estimates with estimates based on decay product radioactivity, or by measuring

the radioactivity of different decay products. As mentioned already, the small size of laboratory sample tends to emphasize the disequilibrium process.

The primary cause of disequilibrium in nature is due to the presence, in the decay series, of radioactive isotopes of very different chemical properties. Several cases concerning the uranium-238 have been reported. As can be seen from Table 2.4, the presence of long-lived U-234, Th-230 and Ra-226 makes the establishment of secular radioactive equilibrium throughout the series a long process; also the different chemical natures of the long-lived intermediate members enhance the chances of chemical fractionation in nature and so the removal or support of any of the long-lived members produces long term disequilibria conditions. The main cause of Uranium to Thorium fractionation is the higher oxidability of tetravalent uranium as compared to thorium. One observed case of disequilibrium in U-238 series which cannot be solely attributed to chemical differences is the depletion of U-234 in weathered rocks and soils and the consequent enrichment in fresh and oceanic waters (Adams and Gasparini, 1970). Thorium-234 occurs between U-238 and U-234 and so the recoil the U-234 nuclei has undergone after one alpha emission may be a cause for the differential behaviour of the two isotopes. Also a number of disequilibrium cases have been reported for the Th-232 series. This is due to the short half-life of the Th-232 daughters which minimize the effect of any removal.

Another cause of disequilibrium is the presence of the isotopes of radon (Rn) in all the series. This, being a gas, can escape from the

series. The chances of Rn escape are highest in U-238 series because of the higher half-life of Rn-222 as compared to Rn-220 and Rn-219. Furthermore Rn-222 has a relatively long-lived daughter Pb-210.

The determination of equilibrium conditions in natural system can be useful in evaluation of sedimentation rate, estimate of weathering and absolute dating of rocks (see Chapter Three). However the use of gamma ray spectrometry to equilibrium determination is restricted by the limited number of sufficiently intense gamma emitters in all three natural series.

CHAPTER THREE

GEOLOGICAL IMPORTANCE OF GAMMA RADIATION

Trace quantities of radioactive materials are found in all rocks. Table 3.1 shows some of the common radioactive minerals while Table 3.2 shows the contents of uranium, thorium and potassium-40 in a few materials of the earth's crust. These elements along with cosmic radiation and radon in air, produce a continuous background reading which may vary from place to place. Cosmic rays consist of atomic nuclei and protons from outer space with high energies of the order of several thousand MeV. These particles interact with atoms in the atmosphere to produce nuclear disintegrations which are accompanied by gamma rays.

Although many elements can be determined by gamma spectrometry, uranium and thorium are the only trace elements whose concentrations can be determined by measurement of their natural radioactivity. The interest in the study of their distribution in rocks is enhanced by their importance in terrestrial heat production, the wide range of variation in different rock types, the sensitivity to various magmatic differentiation processes and their economic importance.

The uses of the determinations of the abundances of natural radioisotopes and their stable end products in a rock or mineral thus include:

- (a) Dating, that is, to estimate the time during which the stable radiogenic isotope accumulated in the system. Each of the natural radioactive series can be used

potentially as a 'radioactive clock'.

- (b) Heat flow studies
- (c) Mapping of petrologic units and
- (d) Exploration work.

<i>Potassium</i>	Mineral	(i) Orthoclase and microcline feldspars [$KAlSi_3O_8$] (ii) Muscovite [$H_2KAl(SiO_3)_3$] (iii) Alunite [$K_2Al_4(OH)_6SO_4$] (iv) Sylvite, carnallite [$KCl, MgCl_2 \cdot 6H_2O$]
	Occurrence	(i) Main constituents in acid igneous rocks and pegmatites (ii) Same (iii) Alteration in acid volcanics (iv) Saline deposits in sediments
<i>Thorium</i>	Mineral	(i) Monazite [$ThO_2 +$ Rare earth phosphate] (ii) Thorianite [$(Th, U)O_2$] (iii) Thorite, uranothorite [$ThSiO_4 + U$]
	Occurrence	(i) Granites, pegmatites, gneiss (ii), (iii) Granites, pegmatites, placers
<i>Uranium</i>	Mineral	(i) Uraninite [Oxide of U, Pb, Ra + Th, Rare earths] (ii) Carnotite [$K_2O \cdot 2UO_3 \cdot V_2O_5 \cdot 2H_2O$] (iii) Gummite [Uraninite alteration]
	Occurrence	(i) Granites, pegmatites and with vein deposits of Ag, Pb, Cu, etc (ii) Sandstones (iii) Associated with uraninite

Table 3.1: Radioactive minerals (after Telford et al, 1976)

	U g/t	Th g/t	^{40}K %
Basalt	0.9	4.2	0.75
Diabase	0.8	2.0	
Granite	3-5	13.0	4.4
Sediments	~1.0	5-12	
Limestone	1.3	1.1	
Oil	100		
Ocean water	0.00015- 0.0016	0.0005	
	%	%	
Uraninite	38-80	0-0.3	
Carnotite	50-63(†)	0-15	
Thorianite	23-26	53-57	
Monazite	0.02-0.7	3.5-16.5	

†Contents of uranium oxide

Table 3.2: Radioactive contents
(after Parasnis, 1979)

3.1. Dating

The use of radioactive decay as a basis of time determination rests on the fact that a parent element decays at a known constant rate into a daughter element, either directly or in a radioactive chain, and that nothing is added or removed during the process. Furthermore, the rock or mineral, at the time it is formed, must either be free of the ultimate daughter isotope or in a known ratio with other isotopes so that the original content of the decay product can be determined.

We recall that the disintegration of a given quantity of any radioactive element can be expressed by the formula

$$N = N_0 e^{-\lambda t} \quad (\text{from equation 2.18}) \quad (3.1)$$

where

N_0 is the number of atoms initially present at time $t = 0$.

From equation 3.1,

$$N_0 = N e^{\lambda t} \quad (3.2a)$$

Hence the amount of parent atoms that have disintegrated or amount of daughter atoms present is given by

$$\begin{aligned} (\text{Daughter})_{\text{present}} &= \text{amount of parent that has disintegrated} \\ &= N_0 - N \\ &= N e^{\lambda t} - N \\ &= N(e^{\lambda t} - 1) \end{aligned} \quad (3.2b)$$

Thus

$$(\text{Daughter})_{\text{present}} = (\text{Parent})_{\text{present}} \cdot (e^{\lambda t} - 1)$$

Hence a determination of the amounts of parent and daughter present, and a knowledge of the rate of decay, λ , of the parent will lead to a solution for the age t of the system.

Most methods, for example, the lead methods, are based on the series decay of uranium and thorium into lead. Also the potassium-argon method involves the direct decay of parent to daughter. The amount of uranium and/or thorium or potassium present can be determined by radiometric method (see equation 2.22b)

3.2. Heat Flow Studies

The decay of radioactive isotopes involves the release of energy which at the end, is converted to heat. This is believed to be the major source of heat production within the earth.

Uranium-238, Uranium-235, Thorium-232 and Potassium-40 are considered the only isotopes of importance for radioactive heat generation in the earth. This is because they are abundant and/or their half-lives are comparable to the age of the earth. The half-lives and heat production for these isotopes are shown in the following Table 3.3.

Isotope	Half-life 10^9 years	Heat generation Cal/g-year
U-238	4.50	0.71
U-235	0.71	4.3
U(ordinary)	-	0.73
Th-232	13.9	0.20
K-40	1.3	0.22
K(ordinary)	-	0.000027

Table 3.3: Half-lives and Heat Production Values (after Birch, 1954)

The measurement of the amount of the above isotopes in rocks will give an idea of the amount of heat generated in the rocks as demonstrated by Wollenberg (1977). The heat production values given above can be converted to 'workable' units of $\text{cal/cm}^3\text{-sec}$ by using the average crustal rock density of 2.68gm/cm^3 .

3.3. Geological Mapping

A comparison of field radioactivity data with the geology of the surveyed area often shows that radiometric data are closely related to petrologic units or to particular geologic features. Several authors, Moxham (1960, 1963), Bates (1966), Demnati and Naudy (1975), just to mention a few, have demonstrated this in their work. This dependence is locally so close that geologic units can actually be mapped from

radiometric data. However, it should be noted while interpreting field data that the gamma ray flux, after correction for background, comes from the upper few centimeters of rocks; and this leads to the consequence that radiometric field data are very sensitive to the occurrence of very thin covers of extraneous materials.

Demnati and Naudy (1975) showed correlations between airborne radiometric, aeromagnetic and geologic maps for the Central part of Morocco. The report shows that the correlations of the total counts (Fig 3.1a) with the geology of the area (Fig 3.1b) are generally very good. In particular the limit between the Carboniferous (relictic rocks) and the more recent formations (carbonates) are easily followed. Furthermore, strong anomalies are located over a granitic intrusion, rhyolites(R) and phonolites(P). More other features are revealed from the detailed contoured maps of the total counts, the thorium channel, the corrected potassium channel(Kc) and the ratio Th/Kc. The uranium distribution maps were not presented, said the report, because the area does not contain characteristic anomalies in this channel.

Bates (1966) concluded from his work that radioactivity data can be used to outline the continuity of geologic units between widely spaced ground traverses, which thus speed the compilation of a provisional geologic map. In areas of deep weathering where geologic relationships are obscured, radioactivity data often may be used to more accurately outlined known rock units and to indicate the presence

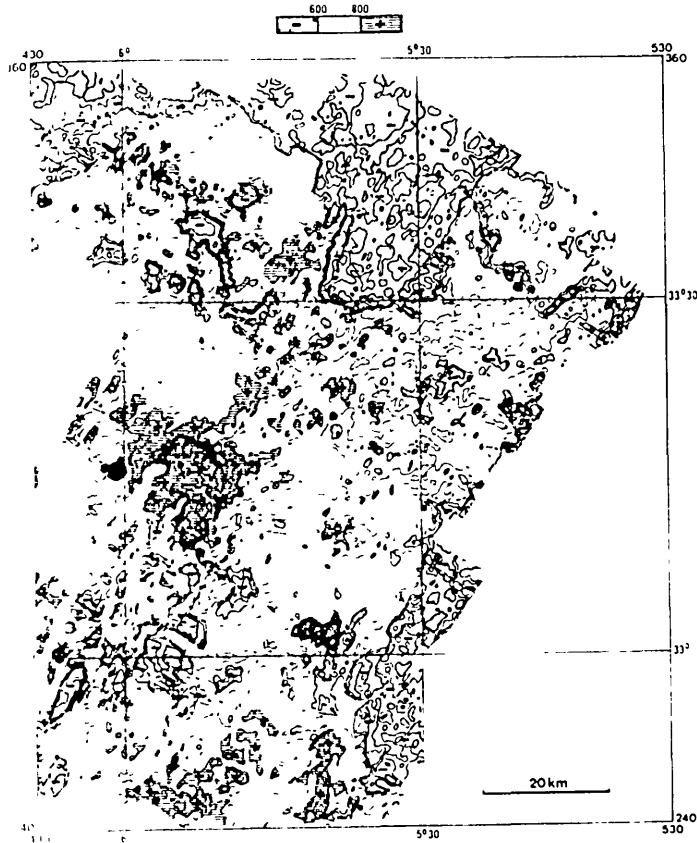


Fig.3.1a: Contour map of total count: contour interval is 50 counts per second (after Demnati and Naudy, 1975)

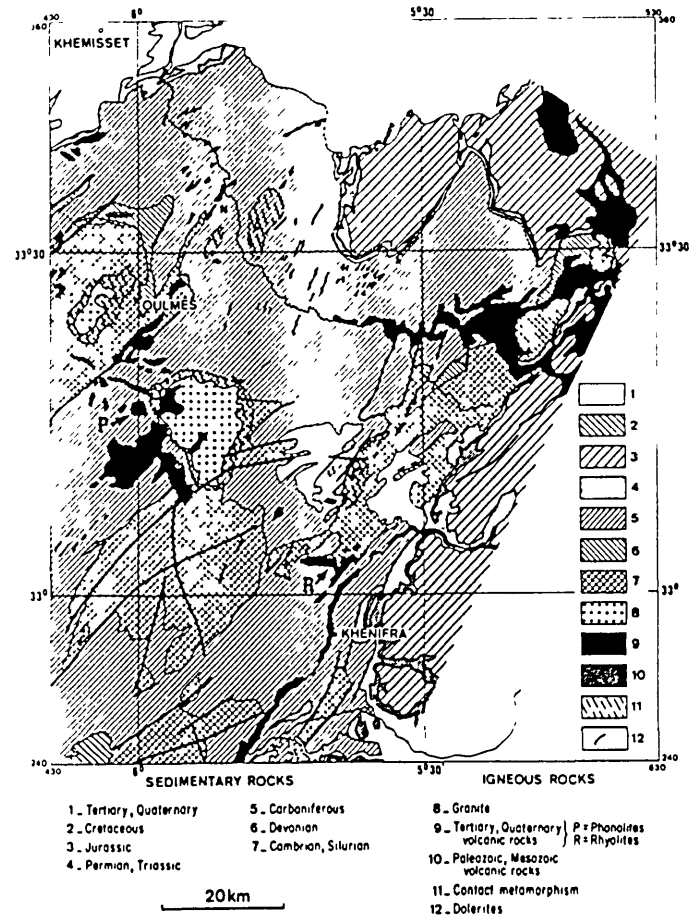


Fig.3.1b: Surveyed area geology (after Demnati and Naudy, 1975)

and configuration of other units. When combined with other forms of geophysical information such as magnetic, subsurface as well as surface configuration of geologic units may be obtained.

3.4. Exploration Work

In the industry, the applications of radiometric to exploration of minerals and petroleum include

- (i) evaluation of uranium ores
- (ii) location of uranium anomalies on a regional and localized basis
- (iii) the use of radioactive minerals as 'pathfinders' for deposit of other placer minerals, e.g. thorium for heavy mineral concentration, and
- (iv) the use of radioactive 'key beds' to interpret subsurface stratigraphic sections and structural relations for petroleum exploration.

Both ground and aerial gamma spectrometric surveys can be used to localize regional or deposit anomalies. These can then be followed by subsurface radiometric survey and laboratory analysis in the evaluation of targets, development and production of resource areas. The following Table 3.4 (after Wollenberg, 1977a) shows the applicability of radiometric methods at different phases of a resource development program.

(1) Exploration For Target Area

- (a) Airborne total gamma and gamma spectral surveys
- (b) Ground field gamma spectrometry on broad scale surveys,
and
- (c) Laboratory gamma spectrometry of selected samples.

(11) Evaluation Of Targets

- (a) Detailed ground field total gamma and gamma spectral surveys over target areas.
- (b) Laboratory gamma spectrometry of specimens from intensely sampled areas, and
- (c) Downhole total gamma and gamma spectral measurements of targets delineated by surface surveys.

(111) Development And Production Of Resource Areas

- (a) Downhole total gamma and gamma spectral measurements for grade control
- (b) Field total gamma and gamma spectral measurements of working faces and benches, and stockpiles; and
- (c) Laboratory gamma and gamma spectrometry of samples from these areas.

Table 3.4: Application of Radiometric methods in Exploration work
(after Wollenberg, 1977a)

In the subsurface survey, differences in the radioactive content of the various rock layers surrounding a well result in corresponding

differences in gamma radiation within the wellbore. By measuring the gamma ray intensity at any depth and plotting the data as a function of depth, a graph is obtained which depicts the radioactivity of the strata (see Fig 3.2). From this curve, the rock strata can be identified and their position and thickness can be determined. For example, in the petroleum industry this is used to distinguish the sandstones and limestones, which are of interest as possible oil-bearing formations, from the clays and shales.

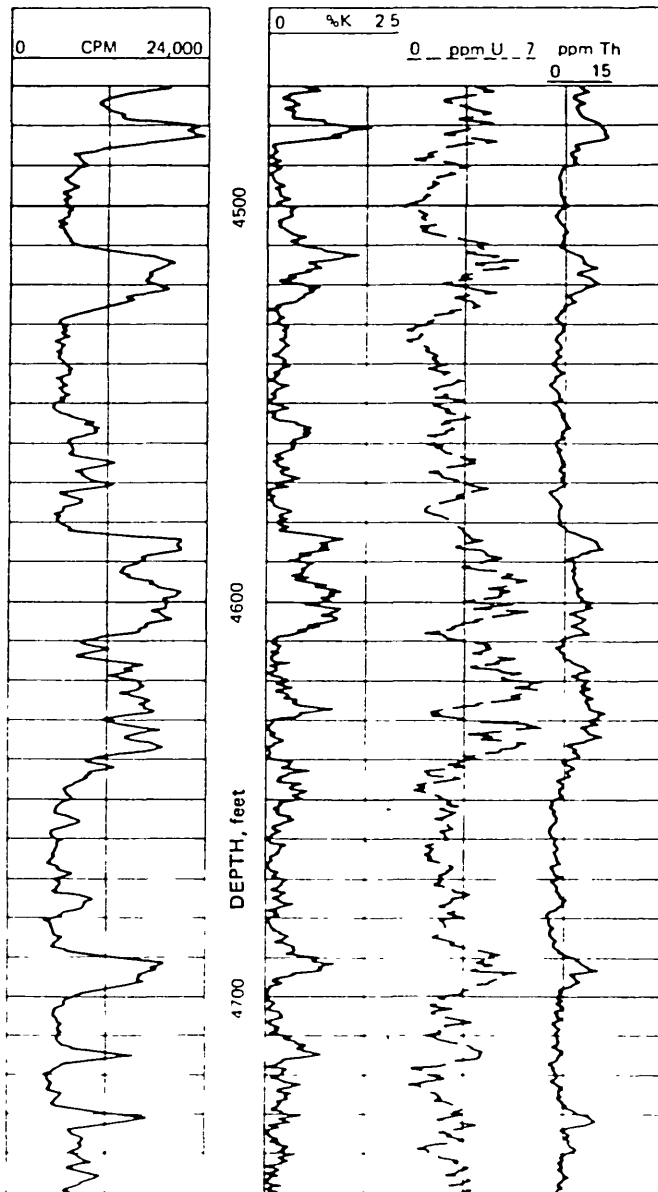


Fig. 3.2: Spectral (left) and natural (right) gamma-ray logs
(after Hilchie, 1977)

In general the gamma ray log is useful because

- (i) shales are usually more gamma-radioactive than other sedimentary formations, and the gamma ray log is frequently able to delineate the shale beds in a sequence.
- (ii) gamma rays are penetrating and give usable logs in cased holes, though with reduced accuracy. Correlations can thus be made in old wells.
- (iii) the gamma ray log usually correlates well with the electrical self-potential log and may be used to tie the electrical log depth scale to the casing collar log, and
- (iv) occasionally a radioactive bed is adjacent to a productive zone over a wide area. Such beds can serve as markers.

The use of gamma ray measurement in mineral exploration has been demonstrated by several authors. For example, Caldwell et al (1977) showed the use of gamma ray spectroscopy in oil and gas exploration and production, while Clayton (1977) demonstrated its use in the coal industry.

CHAPTER FOUR

SURVEY PROCEDURES AND CORRECTIONS

A gamma ray spectrometric survey of the earth's rocks can be carried out either in the laboratory or in the field. The field survey is an in-situ measurement either on the ground surface, subsurface or by means of airborne instruments. For all these measurements, the instrumentation (see chapter Five) required must meet some common requirements, viz, compact, light-weight, rugged with a low power consumption and a detector with a high efficiency and response. The sensitivity of the detection equipment is essential as very slight differences in radioactivity levels of rock units may be geologically significant.

The surveys can be carried out using a three channel or multichannel gamma ray spectrometer. In both cases the concentrations of potassium, uranium and thorium are determined from a comparison of the sample spectral data with at least three sets of 'standard' spectral data.

The recorded signal in a radiometric survey includes background radiation and effects of some other factors (see section 4.2.3). All these effects have to be accounted for and the background removed before any measurement of elemental abundance can be attempted. The elemental abundance in samples are determined after the detection instrument is calibrated using standards of known concentrations.

4.1. Laboratory Measurement

In the laboratory, bulk rock samples are crushed, ground, homogenized and then packed into containers, commonly plastic containers. The filled containers are carefully sealed and weighed, and then left for radon equilibrium to be achieved. The use of the containers ensures that the detector is not contaminated and also ensures that the detector - source geometry is constant for both the samples and the standards. This is necessary because the intensity of radiation from a source is directly proportional to the solid angle subtended by the detector and the boundaries of the source (Bowie et al, 1955). Solid drill cores of regular shapes can also be analyzed non-destructively (Lovborg, 1972).

4.2. Field Measurements

4.2.1. Surface Survey

Ground surveys can be carried out on foot or by using vehicles. The survey may be made either as random examinations on outcrops or along traverses with regular points (stations) marked on them. For foot survey the probe can be mounted on a (photographic) tripod or man-carried in order to control its altitude and hence the resolution or it can be laid on the ground on flat surface. When a vehicle is used the probe is either left in the vehicle or mounted on the roof. The reproducibility of the detector-source geometry during the calibration and the field measurements can be assured by a portable lead collimator placed around the detector (see Fig 4.1)

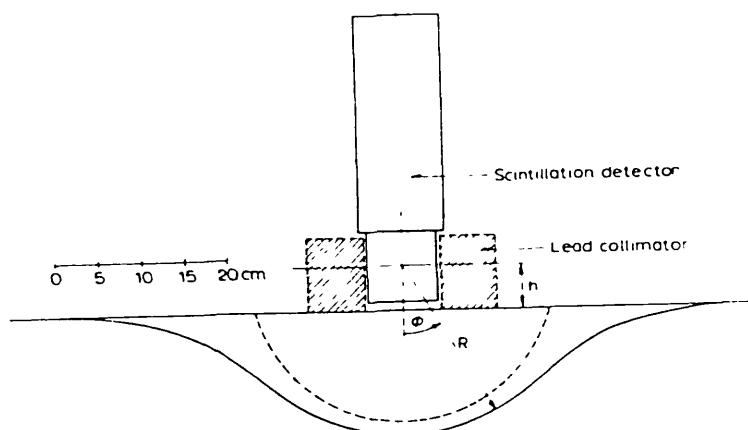


Fig. 4.1: Vertical cross-section showing calculated effective samples obtained by a collimated (dashed curve) and uncollimated (solid curve) detector placed on a flat rock surface. Parameters: $E_\gamma = 2.62 \text{ MeV}$, $\mu = 0.111 \text{ cm}^{-1}$. (after Wollenberg, 1977a)

4.2.2. Airborne Survey

Airborne measurements differ from the ground work mainly in respect of operational procedures. In general the principles of interpretation are the same in both ground and airborne work. The instrumentation is slightly different. The intensity of radiation from radioactive sources on the ground decreases rapidly with the height of the observation point above the source (Parasnis, 1979). The effect is due partly to geometrical divergence and partly to the absorption and scattering of gamma rays in the air. For this reason instruments of higher sensitivity are needed in an airborne work and flight heights

must be kept relatively low. To increase the sensitivity instruments make use of several crystals coupled in parallel.

4.2.3. Factors Influencing Field Survey

Apart from background radiation, certain factors influence the recorded signal in field surveys. These factors include topographic irregularities, absorption of gamma ray by the earth's material, rainfall and/or snow, temperature inversion and survey speed.

Topographic Irregularities

As mentioned earlier, the intensity of radiation is directly proportional to the solid angle subtended by the detector and the boundaries of the source. Topographic irregularities may lead to the situation where a constant detector-source geometry is not valid throughout the survey. This may thus result in false anomalies being recorded, depending whether the reading is taken on a flat surface, cliff, tunnel or hill-top. Fig 4.2 illustrates some detector-source geometries encountered in surface measurements while Fig 4.3 gives similar illustrations and their effects on airborne survey.

The solid angle defines a 'circle of influence' whose radius increases with the height of the instrument from the source. Thus the recorded signal in an airborne survey, because of its comparatively high altitudes, represents a much larger area than ground survey. This leads to a problem of ground follow up of an airborne survey, particularly for a point source.

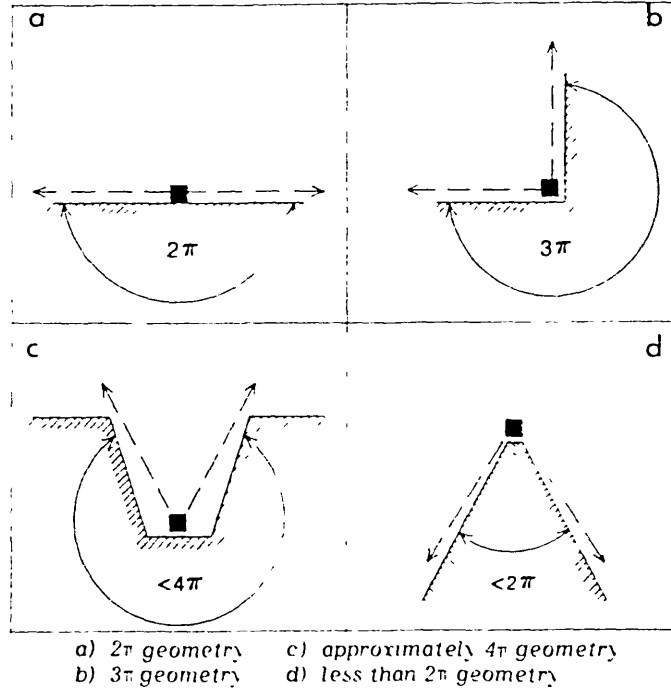


Fig.4:2 : Four different source-detector geometries encountered in surface gamma ray spectrometric measurements in the field. (after Killeen, 1977)

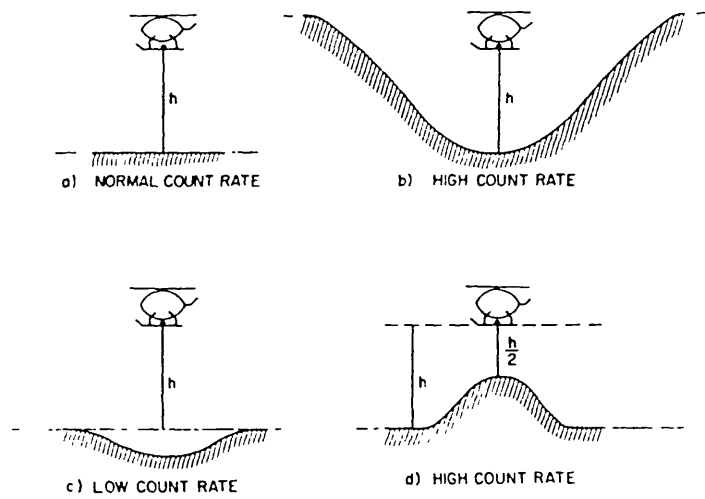


Fig.4.3 : The effect of source geometry and height upon count-rate for airborne gamma ray spectrometric surveys (after Killeen, 1977)

Absorption Of Gamma Ray

The absorption of gamma ray by matter is dependent on the thickness and density of the material, and on the intensity of the gamma ray (see equation 2.3). Because of its limited penetration power, one foot of rock is considered an infinite thick source and additional thickness may not contribute to the detector reading. Also two feet of loose soil may be considered an infinite thick source. In the same way one foot of rock or two feet of loose soil will effectively obscure the radiation from a buried source, no matter how intense the radiation may be. Theoretical curves (Bowie et al, 1955) showing the proportion of gamma radiation from a buried source which would reach the surface through different thicknesses of overburden of various densities are shown in Fig 4.4. These are also the gamma radiation contribution from depths when readings are taken on an outcrop of uniform radioactivity.

Equation 2.3 shows that the amount of absorption of gamma rays depends on the energy level. Thus a potassium-40 source with a primary energy line of 1.46MeV is more readily absorbed and scattered than a gamma ray from a thorium source having an energy of 2.62MeV.

Rainfall And Snow

The effect of rainfall or snow may be twofold. Rainfall can prevent the escape of radon from the ground and thereby increasing the intensity of radiation from the ground. On the other hand, heavy rainfall can drive the radon deeper into the ground, thereby decreasing the radiation from the ground. If rainfall is accompanied

by atmospheric radon and its decay products, there may be a strong

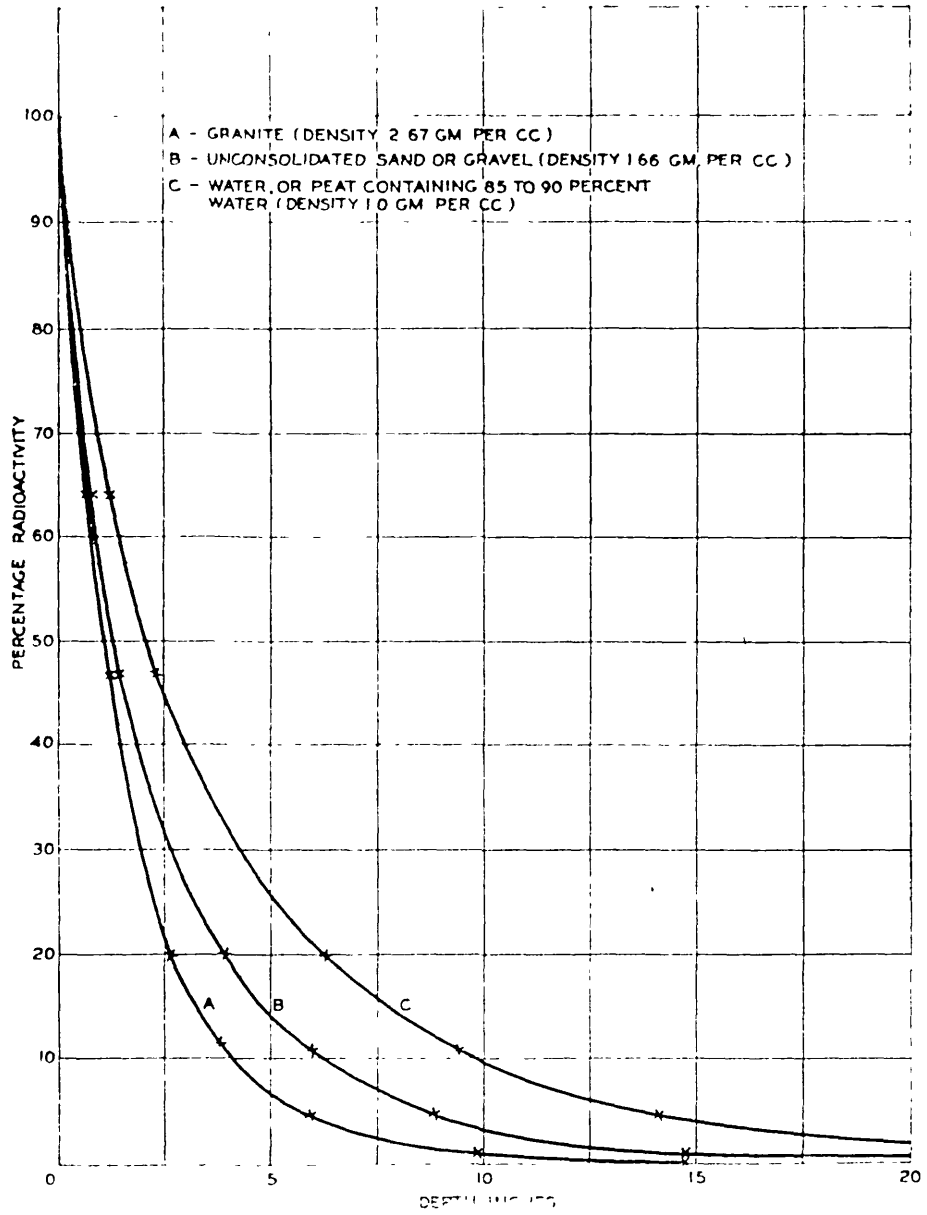


Fig.4.4: Gamma ray absorption curves for overburden material of different densities (after Bowie et al, 1955)

increase in the radiation from the ground. The recovery time after rainfall is about three hours, which corresponds to the decay rates of radon daughter products, lead-214 and bismuth-214.

Effect of snow is similar to that of rainfall. While thin snow tends to increase the gamma emission by trapping radon, thick snow decreases gamma emission by absorbing the radiation.

Temperature Inversion

Normal periods of wind and convection mix radon escaping from the ground thoroughly with the air to form a uniform background. However, temperature inversion produces a blanket of cool air near the ground and this tends to retain radon. Therefore an inversion layer constitutes an inhomogeneity, producing erratic background values. The only solution is to be warned of possible inversion effects either from a meteorological report or a test flight and wait until the inversion has dissipated.

Survey Speed

The confidence that can be attached to any reading is proportional to the square root of the reading (see section 4.4), and obviously the reliability increases as the number of recorded counts increases within safety limits. The choice of the survey speed is determined by the desired accuracy. One way of increasing the number of recorded counts at a given speed is to use large crystal volume. An alternative to this is by flying lower but this is done at the expense of aliasing of short wavelength components (Killeen, et al, 1971).

Also safety limits generally govern terrain clearance. Hence the largest available crystal volume should be used to permit flying at altitudes high enough to minimize the effect of aliasing, while at the same time providing good counting statistics. The volume-velocity relationship thus gives the figure of merit of the system. Darnley(1972) stated that

$$\frac{\text{crystal volume(cu. ins)}}{\text{survey speed(mph)}} \geq 10 \quad (4.1)$$

However, for modern multichannel spectrometric survey, a figure of 20 is preferable (Cowan, personal communication).

4.2.4. Design Parameters For Airborne Survey

The applications of airborne gamma ray spectrometry fall into two main categories : reconnaissance and detailed surveys. Detailed survey is a logical follow-up of the reconnaissance survey. An International Atomic Energy Agency (IAEA) panel (Killeen, 1977) summarized the application of airborne gamma ray spectrometer surveys as follows :

"In practice two rather distinct approaches to airborne gamma ray spectrometry have been developed to meet somewhat different objectives. One method uses a combination of gross-count and a minimal spectral capability to achieve limited objectives. The other utilizes a high sensitivity spectrometric capability to provide a sophisticated multi-parameter geochemical-statistical evaluation. The minimum systems depend on gross-count for rapid regional search for anomalies and rudimentary geological mapping;

spectral measurement of anomalies may identify the primary isotopes, uranium, thorium and potassium. The high-sensitivity spectral method is used for regional and area geochemical-geological mapping and to detect and map variations in lithology and anomalous radioelement ratios. Continuous ratio mapping is used to discover subtle anomalies often not indicated by gamma intensity alone. Sensitive spectrometry is most effectively used to evaluate favourability of broad areas and for preliminary geological mapping".

Thus the first decision to make when planning airborne radiometric survey is the type of survey, viz, whether gross-count or high sensitive spectrometric data be obtained. This decision is however controlled by the desired result and the amount of money available because spectrometric surveys are more expensive than gross-count surveys (Pitkin and Duval, 1980). Other important parameters to consider in designing airborne radiometric survey are line spacing, flight altitudes, detector volume, aircraft speed and sampling time.

Tipper (Killeen, 1977) pointed out that the line spacing commonly 400 to 800 meters, is generally a compromise between cost, the required detail, and the size of the survey area. The size of the radiometric target being sought and the possibility of subsequent more detailed flying must also be taken into account. The ground clearance (flight altitude) should be related to the line spacing and aircraft safety. For detailed survey the aircraft should be flown at a

constant terrain clearance which is as low as possible. However, navigation then becomes more difficult and high quality aerial photography becomes essential for flight path recovery.

Pitkin and Duval (1980) discussed the design parameters for aerial gamma ray surveys and stated that

- (1) the size of the proposed or desired target usually controls the parameters of flight, line spacing and survey altitude. Generally, coarse ($> 3\text{km}$) line spacing is adequate to discover broad, regional anomalies, and for coarsely featured geologic mapping. Fine ($< 3\text{km}$) line spacing is usually needed to detect localized anomalies and to provide aid for detailed geologic mapping. Greater topographic relief in crystalline areas may require a higher flight altitude, while low topographic relief in sedimentary basins may permit a lower flight altitude. However, target detectability or ground resolution (defined as the ability of aerial gamma ray data to differentiate geologic radionuclide concentrations) decreases as the altitude increases (Fig 4.5), and ground coverage (refers to that part of the survey area actually measured by the aerial survey) decreases with decreasing altitude (see Fig 4.6) and decreases with increasing flight line spacing (see Fig 4.7). Also observed count rate decreases as flight altitude increases, because gamma rays are absorbed in air exponentially as the air column increases in

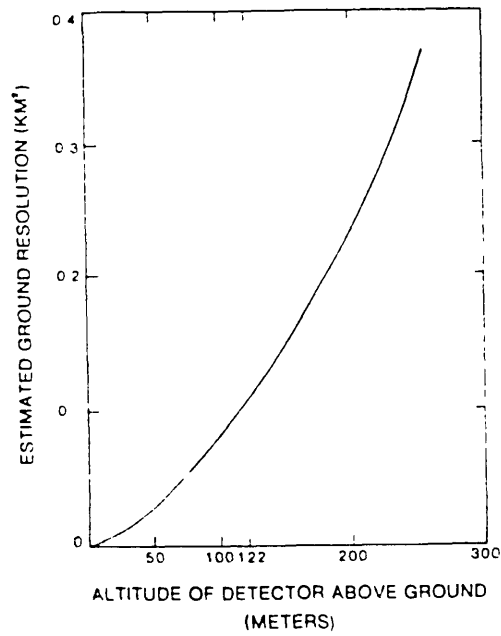


Fig. 4.5: Estimated ground resolution as a function of detector altitude above ground (after Pitkin and Duval, 1980)

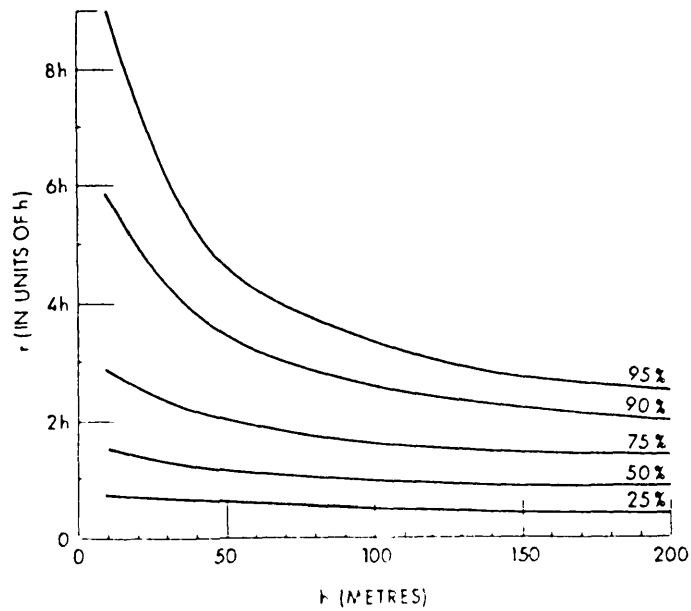


Fig. 4.6: The radius of the circle of investigation versus altitude to percent percentage of infinite source yield (after Duval et al., 1971)

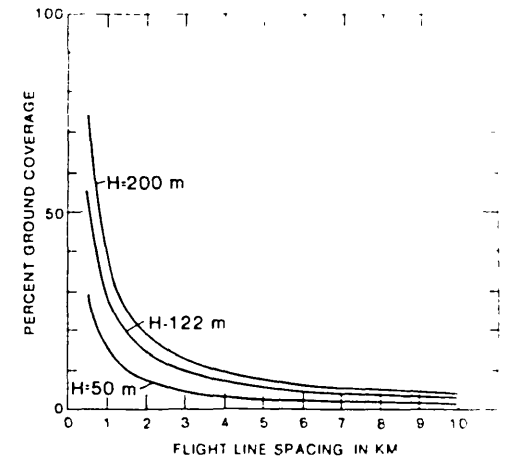


Fig. 4.7: Percent ground coverage as a function of flight line spacing for fixed altitudes (H) above ground level. Data shown are for the 75 percent yield strip (after Pitkin and Duval, 1980)

thickness.

Although quite small targets are resolvable at survey altitudes less than 100 meters, safe operation of the aircraft precludes low altitude design specifications. Thus most aerial surveys are done at a nominal altitude of 122 meters above the ground level. The controlling factors for line spacing are money available, size of survey area, and size of target.

(11) the variation of detector or aircraft velocity and measurement sampling time both affect gamma ray measurement in the same way. For a finite source, the peak yield or maximum detectable count rate is a slowly varying function of both velocity (see Fig 4.8) and sampling time, while the area under the curve decreases rapidly as velocity increases (Fig 4.9) and also as sampling time increases. It can be concluded that an anomaly from a finite source is detectable over a range of velocities, but identification of a specific anomaly could be difficult at the greater velocities. And for an infinite source of uniform intensity, it is shown that the observed count rate has a linear dependence on sampling time and none on velocity. For measurement sampling time, error calculations indicate that the most reasonable range to use is not less than one second and seldom more than three seconds.

(111) the detector volume used controls the quality of data

obtained. The precision of results desired in a given

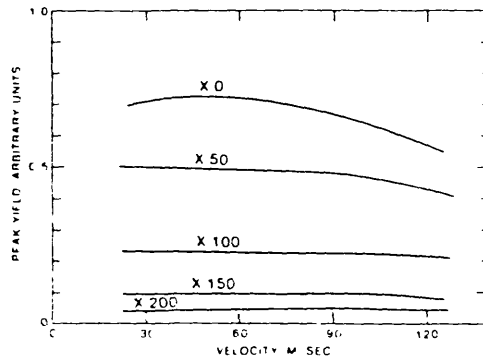


Fig. 4.8: Peak yield of a gamma-ray source as a function of detector velocity for several source positions (X). Source is at ground surface with radius = 30 m intensity = 10 relative to adjacent material X = distance from flight line to center of source in meters. detector flight altitude = 122 m (after Pitkin and Duval, 1980)

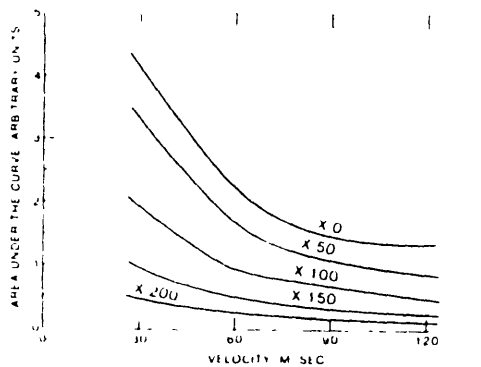


Fig. 4.9: Area under the curve from a gamma-ray source as a function of detector velocity for several source positions (X). Parameters as defined for Fig. 4.8 (after Pitkin and Duval, 1980)

airborne gamma ray survey dictates the detector volume which must be used. The effect of detector volume on precision is shown in Table 4.1, which lists corrected radionuclide count rates and their estimated errors for

Table 4.1: Corrected count rates for K, U_1^a , U_2^b , and Th showing estimated errors for three detector volumes. (Constant ground concentrations are 1.1 percent K, 1.7 ppm eU, and 4.5 ppm eTh. All data normalized to 122-m flight altitude.) (after Pitkin and Duval, 1980)

Detector volume (liters)	K (cps)	K error (percent)	U_1^a (cps)	U_1 error (percent)	U_2^b (cps)	U_2^b error (percent)	Th (cps)	Th error (percent)
54.5	106 ± 20	± 19	28 ± 15	± 54	84 ± 22	± 26	25 ± 8	± 32
27.3	53 ± 13	± 25	14 ± 11	± 79	42 ± 18	± 43	13 ± 5	± 38
13.6	27 ± 9	± 33	7 ± 8	± 114	21 ± 13	± 62	6 ± 4	± 67

^a Assuming only the 1.76-MeV window

^b Assuming summed windows centered at the 1.12- and 1.76-MeV photopeaks

three detector volumes. It can be seen from Table 4.1 that the errors increase as the detector volumes decrease, and they decrease as the concentrations increase. If small detector volumes are used, then count rates should be accumulated for a longer time intervals in order to decrease the statistical errors. However, longer time periods will not increase the signal-to-background ratio.

In order to specify the detector volume, we must be able to predict the count rate per unit volume of the

detector at various flight altitudes. Fig 4.10(a and b) shows the count rates per unit detector volume versus altitude for two high sensitivity spectrometric systems. The data used to construct the curves are background corrected, altitude normalized and for the spectrometric data, corrected for the Compton effect and for an airborne bismuth-214 component.

Killeen et al (1975) stated that the economics of detectors and flying costs must be balanced with the counting statistics, target size and survey parameters; and that the counting statistics for a particular airborne system can be determined by trial flights over areas of known radionuclide content, such as test strips.

4.3. Corrections

The recorded signal in radiometric survey is composed of the radiation from the source being analysed, background radiation, altitude effect and effects due to Compton scattering of gamma rays in the detector crystals. Thus the recorded signal has to be corrected for the effects of the 'unwanted' radiations which include background radiation, altitude and Compton scattering effects. The sequence of correction is as follows (Darnley, 1972):

(i) background correction

(ii) height correction

and/or (iii) Compton scattering correction.

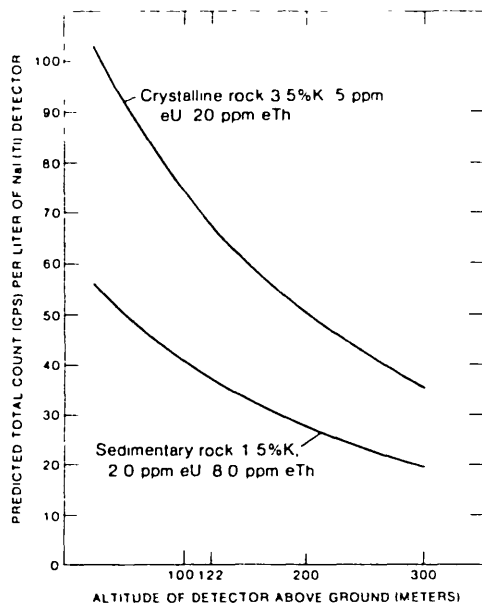


Fig. 4.10a: Predicted total count rate per liter of thallium-activated sodium iodide as a function of detector altitude above ground level for two rock types. Total count window is 0.40 to 2.80 MeV (after Pitkin and Duval, 1980)

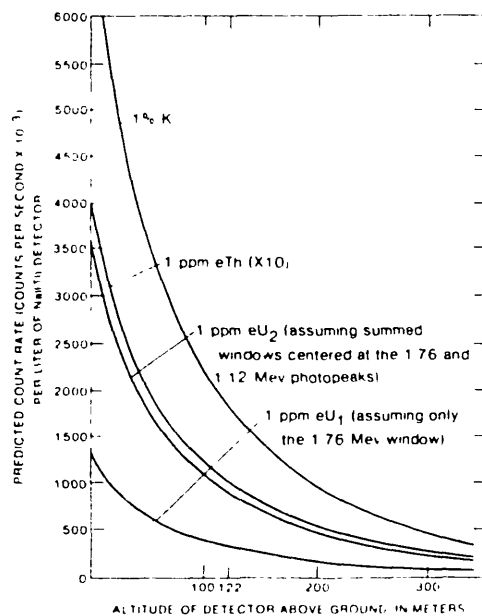


Fig. 4.10b: Predicted count rate per liter of thallium-activated sodium iodide as a function of detector altitude above ground level for specific radioelement concentrations (after Pitkin and Duval, 1980)

4.3.1. Background And Its Correction

The background radiation is any radiation detected by the gamma ray spectrometer but not originating from the source being analyzed. Such radiation include contributions from the system and its surrounding, cosmic rays, radioactivity arising from the daughter product of radon gas and nuclear fallout in the air, potassium-40 and minute quantities of uranium and thorium which are almost always present in rocks (Parasnis, 1979). In the laboratory the detector surrounding refers to the walls, ceiling, floor and the counting chamber or shield; while in the field this refers to the vehicle or aircraft. The background radiation due to the detector system and its surrounding can be minimized if instrument dials or emergency exit signs which are luminized with radium are replaced or removed. Also radium dial wrist watches should not be worn by personnel carrying out surveys and calibration sources should be removed completely or shielded if they must be carried on the survey. If the background is determined during the survey, it is subtracted from the recorded data.

4.3.1.1. Determination Of Background

4.3.1.1.1. Surface Measurement

There are several ways of determining background in surface measurements and these include (Killeen, 1977):

- (a) taking measurement over water in the survey area using a boat or by driving the vehicle onto a bridge (not stone or concrete) over a wide river or onto the ice of a lake.

Since the radioactivity from the underlying rock and water is negligible, this measurement yields background value for the equipment, the vehicle, cosmic rays and the radioactivity in the air. The disadvantage of this method will be mentioned later.

- (b) extrapolating to zero concentration the count rates measured on calibration pads. The pads must be considered to be infinite 2π sources and this will only hold for detectors placed directly on the pad near the centre.

4.3.1.1.2. Airborne Measurement

The radioactivity of the aircraft and its equipment caused by the presence of small quantities of natural radioactive nuclides in the airframe and detector system, is considered constant. The cosmic ray contribution caused by photons generated by cosmic ray interactions with nuclei present in the air, aircraft or in the detection system, increases with aircraft altitude and also varies with the size of the aircraft (Grasty, 1977a). The radon contribution is the largest and most difficult to determine (Burson, 1974). Radon being a gas, can diffuse out of the ground. The rate of diffusion will depend on such factors as temperature, wind, air pressure, soil moisture and ground cover. The radon decay products, lead-214 and bismuth-214, are present as positive ions attached to airborne dust particles and hence their distribution and concentration are strongly influenced by wind patterns. Temperature inversion also creates problems in measuring

the radon background contribution. As explained earlier (see section 4.2.3.), this results in erratic radon background values. It has been reported (Grasty, 1977a) that greater proportion of the photons detected in the uranium window arises from radon daughters occurring in the air. Thus an accurate determination of the atmospheric radiation is of great importance in locating possible uranium targets.

Some of the techniques used to determine background radiation include:

- (i) flights over large volume of water at survey altitude
- (ii) using upward looking crystals, and
- (iii) flight at high altitude of more than 6000 meters above ground level (Pitkin and Duval, 1980). Generally this measurement should be made above radon cloud.

(1) Over Water Background

This method is to establish background values over a large volume of water in the survey area at a given survey flight altitude. Since the concentrations of radioactive nuclides in water are several orders of magnitude lower than that of normal crustal material, the activity measured will be the total background contribution due to the aircraft and its equipment, cosmic rays and atmospheric radiation due to radon. Here it is assumed that the contribution from the water is negligible and that airborne radioactivity over water is at least representative of that over the land survey area. However, the radon contribution varies considerably with time and distance (Burson, 1974) and Geodata

(1979) also explained that it increases significantly as the aircraft flew from water to land at a given altitude, thus illustrating the limitation of the method. Another disadvantage of this method is that background values have to be measured several times during the survey, and one has to use linear interpolation on time base to interpolate between successive measurements.

When large lakes are not available in the survey area, the following methods provide alternatives.

(ii) Upward Looking Crystal

This involves flying a detector system consisting of shielded (2π) and unshielded (4π) detectors over an inland lake and the survey area. The use of this method requires the determination of each of the three background components, aircraft and equipment background, cosmic ray background, and atmospheric (radon) background.

Aircraft (and equipment) and Cosmic Background

These contributions are determined by flying at very high altitudes over water (Geometrics, 1979). Radon radiation is assumed to be negligible at these heights. Thus the count rate may be expressed by

$$C = I_I + I_C \quad (4.2)$$

where

I_I is the aircraft and equipment radiation, and

I_C is the cosmic radiation.

Since I_I is constant, the difference between any two spectra at different altitudes sufficiently separated, typically 2000 feet (Geometrics, 1979), gives the cosmic spectral curve shape (see Fig 4.11). The cosmic spectral shape does not change appreciably with altitude (Burson, 1974). The cosmic ray contribution to energy band is found by correlating the selected energy band count rates to those from an energy band from 3 - 6MeV whose response is due entirely to cosmic radiation (Burson, 1974). Thus in order to calculate the aircraft background and the cosmic ray background for each channel/window, equation 4.2. can be modified as follows:

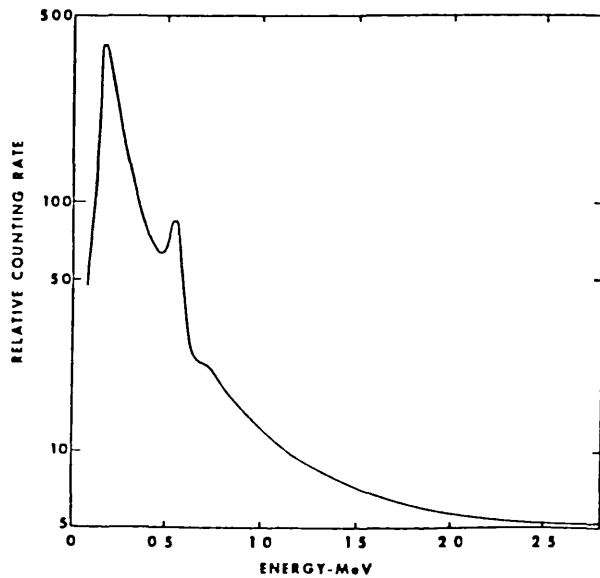


Fig.4.11: Shape of cosmic spectral curve (after Burson, 1974)

$$C_i = I_{Ii} + a_i I_{\text{cos}} \quad (4.3)$$

where

C_i is the count rate in window 1

I_{Ii} is the aircraft background count rate in window 1

a_i is the cosmic stripping coefficient (shape) in window 1, and

I_{cos} is the cosmic count rate in energy band 3 - 6MeV.

It can be seen from equation 4.3 that at least flights at two different altitudes are needed in order to determine the aircraft background and the cosmic spectral shape. It will however, be better to use multi-elevations and least squares' solution. Once the aircraft background and cosmic spectral shape have been determined, they can then be used at survey altitudes since they are independent of height. The cosmic background at survey altitude during the survey can then be determined by monitoring counts in the 3 - 6MeV energy band.

Atmospheric Background

The count rates in the unshielded (4π) and shielded (2π) detectors in the survey area can be expressed as

$$C_{4} = I_G + I_A + I_{I4} + I_{C4} \quad (4.4)$$

and

$$C_2 = kI_G + pI_A + I_{I2} + I_{C2} \quad (4.5)$$

where

C_4 is the count rate in the unshielded detector

C_2 is the count rate in the shielded detector

I_G is the radioactivity from the ground (source)

I_A is the radioactivity from the atmosphere

I_I and I_C are as defined above; and, k and p are constants introduced by the shield in the detector.

k is the amount of the ground signal getting through to the shielded detector, and

p is the response of the shielded detector to the atmospheric signal.

Solving equations 4.4 and 4.5 for I_G and I_A gives

$$I_G = \left\{ p(C_4 - I_{I4} - I_{C4}) - (C_2 - I_{I2} - I_{C2}) \right\} / (p - k)$$

and

(4.6)

$$I_A = \left\{ (C_2 - I_{I2} - I_{C2}) - k(C_4 - I_{I4} - I_{C4}) \right\} / (p - k)$$

The I_I 's and I_C 's are determined as stated above, k and p are determined by flying at a given survey altitude over an inland lake. Since $I_G = 0$ over water, the corresponding count rates in the unshielded and shielded detectors are given by

$$C_{4W} = I_A + I_{I4} + I_{C4} \quad (4.7)$$

and

$$C_{2W} = pI_A + I_{I2} + I_{C2} \quad (4.8)$$

where

C_{4W} is the count rate in the 4π detector over water

C_{2W} is the count rate in the 2π detector over water

and I_A , I_I 's, I_C 's and p are as defined above.

Subtracting equation 4.7 from equation 4.4, and equation 4.8 from equation 4.5 give

$$I_G = C_{4\pi} - C_{4\pi}W$$

and

$$kI_G = C_2 - C_2W$$

Therefore

$$k = \frac{C_2 - C_2W}{C_{4\pi} - C_{4\pi}W} \quad (4.9)$$

Also from equations 4.7 and 4.8,

$$I_A = C_{4\pi}W - I_{I4} - I_{C4}$$

and

$$pI_A = C_2W - I_{I2} - I_{C2}$$

Hence

$$p = \frac{C_2W - I_{I2} - I_{C2}}{C_{4\pi}W - I_{I4} - I_{C4}} \quad (4.10)$$

Having established the values for the aircraft background, cosmic background, k and p , I_G and I_A can be calculated from subsequent flights in the survey area by using equation 4.6. It should be noted that the atmospheric background also contains effects caused by the scattering of thorium gamma rays into the shielded crystal (feed through effect) and this can be corrected by subtracting counts from the 2π total sum count rates based on the corrected thorium count rates determined from the 4π data (Geodata, 1979).

Although this method has the advantage of measuring background

continuously during the survey, its complexity and cost are limiting factors to its use. The shielded detectors require extra space, weight and cost.

An alternative common method of determining the atmospheric background is the use of air filter systems to sample the air during the survey (Burson, 1974). He stated that reasonable estimates of the radon concentrations in the air can be made from the beta or gamma activity of the dust collected on the filter papers.

Also Grasty (1982a) showed that the atmospheric background can be determined by monitoring the count rate in the lead-214 peak at 0.352MeV. He showed a linear correlation between the count rate in the lead-214 peak area and the standard uranium window at 1.76MeV (see Fig 4.12). This relationship can be used to calculate the atmospheric

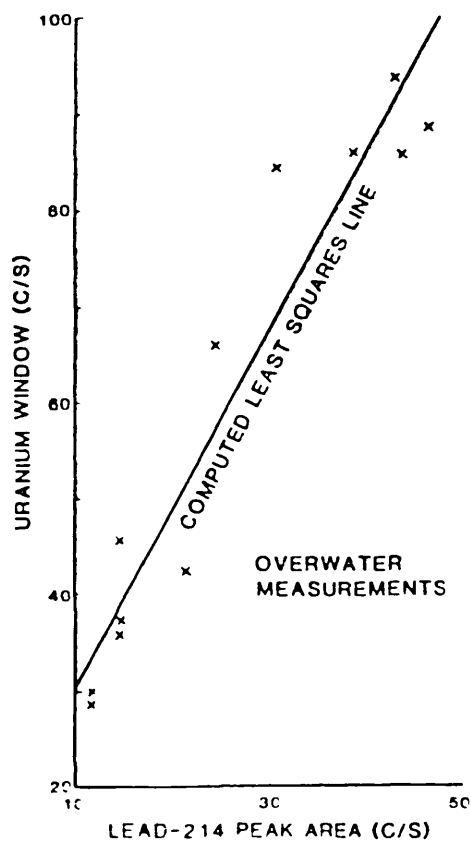


Fig.4.12: Correlation of the uranium window with the lead-214 peak area for overwater backgrounds (after Grasty, 1982a)

background from the lead-214 peak area counts.

(iii) High Altitude

This involves flying at very high altitude, generally at about 800 meters. At this height virtually all the terrestrial (ground) radiation has been absorbed by the atmosphere. The disadvantage of this method is that cosmic radiation increases with height and so at the survey altitude, the cosmic and radon backgrounds may be completely different.

4.3.2. Compton Scattering Correction

High energy photons which are incompletely absorbed in a detector due to its finite size appear as counts in a lower energy window. For instance the counts in the potassium window may be due to potassium photon at 1.46MeV, plus scattered high energy photons of the uranium and thorium decay series at 1.76MeV and 2.62MeV respectively. The same may be true of the uranium and thorium windows. Provided the potassium, uranium and thorium spectrum readings in the detector remain the same, a constant fraction of the counts in the higher energy windows will appear in the lower energy windows. These factors, known as the Compton scattering coefficients or stripping ratios, will be peculiar to each detector system. There are also reverse stripping ratios which may be due to the poor resolution of the detection systems and effect of sum peaks. Fig 4.13 gives a schematic representation of the interplay between the three radioelement windows, potassium, uranium and thorium, and identifying

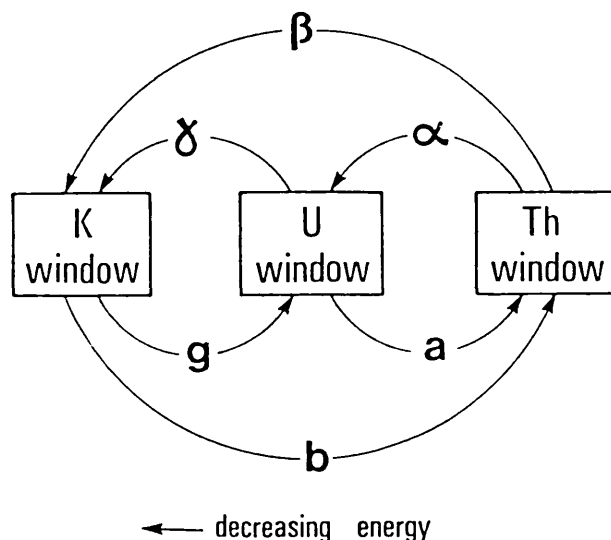


Fig.4.13: Schematic representation of the interaction between the K, U, and Th energy windows indicates the stripping factors which are used to remove the interference denoted by the arrows. Commonly used stripping factors are α , β , and γ . The 'upward' stripping factors a , b , and g are generally small or zero and are often ignored. (after Killeen, 1977)

the stripping ratios. The stripping ratios must therefore be determined before any measurement of elemental abundance can be attempted.

The Compton scattering corrections therefore account for the scatter of one photoelement into the peak of another photoelement. The stripping ratios necessary to remove this effect are determined during the calibration of the measuring instrument (see section 4.5).

The equations relating the corrected count rate in each window to the uncorrected values are given as follows:

$$\begin{aligned}T_U &= T_C + aU_C + bK_C + B_T \\U_U &= U_C + \alpha T_C + gK_C + B_U \\K_U &= K_C + \beta T_C + \gamma U_C + B_K\end{aligned}\tag{4.11}$$

where

T_U, U_U, K_U are the uncorrected count rates,

T_C, U_C, K_C are the corrected count rates,

B_T, B_U, B_K are the background count rates in the thorium, uranium and potassium windows respectively,

α are the counts in the uranium window due to thorium,

β are the counts in the potassium window due to thorium,

γ are the counts in the potassium window due to uranium,

a are the counts in the thorium window due to uranium,

b are the counts in the thorium window due to potassium,

and

g are the counts in the uranium window due to potassium

Generally the background count rates in the windows are known from background measurements (see section 4.3.1). The stripping ratios have been shown to vary with survey altitude (Grasty, 1976, 1982a; Lovborg et al, 1976). Thus flights at several altitudes over the test strip are necessary in order to establish their altitude dependence.

4.3.3. Height Correction

In the field some terrain clearance dependence is always present in data due to geological control. Outcrop may be better on hill tops, providing higher count rates, while valleys may contain alluvium with

low count rates (see Figs 4.2 and 4.3). Thus corrections have to be made to the detector count rates depending on the height of the instrument above the ground. The effect of this correction is to remove the highs and lows caused directly by the variation in ground clearance and smoothen the data. In an airborne measurement, because of the difficulty in maintaining constant terrain clearance, the data are reduced to a mean height and so the deviation of the flight altitude from this mean height has to be corrected for. This can be done using exponential attenuation of gamma ray with height. The method is based on a uniform half space and ignores the effects of varying source geometries.

The detector count rate over a homogeneous ground at an altitude H is given by (Grasty, 1976)

$$N_H = N_0 e^{-\mu H} \quad (4.12)$$

where

N_0 is the count rate at ground level, and

μ is the linear absorption coefficient of gamma rays in air at the energy considered. μ is proportional to the air density.

Thus if H_0 is the mean height to which all readings should be corrected, then the count rate at H_0 is given by

$$N_{H_0} = N_0 e^{-\mu H_0} \quad (4.13)$$

Dividing equation 4.13 by equation 4.12 gives

$$\frac{N_{H_0}}{N_H} = e^{\mu(H - H_0)} = F \quad (4.14)$$

F is called a correction factor. Thus all readings can be normalized (or corrected) to the mean flight height H_0 by using the following equation:

$$N_{H_0} = N_H F \quad (4.15)$$

Fig 4.14 shows the correction factors for both negative and positive ΔH ($\Delta H = H - H_0$). If H_0 is a pre-determined height at standard temperature and pressure (0°C and 760mm of mercury), then H will be given by

$$H = \frac{273 \times P \times H_F}{760 \times T} \quad (4.16)$$

where

H is the effective flying height at 0°C and 760mm of mercury

H_F is the recorded flying height

P is the measured atmospheric pressure, and

T is the measured atmospheric temperature

The effect of this correction is shown on Fig 4.15. The sharp peak at the point marked P of the uncompensated profile (A) is caused by the aircraft flying below the survey altitude of 500 feet (C) as it crossed a sharp topographic high (D). The correct radioactivity level

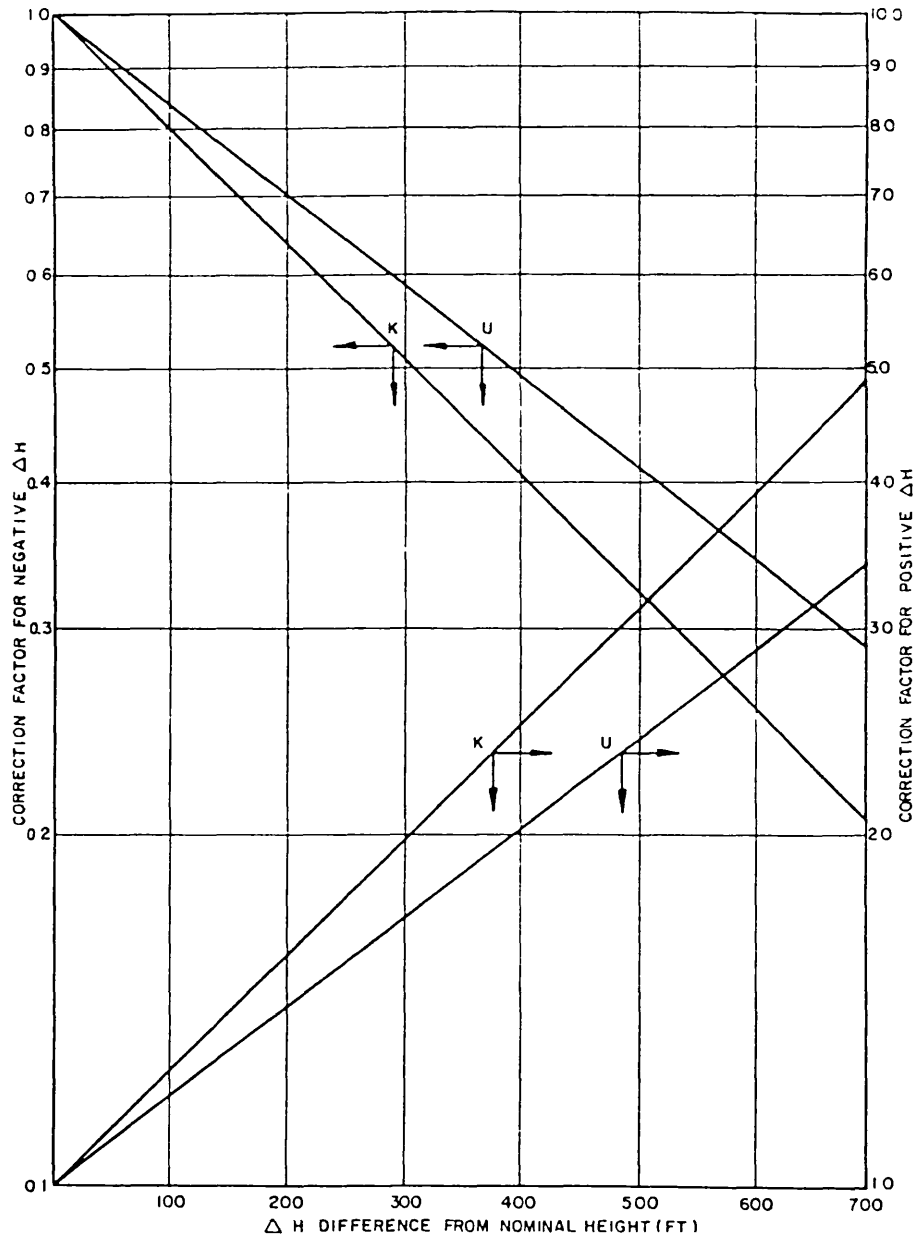


Fig.4.14: Height correction factors

(after Darnley et al, 1968)

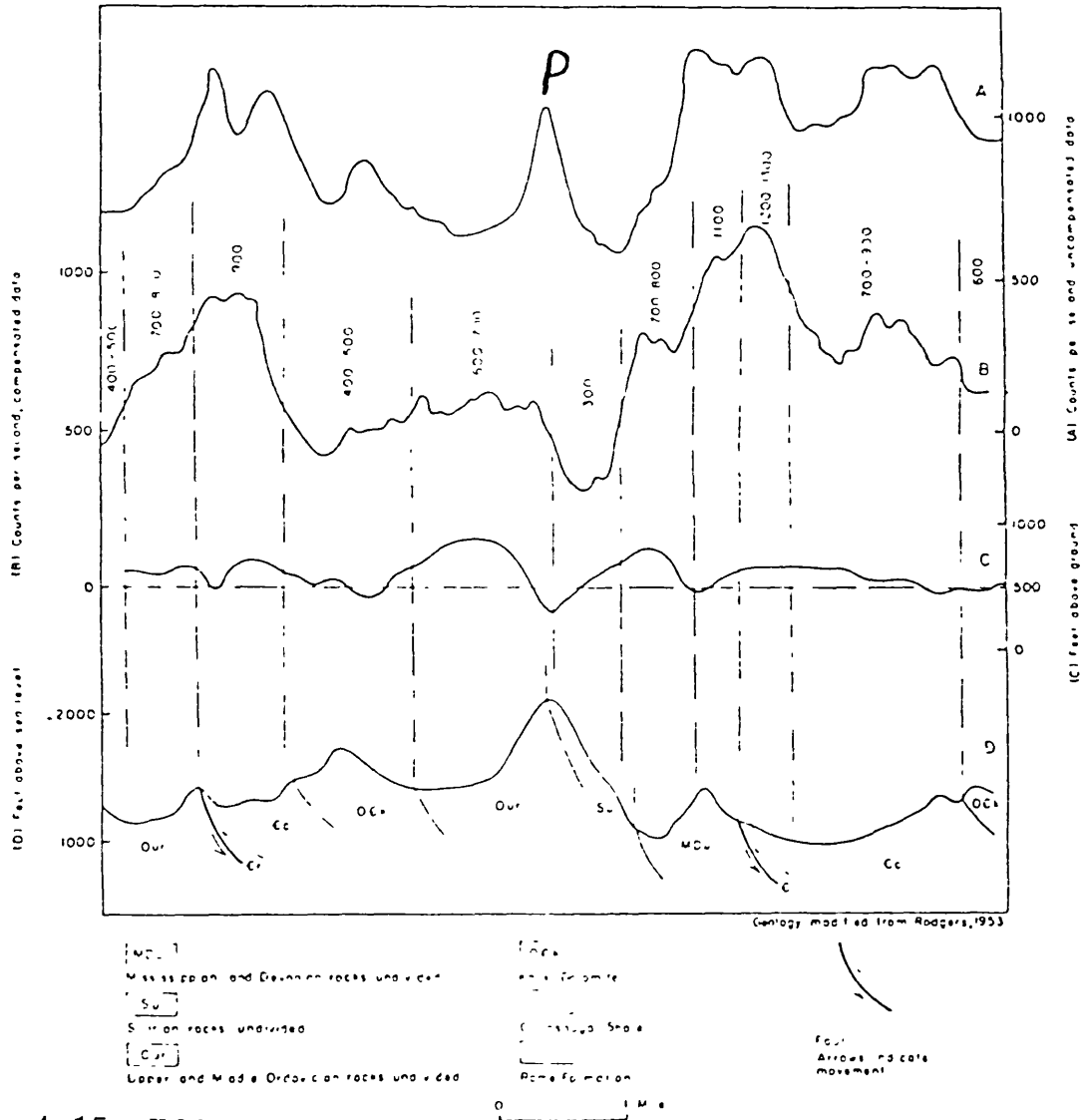


Fig.4.15: Effect of altitude

The amount of spurious signal in precipitation (uncompensated data) by variations in the altitude of the air (C) can be obtained by comparison of the uncompensated data (A) with the compensated data (B). (after Bates, 1966)

of the formation exposed on the topographic high is given by the compensated profile (B). The generally higher level of the uncompensated data (A) is due to the fact that it contains cosmic background which has been removed from the compensated data (B) (Bates, 1966).

Determination Of The Absorption Coefficients

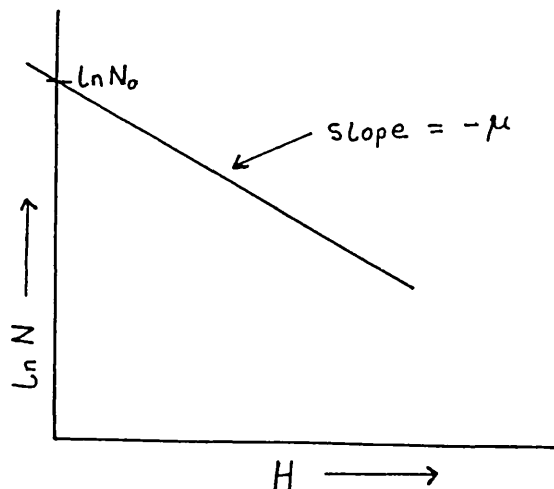
We recall that the count rate over a homogeneous ground at an altitude H is given by

$$N = N_0 e^{-\mu H} \quad (4.12)$$

Taking the Logarithm (natural) of both sides gives

$$\ln N = -\mu H + \ln N_0 \quad (4.17)$$

Thus the graph of $\ln N$ against H will result in a straight line with negative slope, $-\mu$, and intercept, $\ln N_0$, as illustrated below. Hence



the absorption coefficient for potassium, uranium and thorium can be determined by plotting the respective values of count rate in the respective windows against the flight heights. It is recommended (Killeen, 1977) that at least five flights at different altitudes should be used to derive the absorption coefficients and that these flights should span the normal survey altitudes (50 - 300 meters).

It should be noted that the count rates used in equation 4.12 are background corrected. Also the count rates should be stripped before determining the absorption coefficient; except where the stripping ratios are calculated after the data are altitude corrected.

4.4. Survey Statistics

In an experiment it is necessary to report the results of any measurement and also the accuracy with which they were made.

Gamma ray emissions from a source are random events occurring in a large number of nuclei. Thus the measurements of radioactive decay are subject to the random fluctuations inherent in the decay process. These measurements are counting processes since the data collected are merely the number of events occurring in a fixed time interval. This process can be described by Poisson distribution and hence the counting error can be expressed as standard deviation σ given by

$$\sigma = \sqrt{X} \quad (4.18)$$

where

X is the number of counts in a fixed time interval.

4.4.1. Propagation Of Errors

Radiometric (nuclear) data are often processed through subtraction, addition, division, multiplication or other functional manipulations to arrive at a desired number of interest. Since the standard deviation cannot be associated with the square root of any quantity which is not a directly measured number of counts, we must therefore be concerned with how the errors associated with the original number of counts propagate through these calculations. This problem can be mathematically stated as wanting to find the error σ_Y in a random variable Y, where Y is again a function of other random variables. That is

$$Y = f(X_1, X_2, X_3, \dots, X_N) \quad (4.19)$$

where the X's and their associated errors σ_X 's are known.

According to Eichholz and Poston (1979), this problem is very involved, but a relatively simple result can be obtained under the following conditions:

- (1) the various data X_i , $i = 1, 2, 3, \dots, N$, are measured independently; and
- (11) the distributions of the errors in X are unbiased normal distributions.

If both conditions are satisfied then one can assert that

- (a) the best estimate of the mean of Y is the function Y

evaluated at the means of the random variables X_i , $i = 1, 2, 3, \dots, N$; that is

$$\mu_Y = f(\bar{X}_1, \bar{X}_2, \bar{X}_3, \dots, \bar{X}_N) \quad (4.20)$$

and

(b) the variance of Y is given by the expression

$$\sigma_Y^2 = \sum_{i=1}^N \left(\frac{\partial Y}{\partial X_i} \right)^2 \sigma_{X_i}^2 \quad (4.21)$$

where the partial derivatives are evaluated at the means of the variables X_i , and $\sigma_{X_i}^2$ is the variance of X_i .

Equation 4.21 is often referred to as 'error propagation' formula.

4.4.1.1. Application Of Error Propagation Formula In Radiometrics

(1) Addition Or Subtraction Of Counts

$$\text{Let } Y = X_1 + X_2$$

$$\text{or } Y = X_1 - X_2$$

Applying equation 4.21 gives the error in Y as

$$\sigma_Y^2 = \sigma_{X_1}^2 + \sigma_{X_2}^2$$

and from equation 4.18,

$$\sigma_Y = \sqrt{\sigma_{X_1}^2 + \sigma_{X_2}^2} \quad (4.22)$$

This is applicable when subtracting background counts from the source plus background counts to get the net counts due to the source only.

(ii) Multiplication Or Division By A Constant

If $Y = AX$, where A is a constant,

then equation 4.21 gives

$$\sigma_Y = A \sigma_X \quad (4.23a)$$

Similarly, if

$Y = X/B$, where B is a constant, then

$$\sigma_Y = \sigma_X/B \quad (4.23b)$$

An example of the application of equation 4.23b is the calculation of count rates. If X counts are recorded over a time t , then the count rate R is given by

$$R = X/t$$

It is usually assumed that the time t is measured with very small or no error; so that t is considered a constant. Then the error in the count rate is given by σ_R as

$$\sigma_R = \sigma_X/t = \sqrt{X}/t \quad (4.24)$$

(iii) Multiplication Or Division Of Counts

If $Y = X_1 \cdot X_2$

$$\text{then } \sigma_Y^2 = X_2^2 \sigma_{X_1}^2 + X_1^2 \sigma_{X_2}^2$$

Dividing both sides by Y^2 gives

$$\left(\frac{\sigma_Y}{Y}\right)^2 = \left(\frac{\sigma_{X_1}}{X_1}\right)^2 + \left(\frac{\sigma_{X_2}}{X_2}\right)^2 \quad (4.25a)$$

Similarly, if $Y = X_1/X_2$

then

$$\left(\frac{\sigma_Y}{Y}\right)^2 = \left(\frac{\sigma_{X_1}}{X_1}\right)^2 + \left(\frac{\sigma_{X_2}}{X_2}\right)^2 \quad (4.25b)$$

(iv) Mean Value Of Multiple Independent Counts

Consider N repeated counts, $X_1, X_2, X_3, \dots, X_N$, from the same source for equal counting times. The sum of the counts is given by

$$S_N = \sum_{i=1}^N X_i$$

By equation 4.21, the error in S_N is given by

$$\sigma_{S_N}^2 = \sigma_{X_1}^2 + \sigma_{X_2}^2 + \sigma_{X_3}^2 + \dots + \sigma_{X_N}^2$$

and by equation 4.18

$$\sigma_{S_N}^2 = X_1 + X_2 + X_3 + \dots + X_N = S_N \quad (4.26)$$

Equation 4.26 shows that the standard deviation for the sum of the counts is the same as if the measurement had been carried out by performing a single count extending over the entire period represented by all the independent counts.

The mean value for the N independent measurements is

$$\bar{X} = S_N/N$$

From equation 4.24 the error in \bar{X} is given by

$$\sigma_{\bar{X}} = \sigma_{S_N}/N = \sqrt{S_N}/N = \sqrt{\bar{X}/N} \quad (4.27)$$

But the standard deviation of any single measurement X_i is

$$\sigma_{X_i} = \sqrt{X_i} \quad (4.18)$$

Because any typical count will not differ from the mean, $X_i = \bar{X}$. Therefore the mean value based on the N independent counts will have an error which is smaller by a factor of \sqrt{N} compared with any single measurement on which the mean is based.

If the associated precision of the N independent measurements of the same quantity is not nearly the same, then a simple average is no longer the optimal way to calculate a single 'best value'. Instead more weight will be given to those measurements with small values for the standard deviation associated with X_i and less weight to those with large errors.

Let the weighting factor for each X_i be a_i . Then the best value X_B is calculated from the linear combination

$$X_B = \frac{\sum_{i=1}^N a_i X_i}{\sum_{i=1}^N a_i} \quad (4.28)$$

Criterion For Choosing a_i In Order To Minimize The Error In X :

$$\text{Let } \alpha = \sum_{i=1}^N a_i$$

Then equation 4.28 becomes

$$X_B = \sum_{i=1}^N a_i X_i / \alpha \quad (4.28a)$$

From equation 4.2i the error in X_B is given by

$$\begin{aligned} \sigma_{X_B}^2 &= \sum_{i=1}^N \left(\frac{\partial X_B}{\partial X_i} \right)^2 \sigma_{X_i}^2 \\ &= \sum_{i=1}^N (a_i / \alpha)^2 \sigma_{X_i}^2 \\ &= 1/\alpha^2 \left(\sum_{i=1}^N a_i^2 \sigma_{X_i}^2 \right) \\ &= \beta / \alpha^2 \end{aligned} \quad (4.29)$$

where $\beta = \sum_{i=1}^N a_i^2 \sigma_{X_i}^2$ (4.30)

$\sigma_{X_B}^2$ would be minimized with respect to the a_j 's. Thus differentiating equation 4.29 with respect to a typical a_j and setting the result to zero gives

$$\frac{\alpha^2 \frac{\partial \beta}{\partial a_j} - 2\alpha\beta \frac{\partial \alpha}{\partial a_j}}{\alpha^4} = 0 \quad (4.31)$$

But $\frac{\partial \alpha}{\partial a_j} = 1$ and $\frac{\partial \beta}{\partial a_j} = 2 a_j \sigma_{X_j}^2$

Hence equation 4.31 becomes

$$\frac{1}{\alpha^4} (2\alpha^2 a_j \sigma_{X_j}^2 - 2\alpha\beta) = 0$$

Therefore

$$a_j = \beta / \alpha \cdot 1 / \sigma_{X_j}^2 \quad (4.32)$$

If the weighting factors are normalized, then

$$\alpha = \sum_{i=1}^N a_i = 1 \quad (4.33)$$

and equation 4.32 becomes

$$a_i = \beta / \sigma_{X_i}^2 \quad (4.34)$$

From equations 4.34 and 4.30,

$$\beta = \sum_{i=1}^N a_i^2 \sigma_{X_i}^2 = \sum_{i=1}^N \left(\beta / \sigma_{X_i}^2 \right)^2 \sigma_{X_i}^2$$

Therefore

$$\beta = \left[\sum_{i=1}^N 1 / \sigma_{X_i}^2 \right]^{-1} \quad (4.35)$$

From equations 4.35 and 4.34,

$$a_j = 1 / \sigma_{X_j}^2 \left[\sum_{i=1}^N 1 / \sigma_{X_i}^2 \right]^{-1} \quad (4.36)$$

Equation 4.36 shows that each data point should be weighted inversely as the square of its own error.

From equations 4.33, 4.29 and 4.35, the error in X_B is given by

$$\frac{1}{\sigma_{X_B}^2} = \sum_{i=1}^N \frac{1}{\sigma_{X_i}^2} \quad (4.37)$$

Thus the standard deviation σ_{X_B} can be calculated from the standard deviations σ_{X_i} associated with each individual measurement.

Since the standard deviation is a function of the counts, it can

be improved by

- (a) increasing the counting time
- (b) increasing the detector size, or
- (c) moving the detector closer to the source

These three alternatives are relatively easy to accomplish in a laboratory, but in the field, changing these parameters could have various effects.

(a) Increasing The Counting Time

For a portable (or man-carried) gamma ray spectrometer this reduces the number of readings that can be made each day. In a mobile (carborne or airborne) survey, increasing the counting time means that each measurement is taken over a longer distance, and therefore each reading is a larger representative of rock. This smoothing effect may not be acceptable and so the vehicle speed may have to be reduced by a direct ratio to the increase in sample time. In the case of an airborne survey, this could reduce the aircraft speed to the point where the selection of a rotary wing aircraft is required, thus increasing the cost.

(b) Increasing The Detector Size

Increasing the detector size of an airborne package may require a larger and consequently more costly type of aircraft. For a portable or carborne survey, this may be an economical solution.

(c) Moving The Detector Closer To The Source

This may be impossible in the case of a carborne survey, and it may involve flying at unsafe altitudes for airborne surveys. Moving the detector closer to the source will also decrease the sample volume (see Fig 4.6) appreciably and it may be necessary to make more closely spaced measurements for the same ground coverage. This represents an increase in costs.

4.5. Calibration Of Measuring System

For any physical measurement to be meaningful, the measuring device must be calibrated with respect to some reference standards. In radiometrics, two calibrations are necessary. These are:

(i) Energy Calibration

This is done in order to find out how the energies spent by the photons in the detector are related to the channel numbers in the case of the multichannel analyzer.

(ii) Sensitivity Determination

This is done in order to relate the detected radioactivity to the radioelement concentration in the source of the radiation; that is, to determine the sensitivity of the measuring device in terms of counts per unit time interval.

The calibration of spectrometers depends on some known, primary reference standards. Secondary standards are then derived from the primary reference standards. Fig 4.16 shows the connection between

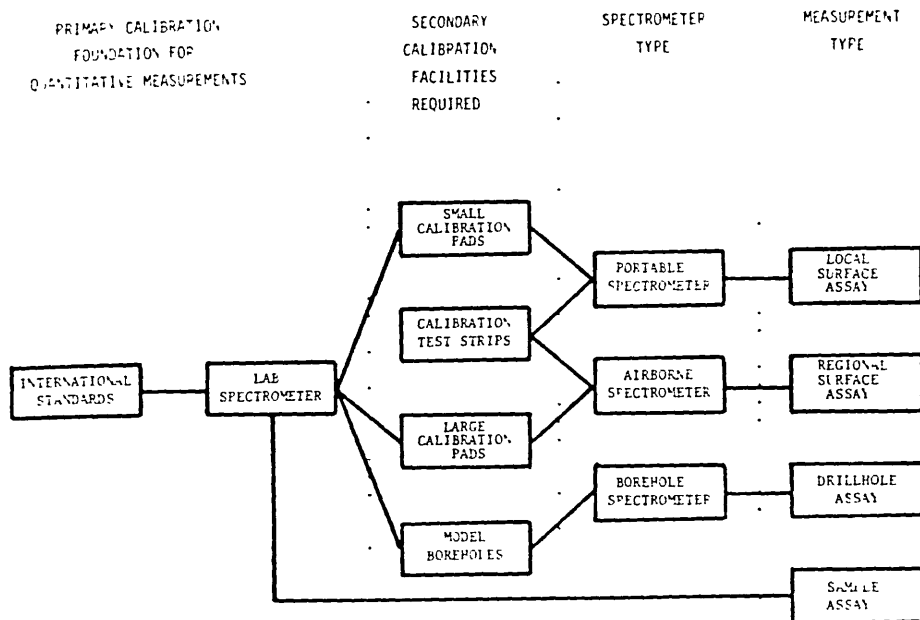


Fig. 4.16: The relationship between primary and secondary calibration facilities for various types of gamma ray spectrometer. International standard samples are used to calibrate lab spectrometers. These in turn analyze calibration pads and model boreholes which can then be used as secondary calibration facilities for field spectrometers. The calibrated field spectrometers can then carry out assays in situ. (after Killeen, 1977)

primary and secondary calibration facilities. The type of spectrometers and relationships of their measurements to the different secondary calibration facilities are also indicated (Killeen, 1977).

It should be noted that an instrument once calibrated is not

calibrated forever, as its characteristics may change with time and it should be re-calibrated periodically. The user should have information about the normal values of the calibration factors for a given instrument. Any changes upon calibration would probably indicate (Killeen, 1977) one of the following:

- (1) a malfunction in the spectrometer
- (ii) an error in recording the counts
- (iii) the counting time was too short to provide good counting statistics
- (iv) an error in entering the data into the computer
- (v) calibration just after a rainfall when all the radon daughters in the air are washed out, increasing background on the pads (standard sources)
- (vi) drifting of energy windows due to changes in temperature of the detector during calibration
- (vii) improper setting of the window locations or window widths
- (viii) low energy power
- (ix) cracked crystal in the detector package, and
- (x) improper energy calibration

Thus calibration, in addition to permitting quantitative measurements, also maintains a check on the performance of the system. It also affords means of standardizing radiometric measurements (Grasty, 1977).

4.5.1. Energy Calibration

In order to measure the energy associated with a spectral peak, the spectrum has to be calibrated against known radiation energies. This means that the proportionality constant between pulse height (or channel number) and energy must be determined. In a properly devised instrument the relationship is roughly linear.

The energy calibration is usually performed by analyzing sources emitting photons of known energy. The following Table 4.2 (Adams and Gasparini, 1970) shows some of the most commonly used sources.

The channel number where the full energy peaks occur are plotted against the energy spent by the photons in the detector. It should be remembered that the pulse height versus energy relationship is only dependent on the internal characteristics of the spectrometer and not the geometry conditions. The pulse height versus energy curve is not constant with time, but exhibits a more or less pronounced instrumental drift. This drift can consist either of a parallel displacement (zero intercept drift) and/or a variation of the slope (slope drift). This can be due to inadequate stabilization of the electronic components and to temperature changes. Where long counts are carried out, as in laboratory analysis, measurable gain drifts have the effects of broadening and lowering all full energy peaks, and smoothening out the Compton continuum. These effects can cause serious errors in the background subtraction and analysis of spectra (see section 4.3.1) particularly where simple techniques using a preset number of channels are applied. However, a combination of high stability electronic components with a temperature stabilized room can

<i>Isotope</i>	<i>Half-life</i>	<i>Gamma-ray energy (keV)</i>
¹⁰⁹ Cd	458 days	25 0 (±0 1)
		87 7 (±0 2)
⁵⁷ Co	270 days	121 97 (±0 05)
		136 33 (±0 04)
²⁰⁷ Bi	30 yr	569 63 (±0 08)
		1063 58 (±0 06)
^{110m} Ag	253 days	1769 71 (±0 13)
		657 61 (±0 15)
		677 36 (±0 20)
		686 80 (±0.25)
		706 28 (±0 25)
		743 99 (±0 25)
		763 77 (±0.22)
		817 87 (±0 30)
		884 46 (±0 25)
		937 2 (±0 3)
		1383 8 (±0 4)
¹³⁷ Cs	30 0 yr	1475.5 (±0 4)
		1504 6 (±0 5)
⁵⁴ Mn	303 days	1561 8 (±0 4)
		661 595 (±0 076)
⁶⁵ Zn	245 days	834 85 (±0 10)
		1115 44 (±0 01)
⁶⁰ Co	5 26 yr	1173 226 (±0 040)
		1332 483 (±0 046)
²² Na	2 60 yr	511 006 (±0 02)
		1274 53 (±0 10)
⁴⁰ K	1 30 10 ⁹ yr	1460 75 (±0 06)*
²³² Th source	1 41 10 ¹⁰ yr	238 61 (±0 01) from ²¹² Pb
		583 139 (±0 023) from ²⁰⁸ Tl
		727 1 (±0 01) from ²¹² Bi
		911 07 (±0 07) from ²²⁸ Ac
		2614 47 (±0 10) from ²⁰⁸ Tl
		241 924 (±0 03) from ²¹⁴ Pb
		295 217 (±0 039) from ²¹⁴ Pb
²²⁶ Ra source	1602 yr	351.992 (±0 062) from ²¹⁴ Pb
		609 37 (±0 16) from ²¹⁴ Bi
		1120 42 (±0 46) from ²¹⁴ Bi
		1764 45 (±0 22) from ²¹⁴ Bi
		2204 25 (±0 48) from ²¹⁴ Bi

* After KING et al (1967)

Table 4.2: Some energy calibration standards
(after Adams and Gasparini, 1970)

reduce the gain drifts.

It is advisable to check before and after each run the position of known full energy peaks in order to monitor the drifts. Because of the possibility of slope drift, at least two points should be checked.

The energy calibration can be done in two ways:

(i) Graphical Method

This is the most accurate but time consuming method. In this method, the peaks due to the known energies, E_1 , E_2 , E_3 and E_4 are superimposed on the same spectrum as that due to the unknown energy E (see Fig 4.17). Vertical lines are drawn through the mean positions

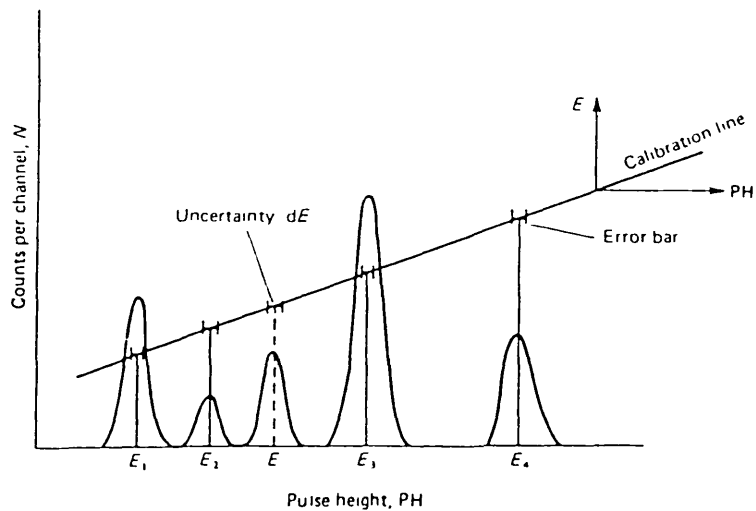


Fig:4.17: Calibration of a pulse height spectrum (after Tait, 1980)

of the known peaks and the heights of these lines are proportional to the energies E_1 , E_2 , E_3 and E_4 . These lines bear no relationship whatsoever to the heights of these peaks, which are proportional to the count rate N . The tops of these vertical lines are then joined by a calibration line as shown in Fig 4.17. This is equivalent to plotting the energies E_1 , E_2 , E_3 and E_4 against the channel numbers where the peaks occur. If the detector has a good linear response for the energy range involved, this is a straight line, but in general it does not extrapolate to the origin since detectors tend to be non-linear at very low radiation energies. The point of intersection of this line with the vertical line through the mean position of the unknown peak gives the energy value of that peak.

(11) Algebraic Method

In this method the dispersion, d , of the spectrometer is calculated. This is the energy interval per unit height interval and is given either as KeV/mV or KeV/channel. It is the energy interval between two calibration peaks, $E_2 - E_1$, divided by the corresponding pulse height interval, $pH_2 - pH_1$, in volts or channels. That is,

$$d = \frac{E_2 - E_1}{pH_2 - pH_1} \quad (4.38)$$

The energy E , of the unknown peak at a mean pulse height pH is then obtained by reference to one of the calibration peaks such as E_1 , by

$$E = E_1 + d(pH - pH_1) \quad (4.39)$$

4.5.2. Sensitivity Calibration

The sensitivity calibration gives the link between count rates (corrected) and concentrations. The sensitivities enable the field values in counts/unit time interval to be converted to ground concentration in parts/million (ppm), or percent (%). The equation connecting the corrected count rates and the concentration of the elements, thorium, uranium and potassium, are expressed as follows:

$$\begin{aligned} \text{Conc(T)} &= T_C/S_T \\ \text{Conc(U)} &= U_C/S_U \\ \text{Conc(k)} &= K_C/S_K \end{aligned} \tag{4.40}$$

where

T_C , U_C , K_C are as defined by equation 4.11, and

S_T , S_U , and S_K are the sensitivities of the instrument to thorium, uranium and potassium respectively.

The stripping ratios defined in equation 4.11 and the sensitivities are determined during the calibration of the instrument. These coefficients are determined as closely as possible to the condition of use of the instrument during a survey.

4.5.2.1. Calibration Of Surface Systems

Surface measurements are usually made with a gamma ray spectrometer either placed directly on the ground surface or elevated such as when man-carried, mounted on a tripod or a vehicle. In all cases, the system should be calibrated with the detector on or near the surface

of a calibration pad to ensure that the pad represents an infinite 2π geometry source, although field measurements with detector elevated will be representative of a larger sample volume. With such correction factors as shown in Fig 4.18, it might be possible to

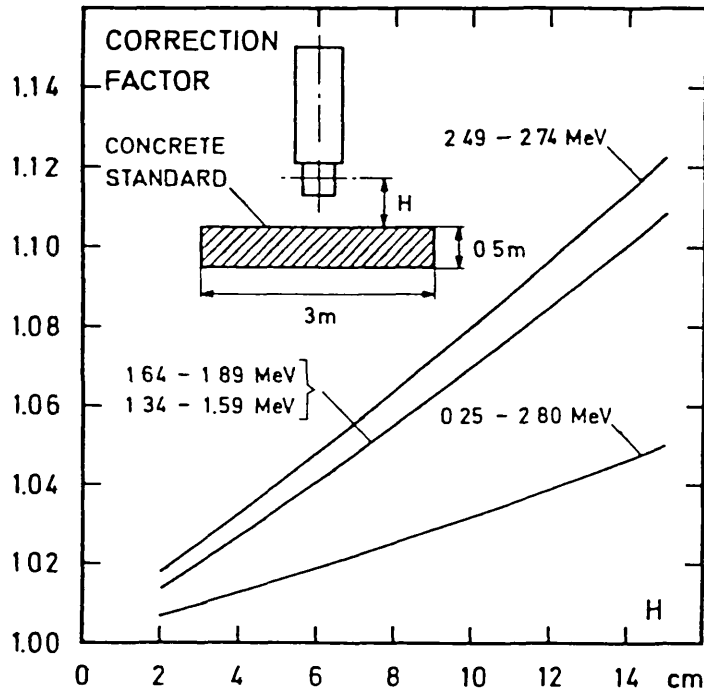


Fig. 4.18: Correction factors for calibrating portable gamma ray spectrometers on calibration pads of less than infinite diameter (after Lovborg et al., 1972). Factors are for a height H above a pad of 3 m diameter as shown in the inset. (after Killeen, 1977)

calibrate spectrometers at elevated positions without having to place them on the calibration pad surface. It should be noted that there is

a possibility of inhomogeneity in the calibration pads and so several measurements at slightly different locations should be averaged. These measurements, combined with the concentrations of the elements, thorium, uranium and potassium, in the pads, are used to solve for the stripping ratios and the sensitivities.

4.5.2.2. Calibration Of Airborne Systems

The calibration of an airborne system requires both calibration pads as well as airborne test strip of known concentrations of thorium, uranium and potassium.

The aircraft can be parked on a set of calibration pads and the measurements made on the pads are combined with the analyses of the calibration pads to derive a set of stripping ratios.

The sensitivities for the airborne system are obtained from flights over a test strip of known concentrations. From these flights (at least five (Killeen, 1977)), the absorption coefficient is calculated (see section 4.3.3). Since airborne data are normalized to a given height, H_0 say, at standard temperature and pressure, the equivalent flight altitude of H_0 at the survey temperature and pressure will be given by (see equation 4.16)

$$H = \frac{760 \times T \times H_0}{273 \times P} \quad (4.41)$$

where T and P are the atmospheric temperature and pressure respectively.

The count rates at this height H are then calculated from

$$N = N_0 e^{-\mu H} \quad (4.12)$$

These calculated count rates are then corrected for background and spectrally stripped using the set of stripping ratios determined on the calibration pads (after being corrected for height). These corrected count rates at height H are then combined with the assay data of the test strip to calculate the sensitivities, using equation 4.40.

To ensure the continuing calibration of the gamma ray spectrometer during a field survey, the system can be monitored with a series of tests which are carried out daily to see that point sources give unchanging results.

The mathematical approach to the background, Compton scattering corrections and isotopic calibration will be discussed in section 6.2.

4.6. Data Presentation

Presentation of data will depend on the purpose of the survey. A uranium survey will require presentation of the uranium channel and probably the uranium/thorium ratio data. A beach sand (thorium rich) survey will require a plot of the thorium values. For mapping purposes, all channels will have equal significance. After all corrections have been made to the raw data, generally by computer, the data are presented as contour maps, stacked profiles, perspective maps or symbol maps. Although contour maps may not be the best form of presentation of the data, it is sometimes more desirable to use the contour method, particularly when comparing radiometric data with some

other types of geophysical data, such as magnetic data, which are usually compiled and studied in contour form.

Several authors have suggested different ways of presenting gamma ray spectrometric data. They are all aimed at easier interpretation of the data.

Darnley (1972) suggested that

- (1) data without any corrections be presented with the use of symbols superimposed on a flight line to indicate an anomaly exceeding an arbitrary background value by some given factor. An example of this is shown in Fig 4.19. According to Darnley this type of presentation, although inexpensive, is unsatisfactory because
 - (a) it is somewhat subjective
 - (b) since there are no Compton scattering corrections, many uranium anomalies would be caused by high thorium values
 - (c) the background used is the average overland radiation level and therefore the information which the overland radiation base level can provide about the general geochemical environment is ignored, and
 - (d) since no terrain clearance correction is applied, some anomalies may be caused by topographic highs and lows.
- (11) the uranium and thorium count rates in the anomaly peak are shown alongside the uranium and thorium background (see Fig 4.20). This improves the amount of information

available on the map.

(111) the thorium content be contoured in addition to the

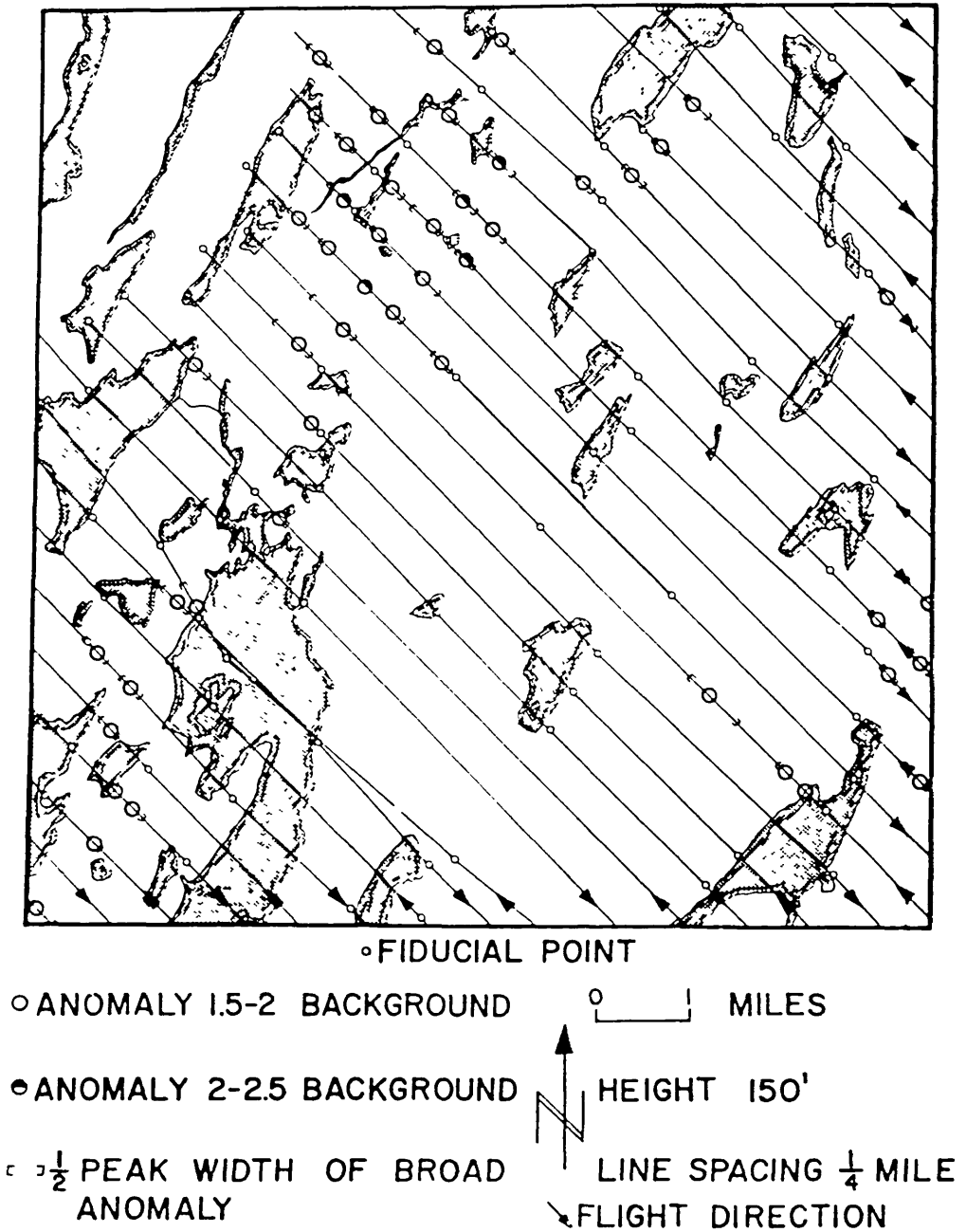


Fig. 4.19: Data presentation example 1 symbols superimposed on a flight line map indicating anomalies exceeding some arbitrary background value by some given factor (after Darnley, 1972)

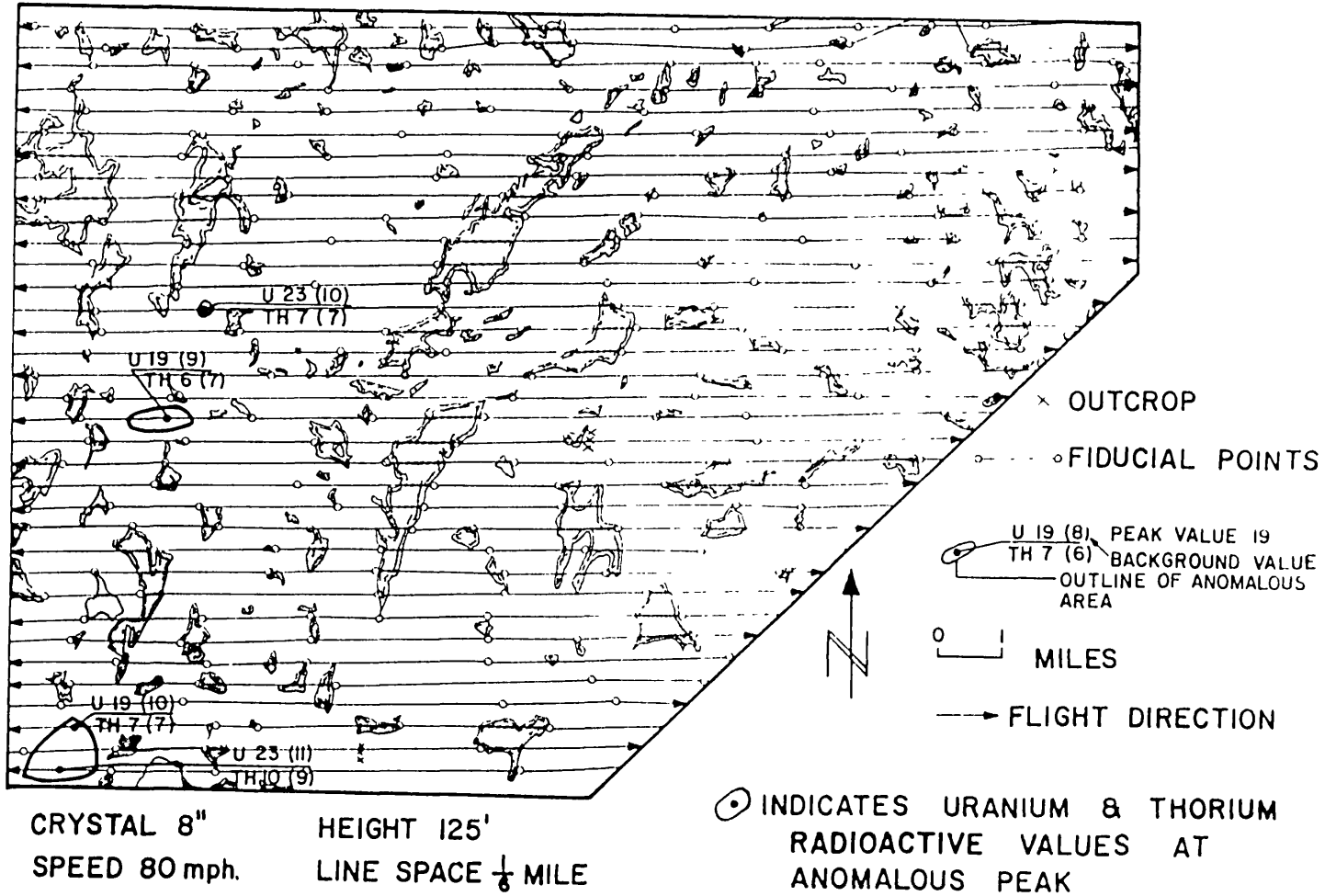


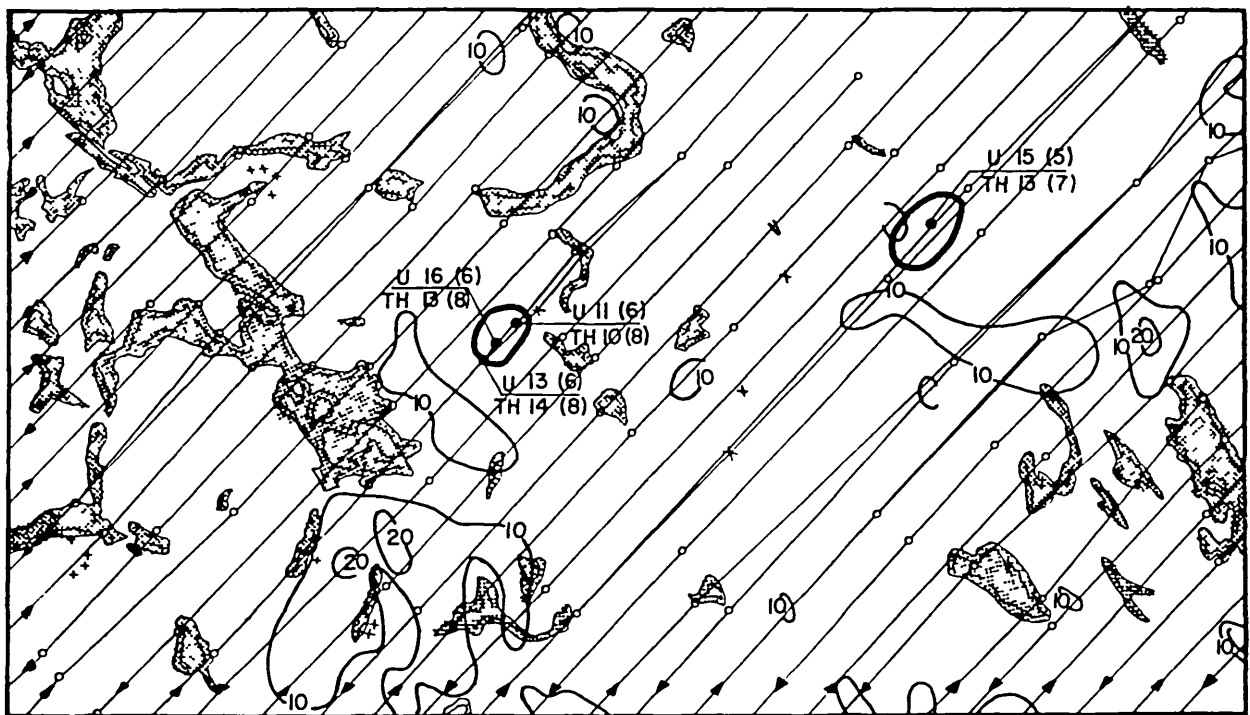
Fig. 4.20: Data presentation example 2 uranium count-rate in the anomaly peak is given beside the uranium background, and the thorium count-rate in the anomaly is given beside the thorium background (after Darnley, 1972).

display (ii) of anomalies as shown in Fig 4.21. Since the thorium is usually more reproducible and statistically more significant than the uranium count, it can be used as an aid in interpreting the geology.

(iv) a profile map (or offset profiles). This is shown in Fig 4.22. Here the strip chart data are plotted on a flight line map along the flight lines. In theory this shows the relationship in radiometric pattern from line to line and similar features can be joined.

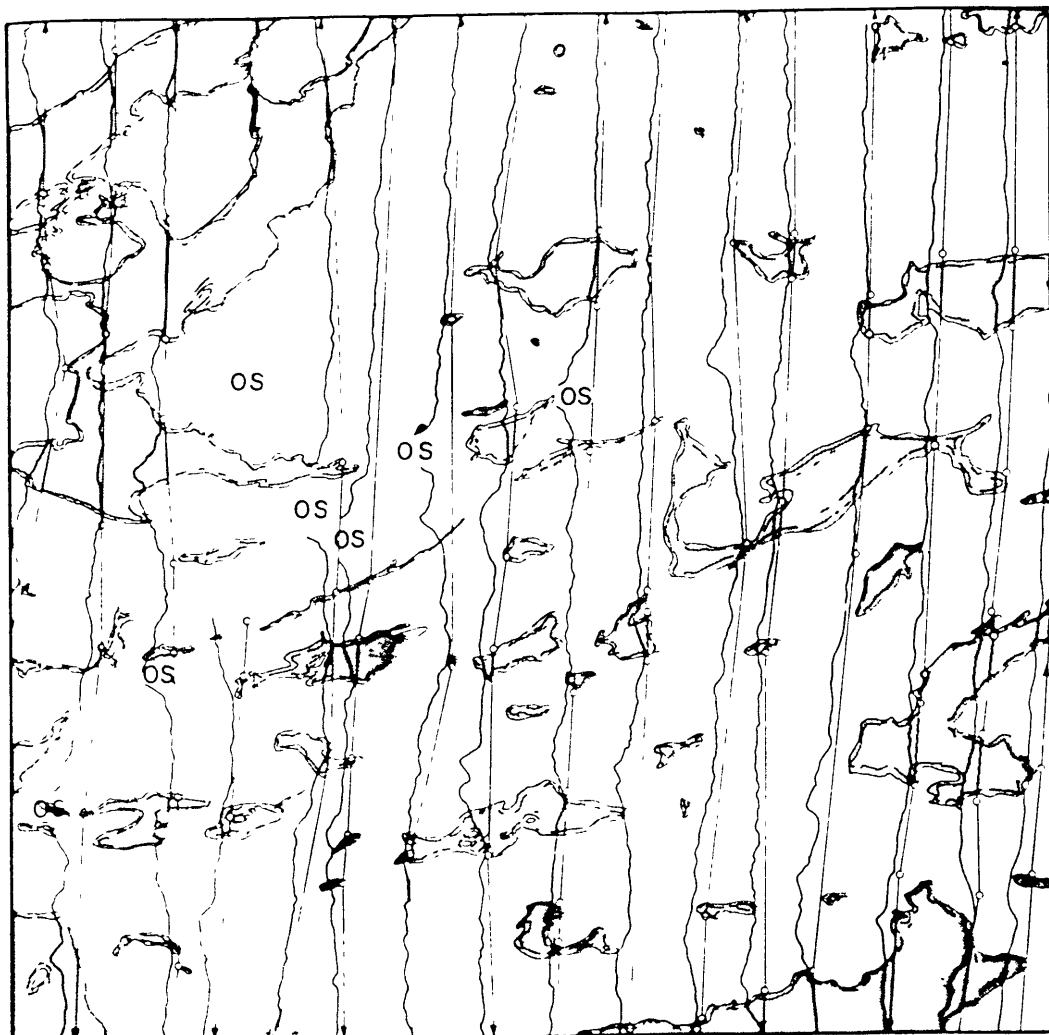
Richardson and Carson (Killeen, 1977) suggested standard deviation maps (or anomaly maps). To produce these standard deviation maps, the mean value of uranium for each flight is calculated and data points that exceed the mean value by 1, 2, 3 or more standard deviations are indicated by 1, 2, 3 or more stars plotted above the flight line (see Fig 4.23). In areas of well known geology, the mean values for all the data measured over each rock unit may be treated in this way and in this case the standard deviations correspond to a given rock unit rather than to the mean values for a given flight line. Potts (1976) presented a contour map of these standard deviations from the mean for uranium, and called it significance factor map. The significance factors are defined as fractional multiples of the standard deviation above or below the mean. Figs 4.24 and 4.25 show respectively the uranium count rate contour map and the significance factor contour map of the uranium data. The two maps show a difference of about 10Km between the area

with the greatest number of standard deviations and the area with the highest uranium count rates.



↗ FLIGHT DIRECTION
 HEIGHT 150'
 ✕✕ OUTCROP
 LINE SPACING $\frac{1}{6}$ MILE
 ○ 20 CONTOURS OF THORIUM RADIATION.
 CONTOUR INTERVAL 10.0cps
 0 1 MILES
 CRISTAL 6"
 PEAK VALUE 19
 BACKGROUND VALUE
 $\frac{U}{TH} \frac{19}{7} \frac{(8)}{(6)}$
 • FIDUCIAL POINTS
 SPEED 55mph.
 INDICATES URANIUM & THORIUM RADIOACTIVE VALUES AT ANOMALY PEAK.

Fig.4.21: Data presentation example 3: similar to Fig. 4.20 but with eTh content contoured in the vicinity of the anomalies (after Darnley, 1972).



° FIDUCIAL POINT
CRYSTAL 6"

FLIGHT DIRECTION ↓
HEIGHT 150'



0 1 MILES

1000 0 (OFF SCALE OS)

PROFILE SCALE

Fig. 4.22: Data presentation example 4. A profile map or 'offset profiles'. The radiometric record is plotted beside the flight lines (after Dainlex, 1972).

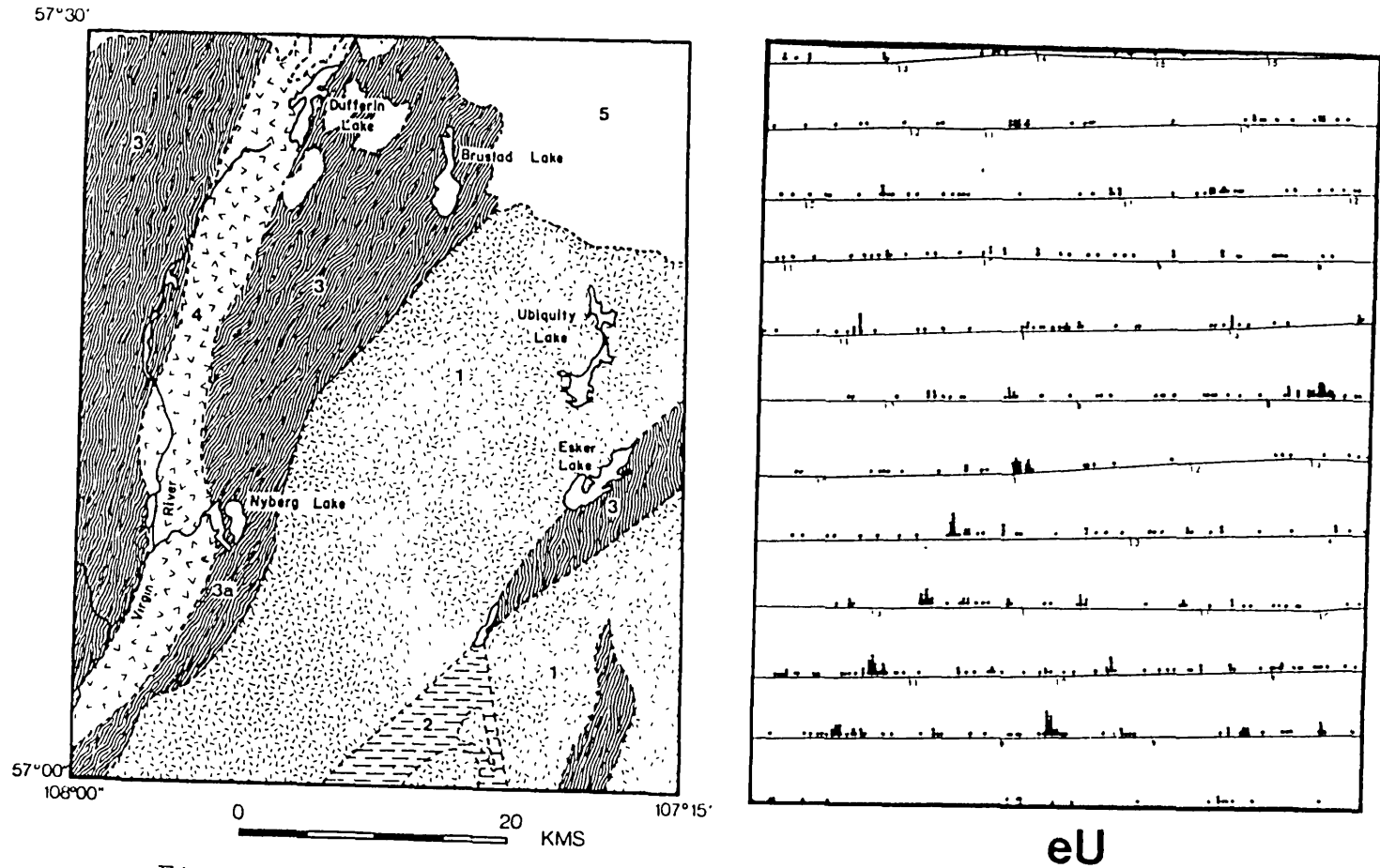


Fig.4.23: Comparison of geology map and eU anomaly map for the Nyberg Lakes - Brustad River area (after Richardson and Carson, 1976). The statistical treatment of the data (described in the text) produces a map which relates to the geology of the area, whereas the simple eU contour map did not. (after Killeen, 1977)

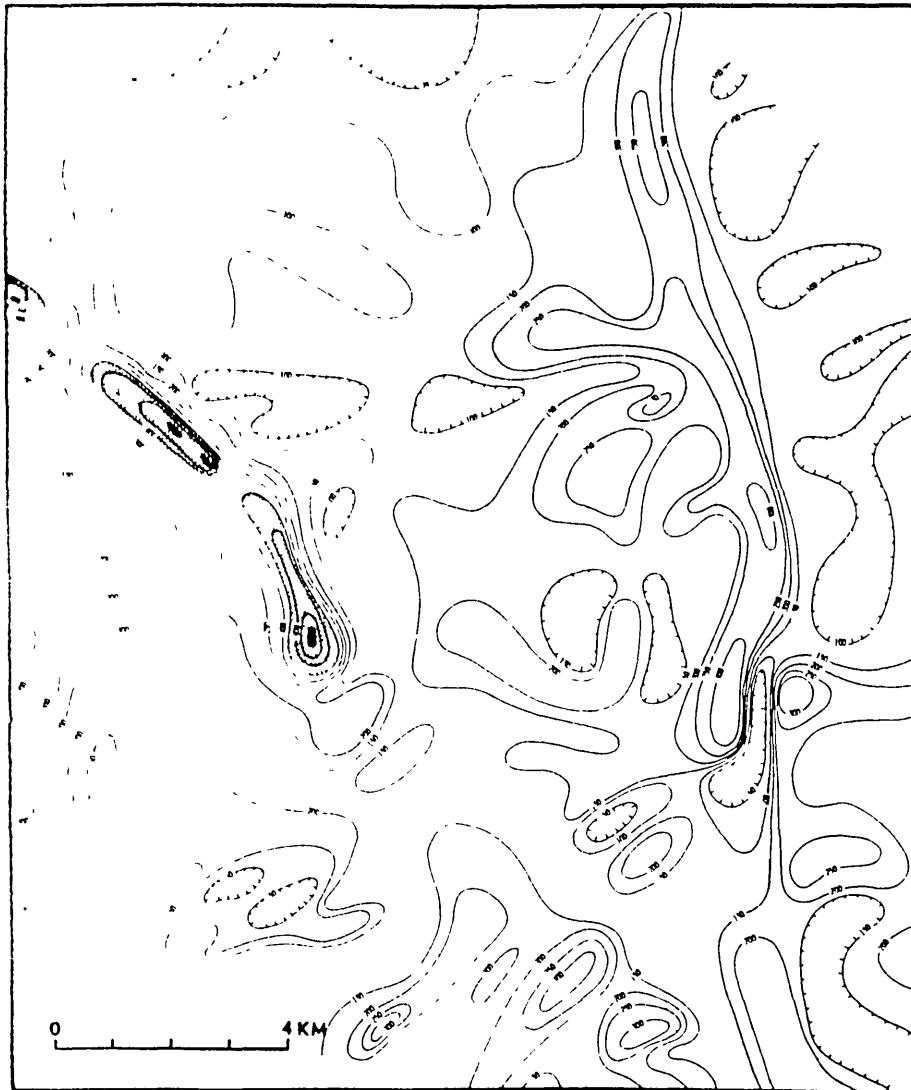
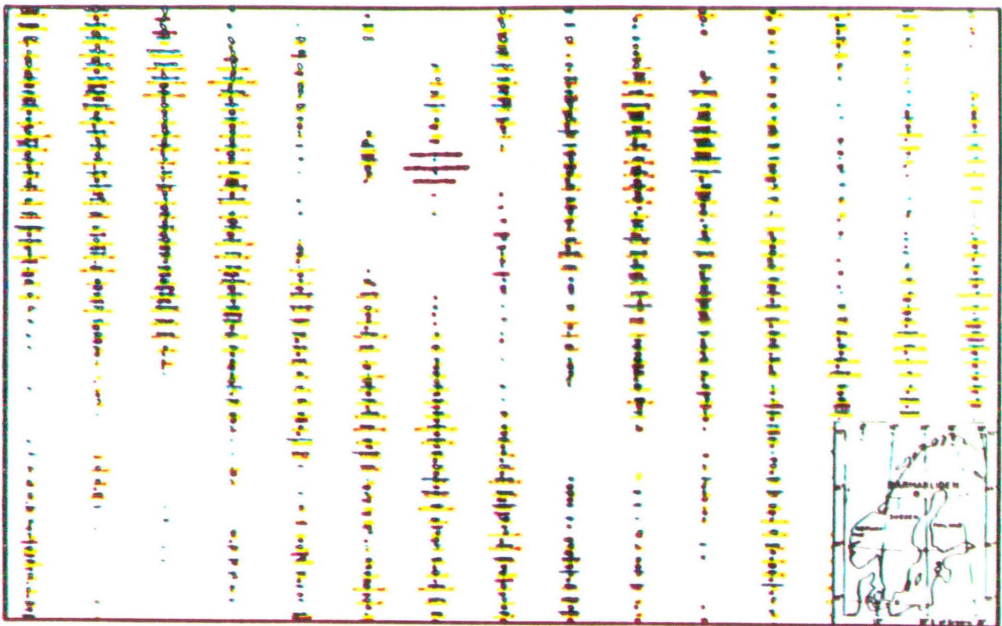


Fig.4.24: Uranium count-rate contour map (counts per 2 seconds) for the area in South America shown in Fig. 4.25 (after Potts, 1976) based on airborne gamma ray spectrometry.



Fig.4.25: Significance factor contour map (described in the text) for the area in South America shown in Fig. 4.24 (after Potts, 1976)

Linden and Akerblom (1976) used colour presentation. This shows the gamma radiation related to potassium, uranium and thorium in the form of coloured columns plotted on the flight lines (see Fig 4.26). This is done by plotting three



*Fig.4.26: Three - Component radiation map
(after Linden and Akerblom, 1976)*

centred-orientated columns on an area described by the length of the flight line and the flight line spacing. The lengths of the columns are proportional to the radiation that relates to each element. Potassium is represented by yellow, uranium by red and thorium by blue. Each group of three columns is separated from the next by a

white field equivalent to the width of one column. In areas of abnormally high or low contents of potassium, uranium and thorium, it is possible to improve the resolution by increasing the contrast between element intensities.

Duval (1983) in addition to the coloured map of the potassium, uranium and thorium (which he called composite element image), also produced coloured composite ratio image, uranium image, thorium image, and potassium image. While the composite ratio image contains eU/eTh , eU/K , and eTh/K , the uranium image contains eU , eU/eTh and eU/K ; the thorium image contains eTh , eTh/eU and eTh/K ; and the potassium image contains K , K/eU and K/eTh . He stated and showed that

"The element image provides a view of the overall pattern of the elements and usually contains patterns related to the various lithologies. The ratio image tends to remove lithologic differences and effects in the data caused by variations in the soil moisture, nonplanar source geometry, and errors associated with altitude corrections. The uranium, thorium and potassium images emphasize the radioelements and highlight areas where the particular radioelement has a relatively higher concentration."

Foote (Killeen, 1977) in his review of data presentation techniques, gave the following summary:

- (a) flight line profiles of intensity of radiation from uranium, potassium, thorium and their ratios.

- (b) histograms showing data distribution
- (c) radiation data by surface geologic unit
- (d) radiation data by flight line showing statistical variation from mean value, and
- (e) data by flight line superimposed on surface geologic map.

Hogg (Killeen, 1977) described

(a) the Zoning Technique in which the boundaries of recognizable changes in the potassium, uranium, thorium and their ratios are marked on a profile (see Fig 4.27). K, U, and T refer to potassium, uranium and thorium respectively, and the signal strength indicated by symbols (+) strong, () average, and (-) weak) which relate to preselected levels. A computer/plotter may then be used to produce a profile coding annotated (see Fig 4.28). These maps may then be coloured for each radionuclide, potassium, uranium and thorium. The advantage of this technique, Killeen stated, is that all the information is presented on one map. The main disadvantage however, is the amount of time involved in the initial steps of the processing.

(b) a computer line printer listing of anomalies meeting specified criteria. For each anomaly a set of statistics is printed including flight line number, fiducial numbers nearest the anomaly, anomaly amplitude, half width (left), area (left side), half width (right), area (right side), total half width, total area as shown in Fig 4.29. Postscripts 1 and 2 refer to parameters calculated from stripped, smoothed, altitude corrected uranium profile with subtraction of

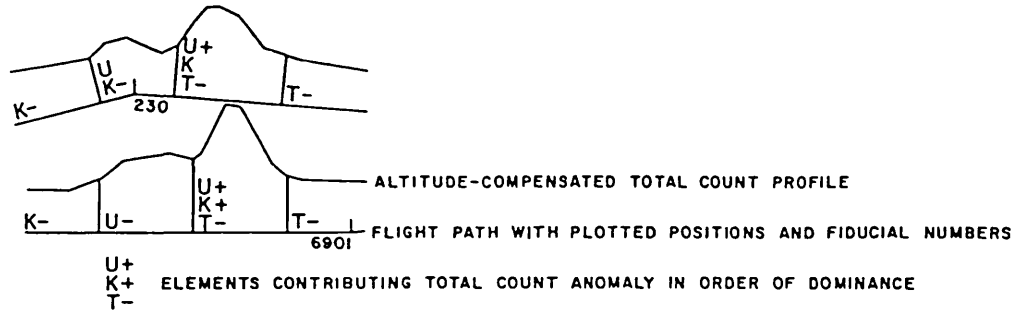


Fig.4.27: The Zoning Technique (after Killeen, 1977)

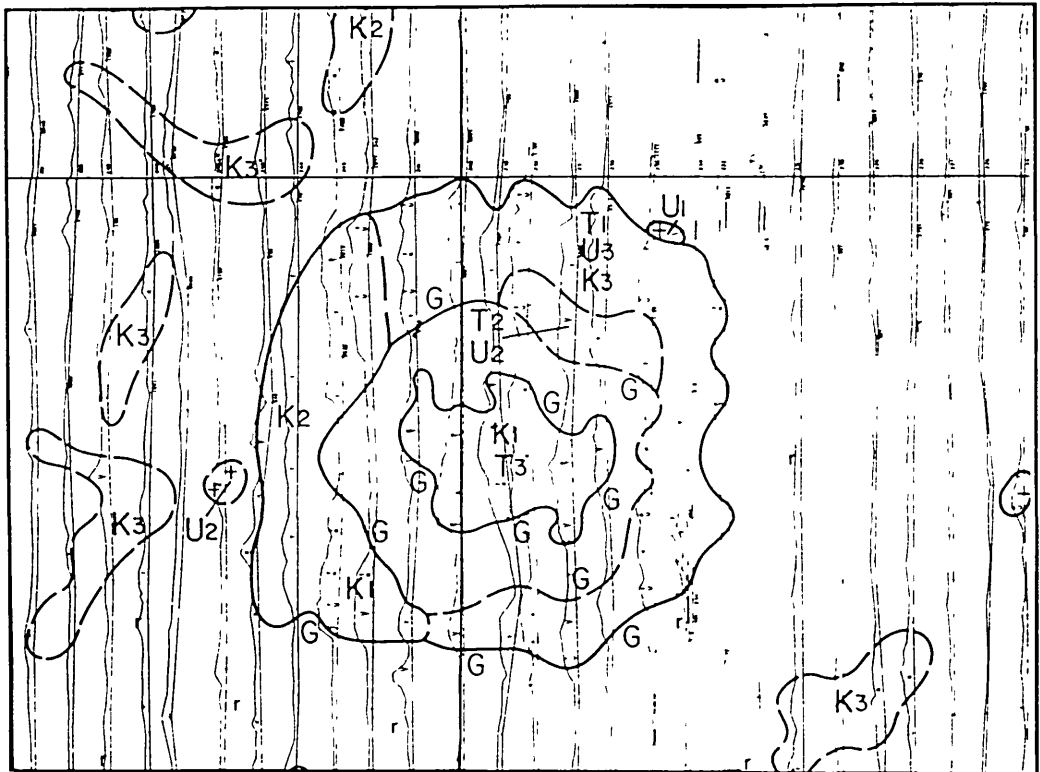


Fig.4.28: The Zoned map based on total count profiles processed as in Fig.4.27 with the zone boundaries joined (after Killeen, 1977)

ADG(1) =										AMP1		HWL1		ARL1		HWR1		ARR1		THW1		TAR1		LINE 12P	
										54.0		.20		10.1		.44		20.2		.64		30.3		FS 6281	
ALBJ(2) =										AMP2		HWL2		HWR2		THW2		TAR2		SBL2					
										34.1		.12		.07		.19		7.6		-44.3					
TOTAL COUNT																									
3444 CPS				150P								P													
POTASSIUM				URANIUM				THORIUM				I													
344				P/100				P/100				I													
I	I	I	I	I	I	I	I	I	I	I	I	I	K	U	TH	TC									
715							U	*				T		1	46	30	22	1061							
720							U	*				T		1	50	23	23	1020							
731											+	T		1	55	16	23	1164							
735							U	*				T		1	54	16	23	1000							
740											U	*		1	49	19	27	1147							
745														1	54	21	26	1263							
750							U	*				T		1	60	22	27	1311							
755											+	T		1	55	23	26	1225							
750							U	*				T		1	54	22	26	1245							
770							U	*				T		1	55	24	26	1211							
775											U	*		1	46	31	27	1119							
780							U	*				T		1	38	35	28	1200							
785							U	*				T		1	44	38	27	1367							
790							U	*				T		1	49	44	23	1493							
795							U	*				T		1	48	44	20	1267							
810							U	*			+	T		1	52	42	23	1346							
810							U	*				T		1	55	55	30	1956							
815							U	*				T		1	52	66	33	2398							
820											U	*		1	49	61	37	2131							
825							U	*				T		1	46	45	40	1773							
830											U	*		1	45	35	32	1591							
840											+	T		1	44	26	25	1249							
845														1	44	17	24	1146							
850							U	*			U	*		1	45	15	22	1092							
855							U	*				T		1	47	17	21	994							
860							U	*				T		1	40	24	20	1020							
865							U	*				T		1	44	30	22	1120							
870							U	*				T		1	48	30	27	1270							
875											+	T		1	36	35	26	1325							
880							U	*				T		1	37	40	24	1371							
890							U	*				T		1	39	37	22	1321							
895							U	*				T		1	35	31	23	1156							
900							U	*				T		1	39	29	23	1142							
910							U	*				T		1	44	29	22	1043							
915							U	*				T		1	43	27	24	1159							

U	TH	K	TC	U/TH	U/K	U/TC(x100P)	TH/K	ALT
64	33	52	2398	2.06	1.31	26.36	.63	327

Fig. 4. 29: A printer-plot anomaly description (after Killeen, 1977)

either (1) atmospheric background or (2) local background plus atmospheric background. A line printer plot may also be produced to illustrate roughly the shape of the anomaly. Below the printer plot are given the count rates and ratios calculated at the uranium anomaly peak.

Morris (Killeen, 1977) also described

a technique where the count rates in the three radioelement channels are expressed as a percentage of the count rates in the total count channel by a normalization process. The position of the anomaly is then located on a ternary diagram as shown in Fig 4.30. The diagram has 100% potassium, uranium and thorium respectively as three points of the triangle. Thus an anomaly can be located on the diagram by the relative percentage contributions to the total count from potassium, uranium and thorium channels. The ternary diagram is divided into nine fields. An example of the application of this anomaly classification system is given in Table 4.3 where three anomalies have been analyzed by this process and they fall into fields S, X and L respectively.

Texas Instrument Incorporation (1977) gave a summary of the presentation of data techniques used in the Natural Uranium Resources and Exploration (NURE) program as follows:

(1) Stacked Profiles:

These are generated from averaged radiometric data and consists of Th/k, U/K, U/Th, gross count, K, Th, U, atmospheric uranium daughter

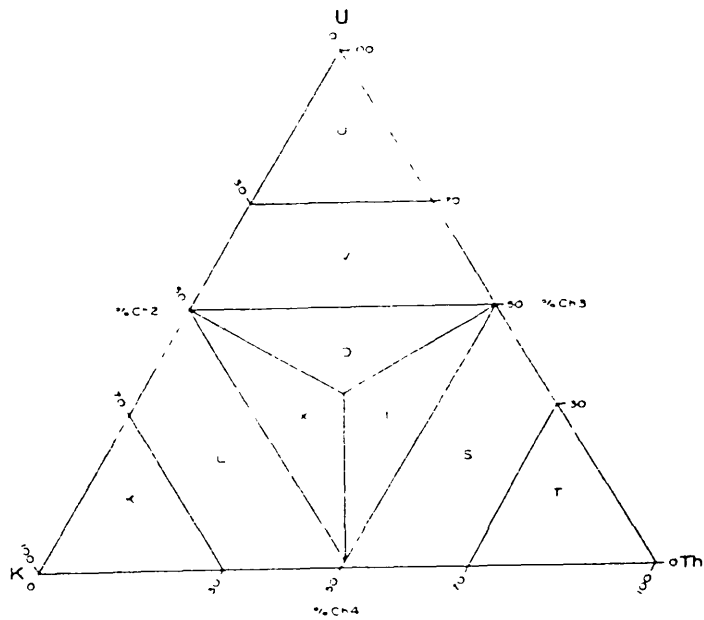


Fig. 4.30: Ternary diagram illustrating a process for classifying airborne gamma ray spectrometric anomalies into nine different fields (after Killeen, 1977)

Table 4.3: Example of three anomalies classified as type S, K, and L using Fig. 4.30 (after Killeen, 1977)

Line 5881										
Anomaly No. 6	Channel 1			Peak	Corrected Counts			%		
	Peak time	6478	Secs		B/ground	Anomaly			U/Th ratio	0.0
	1/2 width time 1	6476	Secs	Channel 1	200	124	76.		Th/K ratio	1.9
	1/2 width time 2	6482	Secs	Channel 2	31.	21	10.	35	Anomaly type	S
	Peak Altitude	426	Feet	Channel 3	11.	10	2.	0	Source	Th-U/K
	Peak raw counts	707	CPS	Channel 4	19.	8	11	65		
	Ch 3 peak time	6475	Secs							
Anomaly No. 7	Channel 1			Peak	Corrected Counts			%		
	Peak time	6578	Secs		B/ground	Anomaly			U/Th ratio	.3
	1/2 width time 1	6575	Secs	Channel 1	131.	59.	72		Th/K ratio	.9
	1/2 width time 2	6605	Secs	Channel 2	29.	13	17.	45	Anomaly type	X
	Peak Altitude	471	Feet	Channel 3	15.	9	6.	14	Source	Mixed(K)
	Peak raw counts	514	CPS	Channel 4	16.	6	9	41		
	Ch 3 peak time	6580	Secs							
Anomaly No. 8	Channel 1			Peak	Corrected Counts			%		
	Peak width time 1	6600	Secs		B/ground	Anomaly			U/Th ratio	1
	1/2 width time 1	6575	Secs	Channel 1	116.	50	67.		Th/K ratio	6
	1/2 width time 2	6605	Secs	Channel 2	31.	10	21	61	Anomaly type	L
	Peak Altitude	468	Feet	Channel 3	13	9	4.	4	Source	K-U/Th
	Peak raw counts	599	CPS	Channel 4	15	6	9	35		
	Ch 3 peak time	6597	Secs							

contribution (UAIR), and average terrain clearance. A geologic strip map with posted record locations annotated at regular intervals appears at the top of the stacked profile, which contains all data collected on one flight line.

(11) Record Location Map:

This is a positional map on which the location of the average record centroids are posted and annotated at regular intervals.

(111) Gamma Ray Anomaly Map:

These are maps on which the position of the averaged record centroids are posted and annotated in such a manner that the statistical significance of the data is indicated. A map is prepared for each of the parameters potassium, uranium, thorium and their ratios, and gross counts.

(iv) Histograms:

These are bar-graph displays plotted for the count rate distribution of data for each of the six gamma ray parameters, potassium, uranium, thorium and their ratios, in each geologic map unit. Information is included on the distribution type, the median value, the absolute values at 1, 2 and 3 standard deviations above and below the mean, and the number of samples included in the data for each parameter (see Fig 4.31) as illustrated by Foute and Humphey (1976).

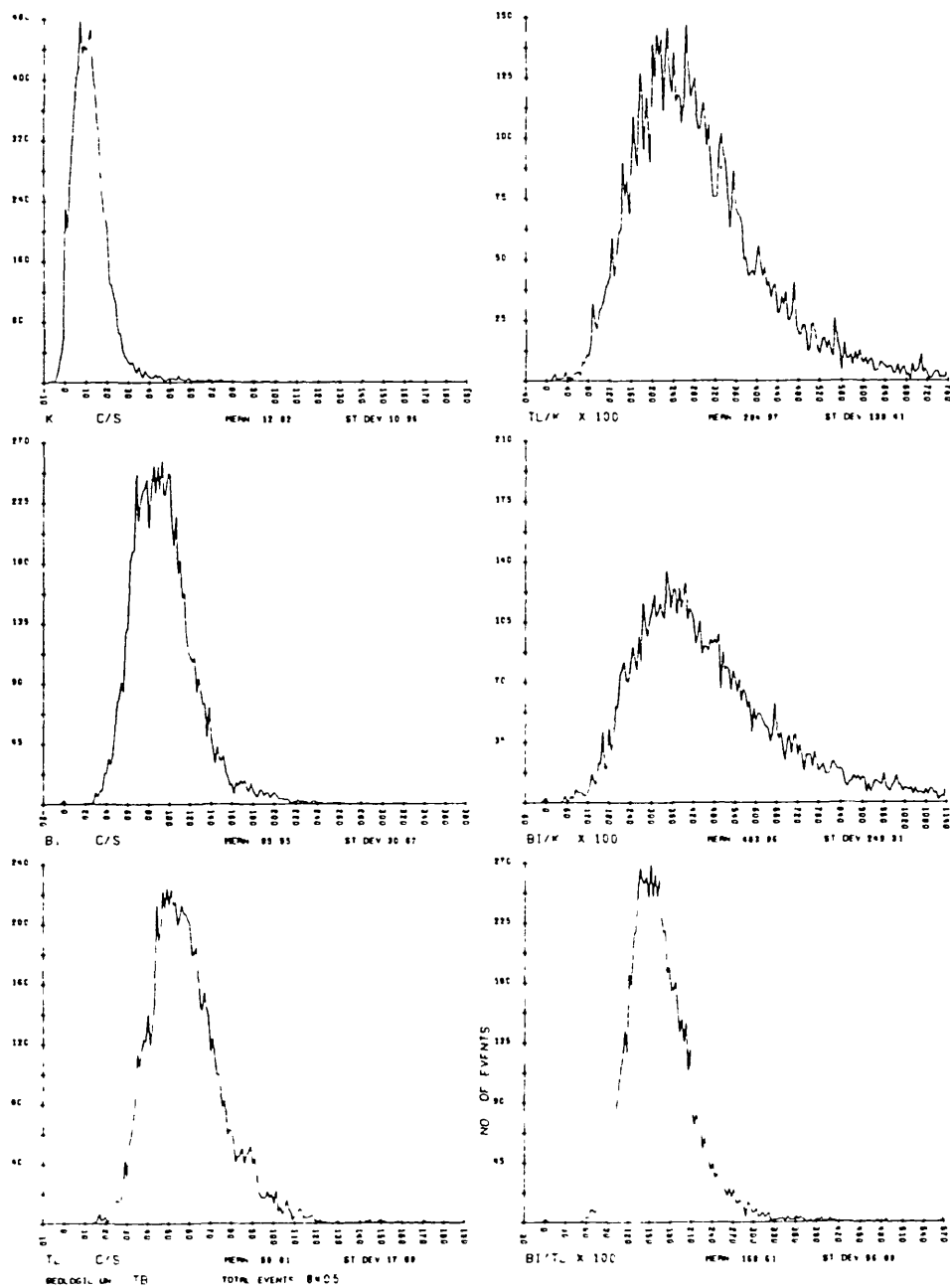


Fig.4.31: Frequency distribution of geology unit Tb Augusta NTMS

(after Foote and Humphrey, 1976)

(v) Computer Listing:

Single record and average record data listings are prepared in microfiche form. The data are arranged by flight line and contain, as heading information on each page, the operator's name, the name of the survey, the flight line number, and the day of year on which the data were collected; and

(vi) Data Tapes:

These consist of the edited field data tape, the single record reduced data tape and the geologic analysis data tape. Each tape consists of all data for the survey. The edited field tape contains the original spectral data prior to any corrections, together with a number of supplemental tag words. The single record data tape contains all totally reduced gamma ray and geologic data, and the geologic analysis data tape contains the general cumulative statistical data obtained from the analysis as well as the individual averaged records with their statistical significance.

CHAPTER FIVE

RADIATION DETECTION AND MEASUREMENT

As mentioned earlier (see chapter Two), the detection of gamma rays is based upon their interaction with matter, which results in the full or partial transfer of energy of the incident radiation to electrons or nuclei of the constituent atoms of the absorber. Thus devices designed to measure gamma rays must be able to promote such interactions and measure the energy transferred to it. This suggests that an instrument for the detection and measurement of gamma rays will consist essentially of a detector, amplifying and counting systems. While the interactions of the photons with matter occur in the detector, the amplifying and counting systems increase the detector's output pulse, count the events and eventually discriminate them according to their energies.

5.1. Detectors

A number of gamma ray detectors have been used and the most important groups are

- (i) Gas-filled detectors
- (ii) Scintillation detectors, and
- (iii) Semi-conductor detectors.

5.1.1. Gas-Filled Detectors

This group of detectors includes ionization chambers, proportional counters and Geiger-Muller tubes. The use of these detectors is based

on the fact that ionization and excitation of gas molecules occur when a charged particle passes through a gas.

All gas-filled detectors consists basically of a chamber filled with a suitable insulating gas. The interaction of ionizing radiation with the gas and/or chamber walls produces ion pairs, which, under the influence of an applied electric field, move towards their respective electrodes. Fig 5.1 shows a schematic diagram of a typical gas-filled detector, where a voltage V is applied between the chamber's wall and the central connecting wire by means of a resistance R , shunted by a capacitance C .

Among other things, the number of charges reaching the collecting electrodes is dependent on the gas filling and the voltage.

The relationship between the number of electrons collected at the anode and applied voltage V is shown in Fig 5.2 (Eichholz and Poston, 1979). At low applied field there is a net drift of the charges in a direction parallel to field lines of forces. For a parallel plate chamber, the net drift velocity v is given by

$$v = (\mu/pd)V \quad (5.1)$$

where

μ is the mobility of the electrons

d is the plate distance

p is the gas pressure, and

V is the applied voltage

When V is very low, as in Region I, the drift velocity is also very small and so the electrons take long time to get to the anode and in

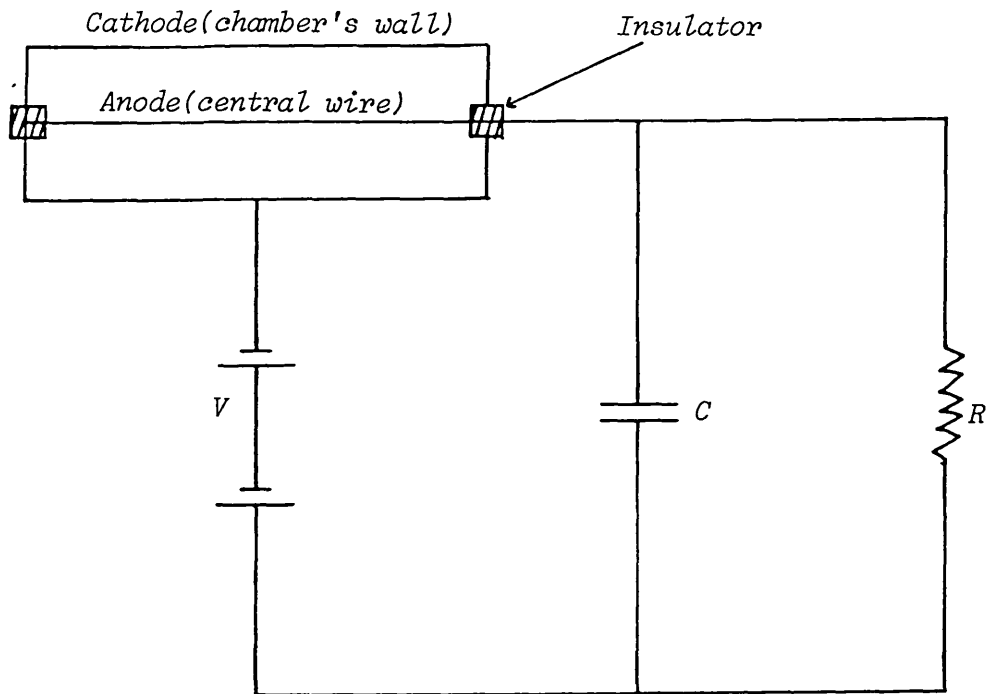


Fig.5.1: Typical gas-filled detector

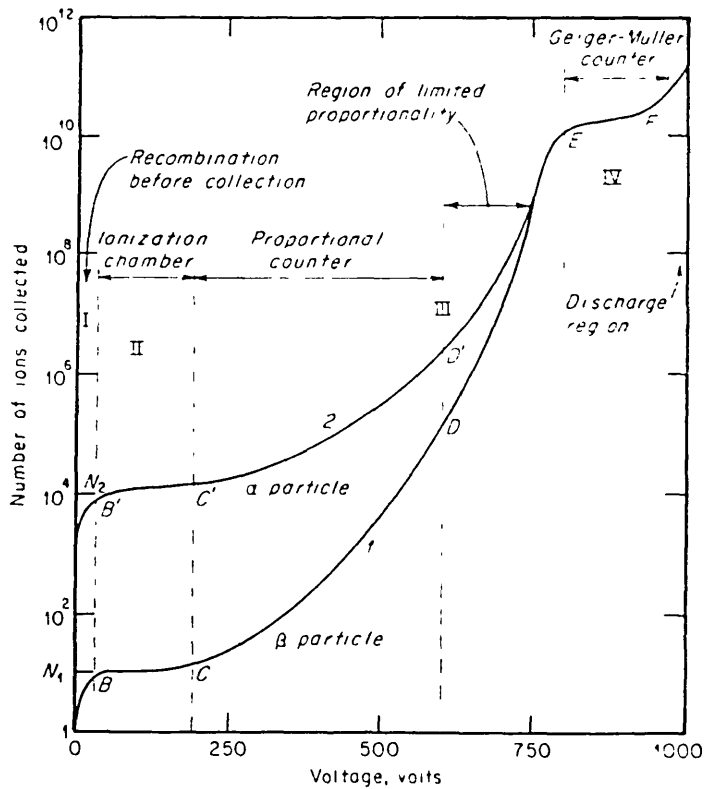


Fig. 5.2: Counting characteristics of gas-filled detectors (after Eichholz and Poston, 1979)

the process some of them recombine with positive ions. Thus the number of electrons collected is less than the number actually produced. In Region II, an increase in the voltage V produces a corresponding increase in the drift velocity, thereby reducing the travelling time of the electrons and thus prevents recombination. Hence all the electrons produced are collected. Further increase in the applied voltage in this region produces no remarkable increase in the number of electrons reaching the anode. This Region II is called the ionization region and the gas-filled detectors designed to operate in this region are called ionization chambers. In Region III, as the applied voltage increases, the electrons may acquire enough energy to produce secondary electrons, which may also possess enough kinetic energy to produce additional ionization. This process, known as gas multiplication, results in the number of electrons collected at the anode being higher than the number produced by the primary radiation. But since the single avalanches do not interfere with each other, the total number of electrons collected is still proportional to the total energy lost by the incident particle in the gas volume. This Region III is called proportional region and the detectors which operate in this region are called proportional counters. In the upper part of Region III, called the region of limited proportionality, a value of V is reached where the size of the avalanches increases to such an extent that their interactions become significant. According to Adams and Gasparini (1970), the magnitude of avalanches at this value is no longer proportional to the initial radiation and this value is lower for the most ionizing radiation. From this point the essentially

parallel curves (1 and 2) begin to converge until they join. Thus Region IV, the Geiger-Muller region, represents a region in which it is impossible to distinguish, as the applied voltage increases, between particles with different ionizing power and the number of electrons collected no longer depends on the initial ionization energy. Radiation detectors which operate in this region are called the Geiger-Muller counters. Gas multiplication process in these counters produces a pulse of a uniform size, regardless of the number of ion pairs formed by the primary ionization. In Region V, called the discharge region, current is produced even after the ionization event has ceased.

In pure gases, positive ions may initiate photoelectrons as they are neutralized at the cathode. These subsequent discharges may be stopped (or quenched) by an external circuit or by adding a small percentage of a lower ionization gas to the filling gas. The external circuit method, designed to reduce the voltage across the detector below the value required to maintain the discharge, is rarely used. The addition of quenching gas results in the interaction of the ions of the main gas with the molecules of the quenching gas thereby preventing ejection of electrons from the cathode.

Table 5.1 gives a summary of some characteristics of the three detector systems mentioned above.

Detector	Output Signal	Amplification Factor	Resolving Time
Ionization chamber	0 - 1mV	1	1μsec
Proportional counter	1 - 100mV	$10^2 - 10^4$	5 - 50μsec
Geiger-Muller tube	0 - 10mV	$10^6 - 10^8$	10 - 1000μsec

Table 5.1: Some Characteristics Of Gas-Filled Detectors (after Eichholz and Poston, 1979)

Geiger-Muller Counter

A simplified Geiger-Muller counter circuit is shown in Fig 5.3. This consists of a sealed glass tube filled with some gas, usually a

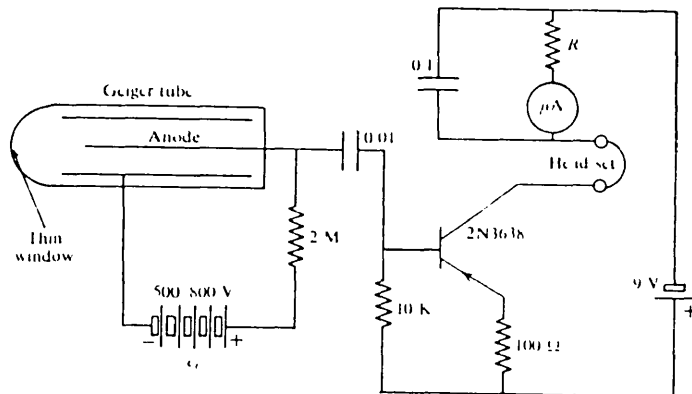


Fig.5.3: Simplified Geiger-Muller counter circuit (after Telford et al, 1976)

mixture of argon and about 10% of alcohol. The gas mixture produces a quenching action which helps to suppress secondary electron emissions from the cathode, caused by positive ion bombardment. The gas is non-conducting and so no current flows. But gamma rays falling on the

tube cause ionization of the gas and the movement of ion pairs to their respective electrodes causes the flow of current. The number of electrons falling on the anode can be registered on a meter or monitored by a pair of headphones.

The Geiger-muller counters are cheap, rugged and easy to operate. They produce an output pulse of sufficient magnitude to require no further amplification. They, however, respond to only a very small amount (1% or less) of incident gamma rays and they register almost all corpuscles including cosmic rays.

5.1.2. Scintillation Counters

These have virtually replaced the gas-filled counters because of their greater sensitivity. They utilize the fact that certain materials scintillate when they absorb gamma rays. The scintillations can be detected by a photocathode in a photomultiplier tube and recorded after amplification.

Principle Of Scintillation

An isolated atom contains discrete electronic energy levels (see Fig 2.1), but interactions between atoms result in the broadening of the outermost energy levels into a series of 'allowed' energy bands in which electrons can move freely. These energy bands are separated by a 'forbidden' gap. A representation of the band system is shown in Fig 5.4. In a normal situation, the lower energy bands, called the valence bands, are completely filled with electrons while the higher energy bands are completely empty. The size E_g of the forbidden gap

between a valence and a conduction band determines whether the material is a conductor, semiconductor or an insulator. E_g is negligibly small for a conductor and relatively large ($>3\text{eV}$) for an insulator. For a semiconductor, E_g lies between these two extremes and it is typically less than 2eV .

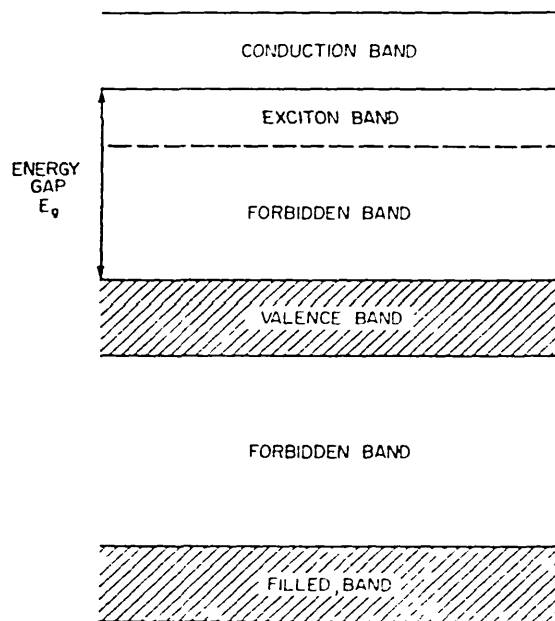


Fig. 5.4 Energy bands in ideal insulating crystal.
(after Birks, 1964)

In the absence of external activation energy, insulators and semiconductors thus have the configuration in which the valence band is completely filled and the conduction band completely empty, and under this condition neither an insulator nor a semiconductor would theoretically show any electrical conductivity. But under the influence of an applied field, there will be some thermal excitation of electrons from the valence band to the conduction band, leaving

vacancies, called holes, in the otherwise full valence band. Hence photoconduction can then occur due to the independent motion of the electrons in the conduction band and of the holes in the valence band. Sometimes the excited electron may remain bound to a hole forming an exciton, the pair possessing not quite enough energy to act as free charges. Such pairs form the exciton band immediately below the conduction band.

Luminescence Process

Luminescence (or emission of light) following the absorption of radiation normally of higher energy than the emission is a molecular property and arises from the electronic structure of the molecules. Thus luminescence process in a scintillator may be described in terms of energy level system comprising of electronic levels and vibrational levels (Schram and Lombaert, 1963). Fig 5.5 shows the absorption and emission

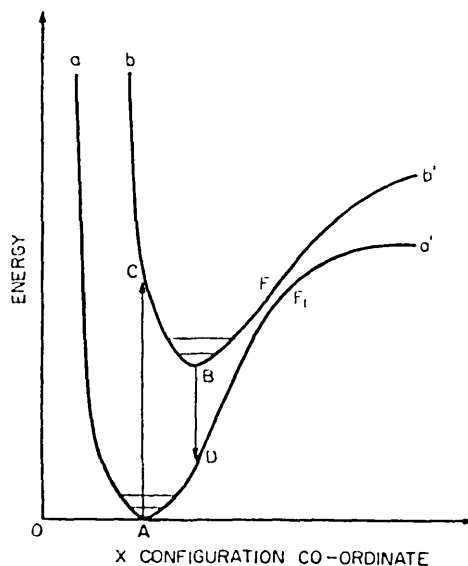


Fig. 5.5: Potential energy diagram of luminescence centre or molecule. aaa' , ground state. bbb' , excited state. AC , absorption transition BD , luminescence emission transition. FF_1 , region of internal quenching (after Birks, 1964)

spectra in which the potential energies of the ground and excited states are plotted against some configurational coordinate (X) (Birks, 1964). The incidence of ionizing radiation on the scintillator causes the excitation of electrons from the valence band (ground state) to the conduction band (excited state). In the excited state, the electrons may simply emit a photon of the same energy as that of the photon it absorbed, thereby returning to the ground state in a single step, or it may give up its vibrational energy by collision before returning to the ground state. This latter phenomena is called fluorescence and in this case the energy of the emitted photon is always lower than that of the absorbed photon. Another possible transition which does not involve the emission of photon, might occur when an electron in the excited state makes a transition to higher vibrational level F, and then dissipates the excess energy thermally.

Activated Scintillators

The above model (Fig 5.4) and discussion apply to 'perfect' scintillators in which there are no impurities and/or crystal lattice defects. According to Knoll(1979), in the pure crystals, the return of the electron to the valence band (ground state) with the emission of a photon (luminescence) is an inefficient process, and also typical forbidden gap widths are such that the resulting photon would be of too high an energy to lie in the visible range. Thus in order to enhance the probability of visible photon emission during the de-excitation process, small amounts of impurities, called activators, are usually added to the scintillators. The presence of the

activators and/or crystal lattice defects causes localized energy bands, usually in the forbidden gap. Fig 5.6 thus shows the energy band structure and the processes which occur in an activated crystal.

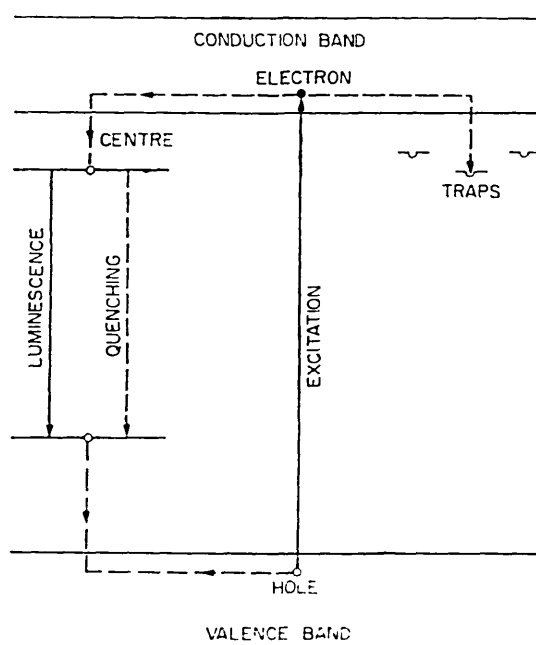


Fig. 5. 6: Energy bands in impurity-activated crystal phosphor, showing excitation, luminescence, quenching and trapping processes.

(after Birks, 1964)

These localized energy bands in the forbidden gap may act as

- (i) luminescence centres in which as described above, an electron can de-excite back into the ground state with the emission of a photon
- (ii) quenching centres in which an excited electron from the conduction band recombines with a hole from the valence band, resulting in a radiationless loss of energy, and
- (iii) traps which have meta-stable levels from which electrons

can return to the conduction band after acquiring enough thermal energy or fall back to the valence band by radiationless transitions

As previously mentioned, instead of the independent migration of electrons and holes, their pairs may migrate together as excitons, drifting freely through the crystal until they reach an activator site where they may de-excite back to the ground state, quenched or trapped.

One important consequence of luminescence through activator sites is that the crystal can be transparent to the scintillation light. While in the pure crystal there is an overlap of the emission and absorption spectrum resulting in substantial self-absorption, this effect will be greatly reduced in the activated crystal because the emission from the activated crystal occurs at an activator site where the energy transition is less than that represented by the creation of the electron-hole pair. As a result the emission spectrum is shifted to longer wavelengths.

Practical Scintillators

A suitable scintillation detector should possess the following properties:

- (1) high atomic number (Z) for the conversion of the kinetic energy of the incident radiation into detectable light with a high scintillation efficiency
- (11) linear conversion - the light yield should be

proportional to the absorbed energy

- (iii) fast response - the decay time of the incident luminescence should be short so that fast signal pulses can be generated
- (iv) high transparency - to its own emission for good light collection
- (v) high purity and subject to manufacture in large sizes
- (vi) high refractive index - near that of glass (about 1.5) to permit efficient coupling of the scintillation light to a photomultiplier tube, and
- (vii) energy gap sufficiently large for operation at room temperature but small enough to maximise resolution

Practical scintillators include inorganic, organic, liquid and plastic crystals. The inorganics tend to have the best light output and linearity, but their response time is relatively slow. Also the high atomic number (Z) of the constituents and high density of inorganic crystals favour their choice for gamma ray spectroscopy. The organics, on the other hand, are much faster, but yield less light. They are preferred for beta spectroscopy and fast neutron detection. Because of the ease with which plastic scintillators can be fabricated and shaped, coupled with the fact that their material is relatively inexpensive, they are often the practical choice where large volume solid scintillators are required. However, their very low density and atomic number make them much less efficient than inorganic scintillators for the detection of gamma rays.

A summary of the characteristics of the best known gamma ray scintillators is given in Table 5.2 (Adams and Gasparini, 1970).

Scintillator	Density (g/cm ³)	Z	Decay time (μsec)	Conversion efficiency	Emission spectrum
NaI(Tl)	3.67	Na 11 I 53	0.3	13%	Band centered at 4,200 Å
CsI(Tl)	4.51	Cs 55 I 53	1.1	~6%	from blue to red with maximum in red
CsI(Na)	4.51	Cs 55 I 53	0.65	~12%	band centered between 4,000 and 5,000 Å
CsF	3.59	Cs 55 F 9	0.005	~0.7%	band centered at 3,900 Å
CaI ₂ (Eu)	3.96	Ca 20 I 53	0.79	twice than NaI(Tl)	peak at 4,700 Å
CaI ₂	3.96	Ca 20 I 53	0.55	twice than NaI(Tl)	peak at 4,100 Å
CdWO ₄	7.9	Cd 48 W 74 O 8	6	~8%	peak at 5,300 Å
Plastic	1.2	H 1 C 6	~10 ⁻³	~2%	band centered between 3,800 and 4,500 Å

Table 5.2: Some properties of the main gamma-ray scintillators (after Adams and Gasparini, 1970)

Sodium Iodide, thallium activated (NaI(Tl)), is the most commonly used crystal. Its high density and high atomic number give rise to large absorption cross sections. But sodium iodide being hygroscopic, its crystal should not be exposed to moisture as this will result in a large drop in resolution. The main disadvantage of sodium iodide crystal is that it always contains potassium impurity, which may lead to an undesirable background.

Cesium Iodide, thallium activated (CsI(Tl)) crystals are probably the main alternative to sodium iodide crystals. They are non hygroscopic and their potassium content is much lower than that of sodium iodide. Also because they are less brittle and more plastic than sodium iodide, they can better withstand shocks and vibrations, as well as sudden temperature change than NaI(Tl). CsI(Na) crystals

have better scintillation characteristics than CsI(Tl). Its resolution is also better and it is particularly suited for measurements in environments with slightly above normal temperature because its maximum conversion efficiency is at about 80°C. It is hygroscopic and so must therefore be sealed against moisture as NaI(Tl).

Although Calcium Iodide (CaI_2) crystals and Europium activated Calcium Iodide ($\text{CaI}_2(\text{Eu})$) crystals have high conversion efficiency and a slightly higher photofraction than NaI(Tl), their use has been restricted by the fact that growth of large crystals has failed due to the formation of parallel cleavage cracks.

In spite of high gamma detection efficiency, CdWO_4 crystals are seldom used. A major disadvantage is their high index of refraction, resulting in a poor light coupling.

Plastic scintillators are less efficient than inorganic scintillators for gamma ray detection. Plastic scintillators made from organic scintillator dissolved in organic solvent, may be manufactured in various shapes and large sizes; hence they are used for anticoincidence annuli (see section 5.1.4).

For portable spectrometers, single cylindrical scintillation crystal with one photomultiplier tube (PMT) (see section 5.1.2.1) are normally used. But for an airborne system, arrays of large cylindrical scintillation detectors connected with several PMTs have been used. The number of PMTs however depends on the size of the arrays. A recent development in the airborne configuration is a prismatic configuration with a 4" X 4" square cross-section by 16"

long with a single PMT mounted on one end (Bristow, 1977a). This configuration leads to a compact package with an array of several detectors laid side by side to form a slab as shown in Fig 5.7. An

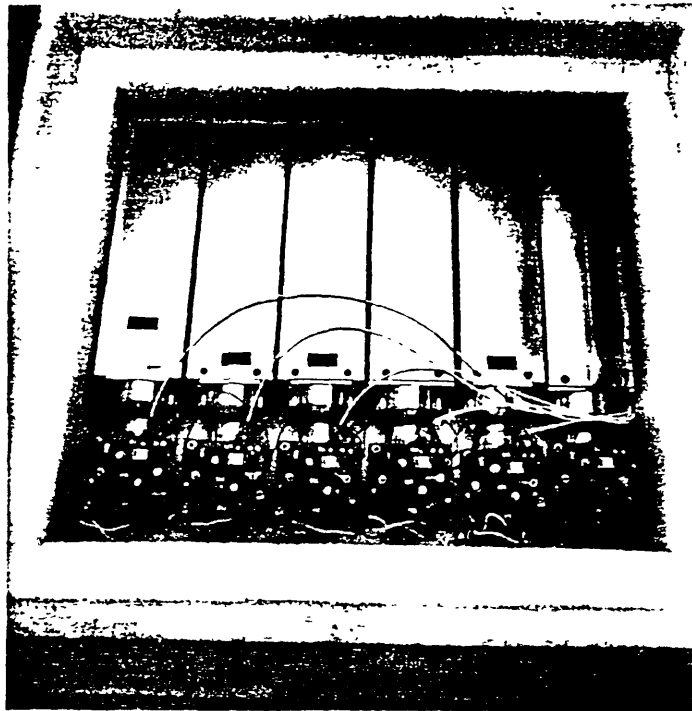


Fig.5.7 : Typical array of six 100 x 100 x 406 mm (4 x 4 x 16 inch) NaI detectors installed in a container designed to provide both thermal and electrical shielding. GSC 203492-k (after Bristow, 1977a)

improvement of this arrangement is the development of an actual slab-shaped detector of 11" x 11" x 4" with four PMTs mounted on the upper surface of the detector (Bristow, 1977a). Another type of scintillation detector is the Phoswich (phosphor sandwich) detector. The Phoswich detector is a combination of two non-similar scintillators optically coupled to a single PMT. This detector

distinguishes between the events that occur in one scintillator from those that occur in both scintillators. The principle of its operation is illustrated in Fig 5.8. In general sodium iodide and cesium iodide are often chosen as the two detector materials because

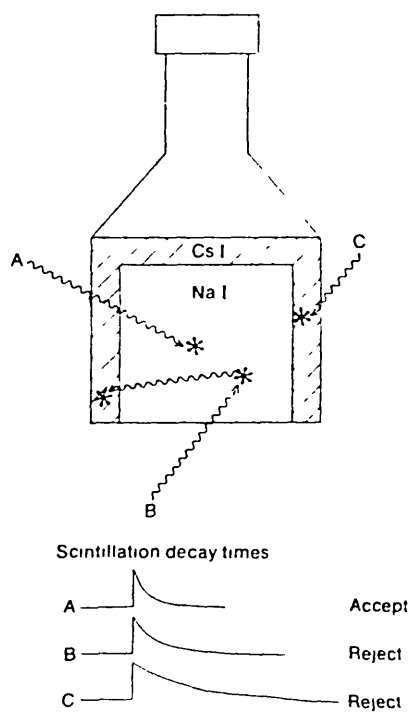


Fig. 5. 8: The PHOSWICH (phosphor-sandwich) Detector.
(after Bristow, 1977a)

their decay times are different by about 4:1 so that it is possible to differentiate between the photons which have been totally absorbed in only the sodium iodide, the main detector and those which have been

partially absorbed and scattered (absorbed by both sodium and cesium iodide detectors). This type of detector will have the advantage of reducing both background and the continuum. It should be noted that the principle and performance of this detector are equivalent to those of an anticoincidence spectrometer (see section 5.1.4).

5.1.2.1. Photomultiplier Tube (PMT)

Photomultiplier tubes are devices which convert the output charge pulses from a scintillation detector into a corresponding electrical signal before passing them to an amplifier for processing. Not only do PMTs convert the charge signals into electrical signals, they also increase the amplitudes of these signals. Hence a PMT may be regarded as a 'converter' and an amplifier for the scintillation detector signals. In its simplest form, a PMT consists of a semi-transparent photocathode connected to the detector crystal, dynodes and a collector electrode (anode). The photocathode material may be Cs-Sb alloys or K-Cs-Sb (bi-alkali). For the dynodes, materials such as Cs-Sb, Cs-Ag-Mg-O, GaA or GaP may be used. Fig 5.9 shows an arrangement of the basic elements of a PMT. The dynodes are maintained at increasing higher potentials of 100 to 200 volts towards the anode.

An incident photon on the photocathode causes the release of an electron which is then accelerated towards the first dynode. The collision of the electron with the first dynode results in the emission of secondary electrons of lower energies, which are in turn accelerated to the next dynode, where again further multiplication

takes place. In this way an avalanche of electrons is collected at the anode. Knoll(1979) stated that most PMTs perform this charge amplification in a very linear manner, producing an output pulse which is proportional to the number of the original photoelectrons over a wide range of amplitude like 10^6 .

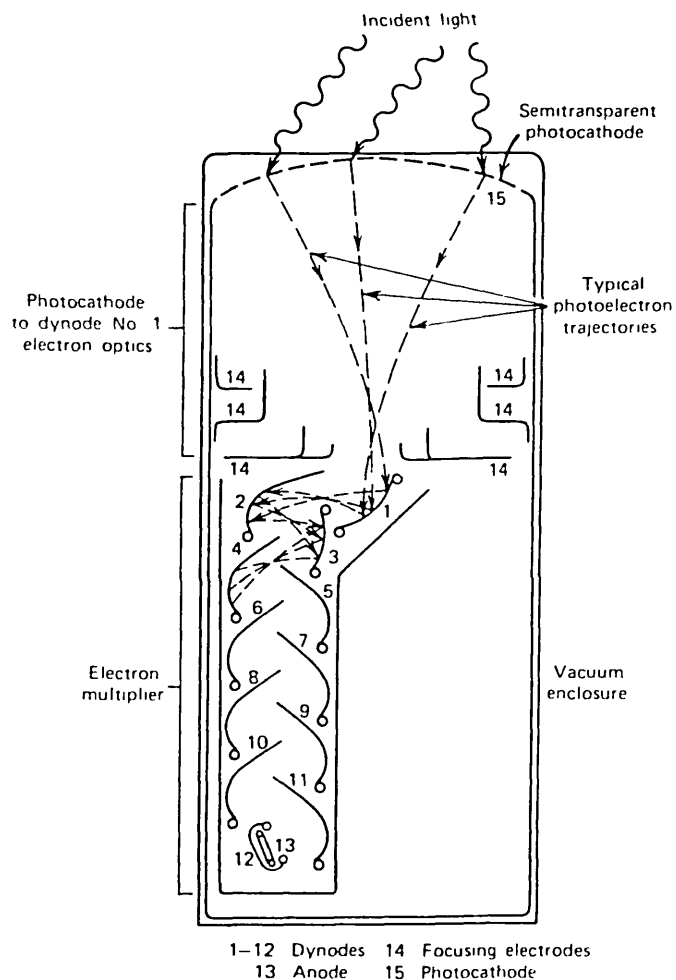


Fig.5.9 : Basic elements of a photomultiplier tube.
(after Knoll, 1979)

The geometry of a PMT must be such that the electric field at the dynode surface is such as to accelerate the secondary electrons away from the surface and onto the next dynode. The principal types and geometries of PMTs are shown in Fig 5.10. The focused types (a and b)

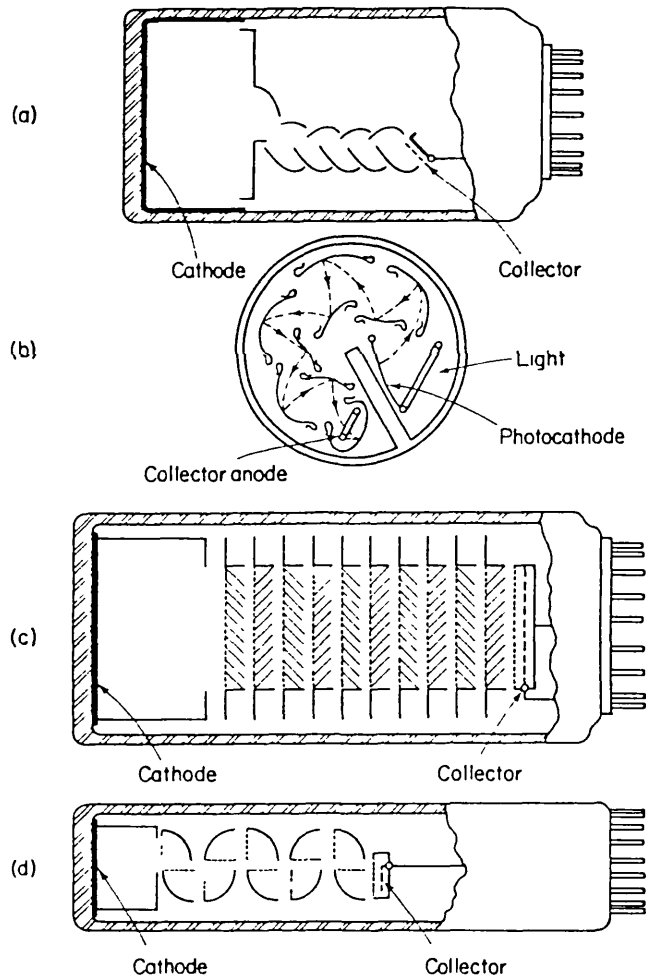


Fig. 5.10: Different photomultiplier tube geometries. (a) and (b) show two types of focused dynode arrangements, (c) the venetian blind geometry and (d) the box and grid arrangement (after Nicholson, 1974)

have smaller spread in electron transit time than the unfocused types (c and d). On the other hand, the larger areas of the unfocused types simplify the problem of efficient and uniform electron collection from the photocathode on to the first anode (Birks, 1964).

5.1.3. Semiconductor Detectors

At present the most exciting alternative to scintillation counters are semiconductor detectors. This is because they have high resolution, fast pulse rise time, compactness and high absorption coefficients. Their main disadvantage is the small sizes of the sensitive volume, resulting in low efficiency for gamma photons of intermediate and high energies. However, even with the present efficiency limitations, these detectors are very useful whenever a detailed study of a complex gamma ray spectrum of high source intensity is required, particularly in the laboratory.

The principle of semiconductor detectors is basically the collection of the electric charges released in a solid by the absorption of photons or charged particles.

Operational Principle Of Semiconductor Detectors

As mentioned in section 5.1.2, energy bands exist in semiconductors and the energy of any electron in these materials must be confined to one of these bands (see Fig 5.4). The probability of an electron being excited to an energy level E is given as

$$f(E) = 1/(1 + \exp(E_g/2kT)) \quad (5.2)$$

where

k is the Boltzmanns constant, and

T is the absolute temperature

If the energy gap E_g is very much greater than kT , the above expression reduces to

$$f(E) = \exp(-E_g/2kT) \quad (5.3)$$

The number of electrons N_e in the conduction band and the number of holes N_h in the valence band for an intrinsic semiconductor is given by

$$N_e = N_h = CT^{3/2} \exp(-E_g/2kT) \quad (5.4)$$

where

C is the proportionality constant which is characteristic of the material

This state of equilibrium is modified when impurities are present in the material. As in the case of the scintillators discussed above, these impurities introduce localized energy levels in the forbidden gap. Fig 5.11 shows the band structure and the processes which can occur in a semiconductor material containing impurities. These localized energy bands may become ionized either by donating an electron to the conduction band or by accepting one electron from the valence band. In either case the energy needed for the process will be less than the gap energy E_g . These levels are said to be 'donors' (n-type) if they donate electrons and 'acceptors' (p-type) when they accept electrons. They can act as traps at which electrons or holes

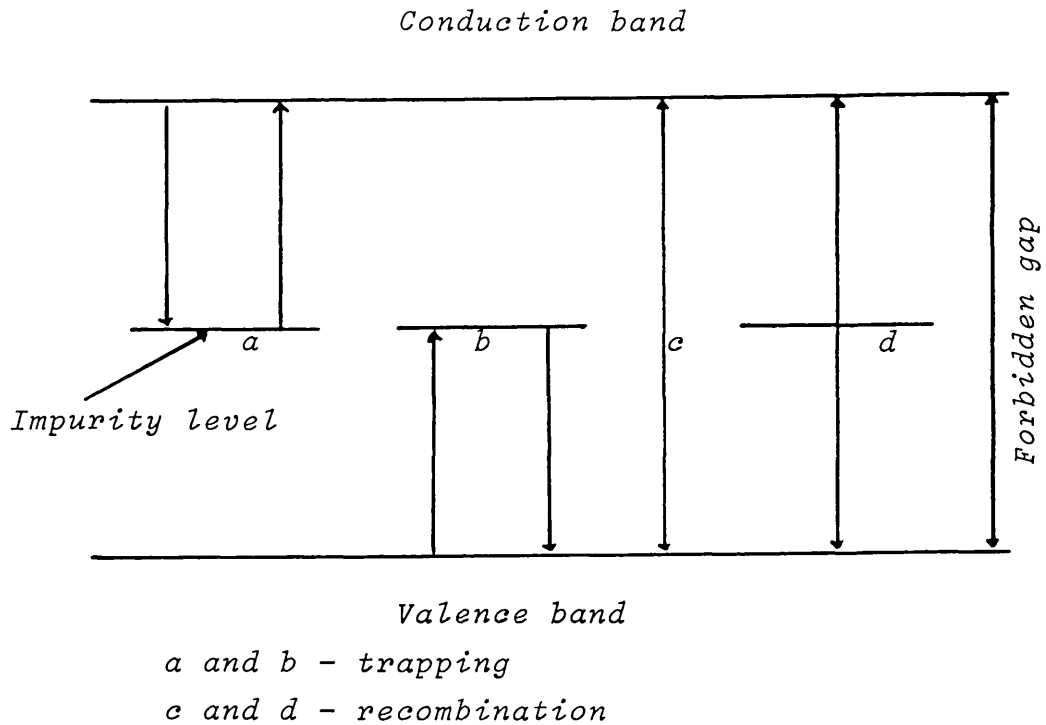


Fig.5.11: Band structure of a semiconductor material containing impurities

are temporarily held for sometimes before returning to the band where they again contribute to the conductivity. They can also act as sites where electrons and holes recombine, resulting in loss of energy. While donors have centres close to the conduction band, acceptors have their centres close to the valence band.

In practice materials used for semiconductor detectors always contain some amount of impurities. Hence a semiconductor spectrometer is regarded either as an n-type or p-type depending on whether the number of electrons produced by donors exceeds the number of holes produced by acceptors or vice versa. If the material corresponds to an n-type say, it is refined (or compensated) by the addition of an appropriate amount of an acceptor impurity so that the material then approximates closely to a pure material. Also if the number of donors

exceeds that of acceptors, the donors are then referred to as majority carrier while the acceptors are called minority carrier and vice versa.

Process Of Charge Collection

The process of charge collection for an 'ideal' semiconductor detector may be illustrated by a homogeneous block of material with a constant electric field passing through it. This is shown in Fig 5.12.

When an ionizing particle (or an electric field) passes through

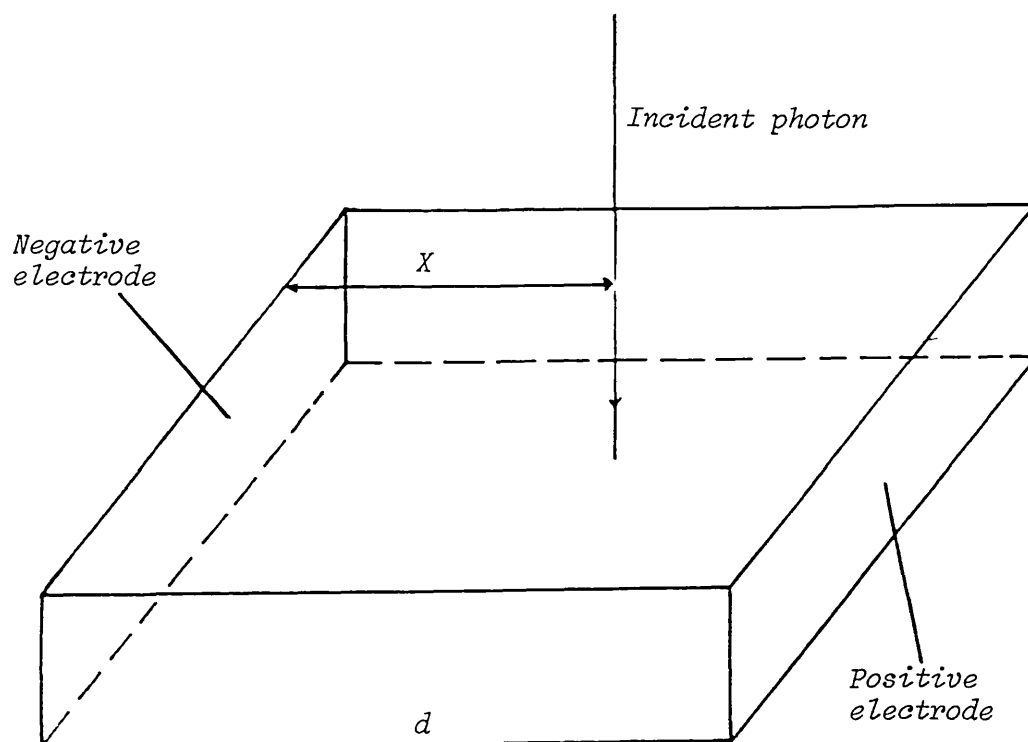


Fig.5.12: Charge collection in an ideal homogeneous crystal

the semiconductor crystal, a number of electrons and holes are created. These will undergo net migration with a net drift velocity parallel to the direction of the applied field. This velocity which is proportional to the applied field is given by

$$v = \mu E$$

where

μ is the mobility of an electron or hole

It should be noted that the mobility of an electron and hole differs from each other. The drift velocity increases slowly at very high fields until eventually a saturation velocity of approximately 10^7 cm/sec (Knoll, 1979) is reached and then becomes independent of further increases in the field. Semiconductor detectors can therefore be among the fastest responding of all radiation detector types.

The electron - hole pairs are separated by attraction to their appropriate electrodes and this movement of individual charges contributes to the current flow. This contribution is given by

$$dI = e\bar{v}/d$$

where

e is the electronic charge

\bar{v} is the velocity of carrier, and

d is the electrode separation

The total current flow between the electrodes, if the carrier completely traverses the detector, will be given by

$$I = \int_0^{d/\bar{v}} \frac{e\bar{v}}{d} dt = e \quad (5.5)$$

Hence if N electron-hole pairs are present, the total current reaching the electrode will be Ne.

The transit time of a carrier is given by

$$t_c = \frac{d}{v} = \frac{d}{\mu E} \quad (5.6)$$

For a charge to be counted, its half-life must be in the same order as its transit time. From the above expressions, it follows that if the incident radiation is at a distance X from the negative electrode, the current contribution by the hole at the negative electrode will be

$$I_H = \frac{NeX}{d} \quad \text{in time } t_c = \frac{X}{\mu_H E} \quad (5.7)$$

and the electrons' contribution at the anode will be

$$I_E = \frac{Ne(d - X)}{d} \quad \text{in time } t_c = \frac{d - X}{\mu_E E} \quad (5.8)$$

where

μ_H is the mobility of a hole, and

μ_E is the mobility of an electron

As mentioned previously, materials used for semiconductor

spectrometers are never ideal and the presence of impurities and/or crystal lattice defects causes trapping and recombination of electrons and holes. These processes affect the amount of current reaching the electrodes and the collection time.

Recombination Effect

Recombination is said to occur when an electron re-unites with a hole and the pair disappears. Hence recombination reduces the amount of current reaching the electrodes, whatever the collection time.

Trapping Effect

Trapping is the process whereby an electron (or hole) is held at an impurity centre and after sometime released into the band where it again contributes to the current flow. When this happens the collection time of the charges is increased; and it is given by

$$t'_C = \left(\frac{t_1 + t_2}{t_1} \right) t_C \quad (5.9)$$

where

t_1 is the mean time spent outside traps, and

t_2 is the mean time spent in traps

Trapping could be of two types, depending whether t'_C is less or greater than the dielectric relaxation time of the detector. The relaxation time is given by

$$\tau = \frac{\rho x}{4\pi} \quad (5.10)$$

where

ρ is the resistivity, and

x is the dielectric constant of the semiconductor

The dielectric relaxation time of the detector is the time constant of the exponential reversion to electrical neutrality after a small disturbance of its equilibrium state.

Short Term Trapping ($t_c' < \tau$)

Although this permits complete collection of charges, the pulse height may be distorted as can be seen in Fig 5.13(11).

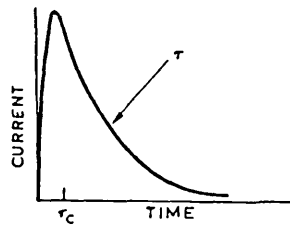
Long Term Trapping ($t_c' > \tau$)

This causes pulse amplification and causes successive events to produce overlapping signals (see Fig 5.13(111)).

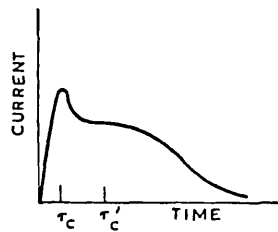
Detector Properties

The properties required for a semiconductor detector material may be listed as follows:

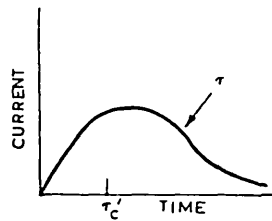
- (i) high atomic number (Z) to give a good photoelectric cross section for gamma rays
- (ii) small energy gap E_g to give a large number of electron-hole pairs



(a)

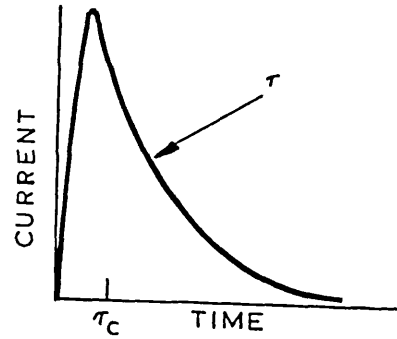


(b)

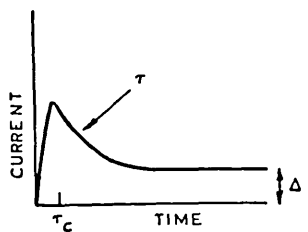


(c)

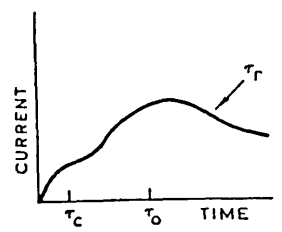
(ii): Current pulses when one carrier is trapped (short term trapping)



(i): Current pulse with complete charge collection (no trapping)



(a)



(b)

(iii): Current pulses with charge amplification due to trapping (long term trapping)

Fig. 5.13: Effects of trapping (after Dearnaley and Northrop, 1966)

- (iii) low carrier density to minimize current noise. This requirement is however incompatible with (ii).
- (iv) high carrier mobilities to give short pulse rise times
- (v) long carrier lifetimes to permit efficient collection of charges, and
- (vi) freedom from traps to give short pulse rise times and in addition to reduce loss of signal, pulse distortion and amplification

The materials that are almost exclusively used currently are silicon and germanium, since it is only with these material that an adequate technology for purification is available (Nicholson, 1974).

Lithium Drifted Detectors

Ion-drifting is the process whereby semiconductor detectors can be fabricated with large active (sensitive) volumes. Theoretically this involves creating a thick region of compensated material in which the number of acceptors is exactly balanced by the number of donors. But in practice, because 'perfect' compensation is difficult to achieve, the compensated material always turns out to be either n- or p- type. It is reported that the present germanium material tends to be p- type mainly because of the presence of boron impurity. Hence donor atoms must be added to the material to accomplish the desired compensation. It has also been reported that out of the alkali metals which tend to form interstitial donors in crystals of germanium (or silicon), only lithium can be introduced into germanium (or silicon) in sufficient

concentration to serve as a compensating impurity.

Ge(Li) detectors have two basic configurations - planar and coaxial. The planar Ge(Li) detector consists of either circular or rectangular cross-section of germanium with a lithium drifted region. The rectangular planar configuration of a lithium-drifted semiconductor detector is shown in Fig 5.14. In the planar configuration, lithium is drifted into one of the surfaces. The

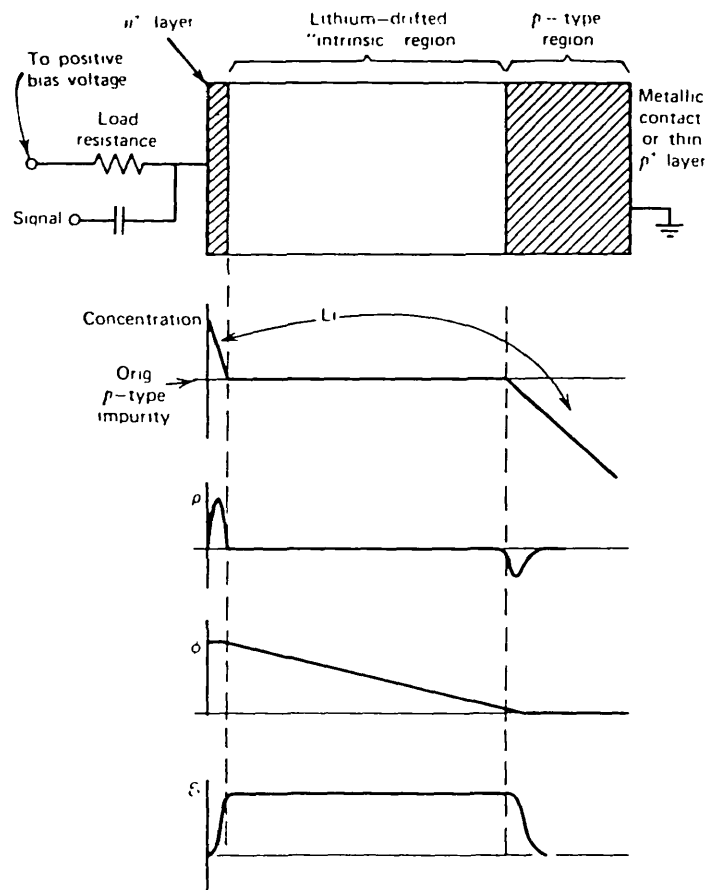


Fig. 5.14: Basic configuration of a lithium-drifted p-i-n junction detector. Also shown are the corresponding profiles for impurity concentration, charge density ρ , electric potential ϕ , and electric field E . (after Knoll, 1979)

excess lithium at the surface from which the drift started, converts that surface into an n - layer. The non-compensated p - region at the opposite side is often given a metallic coating which acts as an ohmic contact. Across the intrinsic region (also called compensated region, depletion or drift depth), the applied electric field is uniform because ideally, no net charge exists in this region. Also because the resistivity of the compensated material is much higher than either the p- or n- region, virtually all the applied voltage appears across the i-region and drops sharply to zero at its boundaries. Therefore the dimensions of the i-region determine the active volume of the detector, and the migration of the charge carriers to the p - i and i - n boundaries gives rise to the basic signal pulse.

At room temperature, the lithium ion mobility is high enough to permit redistribution of the lithium from the compensated region. Thus in order to prevent this and also to reduce the detector noise, lithium-drifted germanium (Ge(Li)) detectors must be stored and operated at low temperatures, usually that of liquid nitrogen (77°K). The leakage currents are also sensitive to surface conditions and so the detector must be cooled under vacuum. Silicon lithium drifted (Si(Li)) detectors are less sensitive to temperature but optimum performances are obtained when they are operated at very low temperatures. Table 5.3 summarizes the main characteristics of both silicon and germanium. Ge(Li) detector which has a very high resolving power, of the order of 50 to 80 times that of NaI(Tl), and higher absorption coefficient than Si(Li) is better suited for gamma ray spectroscopy than Si(Li) which is restricted to intermediate and

low energy X-ray spectroscopy.

In practice the thickness of the intrinsic region of planar Ge(Li) detectors is limited to about 20mm beyond which the drifting process is no longer possible (Steyn, 1973; Knoll, 1979). The coaxial Ge(Li)

	Si	Ge
Atomic number	14	32
Atomic weight	28.06	72.60
Density (300 K)	2.33 g/cm ³	5.33 g/cm ³
Dielectric constant	12	16
Energy gap (300 K)	1.106 eV	0.67 eV
Energy gap (T K)	$1.205 - 2.8 \times 10^{-4} T$ eV	$0.782 - 3.4 \times 10^{-4} T$ eV
Electron mobility (300 K)	1,350 cm ² /Vsec	3,900 cm ² /Vsec
Hole mobility (300 K)	480 cm ² /Vsec	1,900 cm ² /Vsec
Electron mobility (T K)	$2.1 \times 10^9 T^{-2.5}$ cm ² /Vsec	$4.9 \times 10^7 T^{-1.88}$ cm ² /Vsec
Hole mobility (T K)	$2.3 \times 10^9 T^{-2.7}$ cm ² /Vsec	$1.05 \times 10^7 T^{-2.11}$ cm ² /Vsec
Energy per hole-electron pair	3.66 eV	2.96 eV
Intrinsic carrier density (300 K)	1.5×10^{10} /cm ³	2.4×10^{14} /cm ³
Intrinsic carrier density (T K)	$2.8 \times 10^{16} T^{1.45}$ /cm ³	$9.7 \times 10^{15} T^{1.45}$ /cm ³

* Measured only over a limited temperature range (about 100-300 K for Ge and 160-400 K for Si)

Table 5.3: Some properties of silicon and germanium (after Adams and Gasparini, 1970)

detectors are of much larger active volume than the planar type, sometimes active volume of up to 150cm³ (Knoll, 1979). The coaxial types are either double- (or open-) ended or single- (or closed-) ended. In the double-ended coaxial Ge(Li) detector, lithium compensation is achieved by drifting lithium radially from the side surface towards the centre of the germanium crystal and as a result, a p-type core is left along the entire axis. In the single-ended case, lithium is drifted, in addition to radial drifting, along the axis from one end surface, and the end result is a U-shaped p-core along the axis of the crystal. Coaxial types of Ge(Li) detectors are shown in Fig 5.15. While Fig 5.15a shows coaxial cylindrical types,

Fig 5.15b shows coaxial trapezoidal types (Knoll,1979). The well-type detector is a single-ended type with the central core removed. This type of detector in general offers high relative counting efficiency,

DOUBLE OPEN-ENDED

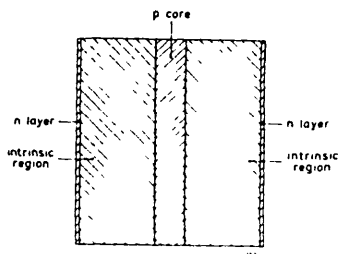
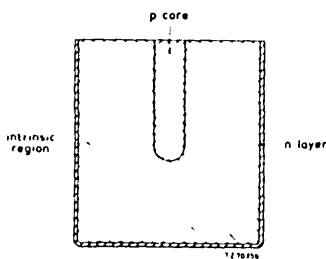
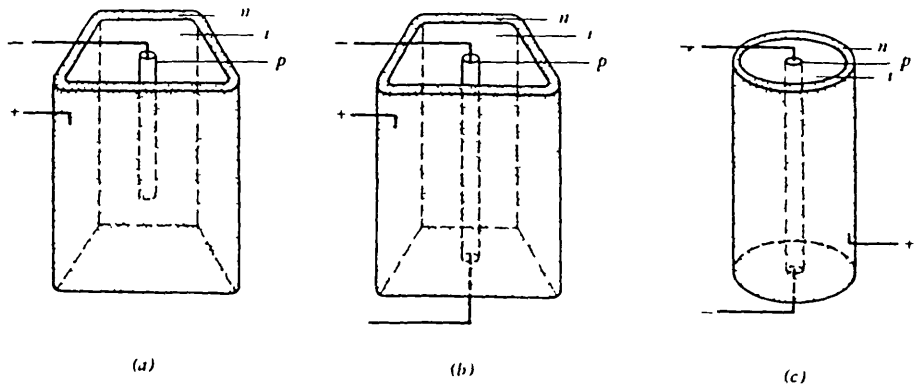
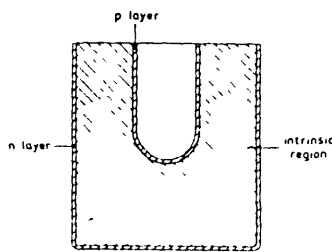


Fig.5.15: Drifted detector configurations

SINGLE OPEN-ENDED



WELL-TYPE



- (a) Single-ended trapezoidal
- (b) Open-ended trapezoidal
- (c) Open-ended cylindrical or "true coaxial."

(i) after Philips, 1975 (ii) after Knoll, 1979

particularly for low-energy gamma rays, for sources placed within the well probably because of its approximate 4π geometry.

In general, although semiconductor detectors have high resolution, their output signal is comparatively very small. Hence a preamplifier with a low noise input stage is required for the signal processing. Currently the field-effect transistor (FET) preamplifier is universally

accepted as having such property. But an optimum performance is obtained from an FET if it is cooled and located close to the detector. Therefore it may be convenient to locate both the detector and the FET in the same enclosure (Adams and Gasparini, 1970).

5.1.4. Coincidence and Anticoincidence Spectrometry

Ideally the response of an infinitely large gamma ray detector will be a well-resolved peak with no associated continuum as is shown in Fig 5.16. But in practice this situation is different owing to the

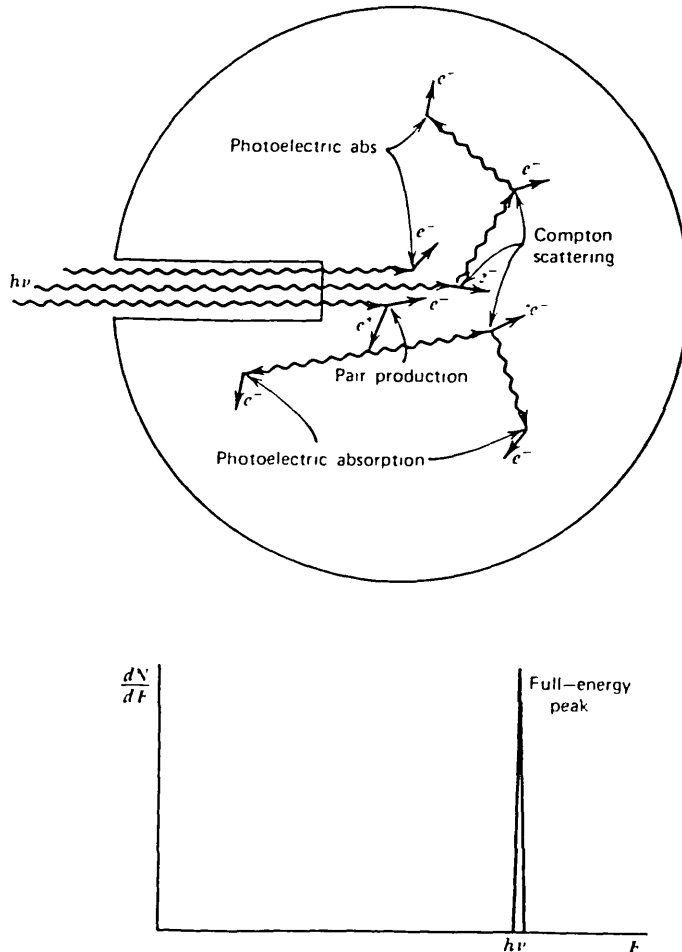


Fig. 5.16 : The “large detector” extreme in gamma ray spectroscopy. All gamma ray photons, no matter how complex their mode of interaction, ultimately deposit all their energy in the detector. Some representative histories are shown at the top.
(after Knoll, 1979)

presence of secondary radiation which might escape from the detector (undetected) because of its finite nature. Also secondary radiation may be produced by the interaction of gamma rays with the materials surrounding the detector. The net effect of these secondary radiations is the production of a spectrum with prominent continua which may obscure low intensity peaks from other gamma ray energies (see Fig 5.17). In order to approach the ideal situation several methods of coincidence and anticoincidence spectrometry are applied. These methods involve the use of two or more detectors of similar or different materials and using coincidence techniques to preferentially select those events that correspond to full-energy absorption. Some of such methods are:

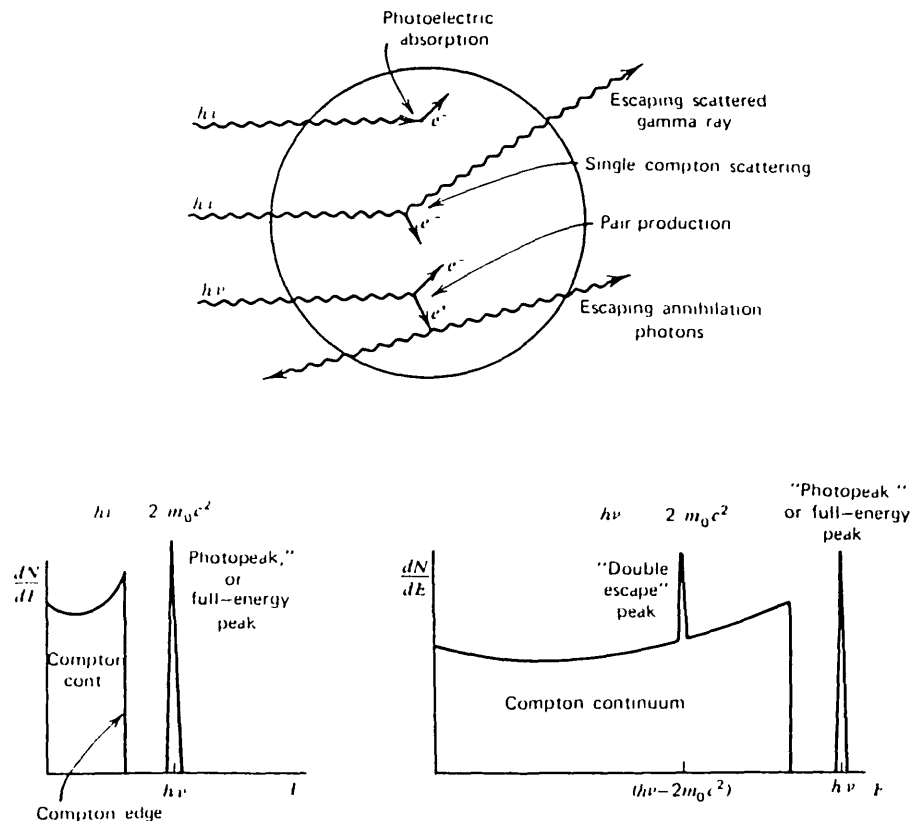


Fig. 5.17. : The "small detector" extreme in gamma ray spectroscopy. The processes of photoelectric absorption and single Compton scattering give rise to the low-energy spectrum at the left. At higher energies, the pair production process adds a "double escape" peak shown in the spectrum at the right. (after Knoll, 1979)

(1) Anticoincidence Shielded Spectrometer

This involves surrounding a primary detector with an annular detector in anticoincidence. In this arrangement, most gamma rays which escape from the primary detector are detected by the annular detector, thus leading to the rejection of these photons. Practically large sodium iodide crystals have been surrounded by sodium or plastic annulus. Signals detected in the annulus originate primarily from background radiation and from degraded gamma rays scattered out of the central (primary) NaI crystal. The signals detected by the annulus are subtracted from those detected by the central crystal; hence by this arrangement reduction of the background and of the continuum could be achieved as shown in Fig 5.18.

The disadvantage of this method becomes obvious when a source with a complex decay scheme is analyzed. From such a source, many gamma

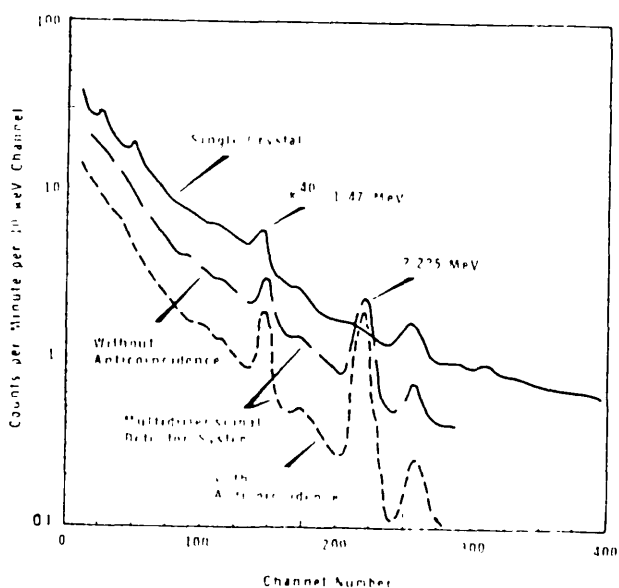


Fig. 5.18: Effect of plastic phosphor shielding on the background of a single 11" in dia \times 6" thick crystal detector system located in a 4" thick lead shield

(after Wogdan et al, 1967)

rays can be emitted in coincidence and it is possible they interact in both detectors. Such events will therefore be rejected, thus leading to unwanted suppression of some full-energy peaks.

An improved version of this method has been used by Wogman et al (1967) where two principal NaI(Tl) detectors are enclosed in plastic phosphor which serves as an anticoincidence shield. A fourth detector, called backscatter detector, is placed between the two principal detectors (see Fig 5.19). This fourth detector, which is optional,

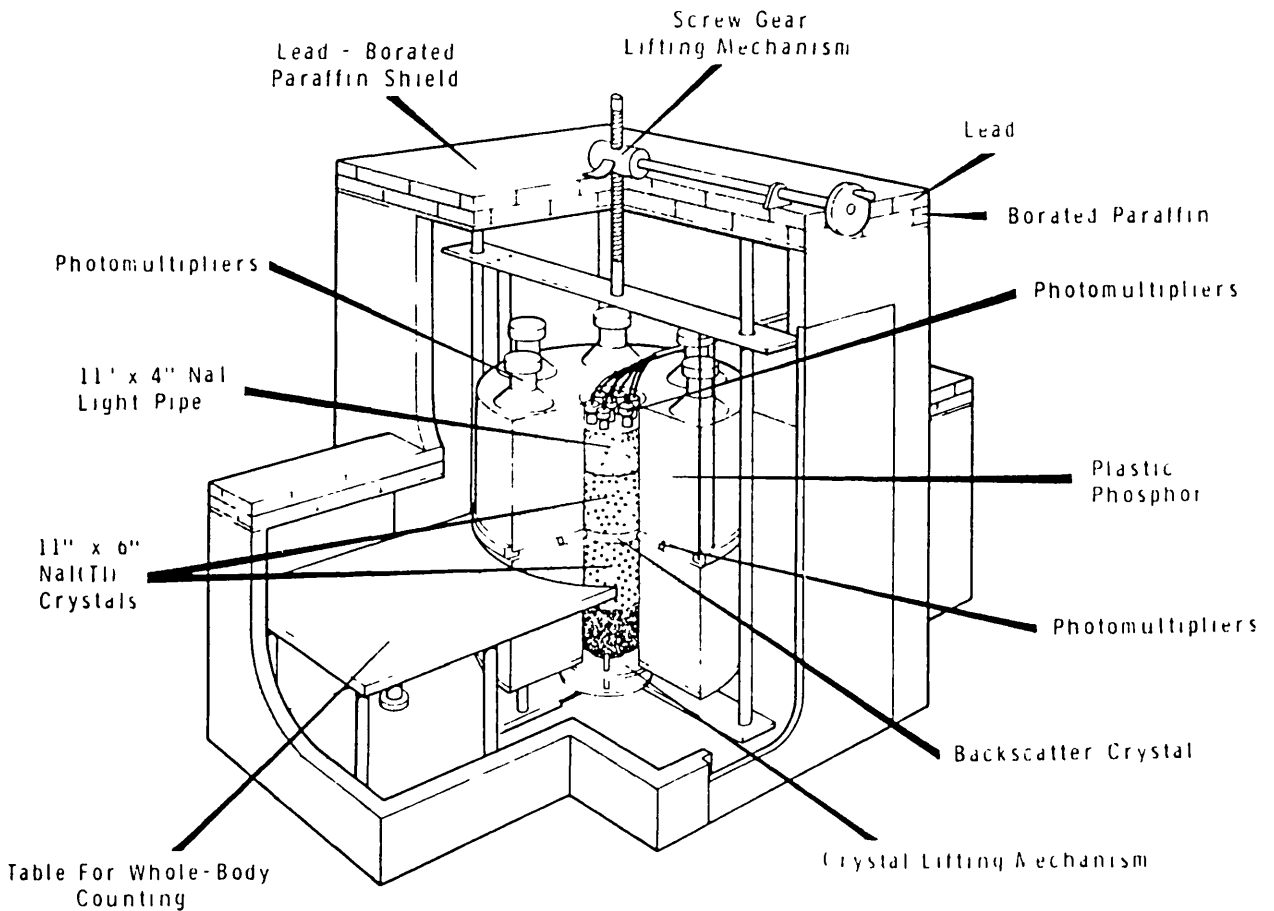


Fig. 5.19: Large crystal multidimensional gamma-ray spectrometer system

(after Wogman et al, 1967)

eliminates much of the systems' backscatter response where small sources are being counted. The sample to be analyzed is placed in the hole of the backscatter detector. Gamma rays which are scattered from the two principal detectors have a high probability of being detected by either the plastic phosphor annulus or by the backscatter detector and thus resulting in the rejection of that particular event. Although this detector arrangement has high counting efficiency, lower Compton and background response, it is not suitable for field surveys.

(ii) Compton Spectrometer

Fig 5.20 shows a schematic diagram of a Compton spectrometer. When the collimated beam of gamma rays from the source strikes the first detector A, some fraction of the scattered gamma ray will travel to the second detector B, where it may also interact to give a second pulse. Because the distance between the two detectors is very small, the pulse will essentially be in time coincidence. Thus by selectively recording only those pulses from the first detector that are in coincidence with a pulse from the second detector, the recorded

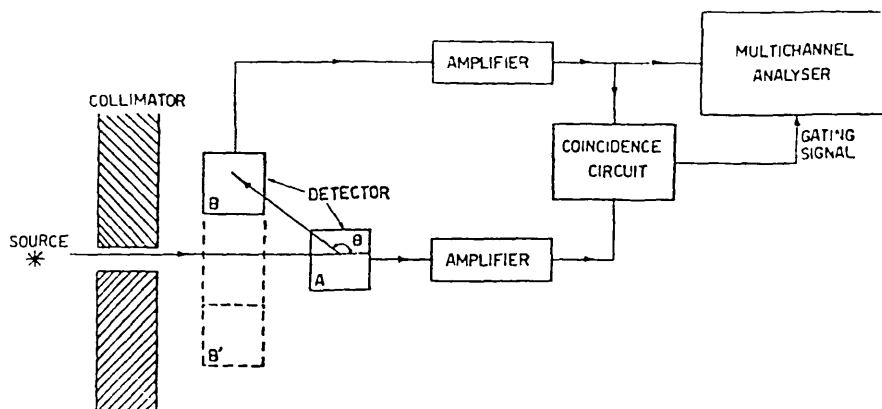


Fig. 5.20 : Schematic of Compton spectrometer.
(after Adams and Dams, 1977)

spectrum will contain only single Compton scattering events. Because the angle of scattering is fixed, a constant amount of energy is deposited for each interaction involving monoenergetic incident gamma rays. Photoelectric and all other events which do not lead to coincidence between the two detectors are also excluded.

(iii) Pair Spectrometer

This is essentially a high energy gamma ray spectrometer. It consists of a central detector surrounded by two other detectors as illustrated in Fig 5.21. The signal of the central detector is analyzed only when there are simultaneous signals from the two other detectors in

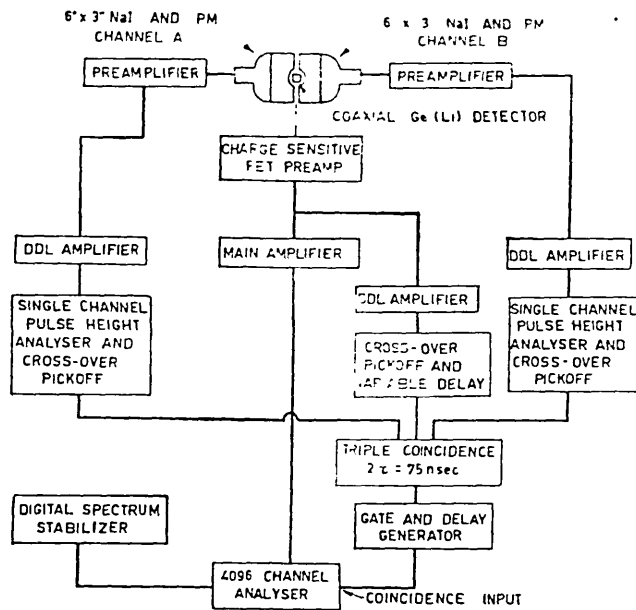


Fig. 5.21: Schematic diagram of a pair spectrometer (after Adams and Dams, 1977)

coincidence. This condition can only be met by pair production process and the detection of the two annihilation photons. Thus the energy measured is 1.022MeV less than the energy of the incident gamma

ray. This method will thus suppress most of the continuum including the background as well as the full-energy peak. Fig 5.22 shows the

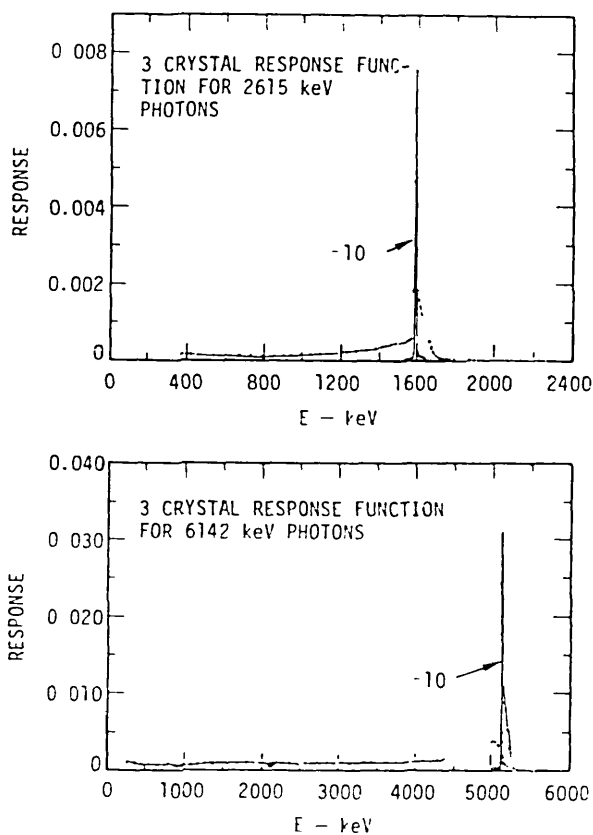


Fig. 5.22: Response functions of a Ge(Li) crystal operated as a pair spectrometer in conjunction with two NaI(Tl) detectors. (after Knoll, 1979)

response function obtained from a pair spectrometer. Further improvement on the performance (response function) can be obtained by using pulse shaping functions (see section 5.2.2.1.) to remove the slow rising pulses from interactions near the edges of the central detector as demonstrated by Robertson et al (1975).

5.2. Amplifying Section

This section consists of preamplifiers and amplifiers. The aim here is to amplify and shape the pulses from the detector before passing them on to the analyzer.

5.2.1. Preamplifiers

Detectors in general have one common characteristic of generating small pulses in the process of detecting events. The main purpose of the preamplifier is thus to amplify these weak pulses generated by the detectors. Fig 5.23 shows the diagram of a typical preamplifier.

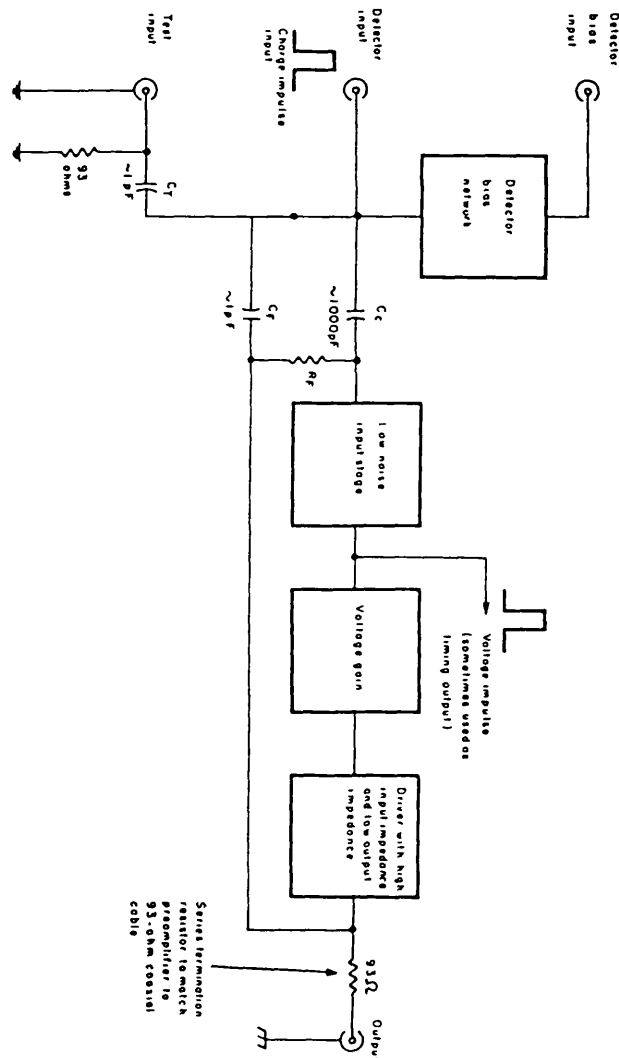


Fig. 5.23: Typical preamplifier block diagram (after Ayers, 1973)

There are three basic types of preamplifiers - current-, voltage- and charge- sensitive types. The type of preamplifier required depends on the type of detector used. For instance, in some detectors, such as the scintillation and GM counters, considerable signal amplification occurs before the signal emerges from the detector and in such a case, the role of the preamplifier is reduced to that of signal pulse shaping (see section 5.2.2.1.). Other types of detectors like the semiconductor and proportional counters, give small signal output that a preamplifier is required for its amplification. The preamplifier is usually located as closely as possible to the detector in order to minimize the signal - to - noise ratio. Thus it is advisable to avoid the use of long interconnecting cables between the detector and the preamplifier.

Of the three types of preamplifiers, the current-sensitive type which is generally used with signal sources of low output impedance, is rarely used (Ayers, 1973; Nicholson, 1974). It is used only when the energy resolution is not determined by the signal - to - noise ratio of the preamplifier (Fairstein and Hahn, 1965).

5.2.1.1. Voltage - Sensitive Preamplifier

Fig 5.24 shows a schematic diagram of a voltage - sensitive preamplifier configuration. This system amplifies any voltage pulse at its input to provide an output voltage larger than its input by its gain factor A. The amplitude of the input pulse is given by

$$V_I = Q/C \quad (5.11)$$

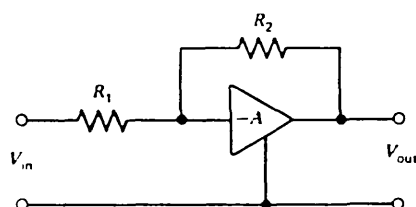
where

Q is the signal charge

C is the input capacitance, and

A the gain of the preamplifier is assumed to be very much greater than R_2/R_1 ($A \gg R_2/R_1$).

$$V_{\max} = \frac{Q}{C}$$



Assume $A \gg R_2/R_1$

$$V_{\text{out}} \cong -\frac{R_2}{R_1} V_{\text{in}}$$

Fig. 5. 24: Schematic diagram of a simplified voltage sensitive preamplifier configuration. R_2 is the feedback resistance. (after Knoll, 1979)

It should be noted that equation 5.11 is true if the time constant (the parallel combination of the input resistance R and the capacitance C) is large compared to the charge collection time of the detector and the input capacitance C is stable (Ayers, 1973; Knoll, 1979). Thus since semiconductor detector capacitance is dependent on its bias voltage (Nicholson, 1974), the capacitance of the detector will fluctuate with temperature changes (Ayers, 1973). Hence it is not desirable to use a voltage - sensitive preamplifier following a semiconductor detector, especially when it is subjected to temperature fluctuations.

5.2.1.2. Charge - Sensitive Preamplifiers

A simplified diagram of a charge - sensitive preamplifier is shown in Fig 5.25. The effective input voltage V_{in} to the preamplifier is

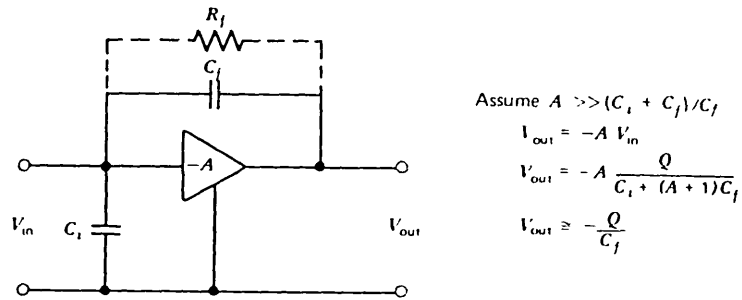


Fig. 5.25 : Simplified diagram of a charge-sensitive preamplifier configuration. If the conditions indicated are met, the output pulse amplitude becomes independent of the input capacitance C_i . The time constant given by the product $R_f C_f$ determines the decay rate of the tail of the output pulse. (after Knoll, 1979)

given by

$$V_{in} = \frac{Q}{C_D + C_f(1+A)} \quad (5.12)$$

where

$C_f(1+A)$ is the effective input capacitance obtained by placing C across the preamplifier

Q is the charge from the detector

C_D is the total capacitance associated with the detector, preamplifier and cables

C_f is the feedback capacitance, and

$-A$ is the gain of the preamplifier.

If $C_f A \gg (C_D + C_f)$, then equation 5.12 reduces to

$$V_{in} = \frac{Q}{C_f A} \quad (5.13)$$

Hence the output voltage V_{out} given by

$$V_{out} = -AV_{in} = -Q/C_f \quad (5.14)$$

is independent of the input capacitance. Hence changes in the input capacitance no longer have an appreciable effect on the output voltage as they do in the case of the voltage - sensitive preamplifier. Thus this type of preamplifier is the type most suitable for semiconductor detectors. However it is also used with other types of detectors such as scintillation, proportional and GM counters, in which the capacitance does not necessarily change (Knoll, 1979).

5.2.2. Amplifiers

In signal processing, nuclear amplifiers have two basic functions of amplitude amplification and pulse shaping. The tail input pulse from the preamplifier has an amplitude of a few tens or hundreds of millivolts and this is too small to be directly counted by the analyzer (see section 5.3). The main amplifier is thus required to reshape the pulse and provide a continuously adjustable gain over a wide range so that low energy as well as high energy spectrum can be made to give full scale output in a spectrum analyzer. The overall gain obtainable from an amplifier could be between 1000 to 2000. The shaping of the pulse is necessary in order to remove pile-up effect

(see section 5.4), especially at high count rates. Shaping also helps to optimize signal - to - noise ratio, although some shaping requirements for high count rate performance may conflict with the best signal - to - noise ratio requirements (Hatch, 1973; Knoll, 1979).

5.2.2.1. Shaping Of Pulse

This is the most important function of the amplifier, since it is required that the signal pulse presented to the counting system (analyzer) has a pulse height which is proportional to the charge collected by the detector. The effect of pulse shaping is illustrated in Fig 5.26. For Fig 5.26b the pulses have been shaped so that their total length is reduced but in a way that does not affect the maximum

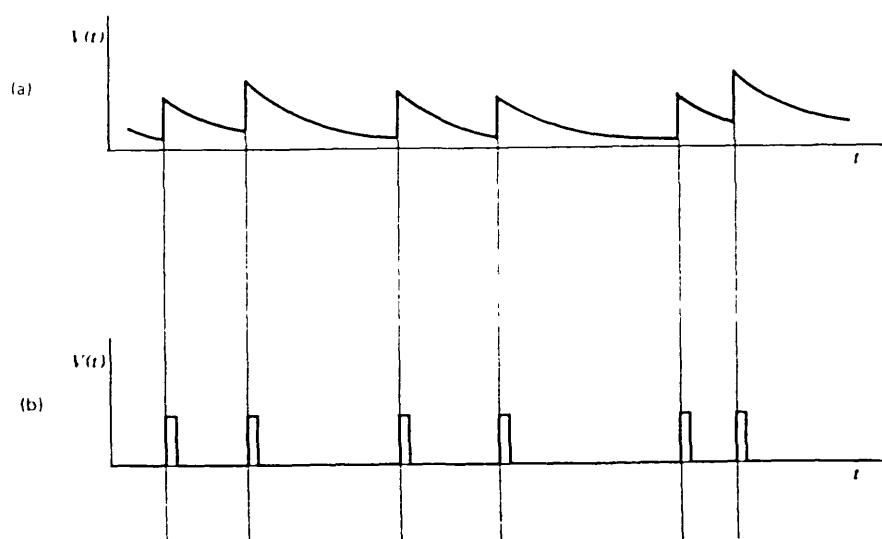


Fig. 5.26: The pulses with long tails shown in part (a) illustrate the apparent variation in amplitude due to pulse pile-up. These effects can be greatly reduced by shaping the pulses as in part (b). (after Knoll, 1979)

amplitude that carries the basic information. The methods employed in pulse shaping include

- (1) CR - RC (Differentiator - Integrator)
- (ii) $(CR)^2$ - RC (Double differentiation)
- (iii) Delay line
- (iv) Delay line and Integrator, and
- (v) Semi-Gaussian Or CR - $(RC)^n$

Detailed discussion of these shaping methods, their individual advantages and limitations can be found in several texts including Nicholson (1974) and Knoll (1979).

5.2.2.2. Pole - Zero Cancellation

It is assumed that the input pulse from the preamplifier to the main amplifier is a voltage step function. But because the decay of the preamplifier pulse is finite, this will give rise to a pulse with an undershoot (or zero crossover) when it is passed through a basic CR - RC circuit (see Fig 5.27). This will then recover back to zero with a time characteristic of the preamplifier decay time. Since preamplifiers have long decay times (of the order of $50\mu s$), the undershoot will persist for a relatively long time and if another pulse arrives during this period, it will be superimposed on the undershoot. This may result in baseline suppression, especially during high count rates. This problem of undershoot which is associated with most unipolar shaping methods (Nicholson, 1974) can be solved by a technique known as pole - zero cancellation where an

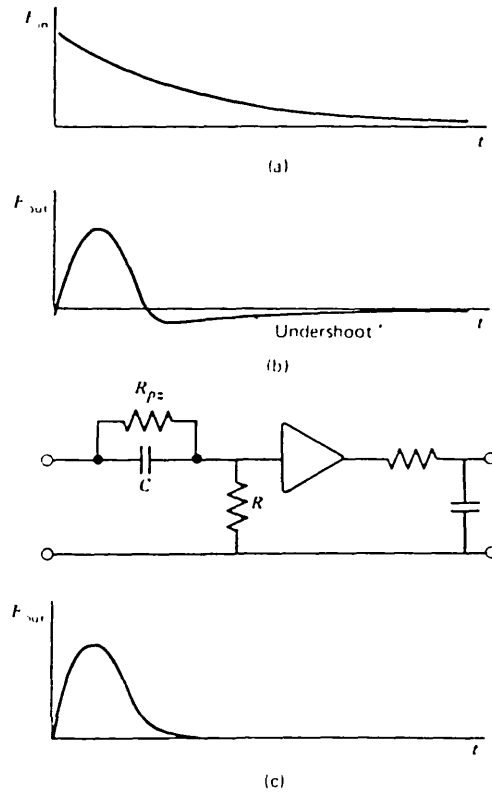


Fig. 5.27: Application of pole-zero cancellation to eliminate the undershoot (plot *b*) normally generated by a *CR-RC* shaping network for an input step with finite decay time. By adding an appropriate resistance R_{pz} to the differentiator stage, a waveform without undershoot (plot *c*) can be obtained. (after Knoll, 1979)

output pulse is stored without an undershoot. This is done by adding a large resistor R in parallel with the capacitor of CR . The effect of the resistor R is to create a zero in the filter which thus cancels one of the poles of the input circuit, resulting in an exponential decay function for a step input. A proper choice for the value of R depends on the value of the input decay time from the amplifier in use (Knoll, 1979).

5.2.2.3. Baseline Shift

Here a baseline is defined as the datum from which pulse heights are measured. The baseline may shift up or down depending on the shape, polarity and count rate of the pulses. Fig 5.28 shows rectangular pulses obtained from CR - RC shaping function. The baseline on which these rectangular pulses are superimposed is suppressed below the true zero level such that the areas enclosed by the output waveform above and below the zero axis are equal. The amount by which this apparent baseline is depressed below the true zero is called the baseline shift. The baseline is chosen at true zero dc (direct current) voltage. Hence ideally the coupling between amplifier stages should have a frequency response going down to dc. A baseline shift results in an analyzer registering a pulse height which is different from the true height.

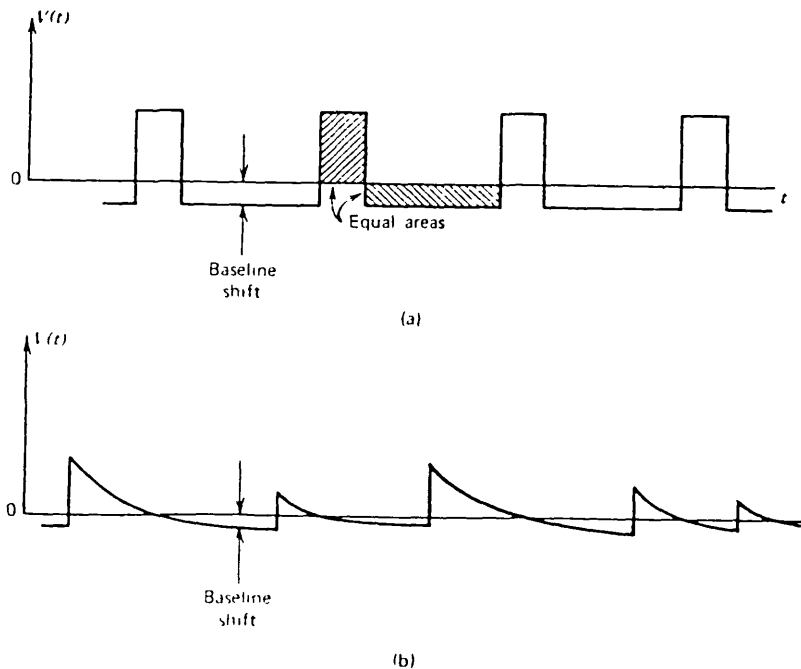


Fig. 5. 28. : Illustrating baseline shift which must take place in ac-coupled circuits. In part (a) uniform and regular pulses lead to fixed baseline shift, but the random pulses of part (b) give rise to variable shift. (after Knoll, 1979)

5.3. Counting Section

The amount of charges (or photons) incident on a detector, after amplification and shaping, has to be sorted and counted according to the energies of the charges. The sorting and counting device, called pulse height analyzer, is constructed in two basic modes - integral and differential modes.

In the integral mode, the signal is classified into a class having only a selected lower energy limit E say. Thus all signals with energies equal to or greater than E are counted. The number of counts N may be defined as

$$N = f(E) \tag{5.15}$$

In the differential mode, the signal is classified into relatively narrower class (called window or channel) having a lower limit E and an upper limit $E + \Delta E$. Only signals whose energies fall within the interval ΔE are therefore counted. The distribution of the counts in this case may be represented by

$$\frac{dN}{dE} = f'(E) \tag{5.16a}$$

or

$$N = f(E+\Delta E) - f(E) \tag{5.16b}$$

An analyzer defined in either of these ways is referred to as a single channel analyzer (SCA). Obtaining the spectrum with a single channel analyzer thus involves changing the value of E , that is, moving the channel along the spectrum as illustrated in Fig 5.29a and the

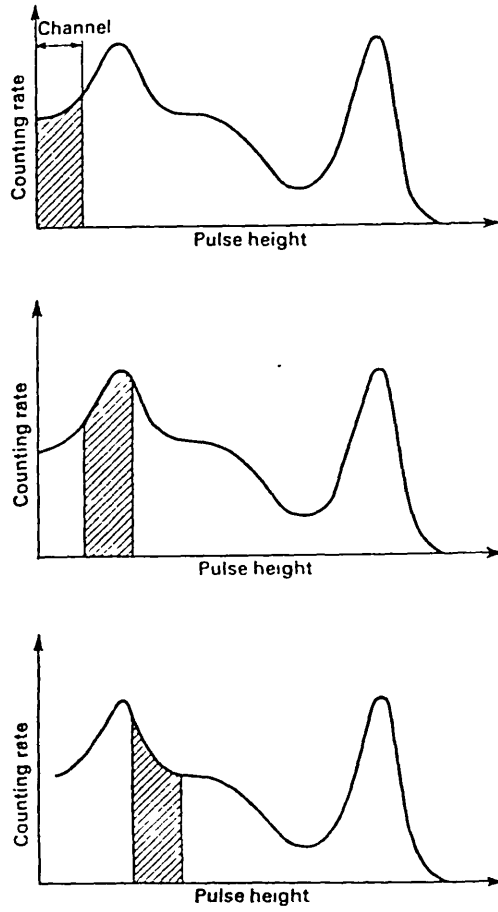


Fig. 5.29a: Principle of taking spectrograms with aid of single-channel spectrometer by shifting channel along spectrum (after Scharf and Lisieski, 1980)

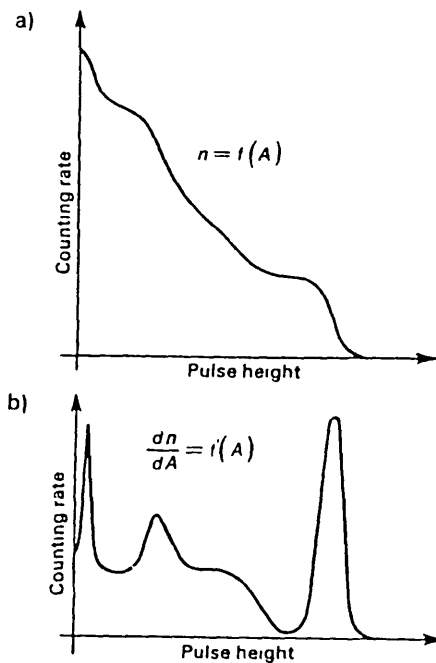


Fig. 5.29b : Amplitude distribution of pulse spectrum: (a) integral spectrum, and (b) differential spectrum. (after Scharf and Lisieski, 1980)

resultant count distribution will be as shown in Fig 5.29b.

As can be envisaged, the measurement of a spectrum with a single channel analyzer (either integral or differential) would require a long time and therefore unsuitable where fast measurements are required. It should also be realized that the SCA can only be used to select one energy range at a time for analysis. To combat these problems, multichannel analyzers (MCA) are developed. These are in principle equivalent to many differential single channel analyzers operating in parallel. Three possible arrangements of such single channels are shown in Fig 5.30. But in general the single channels in a multichannel analyzer are arranged so that the windows are contiguous (the upper limit of one channel coinciding with the lower limit of the next channel). Also there is the possibility of unequal window widths but again in a multichannel analyzer, the window widths are generally made to be equal. However in the conventional three channel spectrometer where windows are centred on peak positions, the windows are inevitably non-contiguous and unequal. The arrangement where the windows are contiguous can permit the spectrum being analyzed to be simultaneously segregated and counted in the relevant channels. The operating principle of a multichannel analyzer is illustrated in Fig 5.31. The pulse from the detector, after amplification and shaping, is fed into an analyzer which has an analogue - to - digital converter (ADC) as its input. The ADC then measures the amplitude (or energy) of this pulse, presents it at its output in digital form and directs it to an appropriate channel whose content then increases by one. The overall process of a multichannel

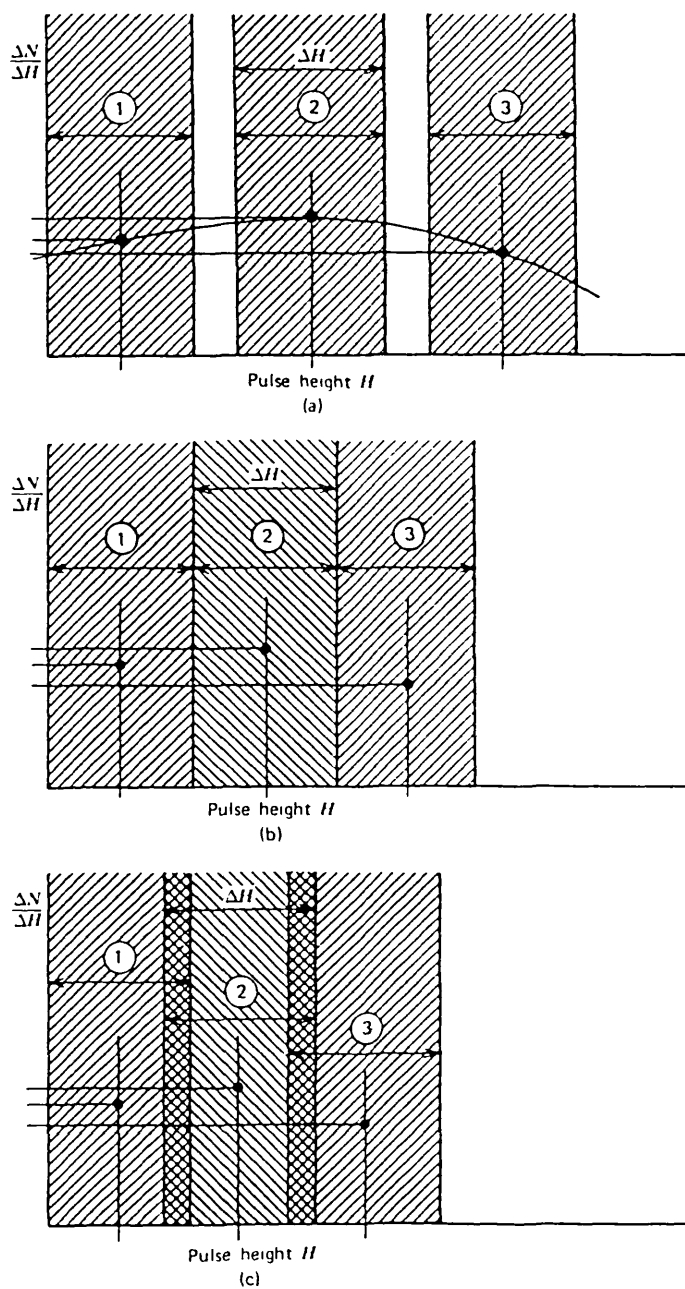
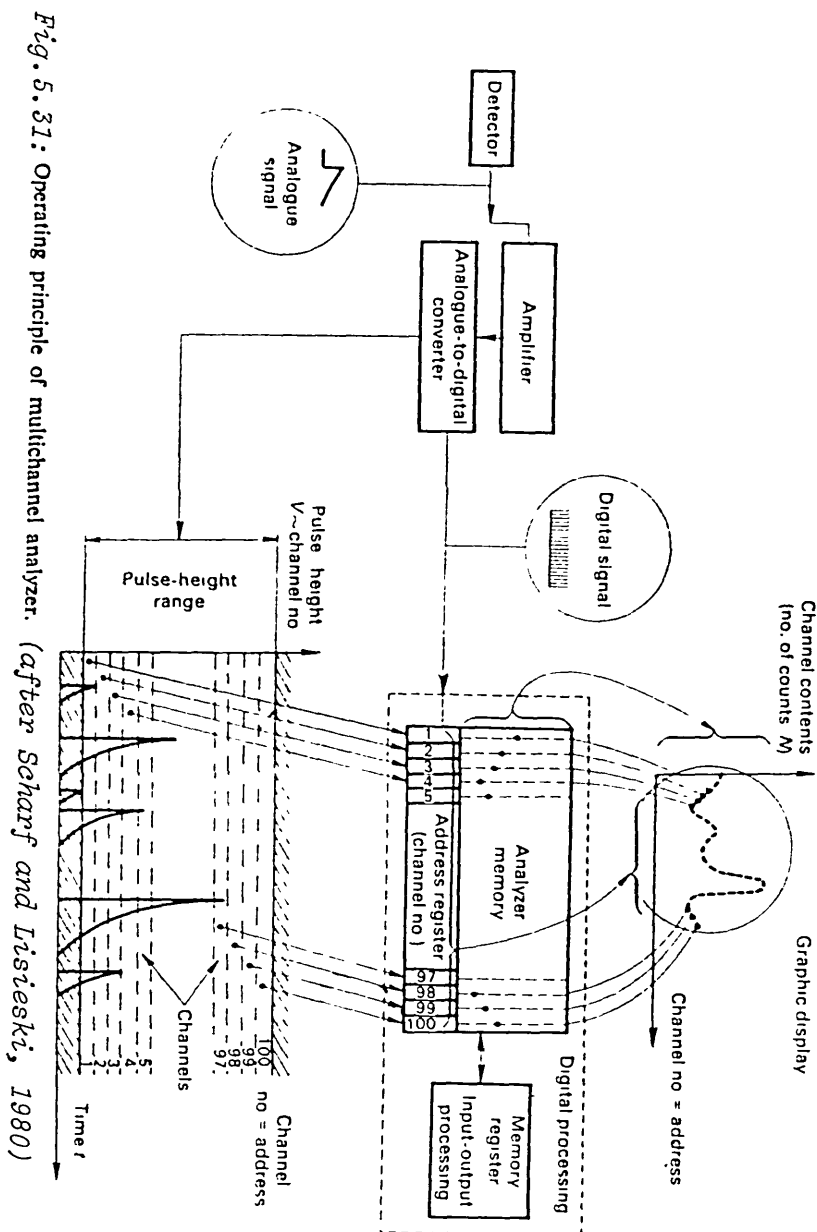


Fig. 5.30: Sequential measurements (labeled ①, ②, ③) using an SCA with a constant window width ΔH . When the number of counts ΔN is normalized by ΔH and plotted at the midpoint of the pulse height interval, a pointwise approximation to the differential pulse height distribution is obtained. Plot (b) is taken with contiguous windows, plot (a) with widely spaced windows, and plot (c) with overlapping windows.

(after Knoll, 1979)



analyzer can thus be viewed as sorting each input pulse from the detector into a corresponding channel and incrementing the content of that channel by one each time a pulse arrives there. At the end of the measuring period, the sum of all the counts will be the total number of pulses from the detector.

There are two basic principles of sorting the detector pulses by the ADC. After the classification of the input pulses into channels,

the coded information in each channel is then sent to a memory where it is logically recorded. The contents of the memory at the end of the experiment is then read out either in digital form to a computer, paper tape, magnetic tape or typewriter, or in analog form to a chart or XY recorder. Standards which coded inputs and outputs should respond are given in Table 5.4.

NIM Logic Levels for Transmission of Digital Data (Preferred Practice)			Fast Logic Levels and Characteristics (Preferred Practice)		
	Output Must deliver	Input Must respond to		Output Must deliver	Input Must respond to
Logic "1"	+4 to +12 V	+3 to +12 V	Logic "1"	-14 to -18 mA	-12 to -36 mA
Logic "0"	+1 to -2 V	+1½ to -2 V	Logic "0"	-1 to +1 mA	-4 to +20 mA

Impedance 50 Ω

Table 5.4: NIM standard (after Costrell, 1973)

The sorting of the detector pulses by the analyzer is done using either of two basic principles - Wilkinson Ramp and Successive Approximation principles.

(a) Wilkinson Ramp Principle

The wilkinson ramp principle is illustrated in Fig 5.32. In this method, an input pulse is made to charge a capacitor until the capacitor voltage is equal to the amplitude of the input pulse. The capacitor is then linearly discharged to zero voltage by a constant voltage current, and this results in a voltage ramp as shown in

Fig 5.32a. At the same time the discharge is started, a comparator (high frequency clock) is switched (gated) on and this is maintained until the ramp voltage is zero. In this way the gate pulse is directly proportional to the ramp voltage and hence directly proportional too to the amplitude of the input pulse from the detector. The gate pulse is used to operate a linear gate 'address register' which opens for a period of time proportional to the amplitude of the input pulse, and so the number of pulses counted is also proportional to the input amplitude.

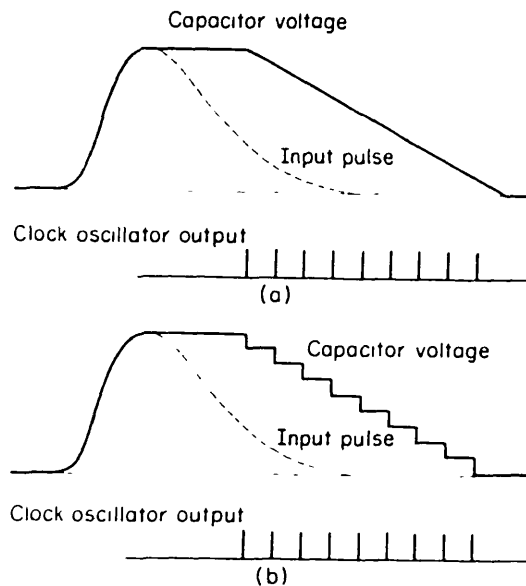


Fig. 5.32: Principle of the Wilkinson type of ADC using (a) a linear discharge and (b) a staircase shaped discharge of the capacitor (after Nicholson, 1974)

An alternative to the linear ramp method is the staircase method illustrated in Fig 5.32b in which the discharge of the capacitor is done in a series of steps, with each step representing equal amount of charge. The number of steps required to completely discharge the capacitor then represents the magnitude (counts) of the input pulse.

This method is however slower than the linear discharge method, thereby comparatively increasing the dead time of the analyzer. On the other hand though, the staircase method, unlike the linear method, does not require a stable clock frequency nor a phase correlated clock to prevent the discharge of the capacitor starting in the middle of a clock cycle. While the linear Wilkinson ADC gives analog coding (binary coded decimal), the staircase type gives a binary coding.

(b) Successive Approximation Method

Fig 5.33 illustrates the principles of the Successive Approximation

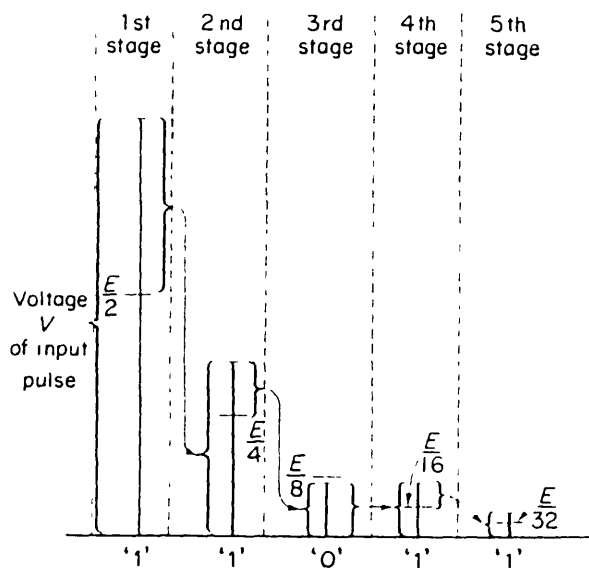


Fig. 5.33 : Schematic representation of a successive binary approximation ADC (after Nicholson, 1974)

method. In this method, the amplitude A of the input pulse is logically compared with a series of standards of varying lengths, starting with the largest standard. If the full scale amplitude of

the analyzer is E , the standards are defined as $E/2$, $E/2^2$, $E/2^3$, and so on. At each stage of the comparison, a '1' or '0' is generated depending on whether or not the amplitude of the input pulse at that stage of the comparison is greater or less than the standard.

At the first stage of the comparison, A is compared with $E/2$ and if A is greater than or equal to $E/2$, then a '1' is generated, otherwise a '0' is generated. If a '1' is generated then $(A - E/2)$ is passed on to the next stage $E/2^2$; but if it is a '0' that is generated, A is passed on to $E/2^2$ unaltered. Thus in each case, the amount of A passed on to the next stage is always less than the present standard. This process is continued in this manner until the amplitude A is reduced to zero (a match is found for A). If n such standards, as defined above, are required before a match is found for A , then an n -bit word will be produced, covering a range of 2^n channels. Thus for an N -channel analyzer, $\log_2 N$ operations are required as compared to N operations using a Wilkinson ramp method. Hence expectedly, successive approximation ADCs are faster and more useful than Wilkinson ADCs when large number of channels are needed. The successive approximation ADCs also have the advantage of producing binary (digital) numbers without further need for encoding. However successive approximation ADCs have poorer linearity, which often results from the cumulative errors in the subtraction processes. This problem is however overcome by channel smoothing technique (Nicholson, 1974).

5.3.1. Choice Of Window Widths For 3-Window Spectrometer

In the three - window spectrometer, the windows are set to count the energies taken within a finite range (differential mode) of the relevant (potassium, uranium and thorium) peaks, allowing for the spreading of the peaks (see Fig 1.2). This may be considered as a multichannel spectrometer but with its window arranged non contiguously (see Fig 5.30a).

The choice of the window widths has raised much controversy and two schools of thought have emerged. While one school maintains that windows should be narrow to increase discrimination between sources and use large detector volumes to keep counting statistics at an acceptable level of significance, the other school maintains that information is contained in the whole spectrum so that wide windows may be used provided they do not overlap (see Fig 5.30c). While it is true that the first suggestion of narrow windows will lead to loss of information contained in the spectrum, the main objection to the use of wide window widths is that we tend to get peaks from another isotope in the window defined for a particular isotope, for example, we may get uranium peak at the lower end of the thorium window. A practical suggestion is that a window should be wide enough to accommodate the finite range of the relevant peak it represents but it should not be too wide as to accept the flanks of adjacent peaks.

5.4. Distortion Of Signal

Certain factors cause distortion in a signal in its journey through a detector to an analyzer. These factors include pulse-up (or sum peak), ballistic deficit, noise, dead time and non-stabilization of

the different components of the entire detecting system comprising the detector, preamplifier, amplifier and analyzer.

Pulse Pile-Up

This results when two or more gamma rays of different energies are counted as one. Since the time interval separating adjacent events are randomly distributed, some may be less than the inherent resolving time of the detector or the pulse processing systems. When this happens, such pulses will be counted together as one pulse whose energy (or amplitude) will correspond to the sum of the individual pulse energies. The probability of pulse pile-up increases rapidly with high count rates. In the amplifying section, pulse pile-up effect can be reduced by shaping to produce pulses with short tails but this is done at the expense of increased noise contribution.

Pulse pile-up is generally of two types - tail pile-up and peak pile-up (sum peak). While tail pile-up results from the superposition of a pulse on the long duration tail of a preceding pulse, peak pile-up occurs when two pulses are sufficiently close together so as to be regarded as one by the analysis system. Peak pile-up does not only lead to the distortion of the recorded spectrum, it also interferes with the quantitative measurements. For instance, the pile-up of two full energy peaks will remove both peaks from their respective positions in the spectrum, and the area under the full energy will no longer be a true measure of the total number of full energy events.

Ballistic Deficit

Ballistic deficit is defined as the amount by which the amplitude of a pulse shaped using a finite time constant differs from the amplitude of the same pulse shaped using an infinite time constant. In other words, ballistic deficit is the measure of the inefficiency of integration by the preamplifier. According to Nicholson (1974), ballistic deficit will be low if the output pulse of a unit charge input pulse is approximately the same as the impulse response having a flat top for at least as long as the total length of the input pulse. Thus in order to minimize the effect of ballistic deficit on energy resolution, large shaping times compared to the rise time of the input pulses, should be used.

Fig 5.34 shows the relative merits of some pulse shaping systems

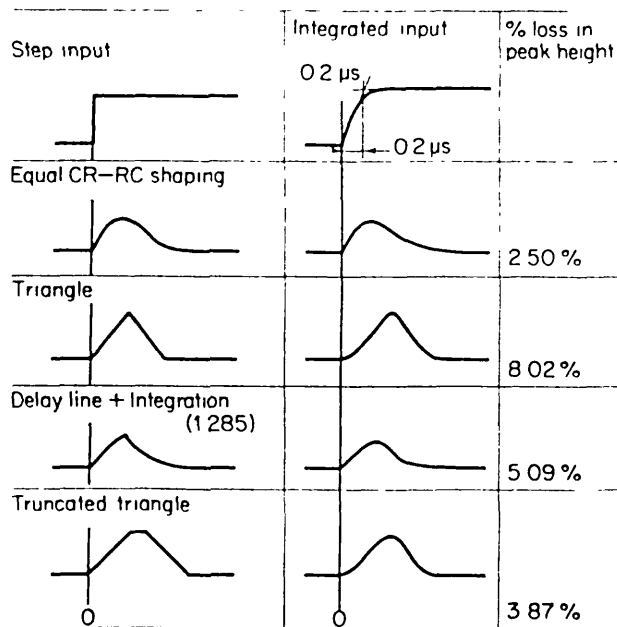


Fig. 5.34: Comparison of the output pulse shapes and the loss in peak height due to the finite rise time of the detector signal (after Nicholson, 1974)

with respect to ballistic deficit. It should be noted that the preamplifier input is not a perfect step function but has a rise time of $0.2\mu\text{s}$ arising from the finite collection time of the charge carriers in the detector. It can be seen from Fig 5.34 that the sharper the apex (peak) of the pulse shape, the larger the ballistic deficit.

Ballistic deficit is more severe for detectors with large variation in charge collection time like proportional counters and Ge(Li) detectors. In cases such as these, consideration of optimum shaping time is based on signal - to - noise ratio or pile-up effect.

Noise

This is defined as any signal measured which is not a part of the original signal generated by the source being analyzed. The effect of noise is to broaden the peak recorded in the analyzer (see Fig 5.35).

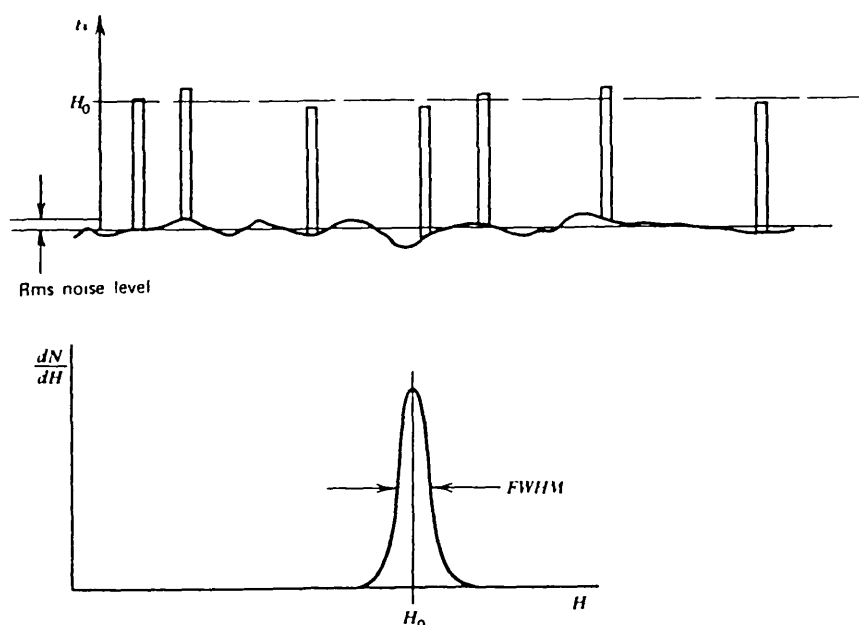


Fig. 5.35: At the top is shown a series of signal pulses of constant amplitude superimposed on a noisy baseline. The effect of the noise is to broaden the peak recorded in the differential pulse height spectrum for these pulses. The full width at half maximum (FWHM) of the peak for Gaussian-distributed noise will be equal to the RMS noise level multiplied by a shape factor of 2.35, provided noise is the only factor in broadening the peak. (after Knoll, 1979)

Since the spectrum of many noise sources is broad, pulse shaping actually amounts to selective filtering of the spectrum in order to remove as much broad spectrum as possible without severely attenuating the useful signal components. Fig 5.36 shows the list of some of the

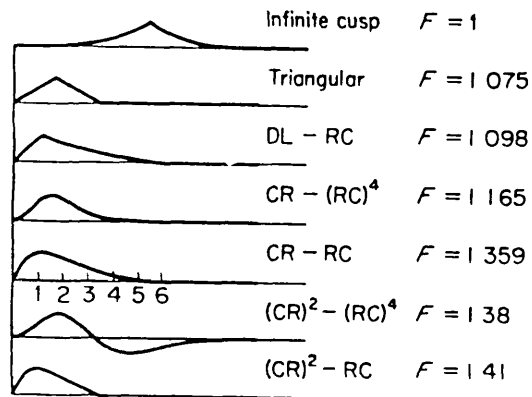


Fig. 5.36 : Pulse shapes, normalized to constant height, for various systems when the time scale of each (i.e. the value of τ) is optimized for the case of a noise corner time τ_c equal to 1.
(after Nicholson, 1974)

common methods of pulse shaping (see section 5.2.2.1) together with signal - to - noise ratio performance compared with the infinite cusp which is theoretically regarded as giving the best signal - to - noise ratio.

Dead Time

In the detection system, either in the detector, preamplifier, amplifier or analyser, two events must be separated by a minimum amount of time so that they can be recorded as separate events. During this time the system is busy processing the first event which

has been detected. This range of time during which the system is insensitive to the passage of any event is called the 'Dead Time' of the system. Dead time is hence dependent on the magnitude of the pulse being processed.

Due to the random nature of radioactive decay, there is always a finite probability that a true event will be lost when it occurs too quickly following a preceding event. Hence dead time losses may become rather large when count rates are high, and so for an accurate measurement to be made under such conditions, correction should be made for the dead time losses. It is recommended that dead time losses should be kept at less than 50% in the worst case and preferably below 10% (Killeen, 1977).

If t_D is the fixed dead time of the system per unit event and C_0 is the observed count rate, then the fraction of the total time for which the system is dead is $C_0 t_D$. Hence the number of counts lost C_L per unit counting time interval is given by

$$C_L = C C_0 t_D$$

where

C is the count rate which would have been observed if the dead time was negligibly small

Therefore

$$C_L = C - C_0 = C C_0 t_D$$

Hence

$$C = \frac{C_0}{1 - C_0 t_D} \quad (5.17)$$

It should be noted that the assumption that t_D is fixed is correct only for comparatively low count rates. At high count rates, t_D fluctuates (Nicholson, 1974).

Measure Of Dead Time

(i) Decay Source Method

This method is used if a short-lived radioisotope source of very short half-life, such as $\text{In}^{116\text{m}}$ (half-life of 54.0 minutes) say, is available. The technique is based on the known behaviour of the true rate C , where C is given by

$$C = C_j e^{-\lambda t} + C_B \quad (5.18)$$

where

C_j is the true count rate at the beginning of the measurement

C_B is the background count rate

λ is the decay constant of the particular isotope used for the measurement, and

t is the measuring time

If C_B is neglected, then equation 5.18 becomes

$$C = C_j e^{-\lambda t} \quad (5.19)$$

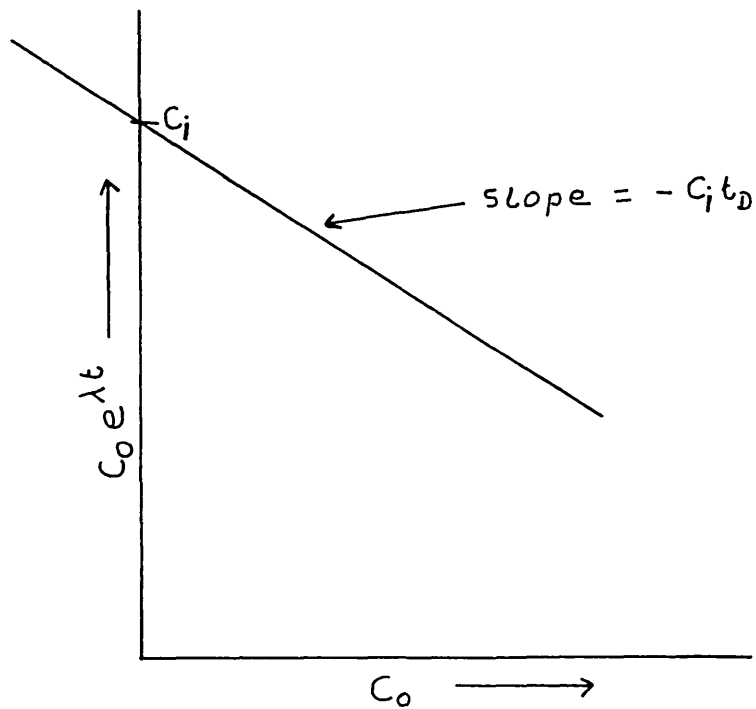
Substituting for C from equation 5.17, we have

$$\frac{C_0}{1 - C_0 t_D} = C_i e^{-\lambda t}$$

Therefore

$$C_0 e^{\lambda t} = -C_i t_D C_0 + C_i \quad (5.20)$$

Thus a graph of $C_0 e^{\lambda t}$ against C_0 will give a straight line whose



gradient is $-C_i t_D$ and intercept C_i . Hence the dead time t_D is given by

$$t_D = - \frac{\text{Slope}}{\text{Intercept}} \quad (5.21)$$

(ii) Two (Paired) - Source Method

This is the most common and practicable method. It involves the comparison of the count rate indicated by the system when two sources are counted simultaneously with the sum of the count rates produced by each of the sources taken individually.

Let R_1 , R_2 , R_{12} be the true count rates due respectively to source 1 minus background, source 2 minus background, and sources 1 plus 2 together minus background. Let C_1 , C_2 and C_{12} be the corresponding observed count rates respectively of sources 1, 2 and 1 plus 2 together. Then

$$R_1 + R_2 = R_{12} \quad (5.22)$$

and by equation 5.17,

$$\frac{C_1}{1 - C_1 t_D} + \frac{C_2}{1 - C_2 t_D} = \frac{C_{12}}{1 - C_{12} t_D} \quad (5.23)$$

Using the approximation

$$\frac{a}{1 - ar} = a + a^2 r$$

equation 5.23 becomes

$$C_1 + C_1^2 t_D + C_2 + C_2^2 t_D = C_{12} + C_{12}^2 t_D$$

Therefore

$$t_D(C_{12}^2 - C_1^2 - C_2^2) = C_1 + C_2 - C_{12}$$

Therefore

$$t_D = \frac{C_1 + C_2 - C_{12}}{C_{12}^2 - C_1^2 - C_2^2} \quad (5.24)$$

It could be seen from equation 5.24 that the accurate measurement of t_D requires highly accurate determination of C_1 , C_2 and C_{12} , since C_1 plus C_2 is nearly equal to C_{12} . Equation 5.24 can be approximated further by substituting $C_1 + C_2$ for C_{12} in the denominator only. Thus

$$\begin{aligned} t_D &= \frac{C_1 + C_2 - C_{12}}{(C_1 + C_2)^2 - C_1^2 - C_2^2} \\ &= \frac{C_1 + C_2 - C_{12}}{2 C_1 C_2} \end{aligned} \quad (5.25)$$

It should be noted that in equations 5.24 and 5.25, it is assumed that t_D is independent of the count rate, and $C_1 t_D$, $C_2 t_D$ and $C_{12} t_D$ all must be less than unity. Although equation 5.25 is only an approximation, it is much more convenient to use than the complex exact equation (Killeen, 1977). Usually dead time loss correction is minimized and hence neglected if 'live' time, instead of actual (real) time, is used in the processing of the data. The technique is however inadequate

for automatic data reduction where, for instance, a source and a background are alternatively analyzed at preset times since the real time is dependent on the count rate. Another way of reducing the dead time losses is the use of a buffer to store an input pulse until the analyzer is free to accept and process it (Nicholson, 1974).

Stabilization

One main problem associated with spectrometers is the drift (or instability) in the detector - preamplifier - amplifier - analyzer system, resulting in the broadening or distortion of the recorded spectrum. The drift may be due mainly to temperature changes, changes in the high voltage power supply, or instabilities in the gain of the amplifiers and analyzer. The net effect of instabilities in the gains of the amplifiers and analyzer will cause say a peak in the spectrum to be shifted over a number of channels. Apart from maintaining the system at a constant temperature by using thermostatically controlled heating coils, the spectrum may be stabilized using automatic gain control (servo) techniques. These techniques may be divided into two classes - those that involve the use of a reference peak and those that do not involve a reference peak. Details of these techniques can be found in Williams et al (1966), Frederick (1968), Bacci et al (1967), Matoba and Sonoda (1971), Nicholson (1974), Yamashita (1974), Johnson et al (1976), Morris et al (1976), Uyttenhove et al (1977) and Knoll (1979). These references also contain other references on the subject. It is worthy to note that in general, even with the in-built automatic drift control in spectrometers, some drifts are still

sometimes noticed in experimental work. When this happens, the effect of drift is corrected for during the analysis of the spectral data (see section 6.6.1).

(a) Reference Peak Technique

This involves the continuous monitoring of a reference peak position in the spectrum and if any change is noticed, an error message signal is generated. This error signal is then used in a feedback loop to restore the peak to its correct (original) position by adjusting the gain in the photomultiplier tube in the case of scintillation counters, amplifiers and analyzer. It should be noted that in the case of a single channel spectrometer, the stabilization circuit encompasses only the detector and the amplifier (Nicholson, 1974). The reference peak may either be a chosen isolated peak in the spectrum being analyzed or superimposed on it by an electrical pulse generator or by a radioactive source of known energy which is permanently or periodically inserted into the viewing range of the detector. Some of such 'monitor' sources include Americium-241, Cesium-137 and Cobalt-57. The use of monitor sources limits the total count range to above the reference peak position (Adams and Gasparini, 1970). This problem can however be avoided by using a separate buffer to monitor the reference peak as in modern airborne systems where a separate buffer is used to monitor the potassium-40 peak drift over a number of scans and correct the channel counts accordingly.

The general principle of the technique using a reference peak as is commonly used is illustrated in Fig 5.37. Here two equal windows are

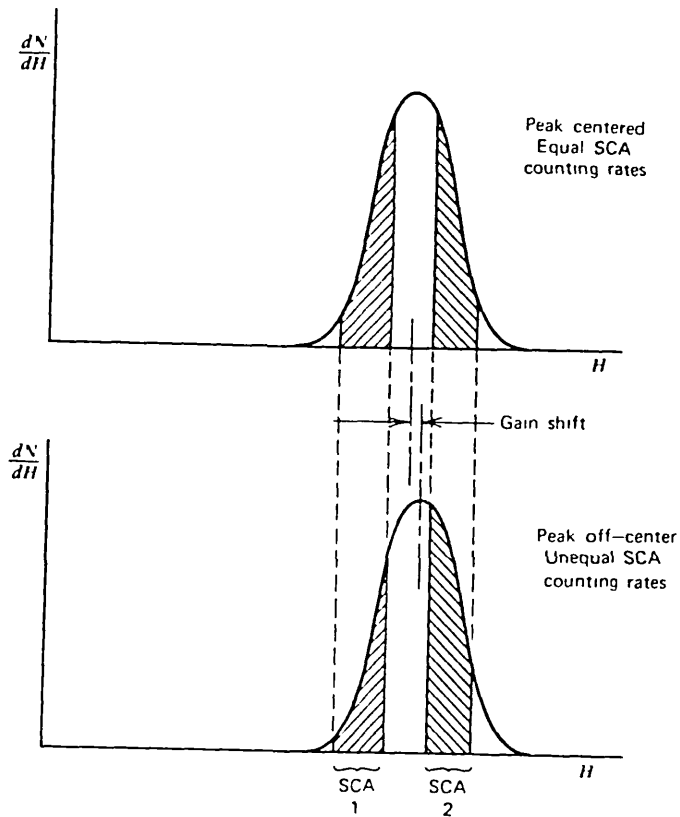


Fig. 5.37: The principle of a spectrum stabilizer based on peak-sensing. An error signal is derived from the counting rate difference in the two SCA windows. (after Knoll, 1979)

set up at the opposite sides of the reference peak position. At the start of the measurement, the gains are adjusted so that the count rates in the two windows are the same. If at any other time during the measurement the reference peak position changes, the count rates in the two windows will no longer be the same and then an error signal will be generated, and the gains correspondingly adjusted to restore

the peak position to its correct position. It is required that the window positions must themselves be very stable because any changes will also be regarded as system gain changes. This is particularly important where a single channel analyzer is used since the stabilization circuit will not include the analyzer. But in the case where a multichannel analyzer is used, the problem of window instability is overcome since the stabilization arrangement is incorporated in the analyzer which processes both the reference and other pulses simultaneously. In an MCA, the reference peak position is held constant by preselected groups of channels which then perform the function of the windows (Knoll, 1979).

(b) No Reference Peak Technique

When a reference peak is not available, the spectrum can still be stabilized by choosing a lower window in the flat region of the spectrum and an upper window in the region where the spectrum drops off rapidly (decreasing region) as illustrated in Fig 5.38 (Matoba and Sonoda, 1979; Knoll, 1979).

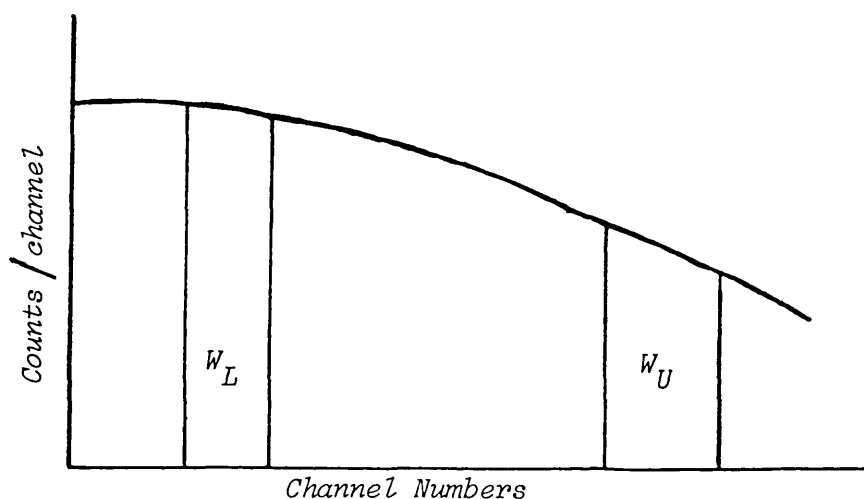


Fig. 5.38: Stabilization without a reference peak

If the window widths W_L and W_U are equal, the count rate C_L in the lower window will always be greater than the count rate C_U in the upper window, and as such no stability point will be found if the usual stabilizer (stated above) is used. Hence in order to achieve a stability point, the count rates in the two windows are made equal. This can be done either by making the upper window larger than the lower window or by multiplying the count rate in the upper window by a factor k . That is

either

$$W_U > W_L$$

or

$$C_L = kC_U, \text{ where } k > 1.$$

Any deviation from the condition of equal count rates in the two windows during the measurement of the spectrum will generate an error signal and so the gains will be corrected accordingly.

This method avoids at least the problems associated with the superposition of a reference peak.

In general, with all these attempts, some drifts are sometimes still noticed in experimental work and when this happens, the effects of drifts are corrected using mathematical approach during the analysis of the data (see section 6.6.1).

CHAPTER SIX

DATA ANALYSIS TECHNIQUES

In order to identify and/or estimate the concentration of isotopes present in a sample from the 'raw' counts obtained from the sample, calibrations of the measuring system are necessary. From the isotopic calibration, the characteristic constants (stripping ratios and sensitivities) of the spectrometer are determined from the spectra of pure potassium, uranium and thorium. While the stripping ratios account for the interactions of the various isotopes with each other, the sensitivities relate the count rates to concentrations.

Generally radiometric data are analyzed using either the graphical method, peak area method or the least squares' method. In this work however, the least squares' method is used in the analysis of the data because, apart from not being subjective, it is suitable for spectra where peaks are superimposed, and also full spectra data as well as photopeak areas can be used.

6.1. Graphical Method

This method involves repetitive subtraction from the sample spectrum of each component spectrum obtained from standards. The method makes use of only those measurements around photopeaks.

Starting with the highest photopeak energy, its standard spectrum distribution is subtracted from the total sample spectrum until, in the judgement of the operator, the correct amount has been subtracted by visual examination of the display. Thus as applied to gamma ray

spectrometry where the concentrations of potassium, uranium and thorium are sorted, the thorium standard will be subtracted first. If f_t is the amount of the thorium standard subtracted from the sample, then the concentration of thorium in the sample will be given by

$$T_{\text{sample}} = f_t T_{\text{standard}}$$

where

T_{standard} is the concentration of thorium in its standard

This procedure is then repeated for the next higher photopeak energy, uranium and continues down to potassium until only background (noise) count is left. This suggests that the quality of results achieved depends on the experience of the operator.

Where there are overlapping (partially resolved) peaks, the stronger peak, in spite of its energy, is subtracted first.

It should be realized that after several subtractions, the lower energy photopeaks will be subjected to higher statistical errors (see section 4.4). This, combined with the fact that the results obtained from the method are highly subjective, makes the graphical method unattractive.

6.2. Peak Area Method

In this method, the peak areas of the same energy gamma rays are compared and their ratio (sample/standard) gives the ratio of the intensities.

If A_0 is the count rate in the channel in which the highest number

of counts occur in a photopeak window, the total area P under the photopeak is given by (see Fig 6.1)

$$P = A_0 + \sum_{i=1}^n A_i + \sum_{i=-1}^{-n} A_i \quad (6.1)$$

In most cases peaks are superimposed on a background or a Compton continuum and a baseline is interpolated to distinguish the counts in the peak from those due to background and /or Compton scattering. The area Q of the baseline located under a peak is calculated as

$$Q = 1/2(A_n + A_{-n})(2n + 1) \quad (6.2)$$

Thus the net area N is given by

$$N = P - Q \quad (6.3)$$

The difficulty with this method is in determining the peak boundaries and the construction of the baseline which can either be linear or non-linear. Quittner (1972) stated that even small deviations of the actual baseline from linearity can cause large errors in the intensity determination. He also pointed out that in order to decrease the variance of the peak area, the boundary selection must be consistent in each spectrum for a given gamma ray energy.

Several authors, Helmer et al (1967), Mariscotti (1967), Routti and Prussin (1969), Quittner (1972), Kozka (1973), Phillips (1979), Phillips and Marlow (1976, 1977), Helmer and Lee (1980), just to mention a few, have suggested methods for automatic peak location and peak area calculation. The International Atomic Energy Agency (IAEA)

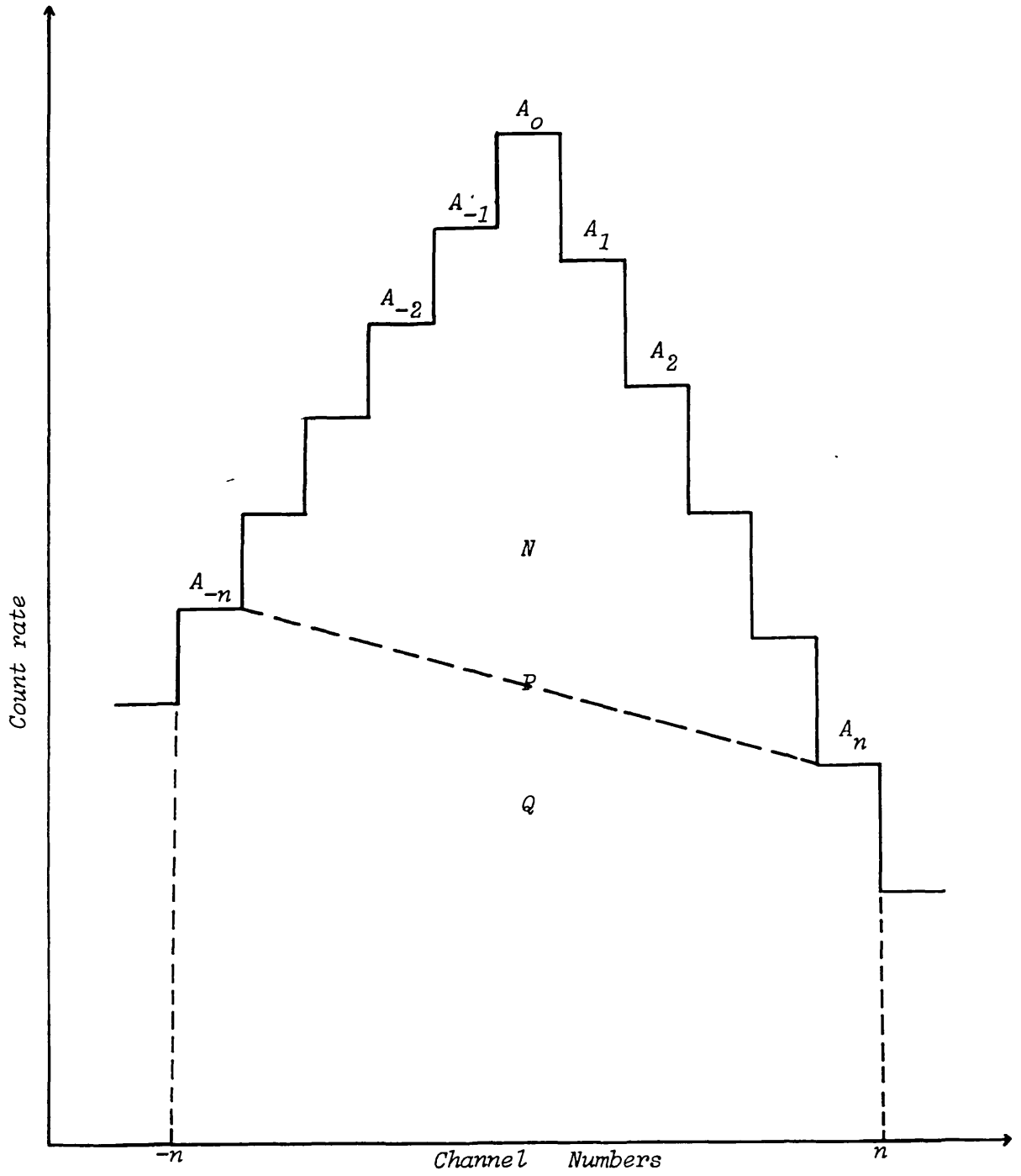


Fig.6.1: Determination of peak area

(Parr et al, 1979) carried out an intercomparison in order to test the accuracy of some of these methods and also to permit a comparison of the different evaluation methods. Their report shows that for:

Peak Detection:

The methods used are shown in Table 6.1. Of the total 192 methods, only two were able to detect the least frequently observed peak, and no single method succeeded in detecting more than 19 of the 22 true peaks. This suggests a drawback in the use of the peak area technique in the quantitative analysis of spectra. The report concluded that in the best hands, visual methods and the use of second derivatives are capable of marginally superior performance. This suggests that, like the graphical method, the peak area method is subjective to the experience of the operator.

Peak Position and Area (single peak):

while Table 6.2 shows the methods used for the peak position determination, Table 6.3 shows the methods used for the peak area estimation. The intercomparison showed that although parabolic fitting is marginally superior for determining peak position and fitting of modified Gaussian function provides the best results for determining peak area, it was pointed out that the degree of success is subjective and that many methods have poor control over the estimation of errors.

Table 6.1: Methods of Peak Detection (after Parr et al, 1979)

Environment	N*	Percent use of specified method†					Unclass.
		Relative max.	First derivative	Second derivative	Cross correlation	Visual	
Manual	5				40	40	20
Minicomputer (single prog)	40	5	28	3	28	10	28
Mini/midi (real time)	31	6	19	16	19	3	35
Batch proc.	116	3	26	39	10	3	18
Interactive	17	12	12	24	12	18	24
Unclass.	3					33	67
All	212	5	23	26	16	7	24

*Number of methods reported.

†The percentage figures refer in each case to the particular working environment.

Table 6.2: Methods of Peak-Position Determination (after Parr et al 1979)

Environment	N*	Percent use of specified method†							Unclass
		Pure Gauss.	Mod Gauss	Mod Gauss +step	Parabol. fitting	Other fitting	Center of gravity	Half area	
Manual	5				40		20		40
Mini (single prog.)	40	13	8	8	5		15	15	38
Mini/midi (real time)	31	19	13	3	10		32	6	16
Batch proc.	116	22	41	6	9	2	9		11
Interactive	17	29	29		6	6	6	6	18
Unclass.	3								100
All	212	20	28	5	8	1	13	4	19

*Number of methods reported.

†The percentage figures refer in each case to the particular working environment.

Table 6.3: Methods of Peak-Area Estimation (after Parr et al, 1979)

Environment	N*	Percent use of specified method†					Unclass.
		Pure Gauss.	Mod. Gauss.	Mod. Gauss. +step	Other fitting	Summation	
Manual	5					80	20
Mini (single prog.)	40	13	8	8		53	20
Mini/midi (real time)	31	26	13	3		45	13
Batch proc.	116	21	41	6	2	25	6
Interactive	17	24	29		6	12	29
Unclass.	3						100
All	212	19	28	5	1	33	13

*Number of methods reported.

†The percentage figures refer in each case to the particular working environment.

Peak Position and Area (double peak):

Table 6.4 shows the methods used. The report stated that although all 144 methods reported were capable of resolving the peak doublet having a separation of six channels and an intensity ratio of 1:1, higher intensity ratios and smaller peak separations were progressively more difficult to evaluate, and only 49 methods (out of the 144) succeeded in providing results for a peak separation of one channel and intensity ratio of 1:10.

Tables 6.5 and 6.6 show the maximum scores (performance) out of 900 for each of the methods used for the determination of the separation of double peaks and ratios of area of double peaks respectively. These values reveal that no method is completely successful in either separating these peaks or determining the ratio of their areas correctly.

6.3. Least Squares' Method

Both the graphical and the peak area methods mentioned above suggest that analysis of spectra involves some form of curve fitting procedure. If this is the case then the best results are likely to be obtained by application of the principle of least squares (Salmon, 1962). Salmon (1962) cited Birge who says:

"Except in especially favourable cases, least squares' results and their computed probable errors are not as reliable as indicated by theory, but alternative methods are without exception, inferior."

Table 6.4: Methods for the Evaluation of Double Peaks (after Parr et al, 1979)

Environment	N*	Percent use of specified method†							Unclass.
		Pure Gauss.	Mod Gauss.	Mod Gauss +step	Other fitting	New Gauss.	2 X undist. part	Right & left parts	
Mini (single prog)	22	9	14	14		18	14	9	23
Mini/midi (real time)	20	35	20	5		25	5	5	5
Batch proc.	94	18	46	9	2	6	7	3	9
Interactive	11	18	45				18		18
All	147	19	37	8	1	10	9	4	11

*Number of methods reported.

†The percentage figures refer in each case to the particular working environment

Table 6.5: Values of the Score for the Determination of the Separation of Double Peaks (after Parr et al 1979)

	Pure Gauss.	Mod. Gauss.	Mod. Gauss +step	Other fitting	New Gauss.	2 X Undist. part	Right & left parts	Unclass.
N*	28	55	12	2	15	12	5	15
Max. value	595	736	573	705	302	200	143	425
Median value	133	383	251	431	78	23	27	55

*Number of methods reported.

Table 6.6: Values of the Score for the Determination of the Ratio of Areas of Double Peaks (after Parr et al 1979)

	Pure Gauss.	Mod. Gauss.	Mod Gauss +step	Other fitting	New Gauss.	2 X Undist. part	Right & left parts	Unclass.
N*	28	55	12	2	15	12	5	15
Max. value	649	672	622	645	441	83	90	577
Median value	100	408	282	419	106	46	44	37

*Number of methods reported.

In 1961, Salmon showed that the least squares' method is more accurate than the graphical method, particularly when the statistical variations in counting are large.

In this work, the least squares' method is used in the analysis of the data. This is because, among other things, the least squares' method is free from subjective errors and it is also suitable for spectra where peaks are superimposed (Salmon, 1962). Also while the graphical and the peak area methods make use of only that part of a spectrum under a photopeak, thereby resulting in loss of some of the information contained in the spectrum, with the least squares' method all information contained in a spectrum can be used. Thus of these three methods mentioned here, only the least squares' method can be used in order to achieve the objective of this project since it is required that full spectral (multichannel) analysis results will be compared with those from conventional three window analysis.

6.4. Theory Of Data Analysis

The direct procedure where only three windows are used for the estimation of the three elements - potassium, uranium and thorium, is only a first approximation in the assessment of the relative concentrations of the radioelements (Crossley and Reid, 1982). While it is an advantage to be able to stabilize the spectrum before summing the window counts, a large part of the spectrum which does not fall within any of these windows, is neglected, thus resulting in loss of some of the information contained in the spectrum. Crossley and Reid (1982) showed that there is a good reason to include all the channels

when solving for the radionuclides.

The theory of processing the radiometric data will be based on a spectrometer with an arbitrary number, n , of channels, of which the three channel (window) spectrometer will be regarded as a special case.

The count rate in channel i due to a sample containing m isotopes may be represented by

$$Y_i = \sum_{j=1}^m X_{ij} \quad (6.4a)$$

where

X_{ij} is the count rate in channel i due to isotope j in the sample

If A_{ij} is the count rate per unit concentration of isotope j in channel i , then equation 6.4a can be written as

$$Y_i = \sum_{j=1}^m A_{ij} X_j \quad (6.4b)$$

where

X_j is the concentration of isotope j in the sample.

In matrix form, equation 6.4b can be written as

$$Y = AX \quad (6.5)$$

It is possible to sum the count rates within the windows centred on the potassium, uranium and thorium peaks respectively, with the width of each window defined (see Fig 1.2). This procedure would then reduce the number, n , of channels to three, and this will be

equivalent to using a three window spectrometer.

From equation 6.4(a and b),

$$A_{ij} X_j = X_{ij} \quad (6.6a)$$

Hence

$$X_j = X_{ij}/A_{ij} \quad (6.6b)$$

Since the concentration and/or count rate of an isotope in a sample can not possibly be negative, the following restrictions are necessary.

$$\begin{aligned} X_j &\geq 0 \\ X_{ij} &\geq 0 \end{aligned} \quad (6.7)$$

Hence $A_{ij} \geq 0$

where

$$j = 1, 2, 3, \dots, m$$

$$\text{and } i = 1, 2, 3, \dots, n$$

Because of the variance in the determination of the count rates Y , A_{ij} and/or X_j cannot be determined simply from the inversion of equation 6.5. An appropriate method of solution has to be sorted.

One way of solving equation 6.5 is by the method of least squares. As stated earlier, Salmon (1962) stated that the least squares' method is the best method for the analysis of spectra.

Based on the principles of least squares, equation 6.5 can be written as

$$Y = AX + E \tag{6.8}$$

where

E_j is the error in channel 1 of the estimated value of Y_j

The values of X are obtained by minimizing the sum of squares of the error E , which is given by

$$E^2 = E^T E$$

where

E is a column vector and E^T denotes the transpose of E

Thus from equation 6.8,

$$\begin{aligned} E^2 &= (Y - AX)^T \cdot (Y - AX) \\ &= Y^T Y - Y^T AX - X^T A^T Y + X^T A^T AX \end{aligned} \tag{6.9}$$

Equation 6.9 is minimized with respect to X or X^T by taking partial derivatives with respect to X or X^T and equating the derivatives to zero. Thus with respect to X^T ,

$$-A^T Y + A^T AX = 0$$

Therefore

$$A^T AX = A^T Y \tag{6.10}$$

If

$$C = A^T A$$

and

$$Z = A^T Y \tag{6.11}$$

Then

$$CX = Z$$

and

(6.12)

$$X = C^{-1}Z$$

where

C^{-1} is the inverse matrix of C

By theory of matrices, only non-singular square matrices have inverses (Stephenson, 1973). Thus since C is a square matrix, its inverse will exist, provided it is non-singular. It should also be remembered that the inverse of C is unique, if it exists. That is, if C^{-1} exists, then

$$C^{-1}C = CC^{-1} = I_m \quad (6.13)$$

where

I_m is the identity matrix, and

m is the order of C

Thus if C^{-1} exists, then the solution of equation 6.12 is unique and it satisfies the data exactly (Jackson, 1972; Richards, 1977a).

The existence of the inverse of C can be investigated when C is factored into the product of its eigenvalues and eigenvectors as

$$C = V \Lambda V^T \quad (6.14)$$

where

V is an orthogonal $m \times m$ matrix whose columns are the eigenvectors V_i and

Λ is the $m \times m$ diagonal matrix whose elements are the eigenvalues λ_i (Jackson, 1972; Wiggins, 1972)

Since V is an orthogonal matrix,

$$VV^T = V^T V = I_m \quad (6.15)$$

where

I_m is an identity matrix of order m .

Therefore

$$\begin{aligned} C^{-1} &= (V \Lambda V^T)^{-1} \\ &= V \Lambda^{-1} V^T \end{aligned} \quad (6.16)$$

where

Λ^{-1} is the $m \times m$ diagonal matrix whose elements are the reciprocals of the eigenvalues ($1/\lambda_i$)

It could be seen from equation 6.16 that C^{-1} will exist, provided none of the eigenvalues is zero.

From equation 6.12,

$$X_K = \sum_{i=1}^m C_{Ki} Z_i \quad (6.17)$$

Thus the X 's are linear combinations of the Z 's. By error theory (see section 4.4), the variance of X_K is given by

$$\text{Var}(X_K) = \sum_{i=1}^m (C_{Ki}^{-1})^2 \text{Var}(Z_i) \quad (6.18)$$

But from equation 6.16,

$$C_{Ki}^{-1} = \sum_{j=1}^m v_{Kj} \lambda_j^{-1} v_{ij} \quad (6.19)$$

Hence

$$\text{Var}(X_k) = \sum_{i=1}^m \left\{ \sum_{j=1}^m (v_{kj} \lambda_j^{-1} v_{ij})^2 \right\} \text{Var}(Z_j) \quad (6.20)$$

Thus though C^{-1} will exist even if the eigenvalues are very small, the corresponding variance of X will be very large if only even a particular eigenvalue is very small.

Because eigenvalues approach zero exponentially (Wiggins, 1972), it is very difficult to distinguish between very small eigenvalues and zero eigenvalues; and so it is necessary to define a lower limit such that all eigenvalues less than such a limit will be ignored. This limit may be set (Wiggins, 1972; Jackson, 1972) by choosing an upper limit T_k , for the variance of X such that

$$\text{Var}(X_k) \leq T_k, \text{ for all } k \quad (6.21)$$

All the above results can also be obtained by taking partial derivatives with respect to X of equation 6.9 and equating the derivatives to zero.

Equation 6.8 can also be solved for A if both Y and X are known. This corresponds to the calibration of the measuring instruments. Taking transpose of both sides of equation 6.8 yields

$$Y^T = X^T A^T + E^T \quad (6.22)$$

Using equations 6.8 and 6.12, the solution of equation 6.22 gives

$$\begin{aligned} A^T &= \{(X^T)^T \cdot X^T\}^{-1} \cdot (X^T) \cdot Y^T \\ &= (X \cdot X^T)^{-1} \cdot X^T \cdot Y^T \end{aligned} \quad (6.23a)$$

Again taking the transpose of both sides of equation 6.23a gives

$$A = Y \cdot X^T \cdot (X \cdot X^T)^{-1} \quad (6.23b)$$

provided $(X \cdot X^T)$ is a non-singular matrix.

Advantages Of Least Squares' Method

Some of the advantages of the least squares' method include

- (i) the method is free from subjective judgement
- (ii) it is suitable for spectra whose statistical variations in counting are large
- (iii) all data in a spectrum can be used and not restricted to those in the region of photopeaks
- (iv) estimates can be made of the variance and the uncertainty of the variance associated with each result, and
- (v) it is amendable to computer calculation

A general disadvantage of the least squares' method, however, is that the calculated coefficients (X or A) may be negative, which of course should not be for physical reasons (see equation 6.7). The least squares' method also leads to handling of large matrices.

Application Of Least Squares In Radiometrics

In general the application of least squares requires that the variance of all observations shall be the same. But in radiometrics, the variance of the count rate in each channel is not constant. Thus a

weighting matrix W is introduced. In defining the weighting matrix, the following assumptions (Eckhoff et al, 1970) are made:

- (1) the count rates are normally distributed
- (11) the errors in the recorded counts are given by the square root of the counts in that channel, and
- (111) the count rates are statistically independent

Using these assumptions, the weighting matrix W is defined as an $n \times n$ square matrix whose elements are given by

$$\begin{aligned} W_{ij} &= 1/\sqrt{y_i} \quad \text{if } i = j \\ &= 0 \quad \text{if } i \neq j \end{aligned} \tag{6.24}$$

where

$$j = 1, 2, 3, \dots, n$$

$$\text{and } i = 1, 2, 3, \dots, n$$

Introducing W into equations 6.8 and 6.10 leads to

$$\begin{aligned} C &= A^T W A \\ Z &= A^T W Y \end{aligned} \tag{6.25}$$

$$\text{and } X = C^{-1} Z = (A^T W A)^{-1} A^T W Y$$

In the calculation of the A 's in equation 6.8, the definition of W is practically impossible because of the number of standards (at least three) used. This difficulty leads to a further assumption in the application of least squares in radiometrics that the coefficients A are known without errors.

6.5. Calibration Of Spectrometer (Isotopic)

The gamma ray spectrometer has to be calibrated in order to relate the detected counts to concentration in the source of radiation. This involves the determination of the coefficients A (see equation 6.23). Equation 6.4b shows that at least $(n \times m)$ equations should be available in order to uniquely solve for the A's. Thus since n channel spectrometer is used, at least m standard sources of known concentrations should be available in order to calibrate the instrument. If l is the number of standard sources used, then equation 6.4b is solvable as long as $l \gg m$, irrespective of the number of channels, n, used. It is also worthwhile to note that equation 6.4b possesses a unique solution only if $n \gg m$. Thus in order to calibrate the spectrometer for the determination of three elements - potassium, uranium and thorium, at least three sources of known concentrations and a spectrometer having at least three channels must be used.

In the calibration of the spectrometer, the matrix of the count rate Y, the calibration coefficient matrix A, and the concentration matrix X are respectively dimensioned as $Y(n,l)$, $A(n,m)$, and $X(m,l)$; where $n \gg m$ and $l \gg m$. The condition $n = m = 3$ gives the conventional three window spectrometer for the simultaneous determination of potassium, uranium and thorium; and in this case, the diagonal elements of the matrix A represent the sensitivities of the instrument to the three elements - potassium, uranium and thorium respectively, whilst the off-diagonal elements in a column divided by the diagonal element in that column give the stripping ratios (see section 6.5.1.).

An absolute calibration of field instrument can be carried out by reproducing as closely as possible the field conditions. The calibration can be done by taking measurements on flat natural geological outcrops in the field (Dug, 1968) or on flat artificially built platforms (Grasty and Darnley, 1971). At least three such outcrops or platforms of known concentrations of potassium, uranium and thorium are necessary. In both cases, the outcrops or platforms should each contain higher concentrations of one of the three radioactive elements (Matolin, 1973) in such a manner that the determinant of the concentration matrix X is not zero. The reproducibility of the geometry during the calibration and the field measurements can be assured by a portable lead collimator placed around the detector.

The in-situ measurements on several outcrops within the survey area and samples taken from these outcrops are then analysed in the laboratory for the potassium, uranium and thorium contents. Dug (1968) used this procedure to calibrate a portable spectrometer but Grasty and Darnley (1971) stated that the method cannot be used for the calibration of airborne systems, probably because of accessibility. A common procedure then for the calibration of field spectrometer, especially airborne, is the use of artificial calibration pads. However in each case, the geometry is very different at survey altitude compared with the ground or pads and Grasty (1982a) used plywood to simulate atmospheric attenuation of pad data. Based on the Grasty's work (1982a), Dickson et al (1981) showed that at any altitude h , gamma ray spectra can be represented by two

components - primary and secondary components, whose amplitudes a , are defined by an exponential function as

$$a(h) = Ae^{-\alpha h} + C \quad (6.26)$$

where

A , α , and C are constants that will be different for potassium, uranium and thorium

Thus instead of calculating the stripping ratios from data obtained on pads at ground level and then correcting them to chosen survey height as stated in section 4.5, the above equation 6.26 may be used to extrapolate the calibration spectra for potassium, uranium and thorium at the desired height before determining the stripping ratios.

6.5.1. Calibration Of 3 - Window Spectrometer

In a 3 - window spectrometer, a window is assigned to potassium, one to uranium, and another to thorium. If the counts in each of these windows are summed and substituted into equation 6.4b, we have, after background subtraction,

$$\begin{aligned} Y_K &= A_{KK}X_K + A_{KU}X_U + A_{KT}X_T \\ Y_U &= A_{UK}X_K + A_{UU}X_U + A_{UT}X_T \end{aligned} \quad (6.27)$$

and
$$Y_T = A_{TK}X_K + A_{TU}X_U + A_{TT}X_T$$

where

the subscripts K, U, and T stand for potassium, uranium and thorium respectively.

In section 4.3.2., Y_K , Y_U and Y_T are defined as

$$\begin{aligned} Y_K &= K_C + \gamma U_C + \beta T_C \\ Y_U &= gK_C + U_C + \alpha T_C \end{aligned} \quad (4.11)$$

and $Y_T = bK_C + aU_C + T_C$

where

$$\begin{aligned} K_C &= p_1 X_K \\ U_C &= p_2 X_U \end{aligned} \quad (4.40)$$

and $T_C = p_3 X_T$

where

p_1, p_2, p_3 are the respective sensitivity of the spectrometer to potassium, uranium and thorium, and

X_K, X_U, X_T are respectively the concentrations of potassium, uranium and thorium in a given sample (or standard).

Combining equations 4.11 and 4.40 gives

$$\begin{aligned} Y_K &= p_1 X_K + \gamma p_2 X_U + \beta p_3 X_T \\ Y_U &= g p_1 X_K + p_2 X_U + \alpha p_3 X_T \end{aligned} \quad (6.28)$$

and $Y_T = b p_1 X_K + a p_2 X_U + p_3 X_T$

and comparing equations 6.27 and 6.28 gives

$$\begin{array}{rcl}
 p_1 & = & A_{KK} \\
 gp_1 & = & A_{UK} \longrightarrow g = A_{UK}/A_{KK} \\
 bp_1 & = & A_{TK} \longrightarrow b = A_{TK}/A_{KK} \\
 p_2 & = & A_{UU} \\
 \gamma p_2 & = & A_{KU} \longrightarrow \gamma = A_{KU}/A_{UU} \\
 ap_2 & = & A_{TU} \longrightarrow a = A_{TU}/A_{UU} \\
 p_3 & = & A_{TT} \\
 \beta p_3 & = & A_{KT} \longrightarrow \beta = A_{KT}/A_{TT} \\
 \alpha p_3 & = & A_{UT} \longrightarrow \alpha = A_{UT}/A_{TT}
 \end{array} \tag{6.29}$$

Sometimes it is assumed that $a = b = g = 0$ (Grasty and Darnley, 1971).

Hence $A_{TU} = A_{TK} = A_{UK} = 0$, and then equation 6.28 reduces to

$$\begin{array}{rcl}
 Y_K & = & A_{KK}X_K + A_{KU}X_U + A_{KT}X_T \\
 Y_U & = & A_{UU}X_U + A_{UT}X_T \\
 \text{and } Y_T & = & A_{TT}X_T
 \end{array} \tag{6.30}$$

This condition assumes that there is no interference from lower energy windows in higher energy windows. However, a has been found to have a value of 0.05 (Grasty, 1975).

In equation 6.5, if $l = m$, the matrix X is square and equation 6.5 has an exact solution given by

$$A = YX^{-1} \tag{6.31}$$

This is equivalent to the "Linear Regression method" (equation 6.30) as used by the Geological Survey of Canada (GSC) (Grasty and Darnley, 1971); or the "Matrix Method" (equation 6.27) as defined by Allan and

Richardson (1974) and Geometrics (1979). But if $l > m$ then equation 6.5 is 'overdetermined' and only the least squares' method (see equations 6.11 and 6.25) is used. In either case, A will be a 3×3 square matrix and equation 6.5 will be exact. Hence using a 3 - window spectrometer, the amount of the three elements - potassium, uranium and thorium in a given sample can be calculated. In this case X is given by

$$X = A^{-1} Y \quad (6.32)$$

6.5.2. Calibration Of Multichannel Spectrometer

In a multichannel spectrometer, the number of channels n is greater than 3. As stated earlier (section 6.5.1.), the number of standards l may be equal to or greater than m ($m = 3$), the number of elements sorted. If $l = 3$, then X has dimension $X(3,3)$. Since X is a square matrix, equation 6.5 will have an exact solution for A, given by equation 6.31. But if $l > 3$, then X is not a square matrix and so equation 6.5 has no exact solution for A, and equation 6.23b is used. It can be seen that in both cases, A will not be a square matrix and so only the least squares' method (equation 6.12 or equation 6.25) is used to determine X.

It should be noted that in the case of the multichannel analysis, there is no equivalent definition of the coefficients, A, for Compton stripping ratios. However the measure of the independence of the data and the resolution of the elements obtained from the data can be determined from two matrices called information density matrix and

resolution matrix respectively.

We recall that the least squares' solution of equation 6.5 is given (see equation 6.12) as

$$\hat{X} = (A^T A)^{-1} A^T Y = HY$$

Thus in the least squares' sense $H = (A^T A)^{-1} A^T$ is the inverse matrix of A in equation 6.5.

The information density matrix S and the resolution matrix R are defined (Wiggins, 1972; Jackson, 1972) as

$$S = AH$$

and

$$R = HA$$

If H is a unique inverse of A , then S will be an identity matrix I_n of order n , while R will be an identity matrix I_m of order m .

If $S = I_n$, then $A\hat{X} = Y$. Hence S is a measure of how well the least squares' model fits the original data. Wiggins (1972) defined the closeness of S to I_n as the degree of independence of the data. But Crossley and Reid (1982) modified the S matrix by defining the relative information (or inversion) importance of the elements of S . They did this by orthonormalizing the rows of S and calling the resultant set of the diagonal elements an information vector. That is, the elements of the information vector are given as

$$S'_{KK} = S_{KK} / \left(\sum_{j=1}^n S_{Kj}^2 \right)^{1/2}, \quad k = 1, 2, 3, \dots, n \quad (6.33)$$

These S'_{KK} 's have limiting values between 0 and 1; and they are interpreted as follows:

a given channel K has no useful information if its inversion importance is 0, and the Kth channel contains completely independent information if its inversion importance is 1
(Crossley, 1982)

Thus the information vector is actually a measure of the independence of each channel relative to its neighbours, hence it indicates the resolution power of the system (spectrometer).

The resolution matrix on the other hand maps the least squares' solution \hat{X} into the actual (true) solution X (Jackson, 1972). Hence the least squares' solution of equation 6.5 may be expressed as

$$\hat{X} = RX$$

If R is an identity matrix then the least squares' solution \hat{X} equals the true solution X and each element of \hat{X} is uniquely determined. But if R is not an identity matrix, then each element of \hat{X} is a weighted sum of the true solution X. This situation may be likened to the three-window analysis discussed above where the effect of any element in the (m x m) R matrix on the other elements can be estimated by dividing each column of R by its diagonal element. The true solution

of the problem will be given by

$$X = R^{-1} \hat{X}$$

provided R is non-singular. Since R is a square matrix, R^{-1} will be unique if it exists.

6.6. Sample Spectrum

The shape of the spectrum of a monoenergetic gamma ray beam is dependent on the photon energy, the absorbing characteristic of the detecting system, the decay mode of the sample and also background count rate around the source or detector (Adams and Gasparini, 1970). However where different sources are measured with the same detecting assembly, and after the removal of the background effect from each spectrum, the resultant shape of the spectrum varies only as a function of the photon energy, count rate and decay mode of the source. Thus to make sense, the spectrometer readings must be corrected for the effect of background and then the instrument calibrated in order to determine its characteristic constants. Also due to instrumental drift (see section 6.6.1. below), the energy represented by a particular channel may change with time during the course of measurement. This effect also has to be corrected for during the processing of the data. Thus the sequence of analysis of data is as follows:

- (i) instrumental drift correction
- (ii) background removal

(iii) Compton scattering and/or height correction, and

(iv) calibration to isotopic concentration

6.6.1. Instrumental Drift And Its Correction

Instrumental drift can be caused by varying experimental conditions such as temperature changes and count rate variation (Quittner, 1972). Although automatic controls are provided in modern instruments, these do not completely eliminate instrumental drift. The resultant effects of drift are gain and/or threshold changes. Thus when drift is noticed in an instrument, its effect has to be corrected for during the processing of the data.

Fig 6.2 illustrates the effect of gain and threshold shifts on count rate in specific channels.

Suppose when a source is counted at two different times there is a change in the energy calibration of the instrument used. The channel position of a given photopeak in the first spectrum will be different from its position in the second spectrum as shown in Fig 6.3. Fig 6.3 shows the gamma ray energy versus channel number (energy calibration) under conditions of different gain and threshold. When the sample is first counted, the first and Nth channels correspond to energies E_1^f and E_N^f , and the threshold is η^f (line 1). On the second count, the first and Nth channels correspond to energies E_1^s and E_N^s , and the threshold is η^s (line 2). The channel corresponding to energy E_i^f has shifted from 1 to 1.

The gradient of line 1 is given by

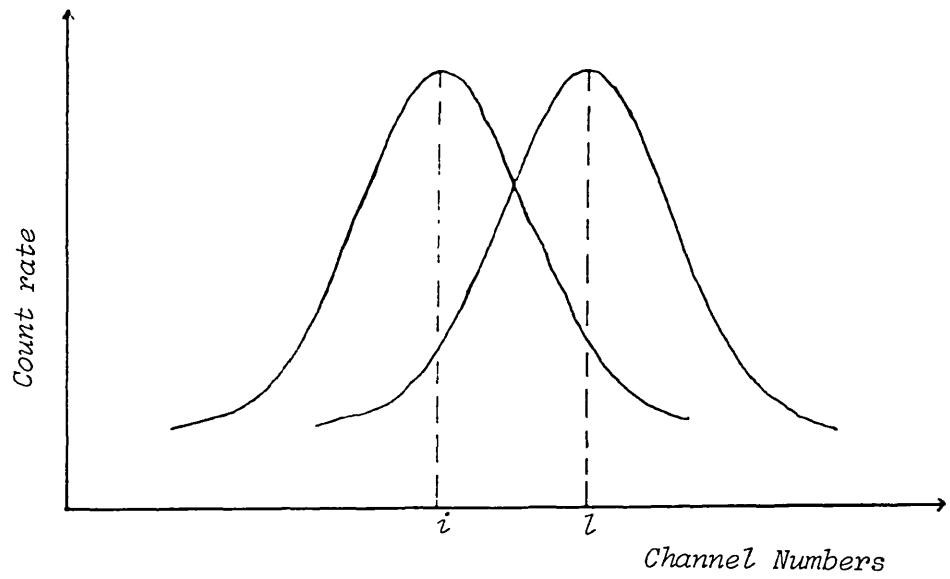


Fig.6.2: Change in peak-position due to gain and threshold changes

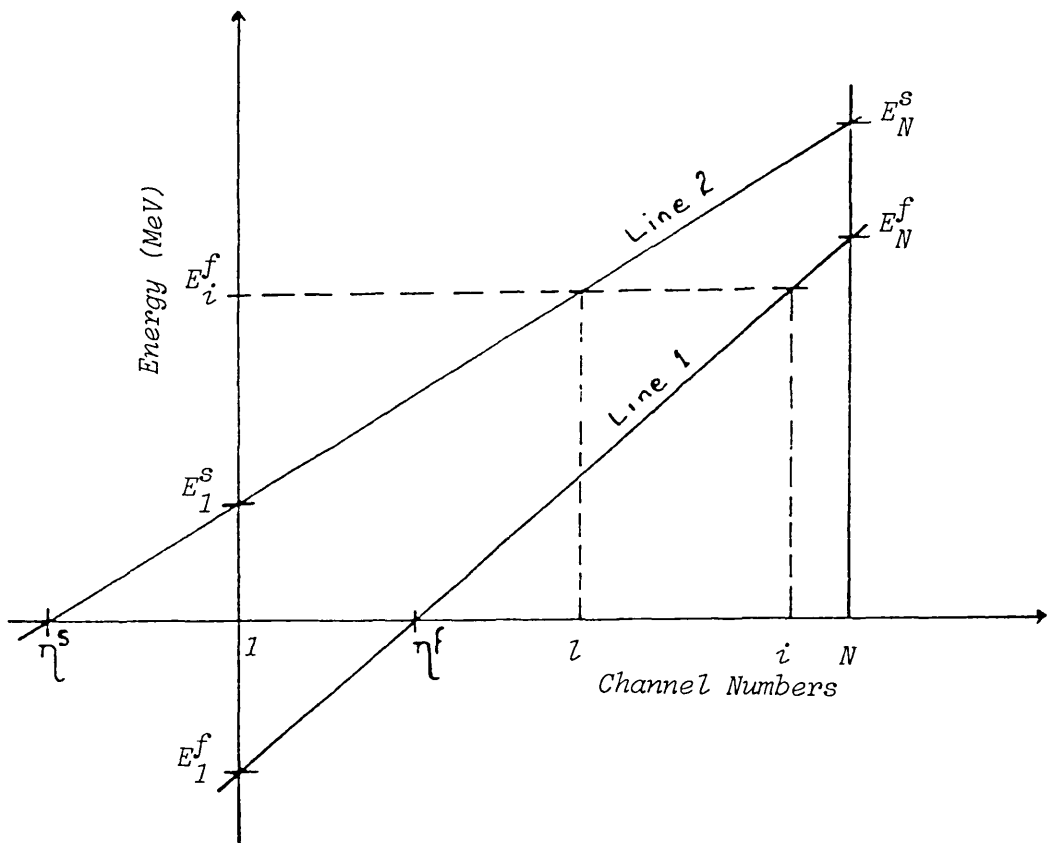


Fig.6.3: Energy calibration under different gain and threshold

$$m_1 = \frac{E_N^f - E_1^f}{N - 1} \quad (6.34a)$$

and the gradient of line 2 is given by

$$m_2 = \frac{E_N^s - E_1^s}{N - 1} \quad (6.34b)$$

According to Schonfeld et al (1966), the new gain instead of remaining 1.0 becomes

$$G = \frac{E_N^f - E_1^f}{E_N^s - E_1^s} = \frac{m_1}{m_2} \quad (6.35)$$

So the

$$\text{Gain change} = G - 1.0$$

and

$$\text{Threshold change} = \gamma^s - \gamma^f \quad (6.36)$$

Several authors, Parr and Lucas, Jr. (1964), Schonfeld et al (1966), Trombka and Schmadebeck (1968), have suggested various methods for compensating for the instrumental drift (gain and threshold changes). But here the linear interpolation method is used because of its simplicity (Parr and Lucas, Jr., 1964; Quittner, 1972). This method assumes that the data in a channel are represented as a histogram (see Fig 6.4). After a change in threshold of Z_c -channels and a fractional change g_c in gain, the new channel boundaries correspond to energies different from the original ones. The new boundaries of channel K for instance, are given by

$$LB_K = K + Z_C + g_C (K - Z_0)$$

and

(6.37)

$$UB_K = K + 1 + Z_C + g_C (K + 1 - Z_0)$$

where

LB and UB are respectively the new lower and upper boundaries of channel K (Parr and Lucas, Jr., 1964; Quittner, 1972).

Z_0 is the original threshold corresponding to the original energy calibration of the spectrometer, and

g_C is the gain change

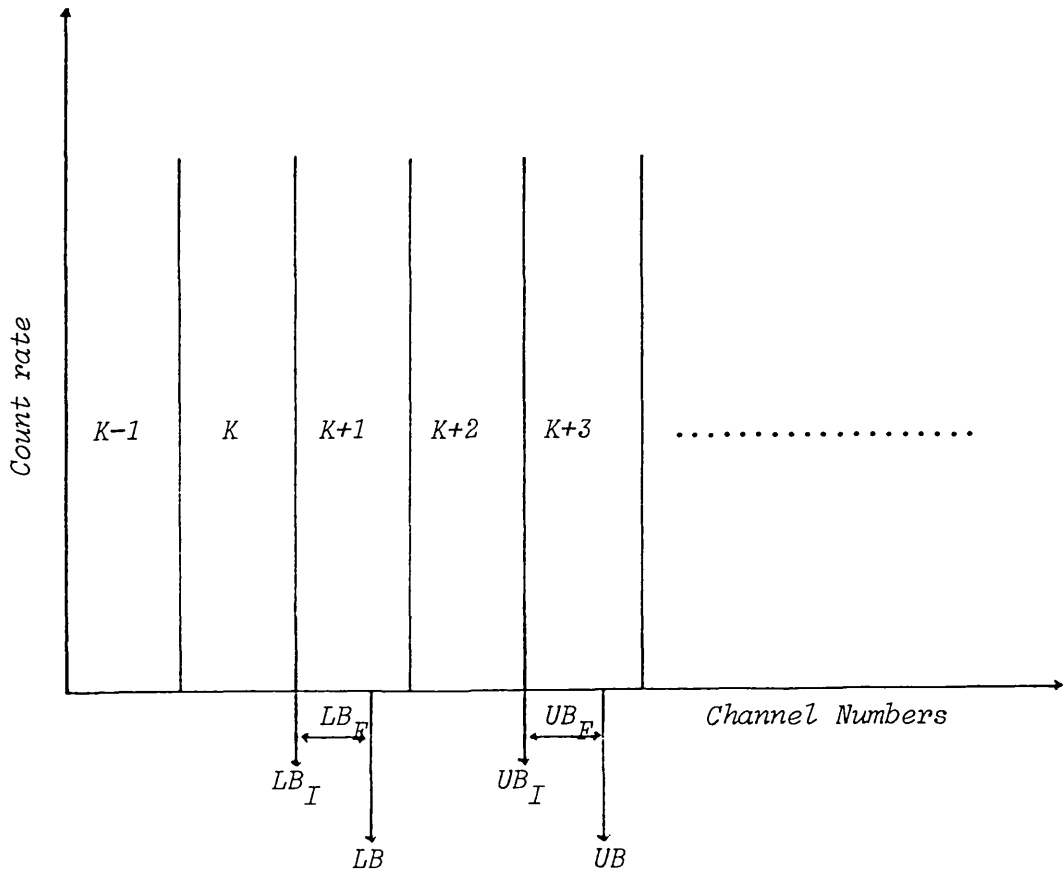


Fig.6.4: Illustration of channel boundary changes due to gain and/or threshold changes

Correspondingly, if Y_K is the count rate in channel K of the shifted spectrum, then the shift corrected count rate in that channel is given by

$$\bar{Y}_K = (1 - LB_F)Y_{LB_I} + Y + UB_F Y_{UB_I} \quad (6.38)$$

where

LB_F and UB_F are respectively the fractional part of LB and UB; and LB_I and UB_I are the integral parts of LB and UB respectively

Y is the sum of the counts between LB_I and UB_I and it is given by

$$Y = \begin{cases} \sum_{I=LB_I+1}^{UB_I+1} Y_I & \text{if } LB_I + 1 \leq UB_I - 1 \\ \emptyset & \text{if } LB_I + 1 > UB_I - 1 \end{cases} \quad (6.39)$$

In order to determine g_c and Z_c in equation 6.37, the peak position in each of the three windows representing potassium, uranium and thorium is determined and these three points are used to recalibrate the instrument, from whence the threshold and gain changes for each spectrum are determined and the counts corrected accordingly.

In order to locate the peak position within each elemental window, the data within each window are first smoothed in order to remove statistical fluctuations. The method used here is based on a least squares' fit of a power (quadratic) function to a small region (window) of the data. Apart from this, the data can also be smoothed using moving average, exponential, symmetrical exponential and

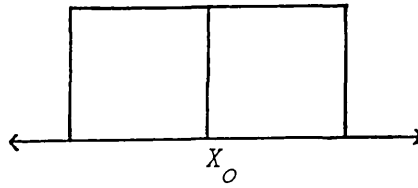
symmetrical triangular functions (see Fig 6.5) (Savitzky and Golay, 1964).

In the least squares' technique, if C_i is the count rate in channel i , then the smoothed value of C_i is defined as D_i and given by

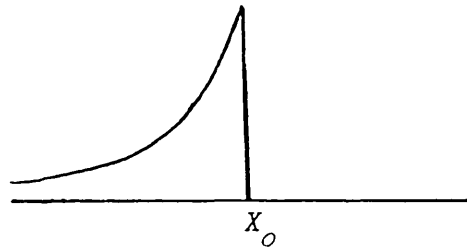
$$D_i = \frac{1}{N_m} \sum_{j=-m}^m (a_{m,j} C_{i+j}) \quad (6.40)$$

The constants $a_{m,j}$ and the normalizing constant N_m are from tables (Savitzky and Golay, 1964) shown in appendix A. Here it is assumed that small regions of the spectrum are approximated by quadratic or cubic power functions, and the values of $a_{m,j}$ and N_m are those derived from these functions. Yule (1966, 1967) pointed out the problems associated with this method. It should be noted however that the smoothed data are not used in further calculations after the peak position has been located.

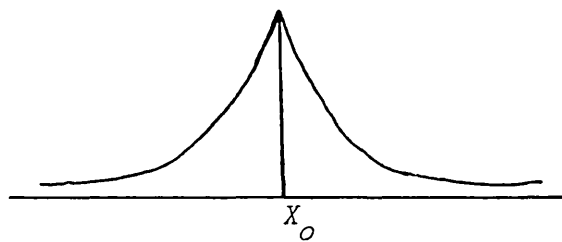
(i) moving average



(ii) exponential function



(iii) symmetrical exponential function



(iv) symmetrical triangular function

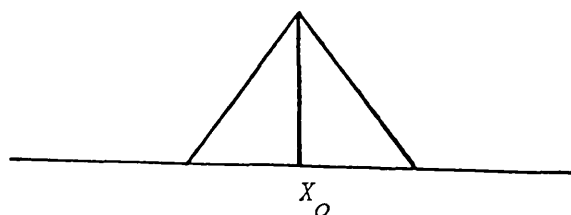


Fig. 6.5: Smoothing functions (after Savitzky and Golay, 1964)

CHAPTER SEVEN

DATA ACQUISITION, ANALYSIS AND INTERPRETATION OF RESULTS

The objectives of this project as stated earlier (see chapter One) include:

- (1) experimental comparison of the performances of a NaI(Tl) detector and a Ge(Li) detector in geological and mineral exploration applications
- (11) comparison of quantitative results obtained from the conventional three window analysis and those from multichannel analysis, and
- (111) comparison of laboratory and field results

In order to achieve these objectives, laboratory and field (airborne) data are used. In the laboratory, a set of samples are analysed using respectively a NaI(Tl) detector and a Ge(Li) detector. These are the only data used in (1) above because of non-availability of field (airborne) data for a Ge(Li) detector. But for (11) both laboratory and field data are used. This will enable us, in addition to comparing the two methods of analysis in different survey environments, see how laboratory and airborne surveys complement one another. The laboratory samples are collected from stations along the same profile the airborne survey was flown.

In the analysis of the data for the comparison of the performances of the NaI(Tl) detector and the Ge(Li) detector, only multichannel spectrometer data will be used, as the definition of window widths in

a window spectrometer is based on the resolution (ability to differentiate between gamma rays of different energies) of the detector. Since it is known that a NaI(Tl) detector has better efficiency (detecting power) than a Ge(Li) detector, while the later has better resolution than the former, this comparison will therefore provide an idea whether or not the acquisition of high efficiency or high resolution data is the essential factor in geological and/or mineral exploration applications of gamma ray spectrometry.

Towards the set goals, the work in this chapter is set out as follows:

- (1) from the laboratory data, comparison will be made between
 - (a) NaI(Tl) and Ge(Li) results from multichannel analysis
 - (b) results obtained from NaI(Tl) multichannel analysis and NaI(Tl) three-window analysis
- (2) from the field (airborne) data, comparison will be made between results obtained from multichannel analysis and those from three-window analysis, and
- (3) comparison will be made between the results from the laboratory NaI(Tl) analyses and those from the field analyses.

Also available (Cowan, personal communication) are results from ground gamma ray spectrometric survey (3 - window analysis) and geochemical analysis of samples from the same profile as the airborne survey. These results will be used to aid in the interpretation of the results

obtained in this project.

7.1. Data Acquisition

7.1.1. Laboratory Data

As stated above, the laboratory analysis will be used to compare both the results from the multichannel analysis and three-window analysis, and also will provide a comparison between the performances of a NaI(Tl) and a Ge(Li) detector in the application of gamma ray to geological and mineral exploration. The laboratory data were obtained by running the same set of samples on a NaI(Tl) detector and then on a Ge(Li) detector. The work was carried out at the Imperial College (University of London) Field Station at Silwood Park, Ascot, where these two detector types are available. All together twenty two samples, including standards for potassium, uranium, thorium and background radiations, were analyzed.

The samples (and the standards), packed in plastic containers, were first each mounted on a cylindrical 3" x 3" NaI(Tl) detector, placed in a shield of dimension 2' x 2' x 2'. The samples were then in turn analyzed using a coaxial Ge(Li) detector, with active volume of 86cc, placed in a Dewar cryostat of volume 34 liter. Each of the detectors was used with the same pulse height analyzer, model NS-700, Northern Econ II series. Fig 7.1 shows the external outline of the analyzer, while Fig 7.2 illustrates the interconnection of each of the detectors and the analyzer. The analyzer consists of three functional subsystems.

(a) Signal Processing Subsystem :

This section contains an analog input circuitry, including a low level amplifier, and an analog - to - digital converter (ADC). The section also includes an internal pre-amplifier/amplifier with charge sensitive

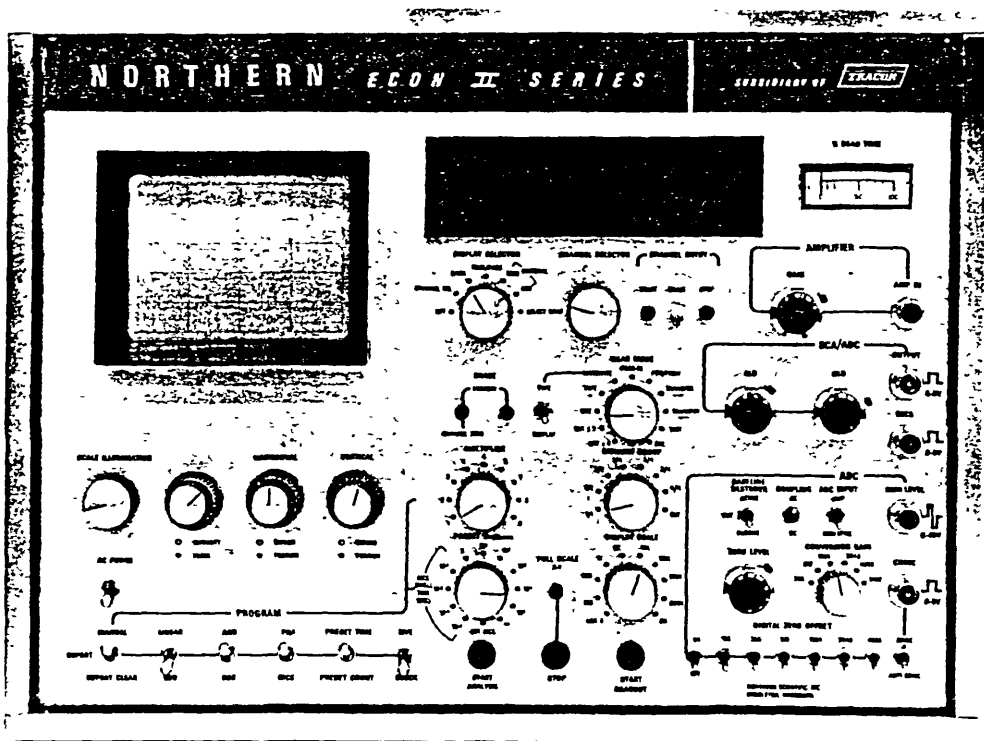


Fig.7.1: External features of the NS - 700 series pulse height analyzer

input designed to accept negative current pulses from a photomultiplier tube anode. After suitable amplification and shaping, the signal is then sent to the ADC for further processing.

(b) The Acquisition and Input/Output Subsystem :

This section consists of a core memory along with its drive circuitry, programmer, and digital - to - analog decoders. The memory is available in three sizes - 1024, 2048 and 4096 channels, each channel with a

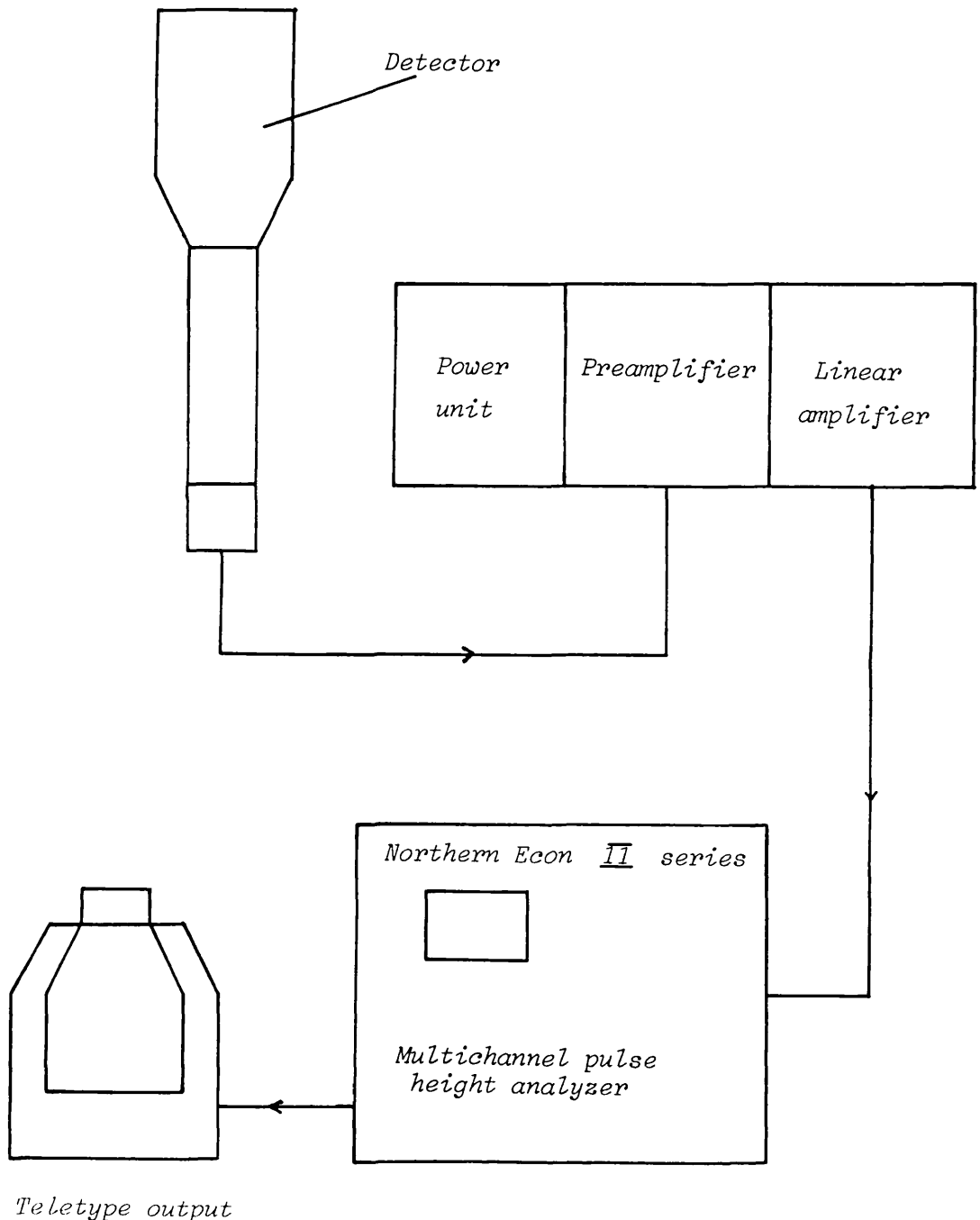


Fig.7.2: System interconnection

capacity to hold $(10^6 - 1)$ counts. Control signal inputs/outputs are available for complete parallel transfer of data to computer interface.

(c) The Display and Analysis Subsystem :

This section contains most of the circuitry which provide for selecting, storing and displaying regions-of-interest from the data in the memory unit. Controls are provided for selecting any channel from the CRT(cathode ray tube) display, reading the address of the selected channel on the digital lights. Thus using only the front panel controls and the CRT, complete quantitative information, including integrals, can be gained easily and quickly.

For more detailed description and operation of the analyzer, see the instruction manual of the Northern Econ II series.

7.1.2. Field (airborne) :

The airborne system consisting of unshielded (4π) NaI(Tl) detector package of 3×10^3 cubic inches, was flown over an aerial test range at several heights from 100feet to 1000feet in steps of 100feet, for a distance of 10kilometers, and over an aerial test range for which the ground concentrations were available. The detector package also included shielded (2π) NaI(Tl) detector of 512 cubic inches. The data for each flight height were recorded in 256 channel analyzer (4π) and 128 channel analyzer (2π) . Background spectrum at each

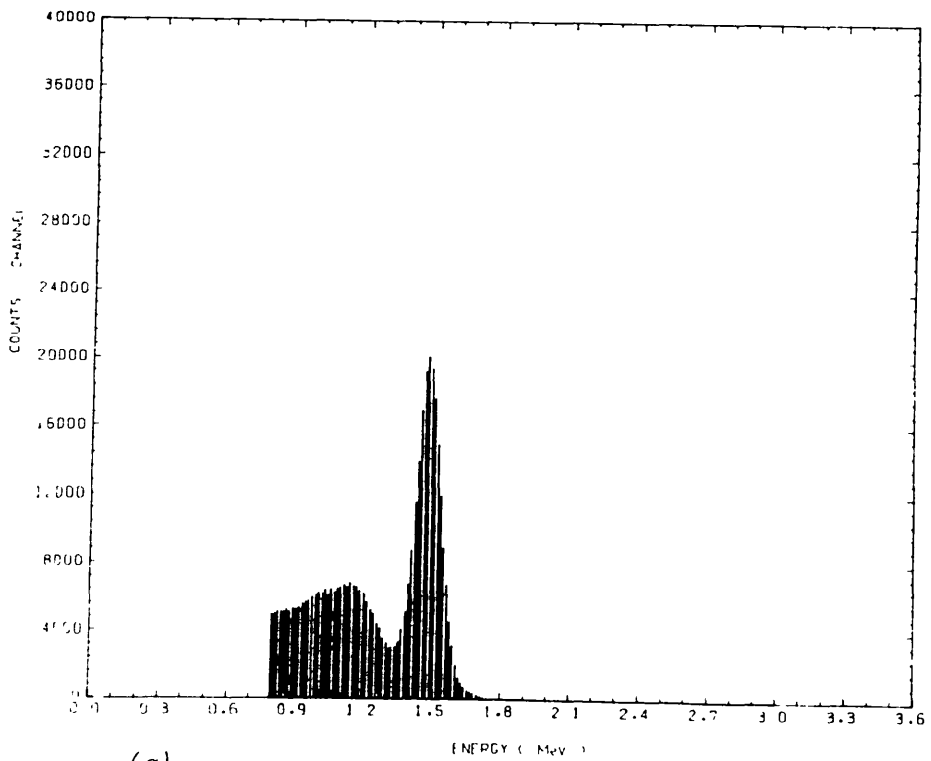
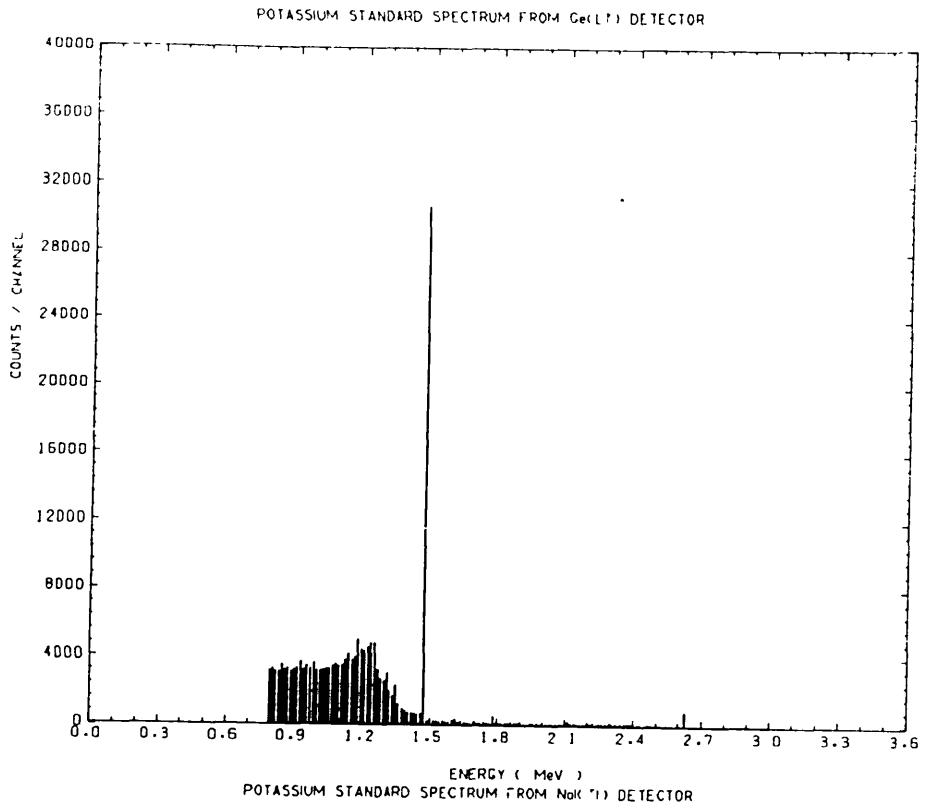
height flown was recorded over water. In addition, high level lines were also flown from 9000 feet in order to determine cosmic/aircraft background (see section 4.3.1.1.2.).

7.2. Calibration Of Instruments And Analysis Of Samples

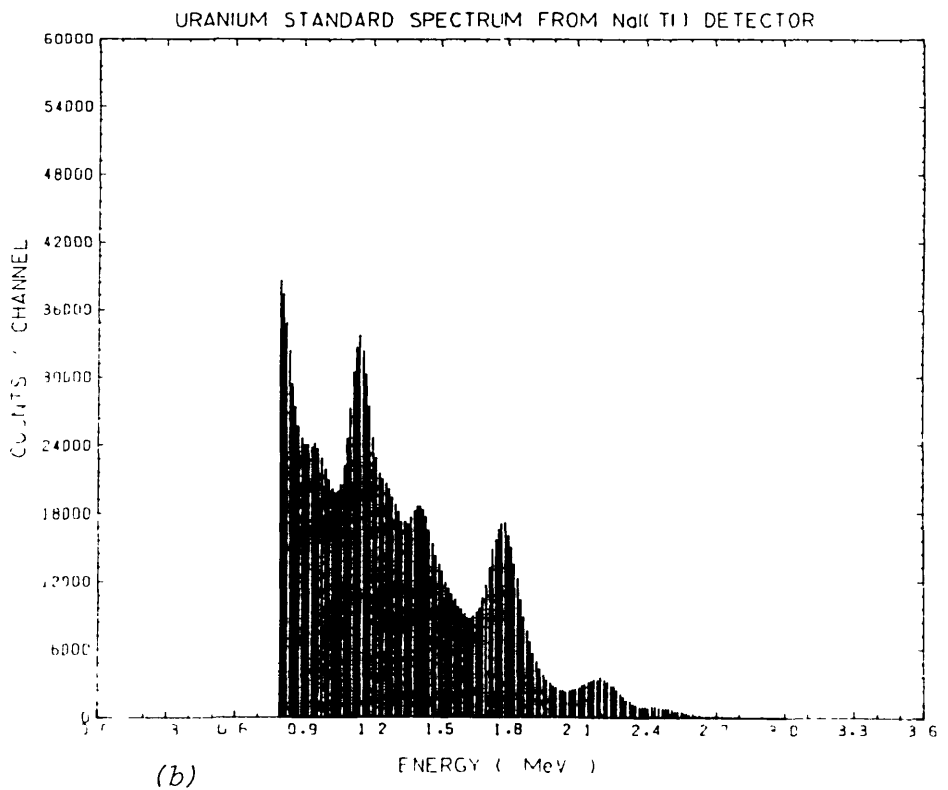
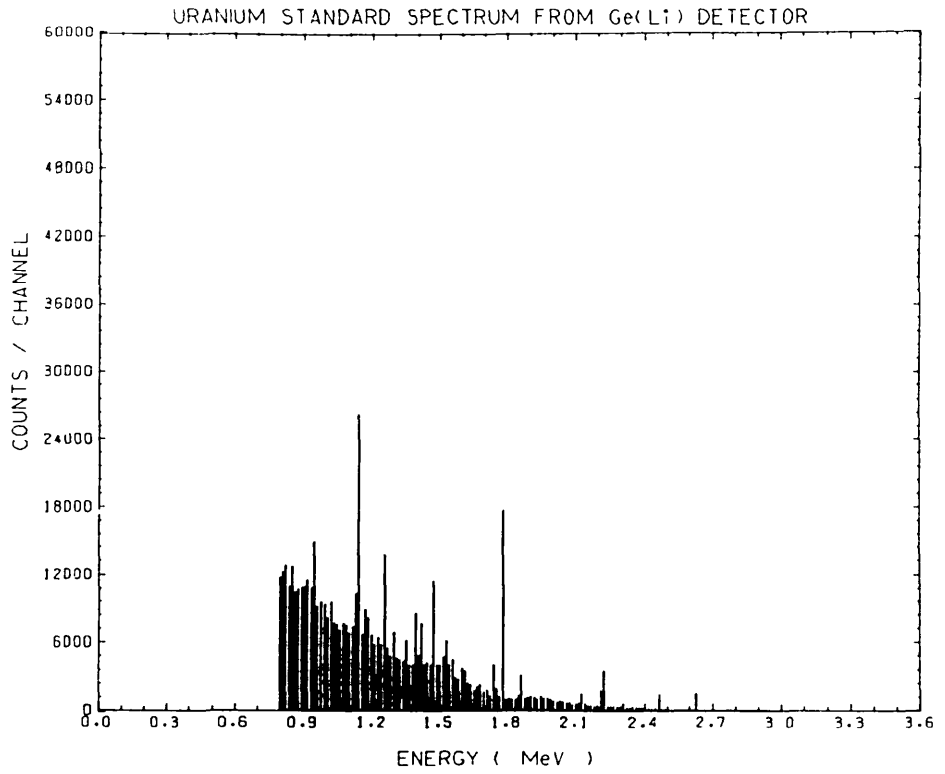
7.2.1. Laboratory :

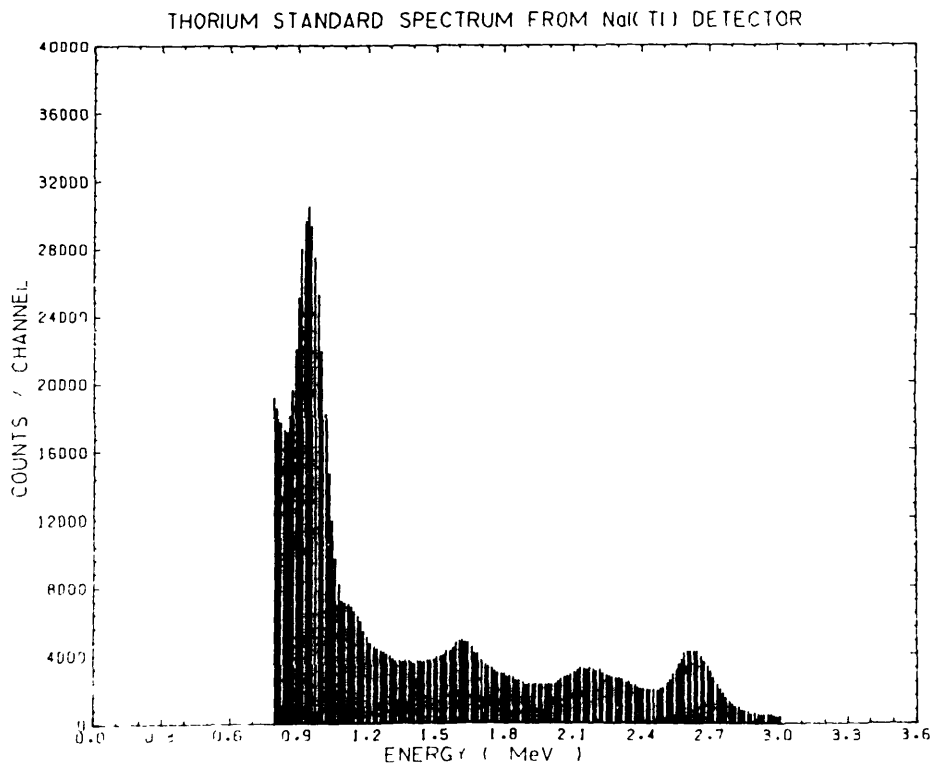
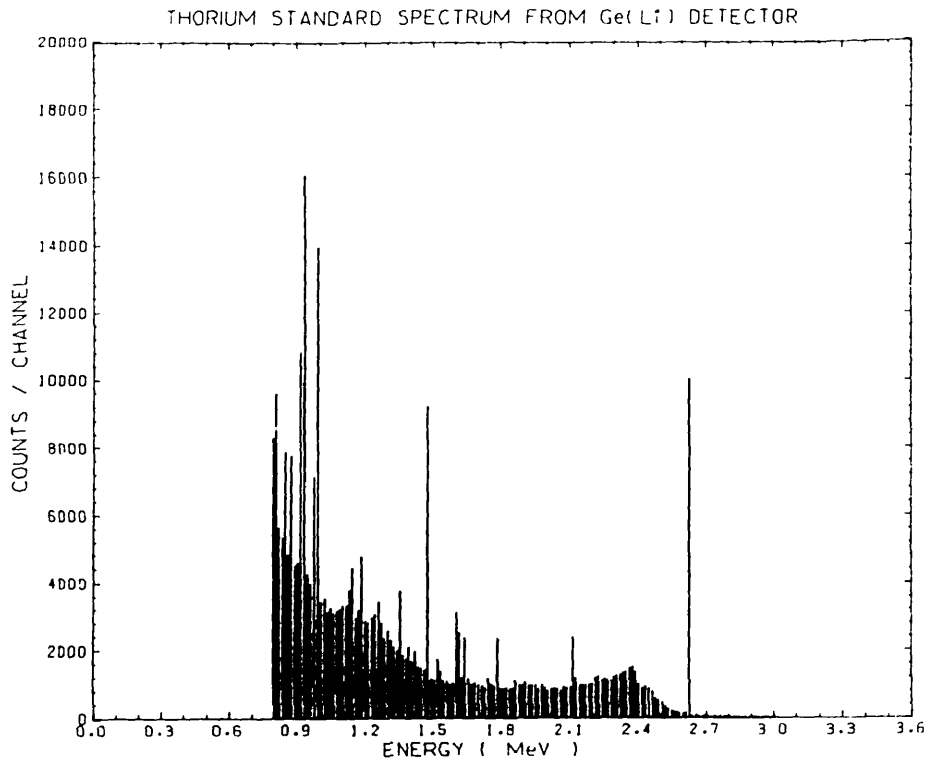
In order to calibrate the instrument (detector and analyzer) used to measure the radioactivity of the samples, standard sources of potassium, uranium and thorium with known concentrations were run using respectively the NaI(Tl) and Ge(Li) detectors with the analyzer described above (section 7.1.1.). The background radiation was monitored by using a sodium chloride standard source. This assumes that the background count rate was constant throughout the experimental period. The length of time for each run was preset and this varied between 10^4 seconds for the NaI(Tl) detector and 2×10^4 seconds for the Ge(Li) detector. This long time was used in order to ensure that statistically significant data are acquired. The problem of dead time was overcome by using live time instead of clock time. The analyzer was set at 1024 channels and at the end of each run, the counts recorded in all 1024 channels were output to a paper tape punch machine, Data Dynamics 390, connected to the analyzer (see Fig 7.2). Typical spectra obtained from some of the standard sources and samples are shown in Fig 7.3 for the Ge(Li) and the NaI(Tl) detectors. Some others are shown in appendix B.

Fig 7.4 illustrates the steps necessary for the complete analysis of the laboratory data.

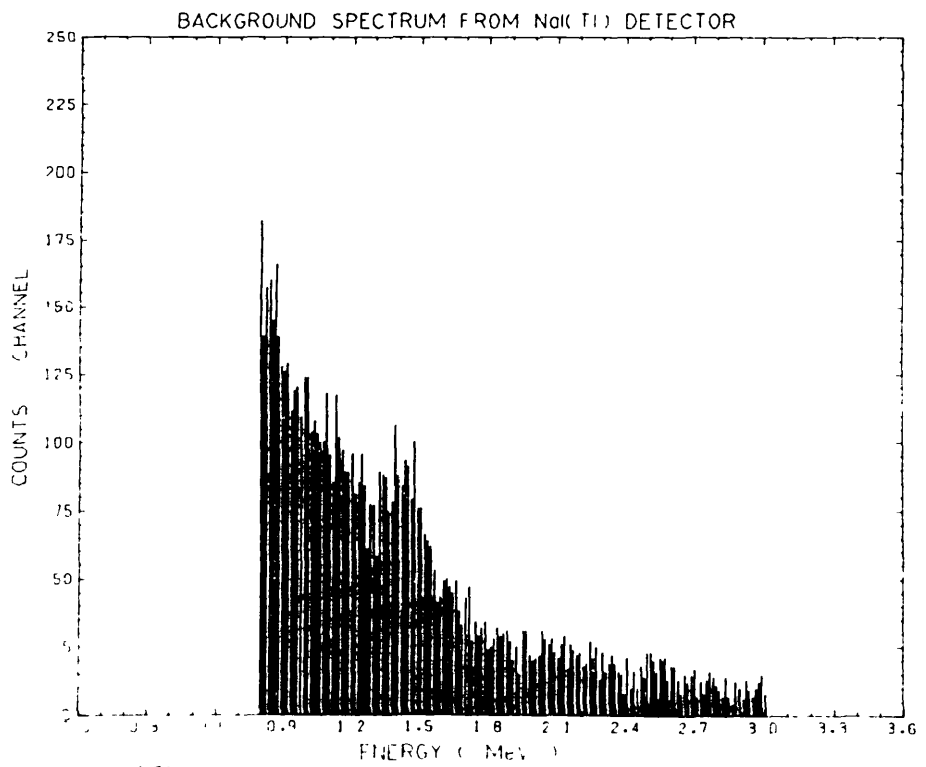
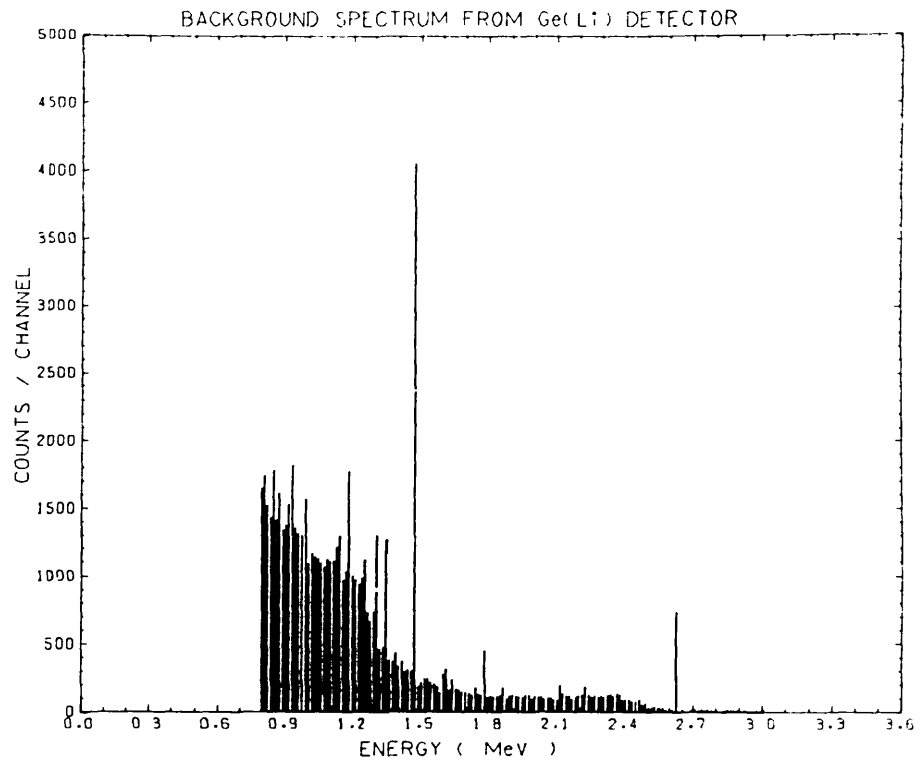


(a)





(c)



(d)

Fig.7.3: Laboratory sample spectra

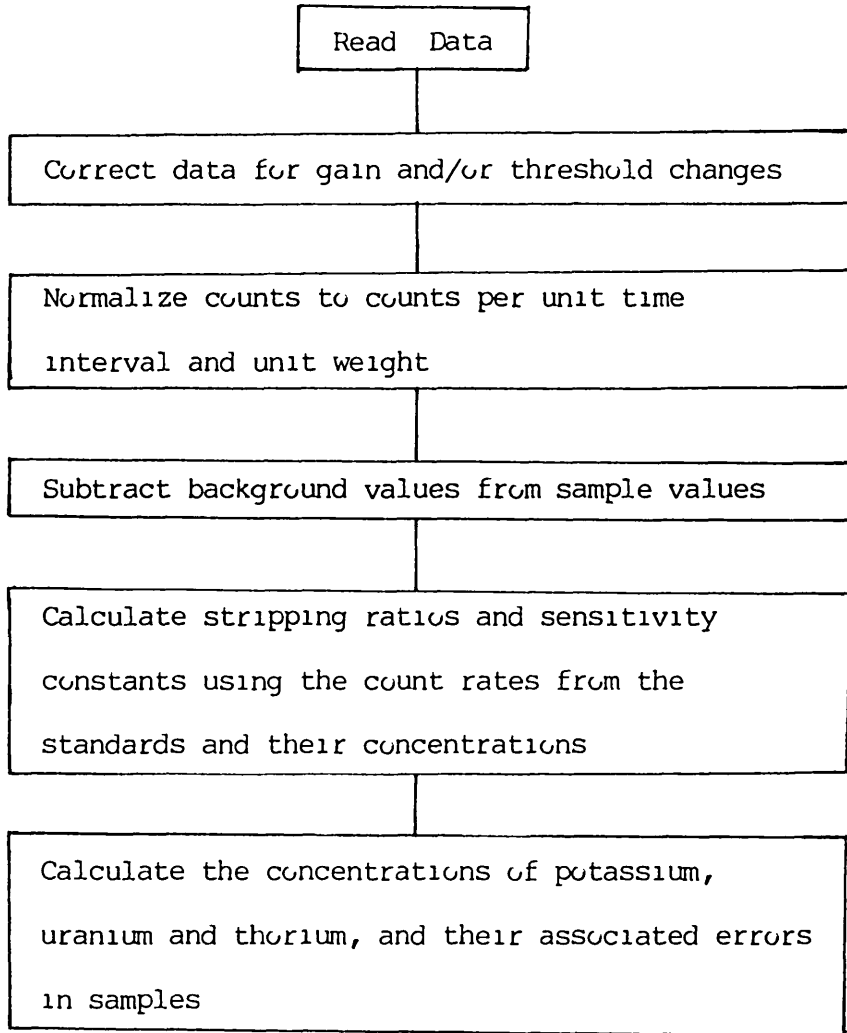


Fig 7.4: Flow chart for laboratory data analysis

7.2.1.1. Multichannel Analysis:

For the multichannel analysis of the data, it was necessary to reduce the number of data points (channel) partly to reduce the statistical fluctuation of the data from channel to channel and partly for easier handling of the data (Richards, 1977a; Knoll, 1979). In doing this,

Careful consideration was given to the preservation of the shape of the spectra and the information they contained. The channels were summed in groups of 2, 4, 8, 16, and 32 to form 511, 255, 127, 63 and 31 channels respectively. From the plots, Fig 7.5, it was found that 1022, 511 and 255 channel groups produce similar spectra. The spectra of channel groups 127, 63 and 31 showed noticeable differences especially in the noise envelope (lower channels). For example, the peaks at about channels 180, 200, 380 and 400 showed up clearly in the spectra of all the groups except for spectra in groups 127, 63 and 31. Thus it was decided to use the 255 channels. Having done this, the energy calibration of the detecting system was performed using the peak positions for potassium, uranium and thorium. Using the algebraic method (see section 4.5.1.), the peak positions were fitted to the peak energies in the least squares' sense. Fig 7.6 is the graph of the energy calibration for the Ge(Li) detector, showing a linear relationship between energy and channel number. Fig 7.6 indicates that there is a zero offset of about three channels and a negative intercept which confirms the non linearity of the system at low energies. The energy equivalence of each channel was calculated and this was used to identify all the isotopes (peaks) present in the samples/standards. This also helps to monitor drift. Since we are only interested in gamma ray energies from 0 to 3MeV, the energy calibration also enables us to pick out these lower and upper channels of energies 0 and 3MeV respectively. Similar procedure was also used to calibrate the NaI(Tl) detecting system and its result (see Fig 7.7) shows a zero offset of about seven channels and a negative intercept.

0 100 200 300 400 500 600 700 800 900 1000 1100
Channel Numbers

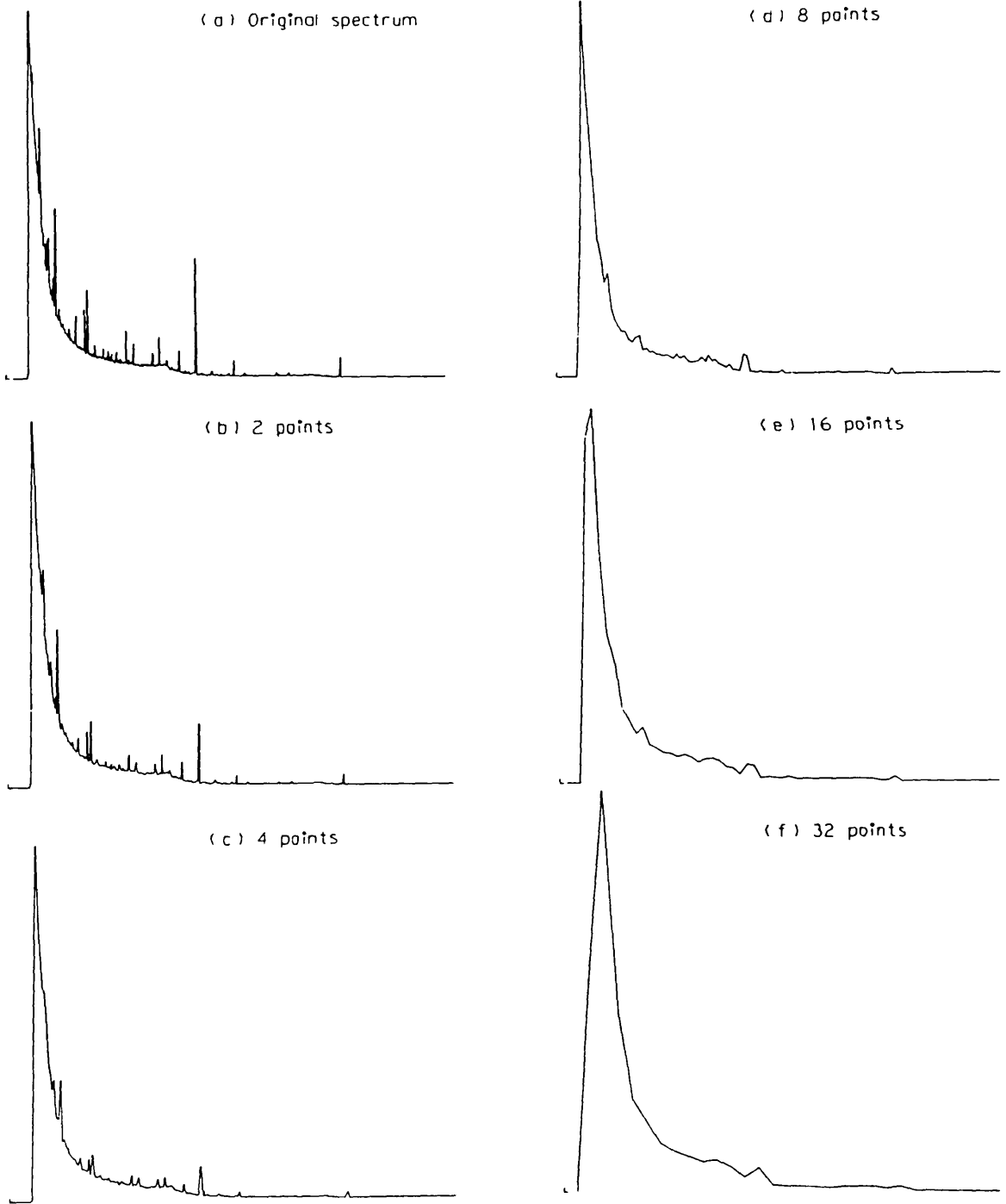


Fig.7.5 Spectrum condensation

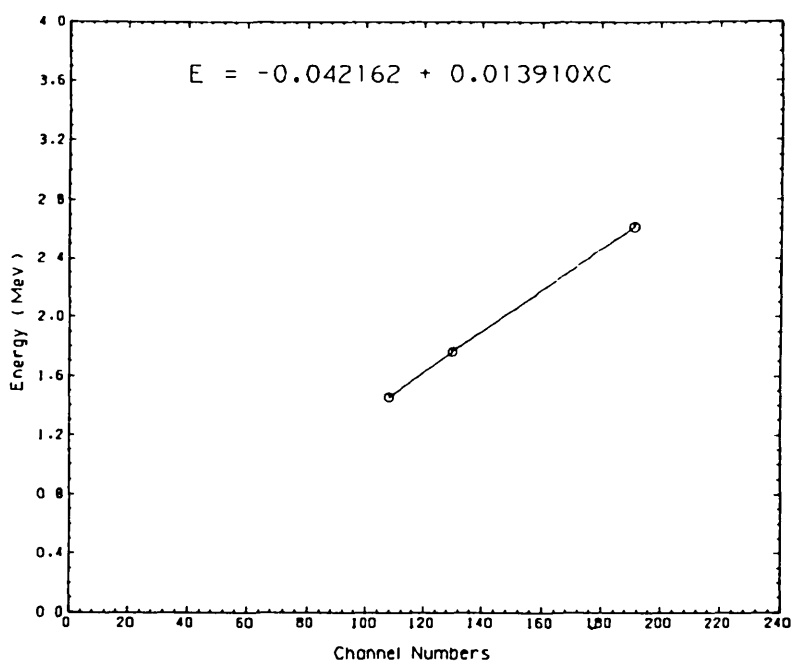


FIG.7.6 Energy calibration for Ge(Li) detector

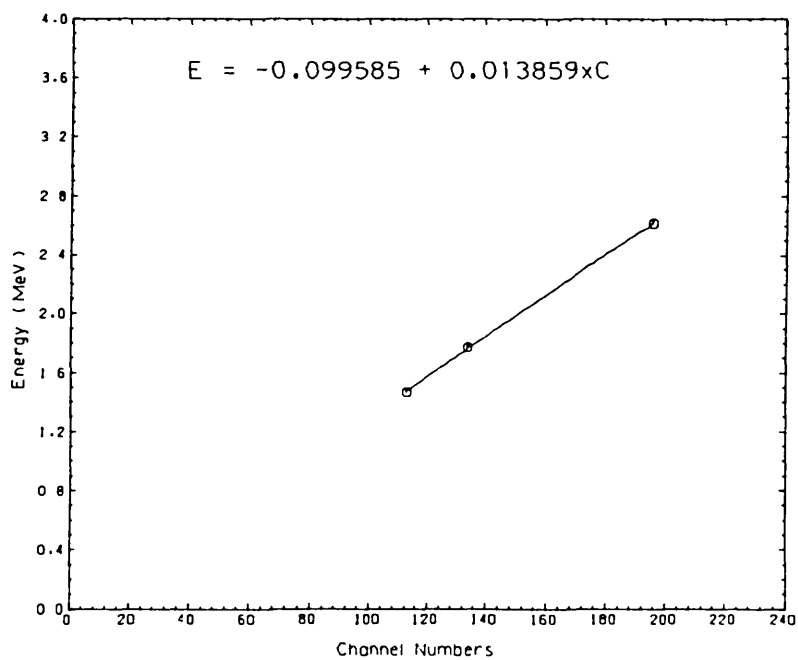


Fig.7.7 Energy calibration for NaI(Tl) detector

In order to avoid the 'noise level' and the Cesium energy peak at 0.662MeV (Grasty, 1982; Crossley and Reid, 1982), a lower energy level of 0.72MeV was chosen. Thus in the analysis of the data, channels of energies from 0.72MeV to 3MeV were used.

After all the spectra were corrected for gain and threshold changes (see section 6.6.1.), the coefficient matrix A was calculated (see equation 6.23b) using the known concentrations (matrix X) and the count rates (matrix Y) of the standard sources after the subtraction of the background count rate (see Fig 7.4). To have an idea of the relative contribution of each channel to the concentration of the elements in the samples, the information vector (see section 6.5.2.) was calculated and plotted (see Fig 7.8). The information vector shows the relative importance of each channel as well as the peaks which stand above the general exponential background (Crossley, 1982). Thus from Fig 7.8, more peaks which stand above the general background can be identified in the information vector for the Ge(Li) detector than in the information vector for the NaI(Tl) detector. For example, while the peaks at energies 0.91 and 0.97MeV are clearly resolved in the information vector for the Ge(Li) detector, these peaks are unresolved in the information vector for the NaI(Tl) detector. The following Table 7.1 shows, within the energy range of 0.72MeV to 3MeV, some isotopes of potassium, uranium and thorium, their energies and relative information 'importance' of the channels they represent. The relative information importance of the channels has values from zero to unity. Also the resolution matrix R for each of the two detecting systems was calculated and the result in each case shows that R is a

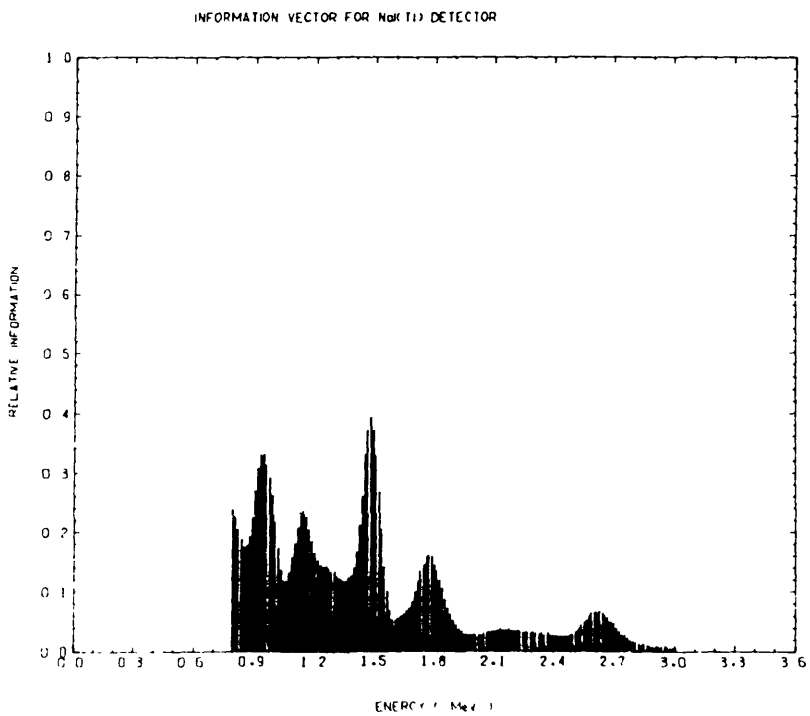
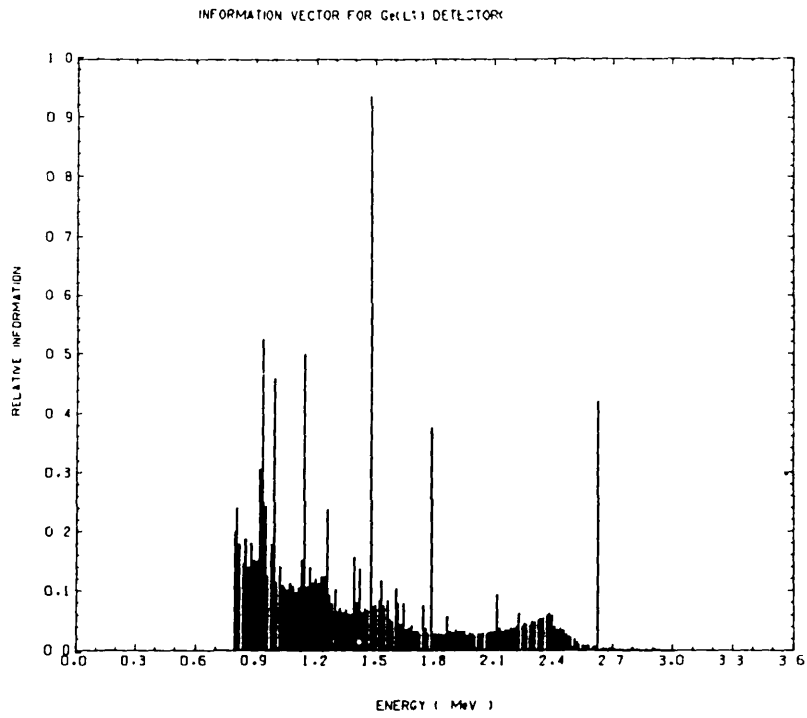


Fig.7.8: Information vector for laboratory systems

'perfect' unit matrix. Hence the concentration results obtained using the calibration matrix A are unique (Jackson, 1972).

Having determined the coefficient matrix A, the concentrations of potassium, uranium and thorium in each sample were calculated by substitution of its count rate, matrix Y, and matrix A into equation

Isotope	Energy (MeV)	Element Represented	Relative Information Importance	
			NaI(Tl)	Ge(Li)
Ac-228	0.91	Thorium	0.31	0.53
Ac-228	0.97	Thorium	0.29	0.47
Bi-214	1.12	Uranium	0.23	0.50
K-40	1.46	Potassium	0.39	0.94
Bi-214	1.76	Uranium	0.16	0.37
Tl-208	2.62	Thorium	0.07	0.42

Table 7.1: Relative Information importance of isotopes (laboratory systems)

6.25. The results of such calculations obtained from the Ge(Li) and the NaI(Tl) detectors are presented in Table 7.2.

In order to compare the performances of the Ge(Li) and NaI(Tl) detectors used, only statistically significant results will be used. Thus it was necessary first to carry out a statistical adequacy test on the results from the respective detectors.

7.2.1.1.1. Statistical Adequacy Test On Results

The statistical test involves defining 'lower detection limit' for each of the three elements - potassium, uranium and thorium. The definition of the lower detection limit carries with it two types of errors:

Type I error which occurs if it is accepted that any or all of the three elements are present (there is an activity) when actually they are not; and

Type II error which, on the other hand, occurs if it is accepted that there is no activity when actually there are some.

Statistically the lower detection limit thus expresses how effectively one can distinguish between a measurement when there is an activity and a measurement when there is no activity (Altshuler and Pasternack, 1963).

Currie (1968) defined three lower detection limits as follows :

- (1) Decision limit at which one may decide whether or not the result of an analysis implies detection. This decision is based on establishing a 'critical value L_C ' such that any of the results from the analysis of the samples is said to be zero or greater than zero according to whether that result is less or greater than the critical value.
- (11) Detection limit at which a given analysis procedure may be relied upon to lead to detection. This again involves

Sample	Ge(L1) Detector			NaI(Tl) Detector		
	K (%)	U (ppm)	Th (ppm)	K (%)	U (ppm)	Th (ppm)
0000	2.37 \pm 0.10	0.82 \pm 0.44	3.57 \pm 0.89	2.47 \pm 0.03	2.21 \pm 0.09	6.15 \pm 0.18
0060	2.53 \pm 0.10	0.82 \pm 0.44	3.36 \pm 0.89	2.99 \pm 0.03	2.21 \pm 0.09	6.77 \pm 0.18
0120	2.30 \pm 0.10	0.84 \pm 0.44	2.30 \pm 0.89	2.54 \pm 0.03	1.79 \pm 0.08	4.74 \pm 0.17
0180	2.65 \pm 0.10	1.23 \pm 0.44	5.78 \pm 0.89	2.80 \pm 0.03	1.73 \pm 0.09	5.96 \pm 0.17
0240	2.02 \pm 0.10	0.95 \pm 0.44	3.23 \pm 0.89	2.29 \pm 0.02	2.04 \pm 0.09	6.48 \pm 0.18
0300	2.37 \pm 0.10	0.34 \pm 0.44	3.40 \pm 0.89	2.24 \pm 0.02	2.20 \pm 0.07	6.84 \pm 0.14
0360	2.51 \pm 0.10	0.91 \pm 0.44	2.52 \pm 0.89	2.75 \pm 0.03	2.29 \pm 0.10	5.48 \pm 0.18
0420	2.36 \pm 0.10	0.75 \pm 0.44	2.86 \pm 0.89	2.70 \pm 0.03	2.30 \pm 0.09	6.17 \pm 0.17
0480	2.16 \pm 0.10	0 \pm 0.44	1.22 \pm 0.89	2.39 \pm 0.02	1.90 \pm 0.09	5.32 \pm 0.17
0540	2.26 \pm 0.10	0 \pm 0.44	2.15 \pm 0.88	2.71 \pm 0.03	1.98 \pm 0.09	5.51 \pm 0.17
0600	2.13 \pm 0.10	1.57 \pm 0.44	3.08 \pm 0.89	2.16 \pm 0.02	1.75 \pm 0.08	4.80 \pm 0.17
0660	1.87 \pm 0.10	1.49 \pm 0.44	4.17 \pm 0.89	1.68 \pm 0.02	2.00 \pm 0.07	5.73 \pm 0.13
0720	2.00 \pm 0.10	0.38 \pm 0.44	3.46 \pm 0.89	2.28 \pm 0.02	2.19 \pm 0.09	6.28 \pm 0.17
0780	2.18 \pm 0.10	0.24 \pm 0.44	3.98 \pm 0.89	2.34 \pm 0.03	2.44 \pm 0.09	7.31 \pm 0.18
0840	2.86 \pm 0.10	2.64 \pm 0.44	5.15 \pm 0.89	2.27 \pm 0.02	1.52 \pm 0.09	5.53 \pm 0.17
0900	3.18 \pm 0.10	3.81 \pm 0.44	5.57 \pm 0.90	2.34 \pm 0.02	1.95 \pm 0.09	5.44 \pm 0.17
0960	1.79 \pm 0.10	1.24 \pm 0.44	3.72 \pm 0.89	2.10 \pm 0.02	2.02 \pm 0.09	6.98 \pm 0.18
1000	2.26 \pm 0.10	0.03 \pm 0.44	1.26 \pm 0.88	2.48 \pm 0.02	1.59 \pm 0.06	4.72 \pm 0.13

Table 7.2: Results obtained from Ge(L1) and NaI(Tl) detectors (multichannel)

defining a small value L_D , such that any measured value of the elements can be expected, with a given degree of confidence, to be greater than or equal to the critical value. Thus L_D actually implies that the amount of an element present is greater than zero, and

- (111) Determination limit at which a given procedure will be sufficiently precise to yield a satisfactory quantitative estimates.

Of these three criteria mentioned above, only the Decision (critical) limit is of relevance to us here since we are interested only in knowing whether or not the results of our analysis imply detection. Thus in this work, the critical level (or minimum detectable limit) will be defined as that limit above which the data are said to be statistically adequate.

We recall that the variance of a sample count is given by

$$\sigma^2 = \sigma_{S+B}^2 + \sigma_B^2 \quad (7.1)$$

where

$$\sigma_{S+B}^2 = \sigma_S^2 + \sigma_B^2 \quad (7.2)$$

σ_S^2 is the variance of the counts associated with the sample alone

and σ_B^2 is the variance of the counts associated with background

Thus

$$\sigma^2 = \sigma_S^2 + 2\sigma_B^2 \quad (7.3)$$

Hence by definition of variance (see section 6.4)

$$\sigma^2 = C_S + 2C_B \quad (7.4)$$

where

C_S is the count rate of the sample alone, and

C_B is the background count rate

The critical limit is given (Currie, 1968) as

$$L_C = K_\alpha \sigma_0 \quad (7.5)$$

where

σ_0 is the standard deviation when $C_S = 0$, and

K_α is the confidence limit at α significant level

Thus from equation 7.5,

$$L_C = K_\alpha \sqrt{2C_B} \quad (7.6)$$

Any signal $S > L_C$ is regarded as a detected signal at a given α level of significance. Because L_C is affected by spectral interference between the various elements and contaminants (Currie, 1968; Norrish and Chappell, 1967), the minimum detectable concentrations for potassium, uranium and thorium are calculated using the same calibration matrix A which was used to estimate their various concentration values from the different samples. This, at least, accounts for the estimates of errors introduced by uncertainties in

the stripping and sensitivity constants (Duval et al, 1972). Table 7.3 shows the critical limits of concentration for potassium, uranium and thorium at two different significant levels.

Detector	5% Significant level			1% Significant level		
	K(%)	U(ppm)	Th(ppm)	K(%)	U(ppm)	Th(ppm)
Ge(Li) - Multichannel	0.266	3.134	4.093	0.377	4.439	5.797
NaI(Tl) - Multichannel	0.031	0.278	0.365	0.044	0.394	0.517
NaI(Tl) - Three-window	0.005	0.077	0.362	0.007	0.110	0.513

Table 7.3: Critical Detection Limits for laboratory systems

7.2.1.2. Window Analysis

In the window analysis, a window is defined for each of the three elements and this is centred on the peak position of the element. Thus while potassium window is centred on 1.46MeV, uranium and thorium windows are respectively centred on 1.76MeV and 2.62MeV. In this conventional three window analysis, only data which fall within these three windows are thus used in the analysis of the spectrum.

The energy windows are set to count the energies taken within a finite range of the relevant peak to allow for spreading of the energy peak. As stated in chapter Five, although the choice of the window widths is controversial, a window should be wide enough to accommodate the finite range of the peak it represents but it should not be so wide as to accept the flanks of adjacent peaks. The window widths used for this analysis (see Table 7.5) are 0.20MeV for potassium and uranium respectively, and 0.40MeV for thorium (Grasty, 1976),

corresponding to the window widths also used in the field (airborne) survey. From the energy calibration of the NaI(Tl) detecting system, described in section 7.2.1.1, the channel numbers corresponding to the peak energies of 1.46MeV, 1.76MeV and 2.62MeV were determined and the summations of the count rates over their surrounding bandwidths were taken, after all the data have been corrected for gain and/or threshold changes. Using equation 6.31, the calibration matrix A was calculated using the count rates and concentration values (matrices Y and X respectively) from the standard sources. After this the concentrations of potassium, uranium and thorium in the samples were calculated using equation 6.32 after the background count rate has been subtracted from the samples' count rates. Table 7.4 shows the concentration values and their associated errors obtained for potassium, uranium and thorium from the window analysis. Also the minimum detectable limits of concentration for the three elements were calculated and results are shown in Table 7.3.

7.2.2. Field (airborne)

Although there is an obvious difference between laboratory and airborne data analysis due to height correction, it should be noted that background radiation in airborne survey is much more complex and difficult to determine than in laboratory work (see section 4.3.1.). While in the laboratory no height correction is necessary because all readings are usually taken from a fixed position, in an airborne survey, flight heights may vary as mentioned in section 4.3.3. Thus corrections have to be made to the detector count rates, depending on

Sample	NaI(Tl) Detector		
	K (%)	U (ppm)	Th (ppm)
0000	2.55 \pm 0.03	2.37 \pm 0.17	4.82 \pm 0.34
0060	3.06 \pm 0.03	2.69 \pm 0.17	4.71 \pm 0.34
0120	2.71 \pm 0.03	1.49 \pm 0.16	3.58 \pm 0.32
0180	3.10 \pm 0.03	1.89 \pm 0.17	4.61 \pm 0.33
0240	2.48 \pm 0.03	1.94 \pm 0.17	5.14 \pm 0.34
0300	2.89 \pm 0.02	1.76 \pm 0.13	5.71 \pm 0.27
0360	2.87 \pm 0.04	2.27 \pm 0.18	3.97 \pm 0.34
0420	2.81 \pm 0.03	2.26 \pm 0.17	4.38 \pm 0.33
0480	2.49 \pm 0.03	1.78 \pm 0.16	4.04 \pm 0.32
0540	2.77 \pm 0.03	2.00 \pm 0.16	4.01 \pm 0.32
0600	2.67 \pm 0.03	0.88 \pm 0.15	4.14 \pm 0.32
0660	2.09 \pm 0.02	1.48 \pm 0.13	4.97 \pm 0.27
0720	2.33 \pm 0.03	2.33 \pm 0.17	4.81 \pm 0.34
0780	2.40 \pm 0.03	2.25 \pm 0.17	5.43 \pm 0.34
0840	2.50 \pm 0.03	2.11 \pm 0.17	4.36 \pm 0.33
0900	2.38 \pm 0.03	2.35 \pm 0.17	3.55 \pm 0.32
0960	2.26 \pm 0.03	1.98 \pm 0.17	5.62 \pm 0.34
1000	2.61 \pm 0.02	1.63 \pm 0.12	2.82 \pm 0.25

Table 7.4: Laboratory results from window analysis of NaI(Tl) detector

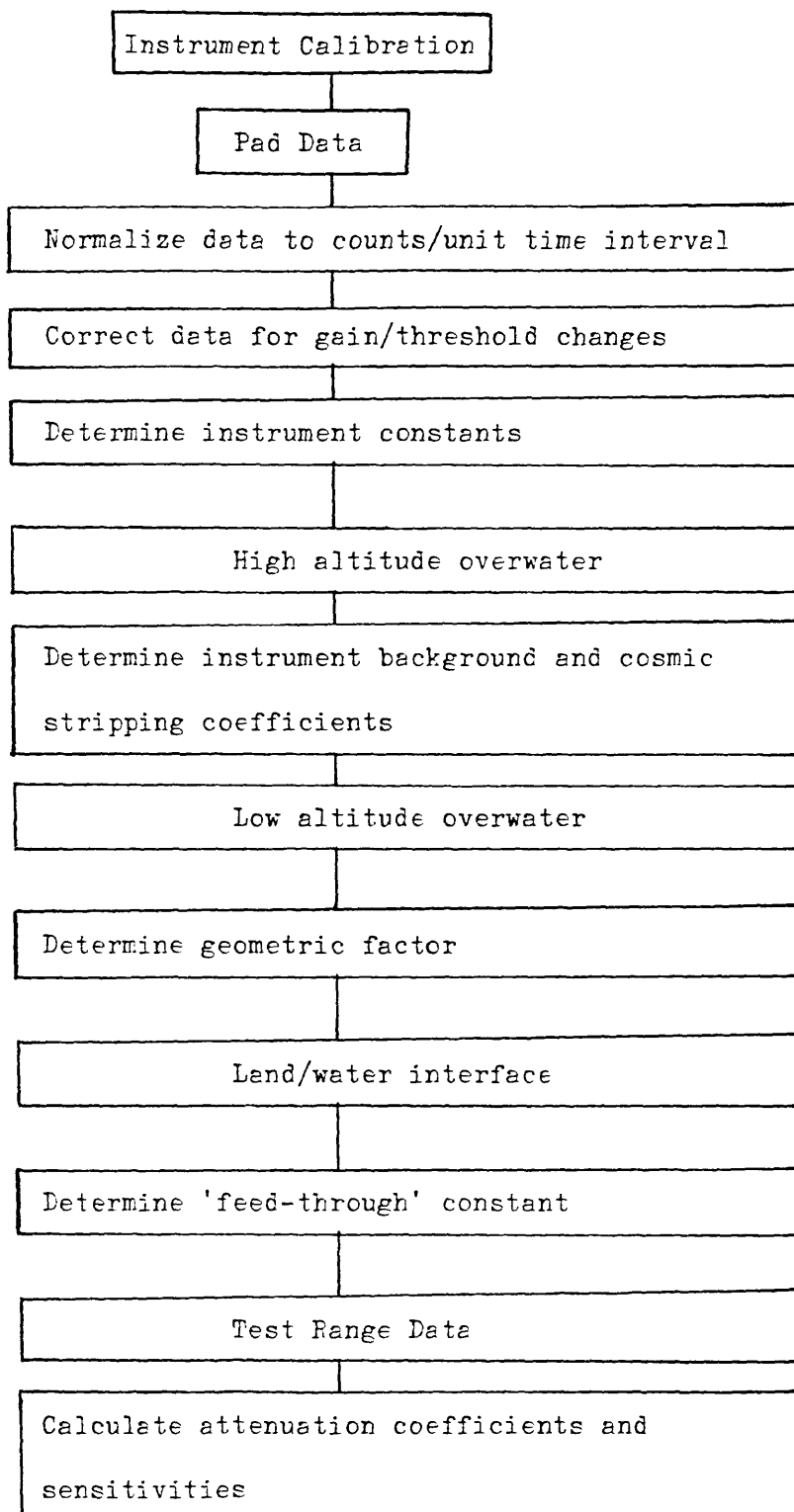
the variation of the flight height from a mean (chosen) height. It is worth noting that height correction and Compton scattering correction are interrelated since the Compton scattering coefficients, as well as the count rates, are altitude dependent (Grasty, 1982).

Several ways of determining background radiation in an airborne survey have been mentioned in section 4.3.1.; and ways of correcting for Compton scattering and height variation have been mentioned in sections 4.3.2. and 4.3.3. respectively. Also the spectra obtained from the airborne survey have to be corrected for gain and threshold changes (see section 6.6.1.). Fig 7.9 thus illustrates the steps necessary for the analysis of airborne data. Table 7.5 shows the windows used to represent the three elements - potassium, uranium and thorium in the 3 - window analysis.

As stated in section 6.5, airborne system can usually be calibrated at ground level on artificially built calibration pads; but because the geometry is different at survey altitudes compared with the ground or pads, the two component method can be used to calculate the calibration spectra for potassium, uranium and thorium at survey heights (Dickson, et al, 1981). In this work, since the detector package used is the same (except in volume) as that used by Grasty (1982a) in his plywood experiment, the calibration spectra for the three elements were calculated at each survey altitude from the primary and secondary spectra provided by him (Grasty) from his plywood experiment.

The first step in using these calibration spectra is to convert them to the same volume as the field (survey) detector package. Since

(a)



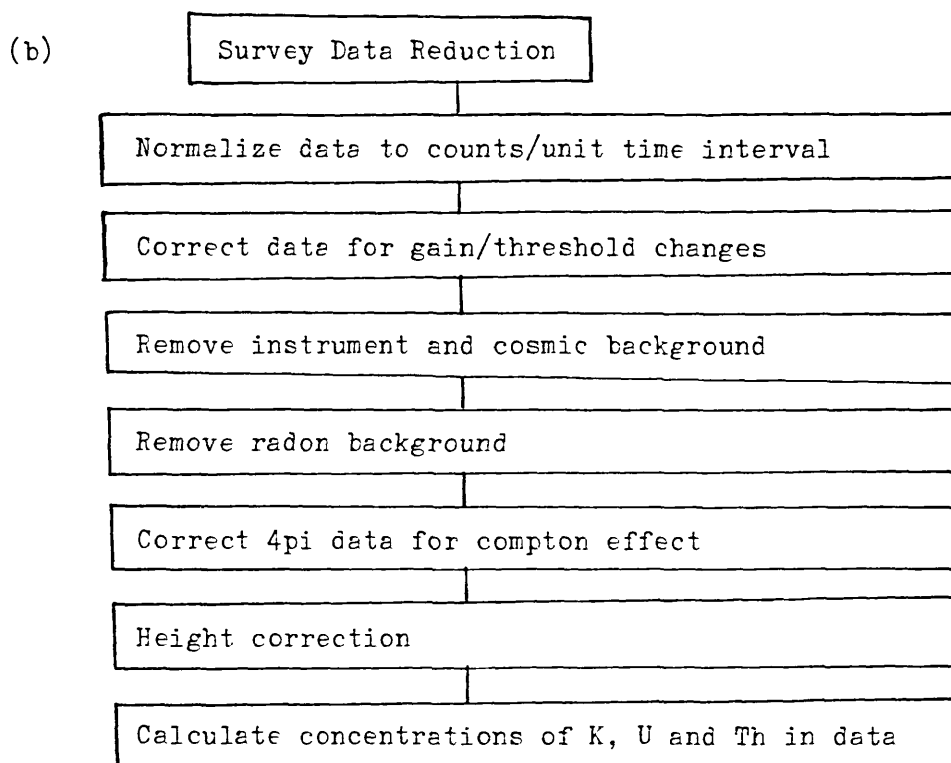


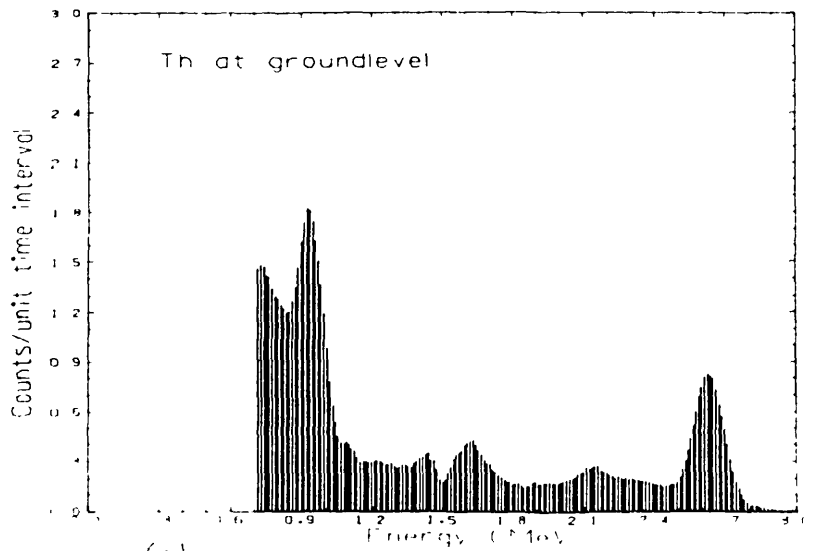
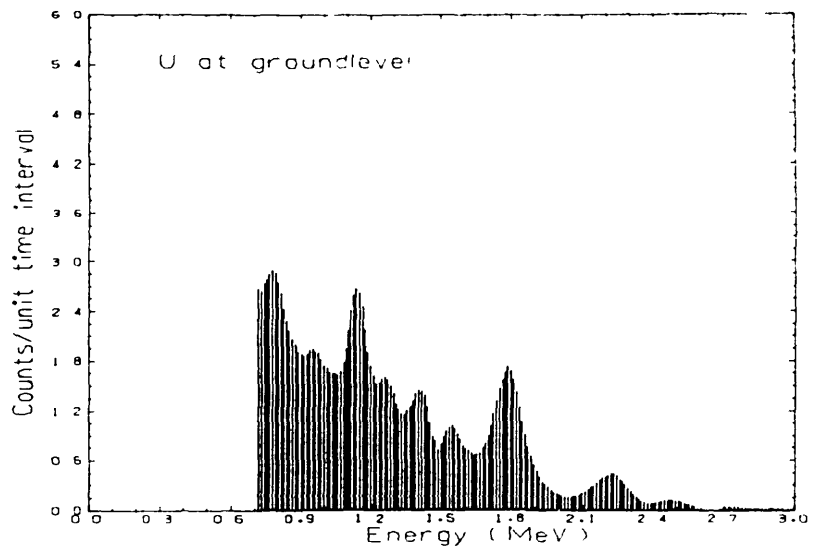
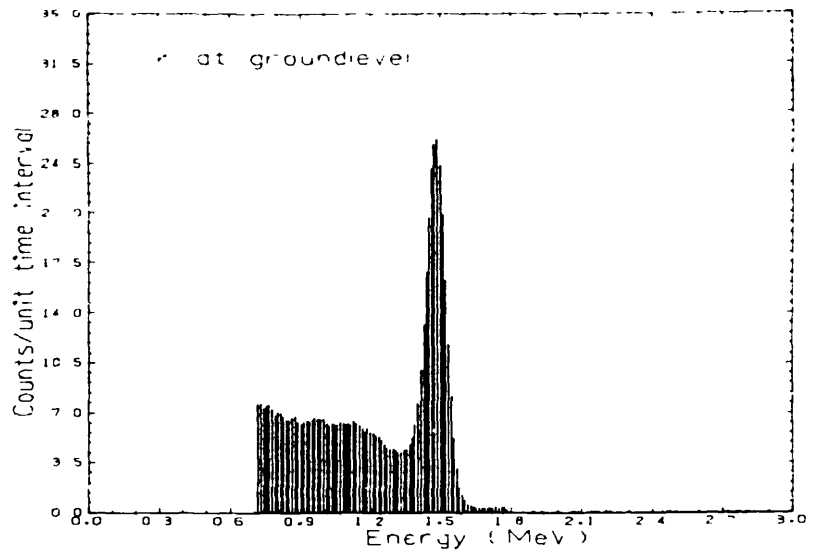
Fig 7.9: Flow chart for multichannel airborne data analysis

Element	Peak Energy(MeV)	Window Range(MeV)
K	1.46	1.37 - 1.57
U	1.76	1.66 - 1.86
Th	2.62	2.41 - 2.81

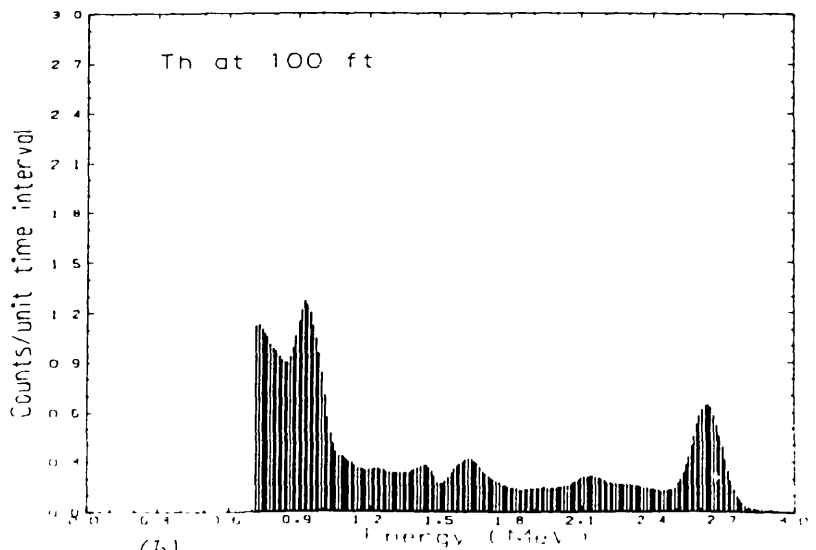
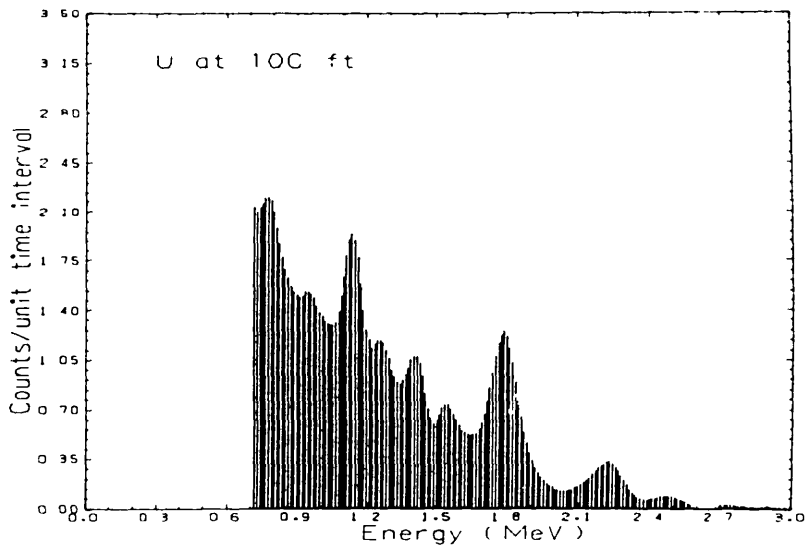
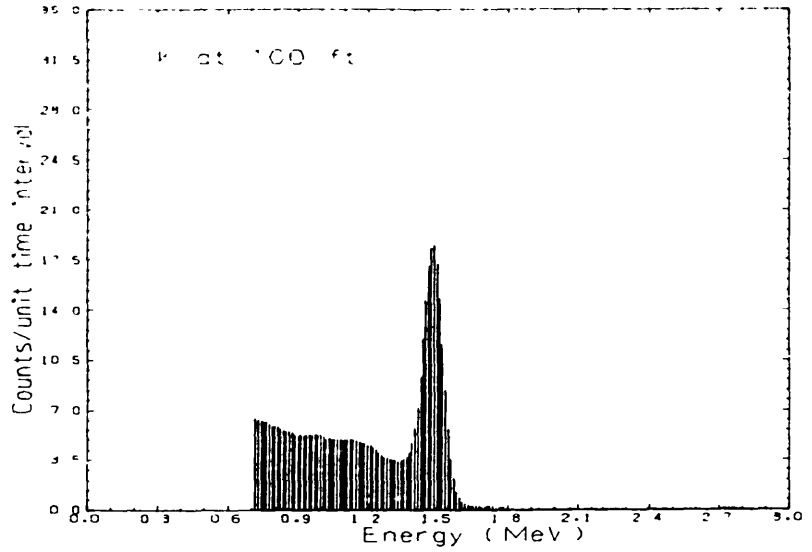
Table 7.5: Window widths used

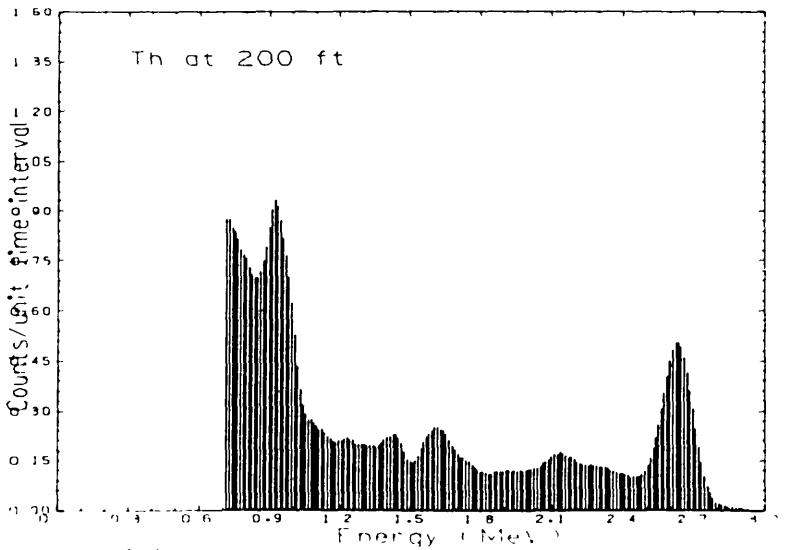
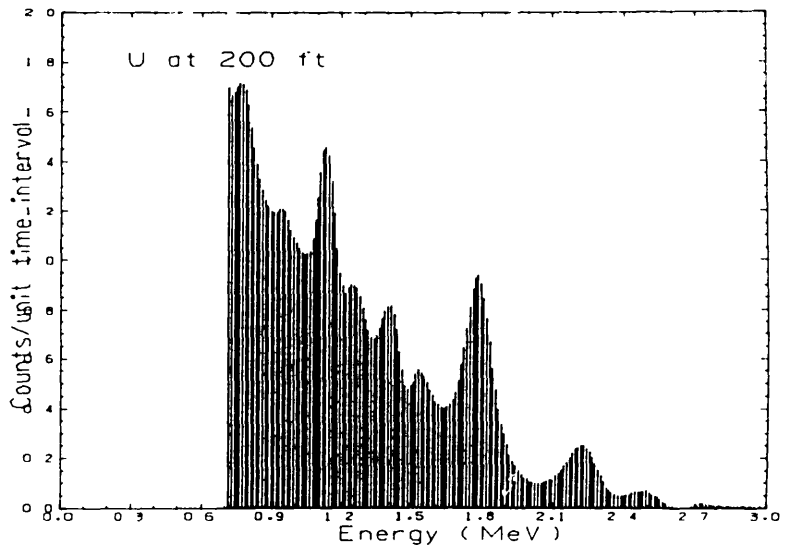
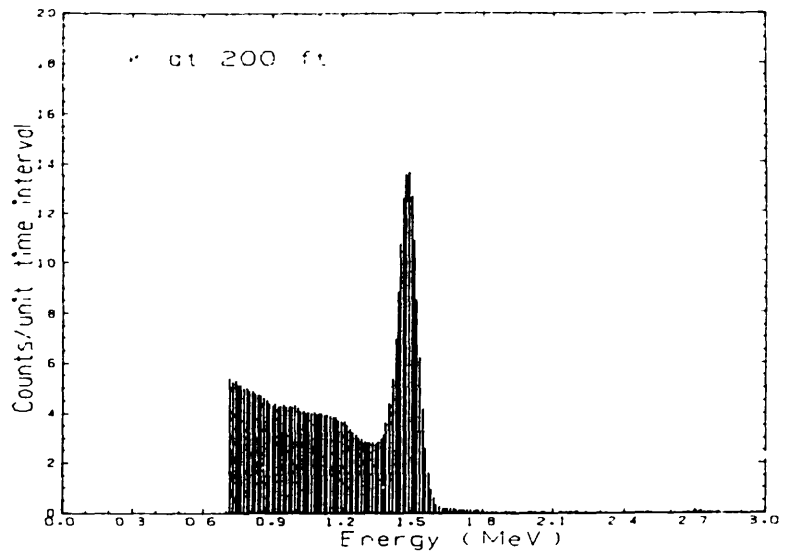
the count rate measured with a given detector package is proportional to the volume of the detector (Darnley, 1973), the count rates measured with a given volume can thus be converted to a similar detector of different volume by determining a scaling factor. This

scaling factor may not be directly proportional to the ratio of the two volumes because the geometric effect of the two detectors will be different at the same height. Thus a more appropriate way to determine the scaling factor will be to compare the count rates measured with the two detector packages at the same height in the same area. For this reason spectra for these two detector packages at the same height were provided. The scaling factor was determined by comparing the normalization coefficient of the respective spectrum from the respective detector since spectra are better compared when normalized. The scaling factor was found to be 2.384. Having determined the scaling factor, the calibration spectra for this survey detector package were calculated using equation 6.26, from the primary and secondary spectra provided. Fig 7.10 shows the calibration spectra for potassium, uranium and thorium at different heights. From these spectra, the information vectors at different heights were also calculated and plotted (see Fig 7.11). The information vector at each height shows at least five prominent peaks above the general exponential background. Like in the laboratory case, the two peaks at 0.91 and 0.97MeV respectively are smeared. Table 7.6 shows the relative information importance of these peaks, their energies and the isotopes they represent. As can be seen from Table 7.6, at ground level, the information importance of the lower energies, 0.91 and 0.97MeV representing thorium, 1.12MeV representing uranium, are greater than the values of the corresponding standard energies of 1.76MeV and 2.62MeV representing uranium and thorium respectively. It is however noticed that while the information values at energies

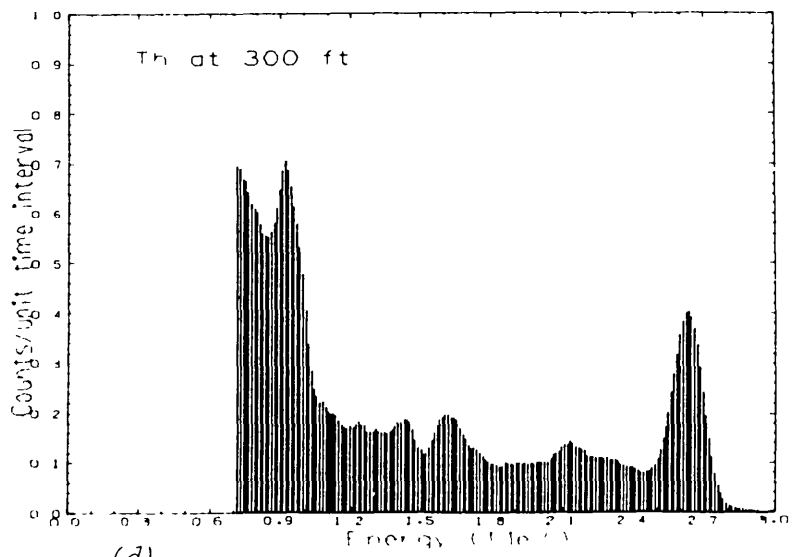
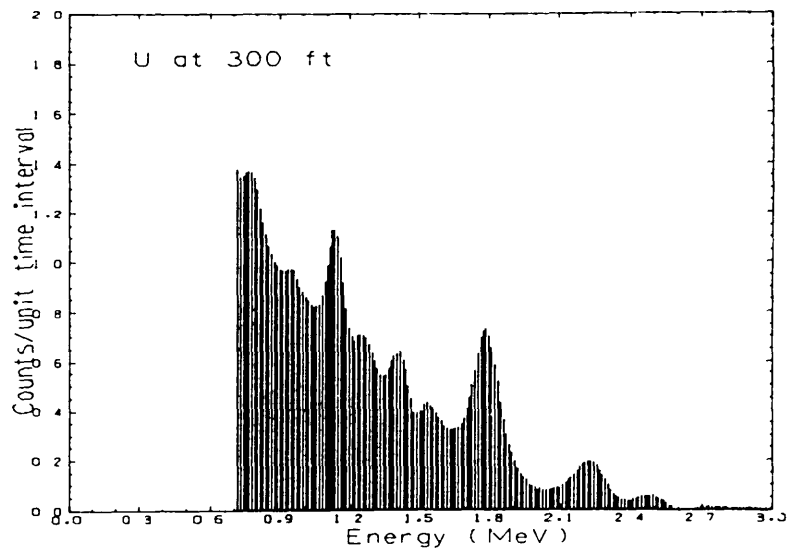
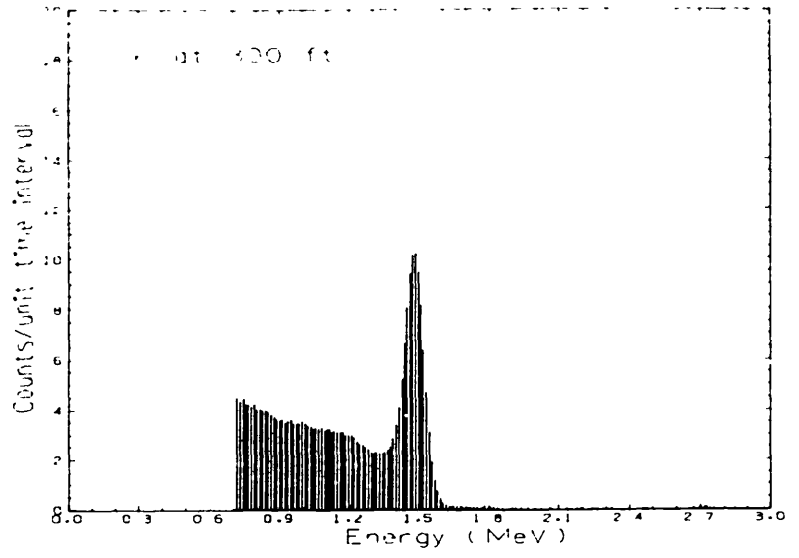


(a)



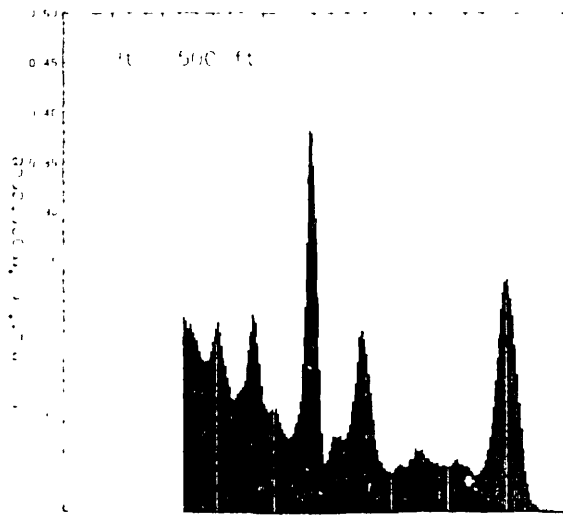
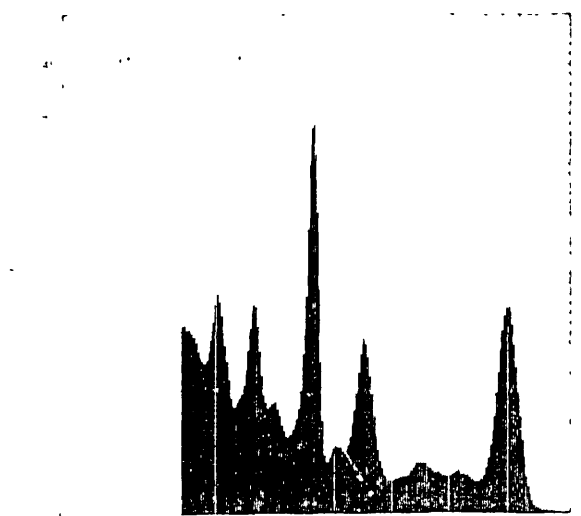
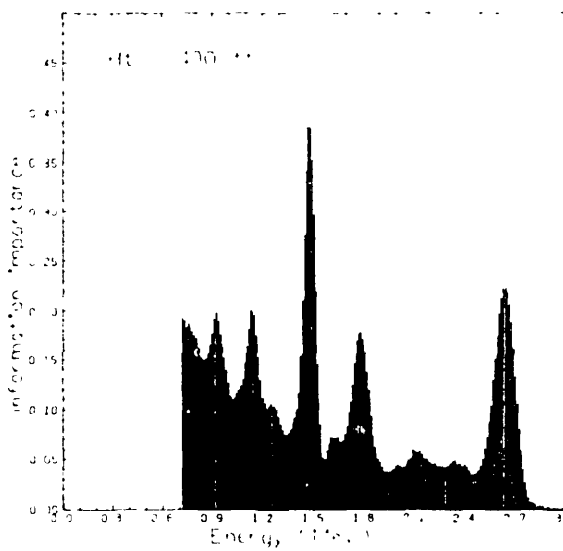
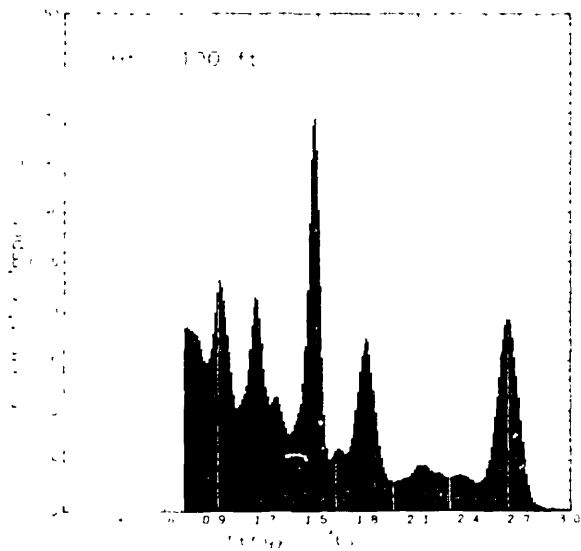
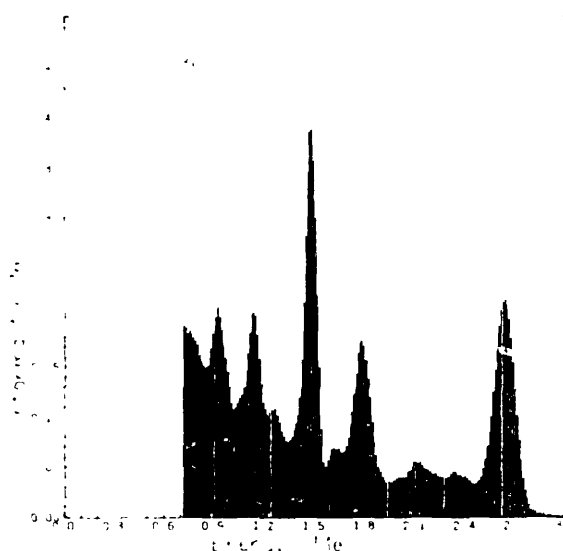
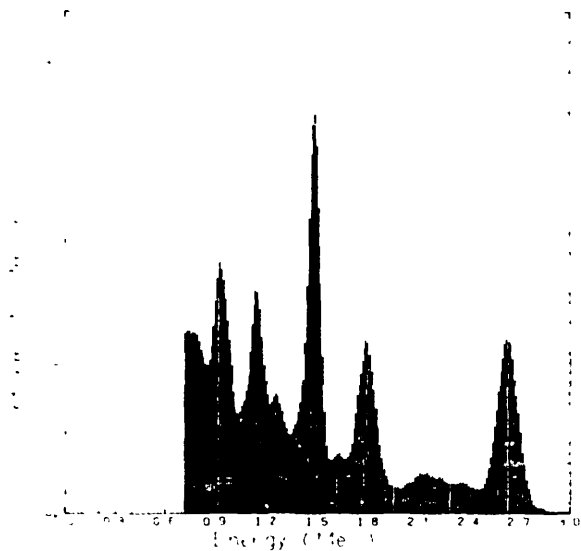


(c)



(d)

Fig.7.10: Calibration spectra at various heights



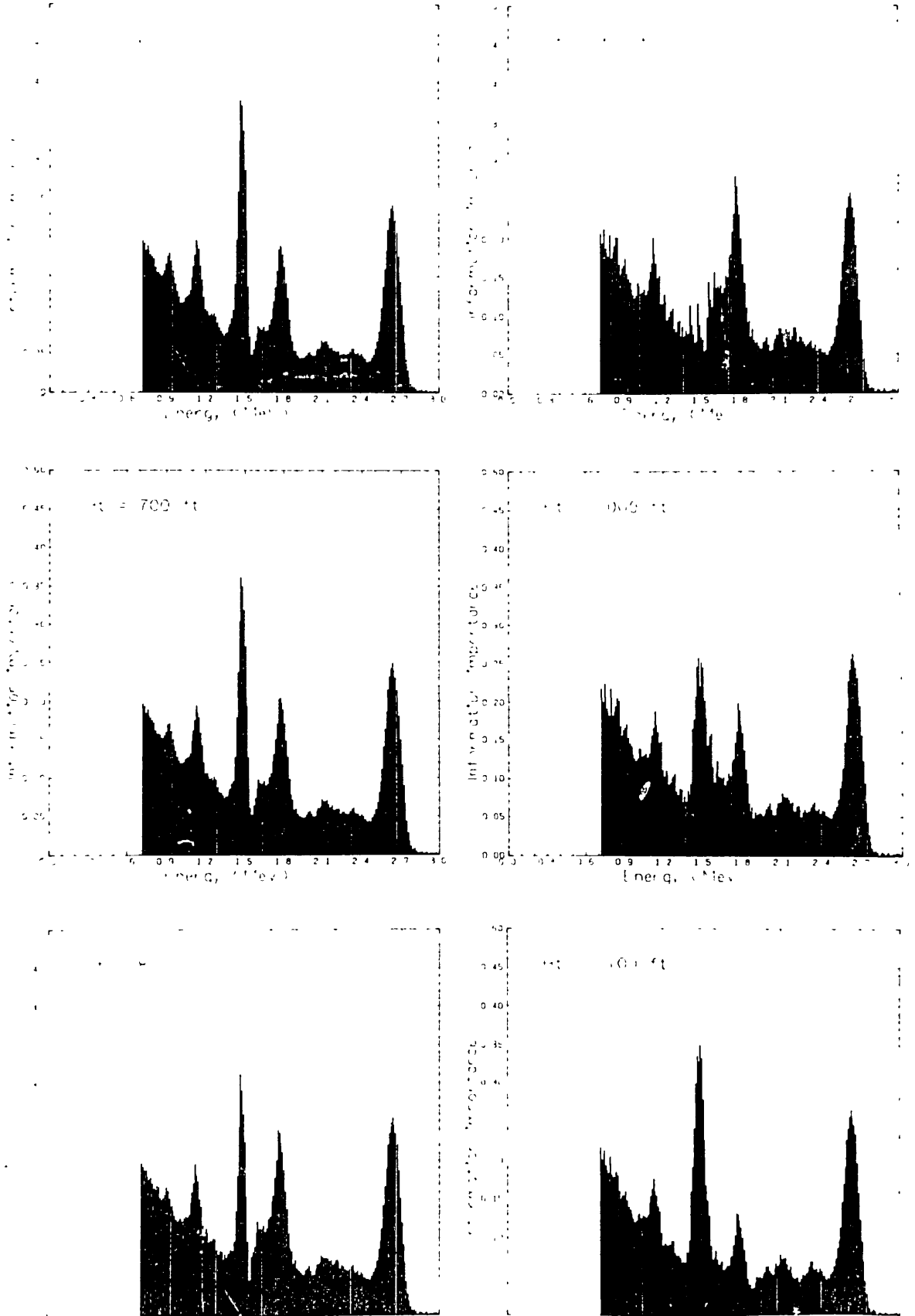


Fig.7.11: Information vector for airborne system at various heights

Isotope	Energy (MeV)	Element it represents	Information Importance at Height (feet)											
			0	100	200	300	400	500	600	700	800	900	1000	1100
Ac-228	0.91	Thorium	0.25	0.23	0.22	0.21	0.20	0.19	0.18	0.17	0.16	0.15	0.15	0.15
Ac-228	0.97	Thorium	0.17	0.16	0.15	0.15	0.14	0.14	0.13	0.13	0.13	0.12	0.12	0.12
Bi-214	1.12	Uranium	0.22	0.22	0.21	0.20	0.20	0.19	0.19	0.18	0.18	0.18	0.17	0.16
K-40	1.46	Potassium	0.40	0.40	0.39	0.39	0.39	0.38	0.37	0.35	0.29	0.12	0.22	0.33
Bi-214	1.76	Uranium	0.17	0.17	0.18	0.18	0.18	0.18	0.19	0.20	0.22	0.24	0.17	0.12
Tl-208	2.62	Thorium	0.17	0.19	0.21	0.22	0.23	0.23	0.24	0.25	0.25	0.26	0.26	0.27

Table 7.6: Relative Information Importance of isotopes (airborne system)

0.91MeV, 0.97MeV, 1.12MeV and 1.46MeV decrease, the information values for 1.76MeV and 2.62MeV increase with increasing survey height.

The resolution matrix R was also calculated at each height and the results show that at each height, the matrix R is a unit matrix; thus implying that the concentration values obtained using the calibration spectra are unique.

From the calibration spectra, the stripping coefficients at each altitude were calculated using the windows defined in Table 7.5. Each stripping ratio was then plotted against height in order to establish its variation with height. Fig 7.12 shows the variation of the stripping ratios with height and the following equations represent the respective lines shown in Fig 7.12.

$$\begin{aligned}\alpha(H) &= 0.43078 + 0.33846E-04 H \\ \beta(H) &= 0.45705 + 0.15695E-04 H \\ \gamma(H) &= 0.94387 + 0.10176E-03 H \\ a(H) &= 0.10708 + 0.69886E-05 H \\ b(H) &= -0.15727E-02 + 0.16431E-04 H \\ g(H) &= 0.15915E-01 + 0.43486E-05 H\end{aligned}\tag{7.7}$$

where

H is the height in feet.

Also the attenuation coefficient for each element was calculated as shown in Fig 7.13 (see equation 4.17) and the results are shown in Table 7.7.

Having established the variation of the stripping ratios with altitude, a composite spectrum at each height was calculated from the

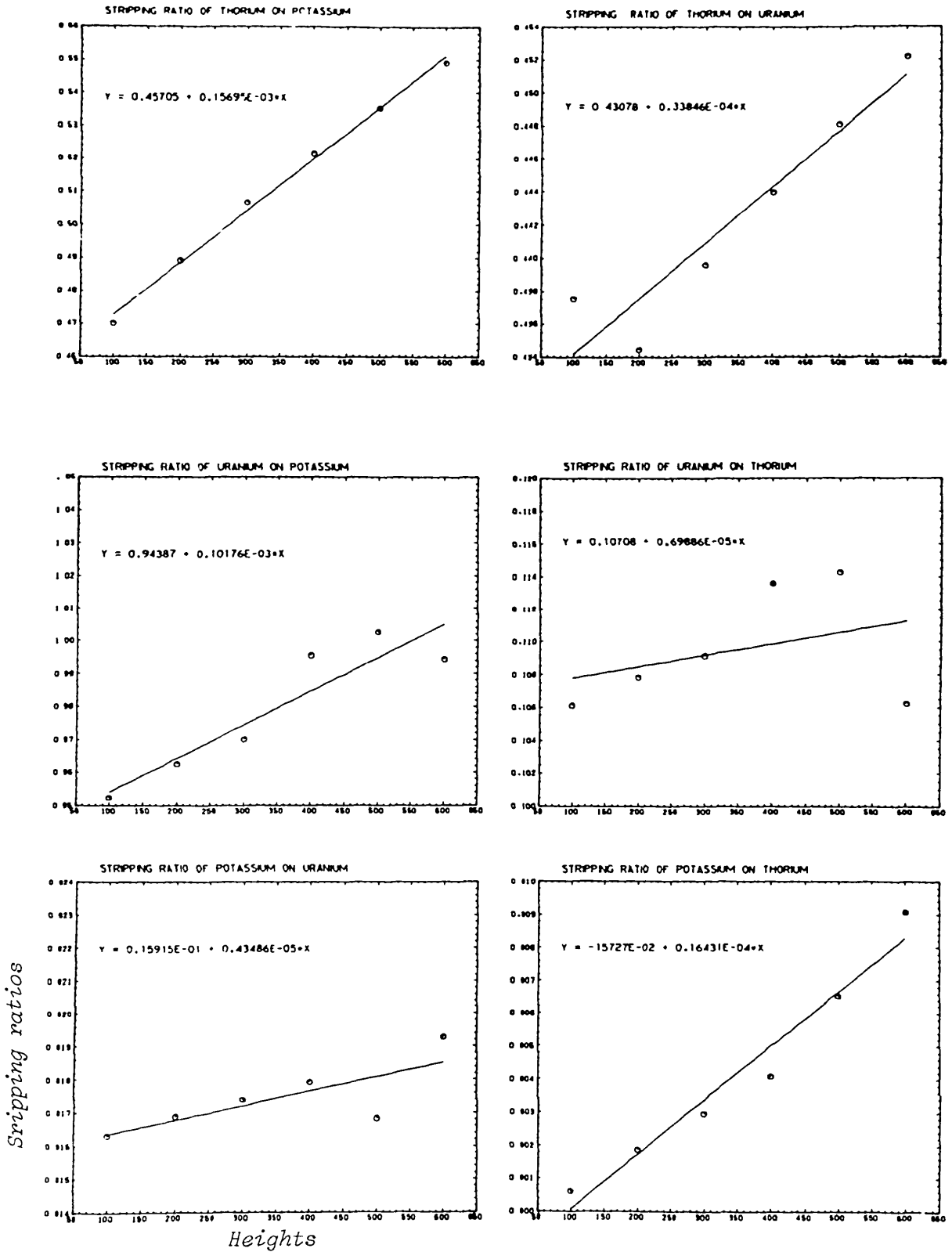


Fig.7.12: Variation of stripping ratios with height

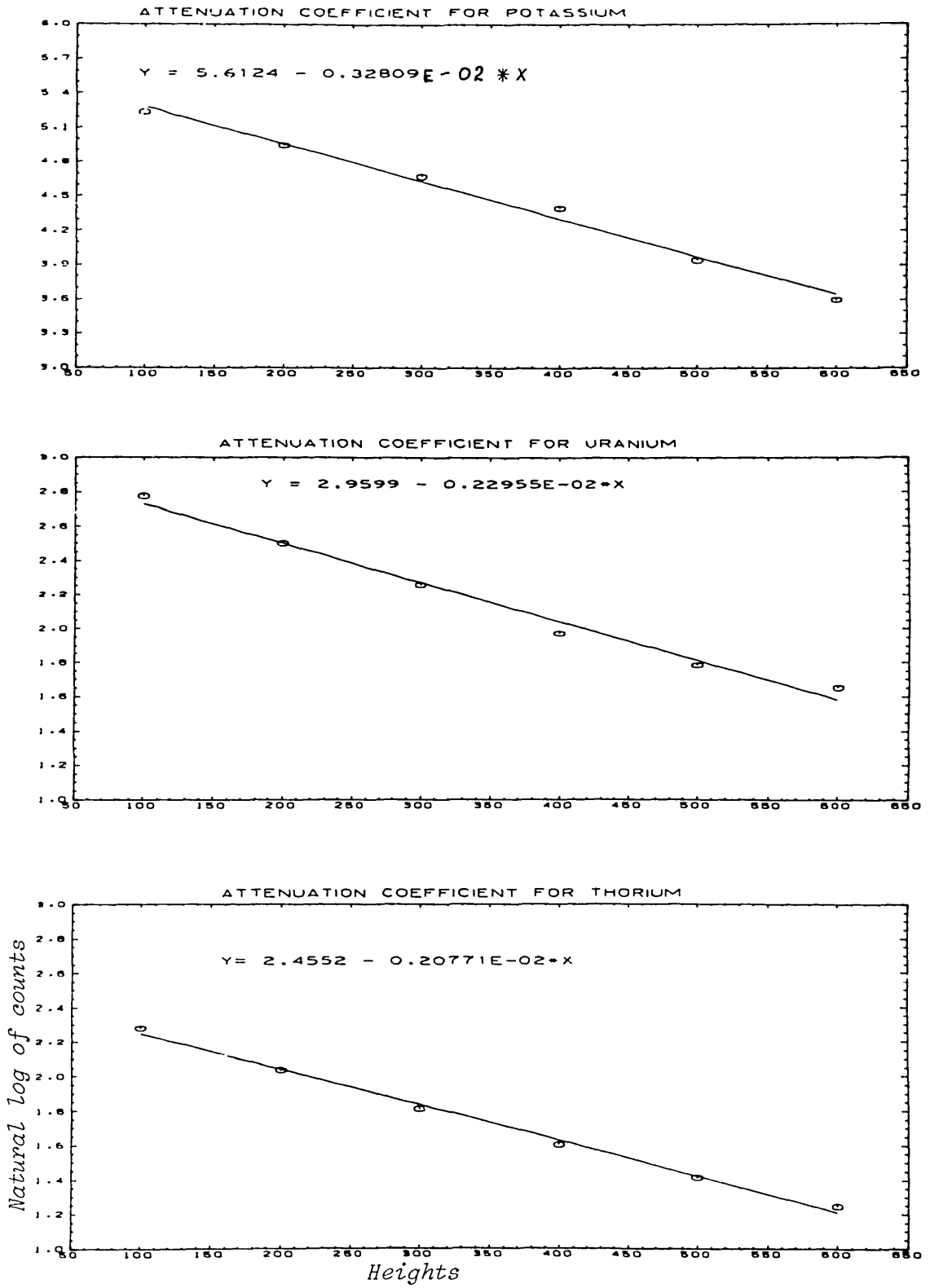


Fig.7.13: Determination of attenuation coefficients

Element	Attenuation coefficient
K	3.28×10^{-3}
U	2.30×10^{-3}
Th	2.08×10^{-3}

Table 7.7: Attenuation Coefficients

primary and secondary spectra, using the following equations:

$$\begin{aligned}
 T &= T_C + aU_C + bK_C \\
 U &= \alpha T_C + U_C + gK_C \\
 K &= \beta T_C + \gamma U_C + K_C
 \end{aligned}
 \tag{7.8}$$

where

T, U and K are the uncorrected thorium, uranium and potassium count rates;

T_C , U_C , K_C are the corrected count rates; and

$\alpha, \beta, \gamma, a, b$ and g are the stripping ratios as defined in section 4.3.2.

The composite spectrum is then given by

$$\begin{aligned}
 C &= T + U + K \\
 &= \{1 + \alpha + \beta\}T_C + \{1 + a + \gamma\}U_C + \{1 + b + g\}K_C
 \end{aligned}
 \tag{7.9}$$

Hence the calibration spectra T_C , U_C and K_C can be fitted to the field spectra, using equation 7.9. The field survey and background spectra

at various heights are shown in appendix B.

Having determined the calibration matrix A and the stripping ratio for the survey detector package, the concentrations of potassium, uranium and thorium in the spectra (after the background spectra have been subtracted) at each height flown, were calculated using equation 6.25 in case of the multichannel analysis and the errors associated with these results were also calculated using equation 6.20. In case of the conventional three window analysis, equation 6.32 was used to calculate the concentrations of the elements. For the background correction, over water background values at each of the heights flown were used, with the assumption that the radon (atmospheric) background is constant and that the background measured over water is at least representative of that over the land survey area (see section 4.3.1.1.2.)

Tables 7.8 and 7.9 show respectively the results obtained using all the channels from 0.72MeV to 3MeV and the conventional three windows defined in Table 7.5. In Tables 7.8 and 7.9 are shown two values at each height. The first line at each height corresponds to the minimum detectable concentrations while the second line is the measured concentrations of potassium, uranium and thorium in the sample.

7.3. Spectra Partitioning

We recall that in order to determine the concentrations of potassium, uranium and thorium in a given sample, the number of channels, n , used must be equal to or greater than three (the number of isotopes). It

Height (feet)	K (%)	U (ppm)	Th (ppm)
100	0.22	0.82	1.35
100	2.63 \pm 0.12	1.39 \pm 0.23	3.00 \pm 0.39
200	0.26	1.00	1.78
200	2.75 \pm 0.15	1.39 \pm 0.29	2.97 \pm 0.46
300	0.34	1.09	2.54
300	2.77 \pm 0.17	1.47 \pm 0.35	3.08 \pm 0.56
400	0.42	1.27	3.23
400	2.92 \pm 0.21	1.38 \pm 0.42	3.14 \pm 0.65
500	0.51	1.44	4.16
500	3.16 \pm 0.26	1.35 \pm 0.48	3.19 \pm 0.75
600	0.61	1.57	5.15
600	3.60 \pm 0.33	1.32 \pm 0.56	3.07 \pm 0.85
800	0.39	2.33	7.62
800	4.71 \pm 0.61	1.08 \pm 0.71	2.76 \pm 1.03
1000	0	5.56	10.81
1000	1.96 \pm 0.97	3.28 \pm 0.69	1.89 \pm 1.13

Table 7.8: Results of multichannel analysis of airborne data

Height (feet)	K (%)	U (ppm)	Th (ppm)
100	0.05	0.27	0.58
100	2.65+0.15	1.06+0.32	2.88+0.50
200	0.06	0.34	0.77
200	2.82+0.18	1.04+0.38	2.81+0.59
300	0.08	0.41	0.94
300	2.86+0.21	1.04+0.46	3.03+0.70
400	0.10	0.53	1.14
400	3.02+0.36	0.98+0.54	3.10+0.81
500	0.12	0.59	1.38
500	3.27+0.32	1.05+0.62	3.15+0.94
600	0.16	0.72	1.63
600	3.90+0.43	0.97+0.71	3.12+1.07
800	0.35	0.87	2.18
800	6.55+0.96	1.01+0.86	2.70+1.31
1000	0	1.05	2.75
1000	0 +8.36	1.22+0.91	4.53+1.50

Table 7.9: Results of window analysis of airborne data

has been stated that $n = 3$ corresponds to the conventional three window analysis, where a window, centred on a photopeak, is assigned to each element. On the other hand, the multichannel analysis requires no photopeak, but one of its main problems is the handling of large matrices. An obvious way of overcoming this is to physically reduce the matrices. This can be achieved by physically reducing n , the number of channels in the spectrometer. This can be done by partitioning (dividing) the spectrum and summing all the counts in each partition. This is possible as long as the number of partitions p , is greater than three, since $n = 3$ corresponds to the conventional three window analysis. That is, $3 < p \leq N$, where p is an integral number and N is the total number of channels from the lower limit to the upper limit (0.72MeV to 3MeV in this case) of the spectrum used.

The number of channels within a partition is given by N/p . Where N is not exactly divisible by p , the remaining channels are left out from the higher energy side of the spectrum. This procedure only reduces the multichannel spectrometer to a 'p' channel spectrometer; but unlike the window analysis, there is no loss of information from the original spectrum since all the spectral data are used in this case.

The following Table 7.10 shows the average results for the heights from 100feet to 400feet obtained from this calculation.

The Table 7.10 shows that all the results are similar to the full spectral analysis (partition 191) except for the thorium values for partition 64 and 128. An investigation of these results reveals that the 63 channels left out from the upper end of the spectra included

No of Partitions				No of channels
P	K (%)	U (ppm)	Th (ppm)	left out
4	2.95	1.24	2.92	3
6	2.79	1.60	2.70	5
8	2.80	1.53	2.86	7
9	3.02	1.07	3.00	2
16	2.96	1.16	3.01	15
32	2.81	1.25	3.39	31
64	2.76	1.15	3.91	63
128	2.75	1.15	3.91	63
191	2.77	1.41	3.05	0

Table 7.10: Average results obtained by partitioning

the thorium photopeak at 2.62MeV. One can thus infer from these results that any number of partitions p of a spectrum is possible provided of course, that $p > 3$ and the region of the spectrum left out does not include the thorium photopeak. When the thorium photopeak at 2.62MeV is not included in the calculation, the estimated concentration of thorium is bound to be unreliable because this amounts to estimating an element which is actually not present in the sample (Salmon, 1962).

7.4. Analysis Program

The program ANASPEC, written in Fortran IV, is used to analyze the survey data. As mentioned earlier, the complete analysis of the survey data involves the following steps:

- (i) correction for gain and threshold changes
- (ii) background correction
- (iii) height correction in case of an airborne survey
- (iv) determination of the characteristic coefficients of the measuring system, and
- (v) calculation of the concentrations of potassium, uranium and thorium in the samples

ANASPEC is written for a spectrometer with arbitrary number ($n \gg 3$) of channels with the conventional three channel spectrometer, where energy windows are centred on peak positions, as a special case.

The program is divided into a main section ANASPEC and four major subroutines - ENERCAL, PICPOS, GTCORR and CSCCS.

Subroutine ENERCAL does the initial and subsequent energy calibration of the spectrometer in order to determine the gain and threshold changes. This subroutine also contains another subroutine NORMEQ which forms the normal least squares' equations. NORMEQ in turn contains subroutine GAUSS which solves these normal equations.

Subroutine PICPOS smoothens the data within the elemental windows and locates the peak positions for potassium, uranium and thorium within

each respective window. The peak position is regarded as the channel number with the highest count rate in the window.

Subroutine GTCORR corrects the data for gain and threshold changes.

Subroutine CSCCS does, after all the data have been corrected for gain and threshold changes, the background subtraction, the determination of the characteristic coefficients of the measuring system and then calculates the concentrations of potassium, uranium, thorium, their ratios - Th/U, Th/K, U/K and the errors associated with these variables.

This subroutine in turn contains the following subroutines

MATINV which finds the inverse of a square matrix

MMULT which finds the product of two matrices A and B, dimensioned as A(N,M) and B(M,L); and

TRANS which finds the transpose of a matrix.

All variables used in the program ANASPEC and its subroutines are defined at various stages (see appendix C).

The input into the program consists of

- (a) peak positions and their corresponding energies for initial energy calibration of the instrument
- (b) degree (integer) which specifies the type of curve to be fitted to the above points. In this case, Degree = 1 since peak positions are linearly related to energies
- (c) number of paired points used in the energy calibration

- (d) the lower and upper limits of the windows for potassium, uranium and thorium
- (e) number of channels the spectrometer really has
- (f) point (channel number) where summing of the data should start. This is necessary because the first few channels may not be useful because they may contain other information which are not count rates
- (g) number of points used in grouping
- (h) number of standard and background sources
- (i) concentrations of potassium, uranium and thorium in the above standard sources
- (j) number of standard and background sources plus number of samples
- (k) the spectra readings
- (l) sampling time for each spectrum
- (m) heights in case of an airborne survey
- (n) weight of each sample (and standard). In the case of the background source and field survey, the weights are all equal to unity, and
- (o) title for each spectrum. In the case of the airborne survey, the title for each spectrum is represented by its height, while in the laboratory, this is represented by the distance along the survey line where the sample is taken.

The output consists of

- (a) the initial threshold and energy per channel of the measuring instrument
- (b) gain and threshold changes
- (c) the concentrations of potassium, uranium, thorium, their ratios - Th/U, Th/K, U/K and the errors associated with these variables, and
- (d) the minimum detectable concentrations for potassium, uranium and thorium.

The complete program is listed in appendix C.

7.5. Comparison Of Results

The laboratory results from the multichannel analysis for Ge(Li) and NaI(Tl) detectors are shown in Table 7.2, while the results for the conventional three window analysis are shown in Table 7.4. Similarly the field (airborne) results from the multichannel and the conventional three window analyses are shown in Tables 7.8 and 7.9 respectively. As mentioned in section 7.2.1.1., only results greater than a minimum detectable limit will be regarded as statistically adequate and only such results will be used in these comparisons. These minimum detectable limits for the laboratory systems are shown in Table 7.3. The minimum detectable limits for the airborne system are included in Tables 7.8 and 7.9.

7.5.1. Experimental Comparison Of NaI(Tl) And Ge(Li) Detectors' Performances

(a) Information Vectors And Spectra From The Two Detecting Systems

The information vectors show the independence of each channel relative to its neighbours. It also indicates peaks which stand above the general exponential background (Crossley, 1982).

Fig 7.9 shows the information vectors for the Ge(L1) and NaI(Tl) detectors. Comparison of these information vectors for the two detector systems shows that for the same energies, the values for the Ge(L1) detector are higher than the values for the NaI(Tl) detector. This indicates that the Ge(L1) detecting system has better resolution than the NaI(Tl) detecting system since the channels in the Ge(L1) detector have higher degree of independence. Also from Fig 7.9, it can be seen that more peaks which stand above the general background can be identified in the plot for the Ge(L1) detector than in the NaI(Tl) detecting system. For example, while the peaks representing thorium at energies 0.91 and 0.97MeV in the Ge(L1) detector are well resolved, these two peaks are not resolved in the NaI(Tl) detector. This fact is also reflected in all the spectra obtained (see Fig 7.3 and appendix B) from the two detecting systems. Thus one may conclude on the basis of these facts that the Ge(L1) detector is preferable to the NaI(Tl) detector in a survey where identification of the isotopes contained in a sample is the objective.

(b) Estimated Concentrations Of Isotopes In Samples

As mentioned earlier, only results which are greater than the minimum detectable limit will be used in this comparison. From Tables 7.2 and 7.3, it could be seen that all the potassium values are significant

for the Ge(L1) detector, but the uranium values are all lower than the critical limit. Hence they may be regarded as not significant. The thorium values are also lower than the critical values except samples 0180, 0660, 0840 and 0900 at the 5% level, while at the 1% level, all the thorium values are also lower than its critical limit. Hence again the thorium values are regarded as not significant at the 1% level. Thus at the 1% level, only the potassium values for the Ge(L1) detector are regarded as being statistically significant. For the NaI(Tl) detector, all the concentration values for potassium, uranium and thorium are greater than their critical limits at both the 5% and 1% significant levels. Hence they are all regarded as being statistically significant at both levels.

Because the Ge(L1) detector values for potassium are statistically valid while uranium and thorium values are not, it was decided to investigate how the Ge(L1) detector will perform in the lower region of the spectrum, that is, in the region which includes the potassium window but excludes the uranium and thorium standard windows. This region was chosen between 0 and 1.61MeV. This was necessary because it has been found from the information vector that the energies representing uranium and thorium in this (lower) part of the spectrum contain more information than the standard uranium and thorium peaks of energies 1.76MeV and 2.62MeV respectively (see Table 7.1).

The results for this investigation are shown in Table 7.11. The comparison of the concentration values with their respective critical limits shows again that only the potassium values are statistically valid at the 1% significant level.

Sample	K (%)	U (ppm)	Th (ppm)
Cl	0.37	5.05	4.01
0000	2.47 \pm 0.11	0 \pm 0.58	1.72 \pm 1.44
0060	2.62 \pm 0.11	0 \pm 0.58	4.78 \pm 1.43
0120	2.38 \pm 0.11	0.46 \pm 0.58	4.42 \pm 1.43
0180	2.74 \pm 0.11	0.85 \pm 0.58	4.59 \pm 1.44
0240	2.12 \pm 0.11	0.53 \pm 0.58	1.94 \pm 1.43
0300	2.50 \pm 0.11	0 \pm 0.58	3.23 \pm 1.44
0360	2.63 \pm 0.11	0.41 \pm 0.58	0.92 \pm 1.43
0420	2.48 \pm 0.11	0.28 \pm 0.58	1.19 \pm 1.43
0480	2.28 \pm 0.11	0 \pm 0.58	0 \pm 1.42
0540	2.41 \pm 0.11	0 \pm 0.58	1.11 \pm 1.43
0600	2.23 \pm 0.11	1.29 \pm 0.58	1.34 \pm 1.43
0660	1.91 \pm 0.11	1.68 \pm 0.58	2.45 \pm 1.43
0720	2.10 \pm 0.11	0 \pm 0.58	3.16 \pm 1.43
0780	2.29 \pm 0.11	0 \pm 0.58	2.33 \pm 1.43
0840	2.79 \pm 0.11	2.67 \pm 0.58	7.14 \pm 1.45
0900	3.08 \pm 0.11	3.82 \pm 0.59	8.34 \pm 1.46
0960	1.89 \pm 0.11	0.78 \pm 0.58	2.71 \pm 1.43
1000	2.40 \pm 0.11	0 \pm 0.58	0.28 \pm 1.43

Cl is the critical limit

Table 7.11: Ge(L1) results for energies from 0 - 1.61MeV

These results from the two detecting systems lead to the suggestion that within the energy range of interest (0 to 3MeV) in gamma ray spectrometry for geological and mineral exploration applications, the NaI(Tl) detector is more reliable than the Ge(Li) detector in the estimation of the concentrations of potassium, uranium and thorium.

It may be worthwhile to recall that statistically adequate results are said to exceed a minimum detectable limit which is dependent on background count rate (see equation 7.6). Thus it may be necessary to look at how the background count rates for the Ge(Li) and the NaI(Tl) detectors were acquired in the laboratory. As mentioned before, the laboratory analyses of the samples were done at Silwood Park, where both the Ge(Li) and the NaI(Tl) detectors are present. These two detectors are however not located in the same room, and also while the NaI(Tl) detector and the samples being analysed were placed in a lead shield, in the case of the Ge(Li) detector, the samples were unshielded, thereby making the detector to register extra radiations in addition to those of the samples being analysed. This effect can be seen in Fig 7.4d where the background spectrum from the Ge(Li) detector is very much higher than the corresponding spectrum from the NaI(Tl) detector. This may explain why the minimum detectable values for the Ge(Li) detector are generally very large, thus resulting in the rejection of the concentration values for uranium and thorium obtained from the Ge(Li) detector. With this observation, it may be recommended not to treat the conclusion about the performance of the Ge(Li) detector in the estimation of the concentrations of potassium,

uranium and thorium in a sample as being of general application.

For further comparison of the performances of the detecting systems, the potassium values from the Ge(Li) detector were plotted against the corresponding potassium values from the NaI(Tl) detector (see Fig 7.14). The 45-degree equivalence line is also indicated in Fig 7.14. If the two sets of results were in perfect agreement, they

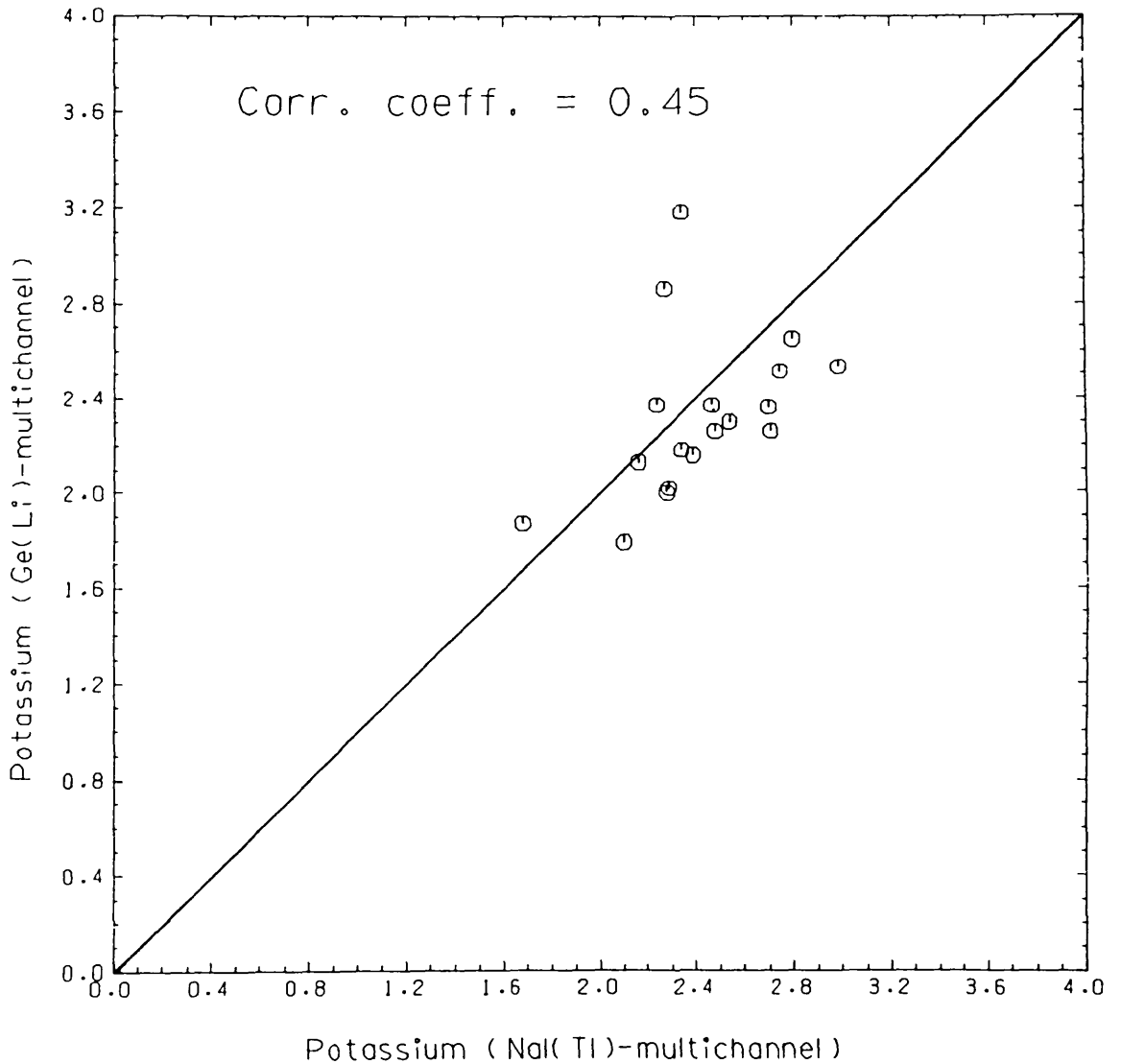


Fig.7.14 NaI(Tl) Versus Ge(Li) results

will lie along the 45-degree line. But as can be seen from Fig 7.14, the Ge(L1) detector values are generally lower than the NaI(Tl) detector values by an average of about 21%.

Also indicated in Fig 7.14 is the regression line of the two sets of values. The correlation coefficient was found to be 0.45, which means that the two sets of values are poorly related. The student - t - test shows that the mean values for potassium obtained from both detectors may be regarded as equal or being drawn from the same population.

These observations imply that where the concentration values are estimated using the Ge(L1) detector, the values are lower than the corresponding values estimated using the NaI(Tl) detector.

7.5.2. Conventional Three Window Versus Multichannel Analysis

It has been seen from Fig 7.9 that for the NaI(Tl) detector, the potassium peak at 1.46MeV has the highest information value. This is followed in sequence by peaks at 0.91MeV and 0.97MeV representing thorium, 1.12MeV and 1.76MeV representing uranium, and 2.62MeV representing thorium (see Table 7.1). This is also the pattern for an airborne system at ground level (see Table 7.6). This suggests that the conventional energy windows centred at 1.76MeV and 2.62MeV respectively for uranium and thorium may not account for all the concentrations of these elements in a sample. Thus illustrates the loss of information in the conventional three window analysis of spectrometric data when the uranium and thorium windows, centred on 1.76MeV and 2.62MeV respectively, are used.

7.5.2.1. Laboratory Results

Table 7.12 shows the concentration values and their relative errors (relative errors are expressed in percentages) from the multichannel and the conventional three window analyses of the same spectrum obtained in the laboratory using the NaI(Tl) detector. Table 7.12 also contains the minimum detectable concentration values for each element. Comparison of the concentration values of each sample from the radiometric analysis with the critical limits shows that all the concentration values are greater than the critical limits, hence they are regarded as statistically significant. It can also be seen from the table that the relative errors in all cases are better in the multichannel analysis than their corresponding values in the window analysis.

Fig 7.15 shows the plot of potassium, uranium and thorium values in the window analysis against their corresponding values in the multichannel analysis. Also indicated in Fig 7.15 is the 45 equivalence line, along which all the points would lie if they were in perfect agreement. It is evident from Fig 7.15 that there are systematic differences between the results obtained from these two methods. The potassium values obtained from the window analysis are systematically greater than those obtained from the multichannel analysis. Since it has been indicated that the windows may not represent the total amount of the elements in a sample, the most probable explanation for this observation would be that in the window analysis, the Compton scattering effect of one element on the other might not be adequately accounted for as in the multichannel analysis.

Sample	Multichannel analysis			Three - window analysis		
	K (%)	U (ppm)	Th(ppm)	K (%)	U (ppm)	Th(ppm)
Cl	0.04	0.39	0.52	0.01	0.11	0.51
0000	2.47 \pm 1.0	2.21 \pm 4.1	6.15 \pm 2.8	2.55 \pm 1.3	2.37 \pm 7.2	4.82 \pm 7.0
0060	2.99 \pm 0.9	2.21 \pm 4.2	6.77 \pm 2.7	3.06 \pm 1.1	2.69 \pm 6.5	4.71 \pm 7.1
0120	2.54 \pm 1.0	1.79 \pm 4.7	4.74 \pm 3.5	2.71 \pm 1.2	1.49 \pm 10.6	3.58 \pm 8.8
0180	2.80 \pm 0.9	1.73 \pm 5.1	5.96 \pm 2.9	3.10 \pm 1.1	1.89 \pm 8.8	4.61 \pm 7.2
0240	2.29 \pm 1.1	2.04 \pm 4.3	6.48 \pm 2.7	2.48 \pm 1.2	1.94 \pm 8.6	5.14 \pm 6.6
0300	2.24 \pm 0.8	2.20 \pm 3.1	6.84 \pm 2.0	2.89 \pm 0.8	1.76 \pm 7.5	5.71 \pm 4.8
0360	2.75 \pm 1.0	2.29 \pm 4.2	5.48 \pm 3.4	2.87 \pm 1.2	2.27 \pm 7.8	3.97 \pm 8.6
0420	2.70 \pm 0.9	2.30 \pm 3.8	6.17 \pm 2.8	2.81 \pm 1.2	2.26 \pm 7.4	4.38 \pm 7.5
0480	2.39 \pm 1.0	1.90 \pm 4.5	5.32 \pm 3.1	2.49 \pm 1.2	1.78 \pm 9.1	4.04 \pm 8.0
0540	2.71 \pm 0.9	1.98 \pm 4.4	5.51 \pm 3.1	2.77 \pm 1.2	2.00 \pm 8.2	4.01 \pm 8.0
0600	2.16 \pm 1.1	1.75 \pm 4.7	4.80 \pm 3.5	2.67 \pm 1.2	0.88 \pm 17.2	4.14 \pm 7.7
0660	1.68 \pm 1.0	2.00 \pm 3.3	5.73 \pm 2.3	2.09 \pm 1.1	1.48 \pm 8.6	4.97 \pm 5.4
0720	2.28 \pm 1.1	2.19 \pm 4.0	6.28 \pm 2.8	2.33 \pm 1.3	2.33 \pm 7.2	4.81 \pm 7.0
0780	2.34 \pm 1.1	2.44 \pm 3.7	7.31 \pm 2.4	2.40 \pm 1.3	2.25 \pm 7.6	5.43 \pm 6.3
0840	2.27 \pm 1.1	1.52 \pm 5.7	5.53 \pm 3.0	2.50 \pm 1.2	2.11 \pm 7.9	4.36 \pm 7.5
0900	2.34 \pm 1.0	1.95 \pm 4.3	5.44 \pm 3.1	2.38 \pm 1.3	2.35 \pm 7.0	3.55 \pm 9.0
0960	2.10 \pm 1.1	2.02 \pm 4.3	6.98 \pm 2.5	2.26 \pm 1.4	1.98 \pm 8.5	5.62 \pm 6.1
1000	2.48 \pm 0.7	1.59 \pm 4.0	4.72 \pm 2.7	2.61 \pm 0.9	1.63 \pm 7.6	2.86 \pm 8.7

Cl is the critical limit

Table 7.12: Laboratory results with relative errors expressed as percentages

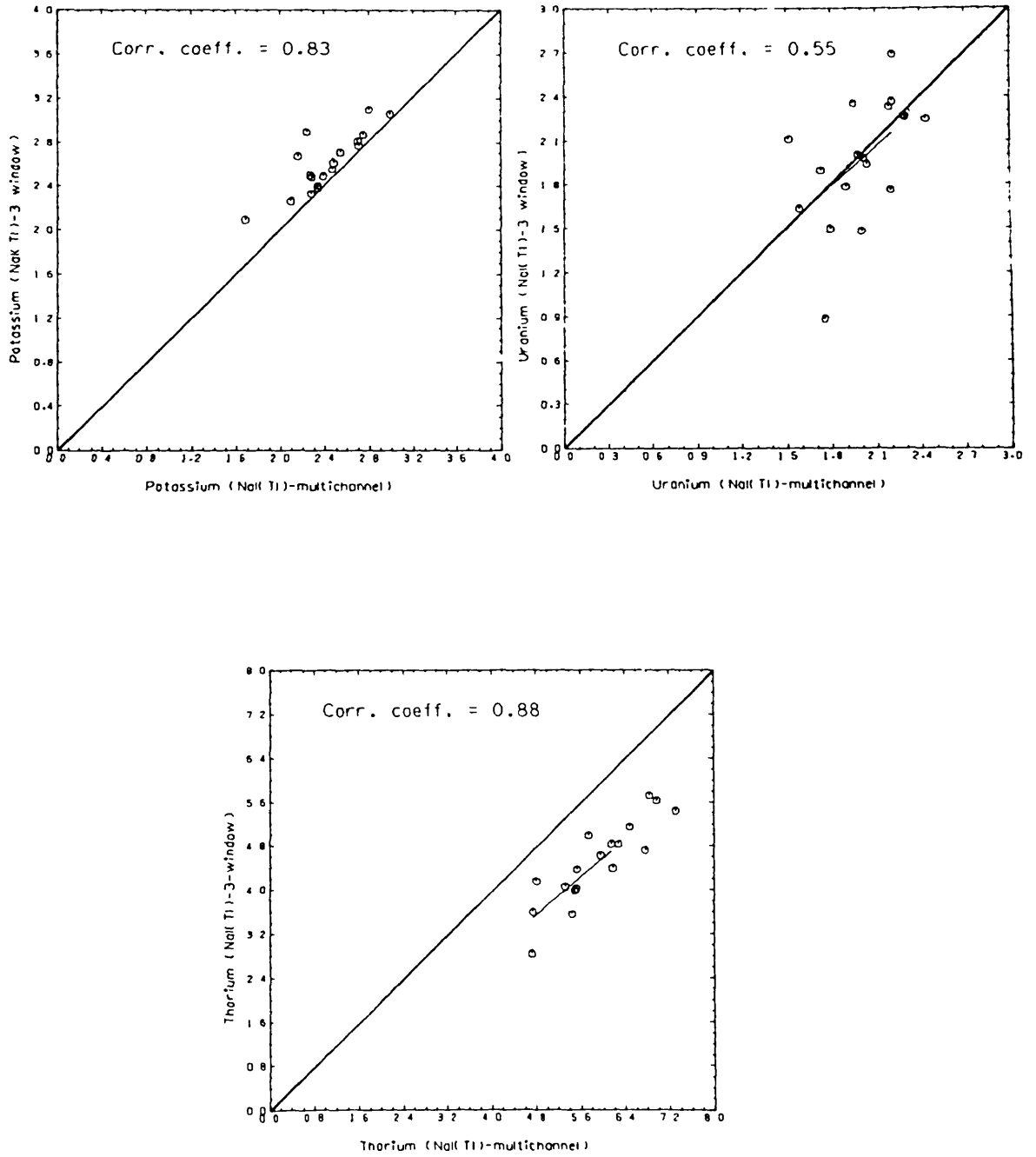


Fig. 7.15 NaK Ti) multichannel Versus 3-window

The uranium and thorium values, however, from the window analysis are systematically smaller than those from the multichannel analysis. This illustrates the fact that in the window analysis, some of the information contained in the spectrum are lost.

Also shown in Fig 7.15 is the regression line. This gives a linear relationship between the corresponding values from the window and the multichannel analyses. The correlation coefficient between the corresponding values for each element was found to be 0.83 for K, 0.55 for U and 0.88 for Th, showing that there is not much difference between the two sets of results. Also the statistical student - t - test indicates that the difference in the mean values of potassium, uranium and thorium from the window and the multichannel analyses can be associated with systematic errors. These suggest that either the window or the multichannel analysis method may be used to estimate the concentrations of the three elements in a sample. But as mentioned before, the accuracy of the results obtained is better when the multichannel analysis method is used.

7.5.2.2. Airborne Results

The results from the airborne survey are shown in Tables 7.7 and 7.8 for the multichannel and the conventional three window analyses respectively. It is seen from Table 7.7 that the results obtained for uranium and thorium above 400feet are very much less than their respective critical limits and hence these results are not used in further work. The abnormality of these results at these heights (500feet to 1000feet) suggests that the calibration spectra may not be

reliably extrapolated outside the range (0 to 433feet) for which they were determined.

Table 7.13 shows the average values of potassium, uranium and thorium obtained for the survey line from the multichannel and window analysis methods. Again, it is seen from Table 7.13 that while the potassium value from the window analysis is larger than that from the

Analysis method	K (%)	U (ppm)	Th (ppm)
Multichannel	2.77±0.12	1.41±0.04	3.05±0.08
Three - window	2.84±0.15	1.03±0.04	2.95±0.14

Table 7.13: Average values from airborne survey

multichannel analysis, the uranium and thorium values from the window analysis are respectively smaller than their corresponding values from the multichannel analysis. This is the same pattern of result observed earlier in section 7.5.2.1. Hence a similar conclusion may be made that the stripping ratios may not have been adequately accounted for in the window analysis and this results in overestimating the potassium values in window analysis.

It is also seen from Table 7.13 that the accuracy of the results is higher when the multichannel analysis method is used.

7.5.3. Laboratory Versus Field Results

It is intended that the laboratory and the field results will

complement one another. However, because of different environmental conditions, some differences are expected in the results (Adams and Gasparini, 1970). The accuracy of field measurements, especially airborne measurements, of potassium, uranium and thorium will always be limited by the effects of vegetation, disequilibria in the uranium-238 and thorium-232 series, variable soil moisture in the upper few inches of the ground, and to some extent the variations of the ground surface from a flat plane; also the field, particularly airborne, survey covers samples that are many orders of magnitude larger than laboratory samples (Adams, 1968)

Table 7.14 shows the average values of the three elements from the laboratory and field surveys. It is seen from Table 7.14 that while

Analysis method	Element	Survey method		
		Lab	Air	Ground
Three - window	K	2.61±0.28	2.84±0.15	2.71±0.21
	U	1.97±0.43	1.03±0.04	1.46±0.25
	Th	4.48±0.76	2.95±0.14	4.60±0.62
Multichannel	K	2.42±0.31	2.77±0.12	-
	U	2.01±0.26	1.41±0.04	-
	Th	5.90±0.78	3.05±0.08	-

Table 7.14: Comparison of laboratory and field results

the field values for potassium are higher than the corresponding

laboratory values, the field values for uranium and thorium, on the other hand, are respectively lower than their corresponding laboratory values. According to Adams and Gasparini (1970), all the three element concentrations obtained from the airborne survey, are expected to be lower than their corresponding values obtained from the laboratory analysis. However, Allan and Richardson (1974) showed a case where at least, the uranium value obtained from an airborne survey is higher than its corresponding value from a laboratory analysis of the samples from the same area (see Table 7.15a). Also Duval et al (1972) presented results where the potassium, uranium and thorium values obtained from field (ground) survey are higher than their corresponding laboratory values (see Table 7.15(b and c)). In the light of this, the potassium values will not be discarded.

The differences between the field and laboratory values lie in the fact that while the field measurements refer to in-situ material which might contain some water moisture, the laboratory measurements are in terms of weight unit of dry samples; the in-situ situation may be characterized by a more severe disequilibrium than the laboratory sample, and also it is not sure if the laboratory sample is fully representative of the in-situ system (Adams and Gasparini, 1970).

7.6. Interpretation of Results

Various forms of data presentation which may lead to easier and better interpretation of radiometric data have been presented in chapter Four. These include contouring the concentration values of the three elements and their ratios in order to determine areas of strong

Table 15a: Results from geochemical and airborne gamma ray spectrometry surveys from the same areas¹ (after Allan and Richardson, 1974)

Method	HARDISTY LAKE MAP SHEET		FORT ENTERPRISE MAP SHEET		RATIO OF HARDISTY LAKE/FORT ENTERPRISE	
	Uranium	Potassium	Uranium	Potassium	Uranium	Potassium
Lake Sediment ⁽²⁾	(ppm U) 70	(% K ₂ O) 33	(ppm U) 28 ⁽³⁾	(% K ₂ O) 30	2.5	1.1
Gamma-Ray Spectrometry ⁽²⁾	3.5	3.2	2.0	2.4	1.8	1.3
Rock Analyses ⁽⁴⁾	6.0 (8.1)	4.7	1.5 (1.7)	2.4	4.0 (4.8)	1.9

1 The bedrock analyses were obtained by Eade and Fahrig (1971) by analyzing composite samples of each rock type found in the area. For Hardisty Lake, only Precambrian rocks of the Bear Province were included in the averages, for both uranium and potassium. For the Fort Enterprise sheet, only rock unit 10 (granite, quartz-monzonite, monzonite) was used for the uranium average; and for potassium only rocks coloured in Eade and Fahrig's map of the area. The rocks came from the following areas: Hardisty Lake 64-65°N and 117-118°W, Fort Enterprise 64-65°N and 112-114°W.

2 Lake-sediment averages were derived as follows: For uranium and potassium the arithmetic mean value was obtained for all sites within the area of 64°30'N to 65°N and 117 to 118°W for the Hardisty Lake Sheet. For the Fort Enterprise Sheet, uranium was the average value for sites overlying Eade and Fahrig's rock unit 10, and potassium was the average for the area coloured on Eade and Fahrig's map. In both cases, averages were from sites north of 64°30'N to 65°N and from 112°W to 114°W.

3 The gamma ray spectrometry averages were calculated over the same areas as the lake-sediment averages. Potassium and uranium count rates over the areas (excluding measurements over water) were averaged, and converted to concentrations using the following correlation: 1%K = 157 counts/2.5 seconds. 1 ppm U = 21 counts per 2.5 seconds.

4 The uranium values were determined by fluorimetric analysis of dissolved samples. Values in parentheses were determined by laboratory gamma ray spectrometry.

5 This value is high, as two of the 42 sites had concentrations of 11 and 13 ppm U. If these two values are excluded the average becomes 2.3 ppm U and the ratio becomes 3.0.

Table 7.15b : Concentrations and estimated errors for K, eU, and eTh at Llano area field sites as determined by field gamma-ray spectrometric systems (Duval et al., 1972)

Site	NaI (TI) detector			Plastic detector			CsI (TI) detector		
	K (percent)	eU (ppm)	eTh (ppm)	K (percent)	eU (ppm)	eTh (ppm)	K (percent)	eU (ppm)	eTh (ppm)
Enchanted Rock granite	4.2 ± 0.5	5.6 ± 1.8	23.7 ± 1.2	4.0 ± 0.9	3.7 ± 1.0	24.4 ± 1.2	4.1 ± 0.7	5.0 ± 1.2	23.6 ± 1.5
Aplite	3.6 ± 0.5	3.3 ± 1.4	19.9 ± 1.1	3.3 ± 0.7	2.6 ± 0.9	20.9 ± 1.1	3.8 ± 0.6	3.2 ± 1.1	24.4 ± 1.5
Contaminated granite	2.8 ± 0.3	3.1 ± 0.7	3.8 ± 0.7	2.4 ± 0.5	3.3 ± 0.6	4.2 ± 0.6	3.2 ± 0.4	1.5 ± 0.4	4.4 ± 0.9
Valley Spring gneiss	2.1 ± 0.3	3.2 ± 0.7	5.0 ± 0.7	2.0 ± 0.4	2.2 ± 0.4	5.1 ± 0.6	2.7 ± 0.4	2.1 ± 0.5	5.3 ± 0.9
Hickory sandstone	0.6 ± 0.1	1.1 ± 0.4	2.9 ± 0.7	0.6 ± 0.1	0.0 ± 0.3	3.1 ± 0.6	0.5 ± 0.1	0.7 ± 0.3	2.8 ± 0.9
Coal Creek serpentine	0.2 ± 0.1	0.4 ± 0.3	0.0 ± 0.7	0.1 ± 0.1	0.2 ± 0.3	0.0 ± 0.5	0.2 ± 0.1	0.8 ± 0.2	0.0 ± 0.8
Town Mountain granite	3.6 ± 0.5	11.3 ± 2.3	24.3 ± 1.2	3.2 ± 1.0	11.1 ± 2.3	26.6 ± 1.3	4.1 ± 0.8	8.5 ± 1.6	23.9 ± 1.5
Marble	0.4 ± 0.1	0.0 ± 0.2	0.4 ± 0.7	0.4 ± 0.1	0.2 ± 0.3	0.5 ± 0.5	0.3 ± 0.1	0.5 ± 0.2	1.0 ± 0.8
Big Branch gneiss	1.3 ± 0.2	4.7 ± 0.9	6.3 ± 0.7	1.4 ± 0.4	4.3 ± 0.9	7.5 ± 0.7	1.6 ± 0.3	3.4 ± 0.6	6.2 ± 0.9
Youghlood Creek aplogranite	2.6 ± 0.8	26.5 ± 6.1	78.8 ± 3.3	2.7 ± 1.7	22.7 ± 6.8	86.0 ± 3.6	3.6 ± 1.3	13.5 ± 3.7	85.8 ± 3.9

Table 7.15c: Concentrations and estimated errors for laboratory determinations of K, eU, and eTh in Llano area field samples (Duval et al., 1972)

Source	K (percent)	eU (ppm)	eTh (ppm)
Enchanted Rock granite	4.78 ± 0.06	1.6 ± 0.4	24.6 ± 0.7
Aplite	4.04 ± 0.05	1.6 ± 0.5	21.4 ± 1.5
Contaminated granite	3.10 ± 0.05	1.8 ± 0.3	3.5 ± 1.5
Valley Spring gneiss	2.66 ± 0.08	2.5 ± 0.7	4.6 ± 0.6
Hickory sandstone	0.73 ± 0.03	0.8 ± 0.3	3.9 ± 1.5
Coal Creek serpentine	0.02 ± 0.03	0.1 ± 0.2	0.0 ± 0.6
Town Mountain granite	4.05 ± 0.09	4.4 ± 0.3	25.2 ± 2.5
Marble	0.07 ± 0.05	0.3 ± 0.3	0.5 ± 0.5
Big Branch gneiss	1.61 ± 0.03	1.3 ± 0.2	4.5 ± 0.5

anomaly. Since only a single line data are used in this project, this form of data presentation, like many others mentioned in chapter Four, will not be possible here. Furthermore, this survey provides only an average (single) value for each of the three elements for the single line surveyed. Hence many forms of data presentation discussed in chapter Four are unlikely to be valid here. However, an attempt is made to interpret the laboratory, ground radiometric and geochemical results in terms of the three elements and their ratios.

Fig 7.16 shows the concentrations of potassium, uranium, thorium and their ratios, U/K, Th/K and Th/U, from the laboratory analysis, along the survey line. The potassium values vary from 1.68% to 2.99% with a mean of 2.42%. The uranium values vary from 1.52ppm to 2.44ppm with a mean of 2.01ppm; and the thorium values vary from 4.72ppm to 6.98ppm with a mean of 5.90ppm.

The average value of Th/U is 2.94, indicating that the materials in the survey area are completely weathered and leached of uranium or are mixtures of materials from low ($\text{Th/U} < 2$) and high ($\text{Th/U} > 7$) ratio environments (Adams and Weaver, 1958).

From Fig 7.16, thorium anomalies are clearly shown at 2.4Km, 7.8Km and 9.6Km. While the thorium anomaly at 9.6Km has associated uranium anomaly, the other anomalies have no associated uranium or potassium anomaly.

Fig 7.17 shows the plots of U against K, Th against K, and Th against U. The scatter of U against K, and Th against K respectively, indicates that there is little or no correlation between uranium and potassium, and also between thorium and potassium. But Th against U

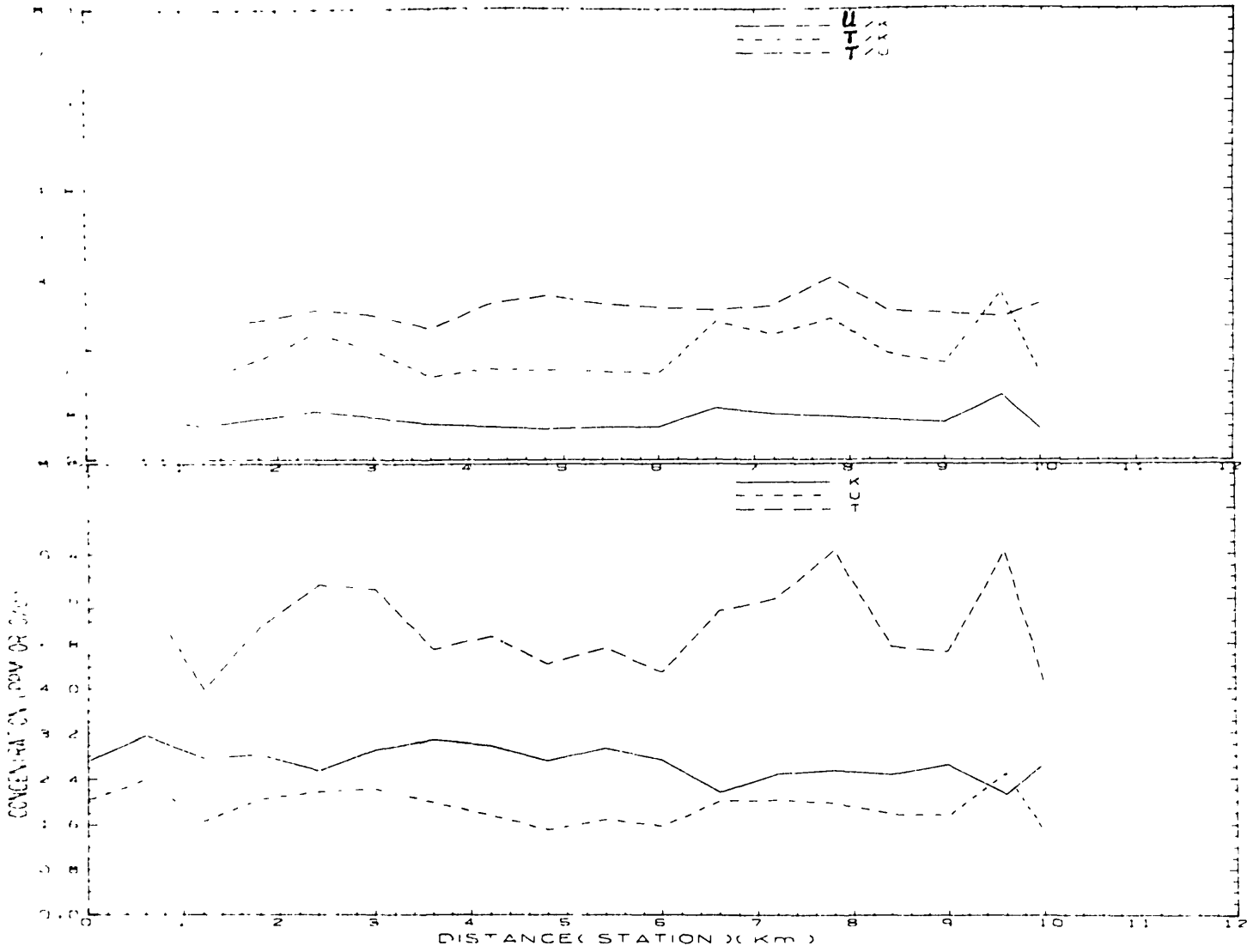


Fig.7.16 : CONCENTRATION OF ELEMENTS ALONG SURVEY LINES (laboratory)

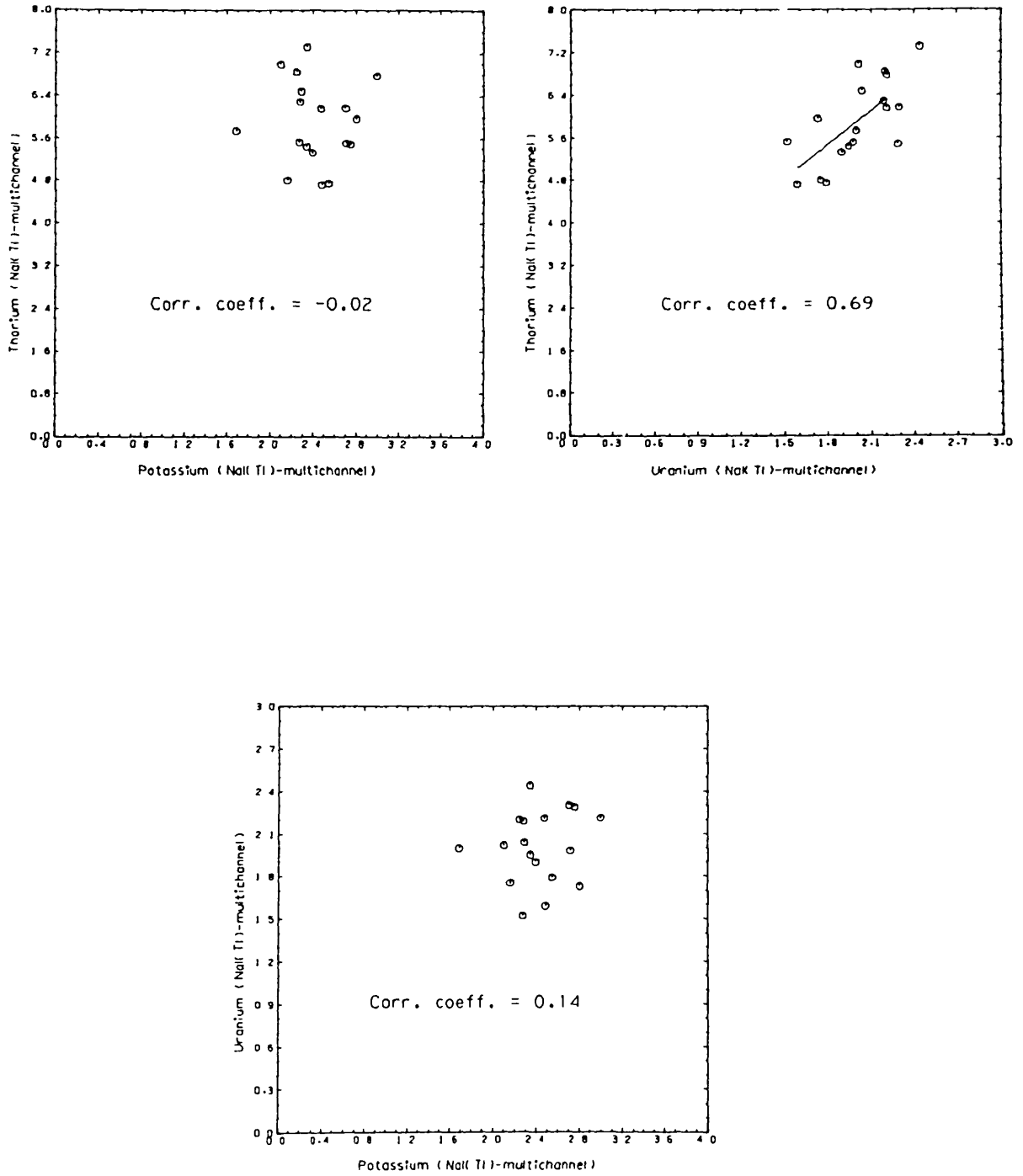


Fig.7.17 Correlation between potassium,uranium and thorium (*laboratory*)

shows a high correlation coefficient 0.69. These results indicate that the potassium concentration is independent of the presence of uranium and/or thorium in the area, whilst uranium and thorium are dependent on each other. It is likely that Th/U and K are independent processes.

The results of the ground profile shown in Fig 7.18 also indicate the thorium anomaly shown between 1.2Km and 3.4Km in Fig 7.17 but extended to 4.0Km. This difference in the extent of the anomaly is due to the density of sampling (the stations were spaced at 0.2Km while the laboratory samples were collected at 0.6Km interval). Also other thorium highs can be seen between 6.0Km and 8.4Km, and two isolated highs at 8.8Km and 9.6Km respectively. The uranium profile follows almost the same pattern. The potassium profile however seems to indicate lows where there are high thorium or/and uranium. Fig 7.19 shows the relationship between potassium and thorium, potassium and uranium, and uranium and thorium. While the correlation coefficient between potassium and thorium is -0.38, that between potassium and uranium is -0.34, and that between uranium and thorium is 0.70. These values again show that while there is little or no association between the occurrence of potassium and thorium/uranium, uranium and thorium are highly associated. The geochemical results are shown in Fig 7.20.

Fig 7.21 shows the histograms for potassium, uranium and thorium concentrations and their ratios from the ground survey. These histograms show that potassium values vary from 2.4 to 3.0% with a mean of 2.71%, and its distribution is bimodal; the uranium has a

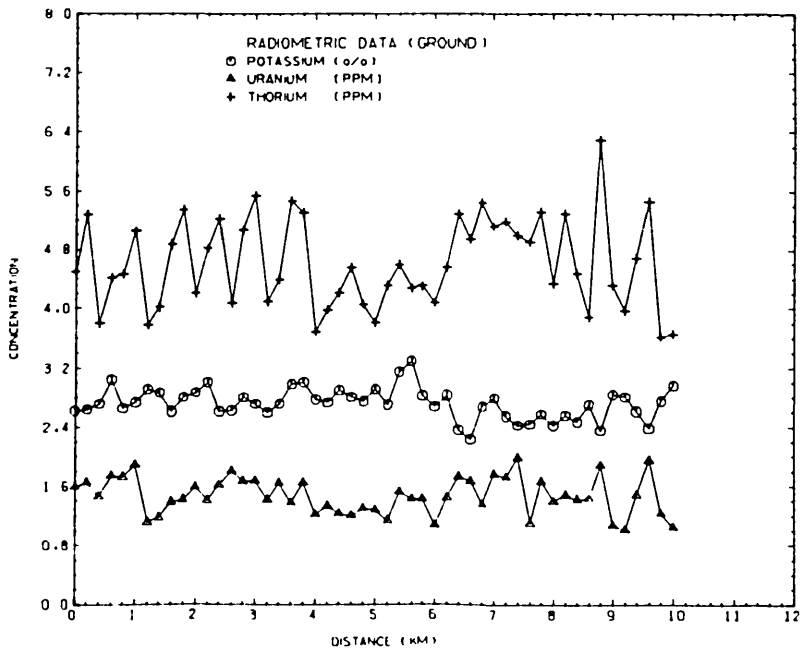
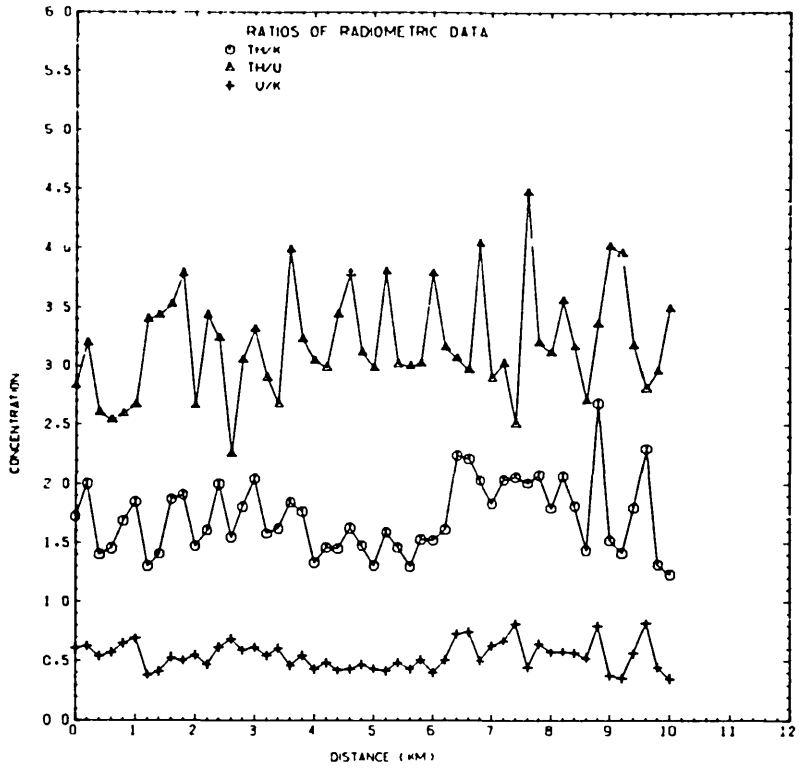


Fig.7.18: Concentration of elements along survey line (ground)

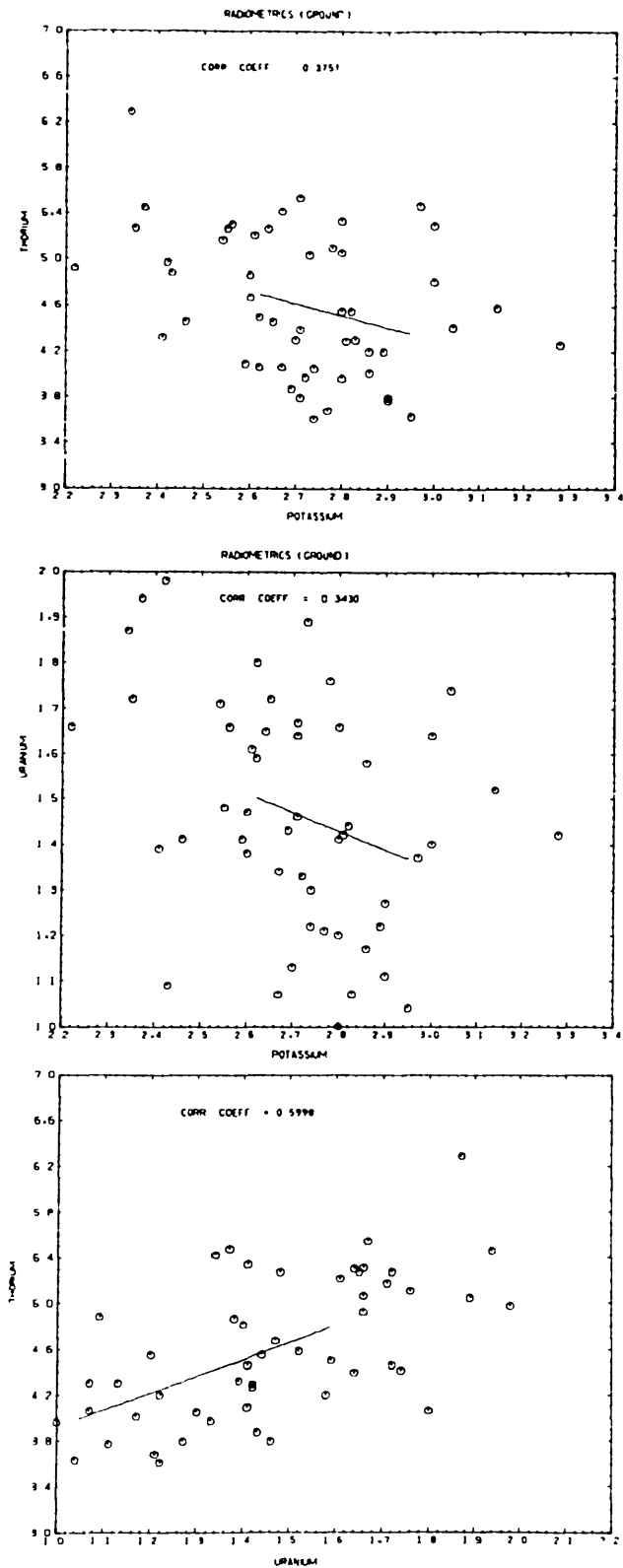


Fig.7.19: Correlation between potassium, uranium and thorium (ground)

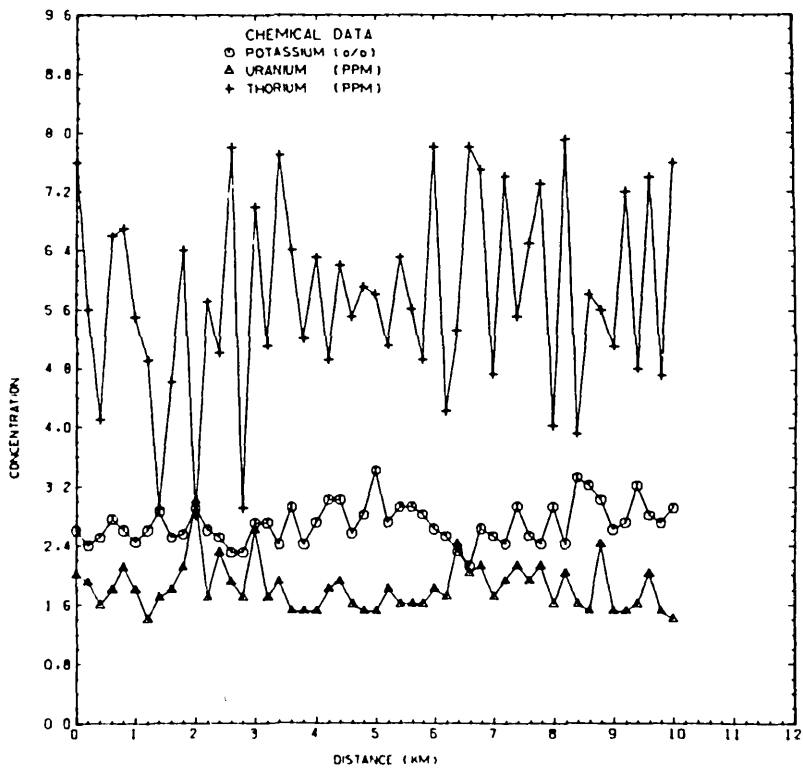
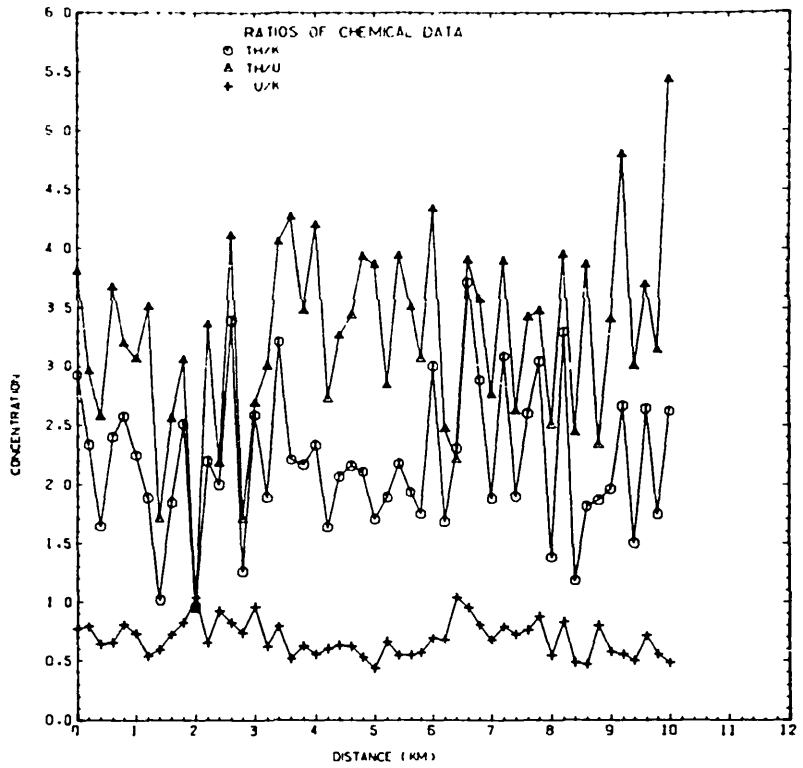


Fig.7.20: Concentration of elements along survey line (chemical)

Fig. 7. 21: Histograms of ground radiometric results

AVER C4 = 4.6025
 STAN C4
 ST.DEV. = .61794
 MEDI C4
 MEDIAN = 4.5000
 HIST C4

T_h

C4

MIDDLE OF INTERVAL	NUMBER OF OBSERVATIONS	
3.6	6	*****
4.0	8	*****
4.4	15	*****
4.8	6	*****
5.2	11	*****
5.6	4	****
6.0	0	
6.4	1	*

AVER C3 = 3.1951
 STAN C3
 ST.DEV. = .46347
 MEDI C3
 MEDIAN = 3.1154
 HIST C3

C3

MIDDLE OF INTERVAL	NUMBER OF OBSERVATIONS	
2.2	1	*
2.4	0	
2.6	7	*****
2.8	4	****
3.0	12	*****
3.2	9	*****
3.4	7	*****
3.6	2	**
3.8	4	****
4.0	4	****
4.2	0	
4.4	1	*

T_h/U

AVER C3 = 1.4641
 STAN C3
 ST.DEV. = .25201
 MEDI C3
 MEDIAN = 1.4300
 HIST C3

U

C3

MIDDLE OF INTERVAL	NUMBER OF OBSERVATIONS	
1.0	2	**
1.1	5	*****
1.2	5	*****
1.3	4	****
1.4	11	*****
1.5	4	****
1.6	5	*****
1.7	9	*****
1.8	2	**
1.9	3	***
2.0	1	*

AVER C4 = .54554
 STAN C4
 ST.DEV. = .11878
 MEDI C4
 MEDIAN = .53870
 HIST C4

C4

MIDDLE OF INTERVAL	NUMBER OF OBSERVATIONS	
.35	2	**
.40	6	*****
.45	9	*****
.50	6	*****
.55	9	*****
.60	7	*****
.65	5	*****
.70	2	**
.75	2	**
.80	3	***

U/K

AVER C2 = 2.7131
 STAN C2
 ST.DEV. = .21129
 MEDI C2
 MEDIAN = 2.7100
 HIST C2

K

C2

MIDDLE OF INTERVAL	NUMBER OF OBSERVATIONS	
2.2	1	*
2.3	1	*
2.4	5	*****
2.5	2	**
2.6	9	*****
2.7	12	*****
2.8	9	*****
2.9	5	*****
3.0	5	*****
3.1	1	*
3.2	0	
3.3	1	*

AVER C2 = 1.7133
 STAN C2
 ST.DEV. = .31304
 MEDI C2
 MEDIAN = 1.6250
 HIST C2

C2

MIDDLE OF INTERVAL	NUMBER OF OBSERVATIONS	
1.2	2	**
1.4	14	*****
1.6	11	*****
1.8	10	*****
2.0	10	*****
2.2	3	***
2.4	0	
2.6	1	*

T_h/K

multimodal distribution and its values vary from 1.00ppm to 2.00ppm with a mean of 1.46ppm; while thorium, also with multimodal distribution, ranges from 3.60ppm to 5.60ppm with a mean value of 4.60ppm. The average value of the Th/U ratio is 3.20 and this indicates, like the laboratory results, that the materials are completely weathered and leached of uranium or are mixtures of materials from low and high ratio environments.

The histograms for the geochemical results presented in Fig 7.22, show that the potassium values range from 2.30% to 3.00% with a mean of 2.68%; uranium values range from 1.40ppm to 2.60ppm with a mean of 1.82ppm; and thorium values range from 4.00ppm to 8.00ppm with a mean of 5.78ppm. The mean value of the Th/U ratio is 3.25, again showing the same result as indicated above.

Fig. 7.22: Histograms of chemical results

AVER C7 = 5.7843
 STAN C7 = 1.3565
 MEDI C7 = 5.6000
 HIST C7

M

MIDDLE OF INTERVAL	NUMBER OF OBSERVATIONS
3.0	3 ***
3.5	0
4.0	4 ****
4.5	3 ***
5.0	9 ****
5.5	8 ****
6.0	4 ****
6.5	7 ****
7.0	2 **
7.5	7 ****
8.0	4 ****

AVER C7 = .68709
 STAN C7 = .14862
 MEDI C7 = .66670
 HIST C7

C7

MIDDLE OF INTERVAL	NUMBER OF OBSERVATIONS
.45	2 **
.50	4 ****
.55	9 ****
.60	3 ***
.65	8 ****
.70	6 ****
.75	4 ****
.80	7 ****
.85	2 **
.90	2 **
.95	2 **
1.00	0
1.05	2 **

U/K

AVER C6 = 1.8176
 STAN C6 = .32293
 MEDI C6 = 1.8000
 HIST C6

U

C6

MIDDLE OF INTERVAL	NUMBER OF OBSERVATIONS
1.4	2 **
1.6	17 ****
1.8	12 ****
2.0	10 ****
2.2	5 ****
2.4	3 **
2.6	1 *
2.8	0
3.0	1 *

AVER C6 = 3.2499
 STAN C6 = .81870
 MEDI C6 = 3.3529
 HIST C6

C6

MIDDLE OF INTERVAL	NUMBER OF OBSERVATIONS
1.0	1 *
1.5	2 **
2.0	2 **
2.5	9 ****
3.0	10 ****
3.5	12 ****
4.0	11 ****
4.5	2 **
5.0	1 *
5.5	1 *

M/U

AVER C5 = 2.6814
 STAN C5 = .27331
 MEDI C5 = 2.6000
 HIST C5

K

C5

MIDDLE OF INTERVAL	NUMBER OF OBSERVATIONS
2.1	1 *
2.2	0
2.3	3 ***
2.4	6 ****
2.5	7 ****
2.6	9 ****
2.7	6 ****
2.8	4 ****
2.9	8 ****
3.0	3 ***
3.1	0
3.2	2 **
3.3	1 *
3.4	1 *

AVER C5 = 2.1909
 STAN C5 = .61504
 MEDI C5 = 2.1569
 HIST C5

C5

MIDDLE OF INTERVAL	NUMBER OF OBSERVATIONS
.8	1 *
1.2	4 ****
1.6	7 ****
2.0	17 ****
2.4	9 ****
2.8	6 ****
3.2	6 ****
3.6	1 *

M/K

CHAPTER EIGHT

CONCLUSION

8.1. SUMMARY

This project is concerned with the evaluation of gamma ray spectrometric data analysis techniques with specific objectives as follows:

- (1) comparison of the performances of NaI(Tl) and Ge(Li) detectors in geological/mineral exploration applications
- (11) comparison of three-window and multichannel analysis results, and
- (111) comparison of laboratory and field results

For better understanding of the subject of gamma ray spectrometry, the principles (chapter Two), survey procedures and corrections (chapter Four), and instrumentation (chapter Five) for gamma ray detection have been included. A review of the methods of analysis (chapter Six) of gamma ray data is made and the least squares' method is used for the analysis of laboratory and field data. The least squares' method is specifically chosen in preference to the graphical and peak area methods because these later two methods make use only of that part of a spectrum around photopeaks and so they do not give all the results required in this project. The graphical and peak area methods are also subjective and have poor performances where peaks are superimposed. The least squares' method on the other hand has the advantage of being

- (a) not subjective
- (b) suitable for spectra whose statistical variations in counting are large, and
- (c) able to use all the data in a spectrum as well as those around photopeaks.

However, the least squares' method has the disadvantages of leading to handling of large matrices (of the order of the number of channels in the spectrometer used) and the calculated coefficients (concentrations of isotopes and the characteristic constants of the spectrometer) may be negative, which of course should not be for physical reasons.

The complete analysis of gamma ray data involves

- (i) instrumental drift correction which accounts for the effect of gain and/or threshold changes
- (ii) background correction which removes the contribution to the recorded counts due to instrument, cosmic and atmospheric (radon) radiations
- (iii) Compton scattering correction and/or height correction. The order of these corrections are interchangeable since the stripping ratios are also height dependent; and
- (iv) determination of the sensitivity constants and then the concentrations of potassium, uranium and thorium in a sample.

Since the definition of window widths in a window spectrometer depends on the resolution of the detector, only multichannel analysis results are used in the comparison of the performances of the NaI(Tl)

and Ge(Li) detectors. The airborne data and the laboratory data for the NaI(Tl) detector were processed using both multichannel and three-window analysis methods.

In the comparison of results, only statistically adequate results were used. The statistical adequacy test involved the determination of a critical limit of detection from the background counts of the system used.

The results of all the analyses and interpretation of these results are presented in chapter Seven. From the results, the following observations were made:

- (i) a Ge(Li) detector is preferable to a NaI(Tl) detector in gamma ray survey where identification of isotopes contained in a sample is the objective.
- (ii) a Ge(Li) detector has poor performance as compared to NaI(Tl) detector in the determination of the concentrations of the isotopes (potassium, uranium and thorium), especially for uranium and thorium. It should be noted that this conclusion is highly dependent on the critical detection limit.
- (iii) although either the conventional three-window or multichannel analysis method can be used in the estimation of the amounts of potassium, uranium and thorium in a ^{laboratory} sample, the accuracy of the results obtained is higher when the multichannel analysis method is used. It is also observed that in the three-window analysis,

three-window analysis, the potassium value may be overestimated because the stripping ratios are not adequately accounted for as in the multichannel case.

- (iv) for airborne data, the three channel analysis underestimate equivalent uranium (eU) and equivalent thorium (eTh) and overestimate potassium. For the eU calculation, the three channel analysis underestimated the eU by about 40% compared with the multichannel analysis. This error could have serious consequences for uranium surveys processed using conventional three window techniques.
- (v) the problem of handling large matrices may be minimized or overcome by spectrum partitioning provided the number of partitions, p , is greater than three and the portion of the spectrum left out at the higher energy end of the spectrum does not include the thorium photopeak at 2.62MeV.
- (vi) comparison of multichannel airborne results with ground and laboratory results revealed a consistent picture. The airborne and ground eU results were in good agreement but both sets of results were lower than the laboratory sample results, probably reflecting factors such as sampling and moisture content. The laboratory potassium values were slightly lower than both ground and airborne data and the eTh multichannel laboratory data significantly higher than the ground spectrometer data

which in turn was greater than the airborne data.

- (vii) the e_{Th}/e_U ratios from the laboratory and field surveys all indicate that the materials in the survey area might be completely weathered and leached of uranium or are mixtures of materials from low ($e_{Th}/e_U < 2$) and high ($e_{Th}/e_U > 7$) ratio environments; and while thorium and uranium may be interdependent, potassium is probably independent of thorium/uranium.

The results indicated that the test range was relatively homogeneous and despite sampling problems, the data indicate that uranium-238 was in equilibrium. The multichannel laboratory data were fairly close to the chemical results (within one standard deviation) but the ground and airborne data showed the effects of different sampling, moisture, etc.

8.2. Limitations And Recommendations For Future Work

In general, gamma ray surveys are limited by the fact that the method assumes secular equilibrium between the parent isotopes Uranium-238 and Thorium-232 and their respective daughter products Bismuth-214 and Thallium-208. This condition of secular equilibrium may not always be met. Several cases of disequilibrium in the uranium series have been reported and this puts some doubts on the results obtained from gamma ray survey. Also correction for background radiation which includes instrument, cosmic and atmospheric radiations, may be difficult in field surveys, especially in the case of airborne survey. Where an

overwater background correction is made, this is done with the assumption that overwater background is the same as that over the survey area. But, as pointed out by Burson (1974) and Geometrics (1979), the overwater background may not be representative of the background over the surveyed area, as the radon distribution may be quite different.

It is recalled that the laboratory analysis of samples with the Ge(Li) detector was performed without shielding the samples. This may be responsible for the high background count rates obtained for the Ge(Li) detector and the consequence of this is the high values for the critical limit of detection which resulted in the rejection of the concentration values for uranium and thorium. In future work, in order to remove this ambiguity, the samples as well as the detector should be shielded so that it will be sure that extraneous radiations are avoided.

The results of the spectra partitioning should be regarded as a preliminary work in the possibility of reducing the large matrices involved in the multichannel analysis of radiometric data. Further investigation may be required in order to establish firm conditions of its application.

The results obtained in this work emphasize the need to utilise the full spectrometer data set, particularly for uranium exploration and more work is needed in this area.

BIBLIOGRAPHY

- Adams, F. and Dams, R. (1977):
Applied gamma ray spectrometry, 2nd edition. Pergamon Press, Oxford.
- Adams, J. A. S. (1968):
Total and spectrometric gamma ray surveys from helicopters and vehicles. in Nuclear Techniques and Mineral Resources, Proc. Symp. held in Buenos Aires, 5 - 9 Nov. 1968, IAEA, Vienna, 1969; pp.147 - 161.
- Adams, J. A. S. and Gasparini, P. (1970):
Gamma ray spectroscopy of rocks. Elsevier Publishing Company, London.
- Adams, J. A. S. and Weaver, C. E. (1958):
Thorium - to - Uranium ratios as indicators of sedimentary process: example of concept of geochemical facies. Bull. Amer. Assoc. Petrol. Geol., Vol.42, No.2, pp.387 - 430.
- Allan, R. J. and Richardson, K. A. (1974):
Uranium and Potassium distribution by lake - sediment geochemistry and airborne gamma ray spectrometry: A comparison of reconnaissance techniques. Can. Min. Met. Bull., Vol.67, No 746, pp.109 - 120.
- Altshuler, B. and Pasternack, B. (1963):
Statistical measures of the lower limit of detection of a radioactivity counter. Health Physics, Vol.9, pp.293 - 298.
- Ayers, J. B. (1973):
Preamplifiers. in Instrumentation in Applied Nuclear Chemistry, edited by Jan Krugers, Plenum Press, London; pp.173 - 202.
- Bacci, C., Bidoli, V. and Baldini-Celio, R. (1967):
Automatic gain control of photomultiplier and relative electronic linear chain. Nucl. Instr. and Meths., Vol.57, pp.100 - 104.
- Bates, R. G. (1966):
Airborne radioactivity surveys, an aid to geologic mapping. Society of Exploration Geophysicists, Mining Geophysics, Vol.1, Case Histories, pp.67 - 76.
- Birch, F. (1954):
Heat from Radioactivity. in Nuclear Geology, edited by H. Faul, John Wiley and Sons, Inc., London; pp.148 - 174.
- Birks, J. B. (1953):

Scintillation counters. Pergamon Press Ltd, London.

----- (1964):

The theory and practice of scintillation counting. Pergamon Press Ltd, London.

Bjerhammar, A. (1973):

Theory of errors and generalized matrix inverses. Elsevier Scientific Publishing Company, London.

Blackburn, J. A. (1965):

Computer program for multicomponent spectrum analysis using least squares method. Analytical Chemistry, Vol.37, pp.1000 - 1003.

Bowie, S. H. U., Hale, F. H., Ostle, D. and Beer, K. E. (1955):

Radiometric surveying with a car-borne counter. Bull. Geol. Surv. Gt. Brit., Vol.10, pp.1 - 23.

Bristow, Q. (1977):

A system for the offline processing of borehole gamma ray spectrometry data on a Nova minicomputer. in Report of Activities, Part A, Geol. Surv. Can., paper 77-1A, pp.87 - 89.

----- (1977a):

Gamma ray spectrometric methods in uranium exploration: airborne instrumentation. in Geophysics and Geochemistry in the search for metallic ores, Peter J. Hood, editor; Geol. Surv. Can., Economic Report 31, pp.135 - 146, 1979.

Burson, Z. G. (1974):

Airborne surveys of terrestrial gamma radiation in environmental research. IEEE Trans. Nucl. Sci., Vol. NS-21, No.1, pp.558 - 571.

Caldwell, R. L., Mills, Jr. W. R., Orr, W. L. and Allen, L. S. (1977):

Nuclear Techniques in Oil and Gas Exploration and Production in Nucl. Tech. and Min. Res., Proc. Series, IAEA, Vienna, 1977; pp.3 - 42.

Cameron, G. W., Elliot, B. E. and Richardson, K. A. (1976):

Effects of line spacing on contoured airborne gamma ray spectrometry data. in Exploration for uranium ore deposits, Proc. Series, IAEA, Vienna, 1976; pp.81 - 92.

Charbonneau, B. W., Killeen, P. G., Carson, J. M., Cameron, G. W. and Richardson, K. A. (1976):

Significance of radioelement concentration measurements made by airborne gamma ray spectrometry over the Canadian Shield.

- in Exploration for uranium ore deposits, Proc. Series, IAEA, Vienna, 1976.
- Choy, S. C. and Schmitt, R. A. (1965):
Gamma ray spectra analysed by computer programme using the peak area method. *Nature*, Vol.205, No.4973, pp.758 - 760.
- Clayton, C. G. (1977):
Applications of nuclear techniques in the coal industry in *Nucl. Tech. and Min. Res.*, Proc. Series, IAEA, Vienna, 1977; pp.85 - 118.
- Conaway, J. G. (1980):
Exact inverse filters for the deconvolution of gamma ray logs. *Geoexploration*, Vol.18, No.1, pp.1 - 14.
- Costrell, L. (1973):
NIM standard. in *Instrumentation in Applied Nuclear Chemistry*, edited by Jan Krugers, Plenum Press, London; pp.153 - 171.
- Cramer, H. (1962):
The element of Probability Theory. John Wiley and sons, Inc., New York.
- Crossley, D. J. (1982):
Optimum use of multichannel gamma ray data. in *Technical Program Abstracts and Biographies. SEG 52nd Ann. Intern. Meeting and Exposition, Oct. 17 - 21, 1982, Dallas, Texas; pp.453 - 455.*
- Crossley, D. J. and Reid, A. B. (1982):
Inversion of gamma ray data for element abundances. *Geophysics*, Vol.47, No.1, pp.117 - 126.
- Currie, L. A. (1968):
Limits for the quantitative detection and quantitative determination. *Analyt. Chem.*, Vol.40. No.3, pp.586 - 593.
- Darnley, A. G. (1970):
Airborne gamma ray spectrometry. *Can. Min. Metall. Bull.*, Vol.73, pp.20 - 29.
- (1972):
Airborne Gamma Ray Survey Techniques. in *Uranium Prospecting Handbook*, edited by S. H. U. Bowie, Michael Davis and Dennis Ostle. The Inst. Min. and Metall., London; pp.174 - 211.
- (1973):
Airborne gamma ray survey techniques - present and future.

- in Uranium Exploration Methods, Panel Proc. Series, IAEA, Vienna, 1973; pp.67 - 108.
- Darnley, A. G., Bristow, Q. and Donhoffer, D. K. (1968):
Airborne gamma ray spectrometer experiments over the Canadian Shield. in Nuclear Techniques and Mineral Resources, Proc. Symp. held in Buenos Aires, 5 - 9 Nov., 1968, IAEA, Vienna, 1969; pp.163 - 186.
- Darnley, A. G. and Grasty, R. L. (1972):
Airborne radiometric survey of the Fort Smith area. Geol. Surv. Can. Open File 101.
- Darnley, A. G., Grasty, R. L. and Charbounneau, B. W. (1969):
Highlights of GSC airborne gamma ray spectrometry in 1969. Can. Min. Journ., pp.98 - 101.
- Davis, J. C. (1973):
Statistics and Data Analysis in Geology. John Wiley and Sons, New York.
- Davis, M. (1972):
Uranium Supply and Demand. in Uranium Prospecting Handbook, edited by S. H. U. Bowie, Michael Davis and Dennis Ostle. The Inst. Min. and Metall., London; pp.17 - 32.
- Dearnaley, G. and Northrop, D. C. (1966):
Semiconductor counters for nuclear radiations. E. and F. N. SPON Ltd., London.
- Demnati, A. and Naudy, H. (1975):
Gamma ray spectrometry in Central Morocco. Geophysics, Vol.40, No.2, pp.331 - 343.
- Dickson, B. H., Bailey, R. C. and Grasty, R. L. (1981):
Utilizing multi-channel airborne gamma ray spectra. Can. Journ. Earth Sci., Vol.18, pp.1793 - 1801.
- Dickson, B. L., Clark, G. J. and McGregor, B. J. (1979):
Technique for correcting for overburden effects in ground level radiometric surveys of uranium ore bodies. Geophysics, Vol.44, No.1, pp.89 - 98.
- Doig, R. (1968):
The natural gamma ray flux: in-situ analysis. Geophysics, Vol.33, No.2, pp.311 - 328.
- Draper, N. R. and Smith, H. (1966):
Applied Regression Analysis. John Wiley, New York.
- Duval, J. S. (1983):

Composite color images of aerial gamma ray spectrometric data. *Geophysics*, Vol.48, No.6, pp.722 - 735.

Duval, J. S., Cook, B. K. and Adams, J. A. S. (1971):
A study of the circle of investigation of an airborne gamma ray spectrometer. *Journ. Geophys. Research*, Vol.76, pp.8466 - 8470.

Duval, Jr. J. S., Worden, J. M., Clark, R. B. and Adams, J. A. S. (1972):
Experimental comparison of NaI(Tl) and solid organic scintillation detectors for use in remote sensing of terrestrial gamma rays. *Geophysics*, Vol.37, No.5, pp.879 - 888.

Dwyer, P. S. (1944):
A matrix presentation of least squares and correlation theory with matrix justification of improved methods of solution. *Annals of Mathematical Statistics*, Vol.15, pp.82 - 89.

Eckhoff, N. D. (1969):
COR GAM - A correlation algorithm for gamma ray spectra. *Nucl. Instr. and Meths.*, Vol.74, pp.77 - 85.

Eckhoff, N. D., Ervin, P. f. and Haskin, F. E. (1970):
A study of statistical properties of polyenergetic gamma ray spectra. *Nucl. Instr. and Meths.*, Vol.83, pp.272 - 276.

Eichholz, G. G. and Poston, J. W. (1979):
Principles of Nuclear Radiation Detection. Ann Arbor Science Publishers, Inc., Michigan.

Ewan, G. T. (1968):
Semiconductor spectrometers. in Farley, F. J. M. (editor), *Progress in Nuclear Techniques and Instrumentation*, Vol.3, pp.67 - 157.

Fairstein, E. and Hahn, J. (1965, 1966):
Nuclear Pulse Amplifiers - Fundamentals and design practice, Parts 1 - 5. *Nucleonics*, Vol.23, No.7, pp.56; Vol.23, No.9, pp.81; Vol.23, No.11, pp.50; Vol.24, No.1, pp.54; Vol.24, No.3, pp.68.

Foot, R. S. (1968):
Improvement in airborne gamma radiation data analysis for anomalous radiation by removal of environmental and pedologic radiation changes. in *Nuclear Techniques and Mineral Resources, Proc. Symp. held in Buenos Aires, 5 - 9 Nov., 1968, IAEA, Vienna, 1969; pp.187 - 196.*

- Foote, R. S. and Humphrey, N. B. (1976):
Airborne radiometric techniques and applications to uranium exploration. in *Exploration for Uranium Ore Deposits, Proc. Series, IAEA, Vienna, 1976*; pp.17 - 34.
- Frederick, D. E. and Hildebrand, J. R. (1968):
The use of labeled pulser pulses as an aid in monitoring the quality of nuclear physics experiments. *Nucl. Instr. and Meths., Vol.61, pp.205 - 208.*
- Galbraith, J. H. and Saunders, D. F. (1983):
Rock classification by characteristic of aerial gamma ray measurements. *Journ. Geochem. Explor., Vol.18, pp.49 - 73.* Elsevier Scientific Publishing Company, Amsterdam.
- Geodata International Inc. (1979):
Aerial Radiometric and Magnetic Survey. Seguin National Topographic Map Texas Gulf Coast. Report prepared for the U.S. Dept. of Energy, under Bendix Field Engineering Corporation Subcontract No.77 - 036 - S.
- Geometrics (1979):
Aerial gamma ray and magnetic survey. Rockies/Laramie Range Quadrangles, Colorado. Final Report. Vol. 1.
- Grasty, R. L. (1972):
Airborne gamma spectrometry data processing manual. Open File 109, June, 1972. *Geol. Surv., Ottawa.*
- (1975):
Uranium measurement by airborne gamma ray spectrometry. *Geophysics, Vol. 40, No.3, pp.503 - 519.*
- (1976):
A calibration procedure for an airborne gamma ray spectrometer. *Geol. Surv. Can.; paper 76-16.*
- (1977):
A general calibration procedure for airborne gamma ray spectrometers in Report of Activities, Part C; *Geol. Surv. Can., paper 77-1C, pp.61 - 62.*
- (1977a):
Gamma ray spectrometric methods in uranium exploration - Theory and Operational procedures. in *Geophysics and Geochemistry in the search for metallic ores*; Peter J. Hood, editor; *Geol. Surv. Can., Econ. Report 31, 1979, pp.147 - 161.*
- (1980):
Skyshine and the calibration of ground gamma ray

spectrometers. in Current Research, Part A, Geol. Surv. Can., paper 80-1A, pp.133 - 135.

- (1982):
Direct snow-water equivalent measurement by air-borne gamma ray spectrometry. Journ. Hydrology, Vol.55, pp.213 - 235; Elsevier Scientific Publishing Company, Amsterdam.
- (1982a):
Utilizing experimentally derived multi-channel gamma ray spectra for the analysis of airborne data. Prepared for symposium on uranium exploration methods review of the NEA/IAEA R and D programme parts, 1st - 4th June, 1982.
- Grasty, R. L. and Darnley, A. G. (1971):
The calibration of gamma ray spectrometers for ground and airborne use. Geol. Surv. Can. paper 71 - 17.
- Green, J. R. and Margerison, D. (1978):
Statistical treatment of experimental data. Physical Sciences Data 2. Elsevier Scientific Publishing Company, Oxford.
- Guillon, H. (1966):
Review of basic instruments and trends. Nucl. Instr. and Meths., Vol.43, pp.230 - 239.
- (1966a):
Review of multichannel and multiparameter analyser systems. Nucl. Instr. and Meths., Vol.43, pp.240 - 247.
- Hamming, R. W. (1962):
Numerical methods for Scientists and Engineers. McGraw-Hill Book Co. Inc., London.
- Hatch, K. F. (1973):
Amplifiers. in Instrumentation in Applied Nuclear Chemistry, edited by Jan Krugers, Plenum Press, London; pp.203 - 243.
- Heath, R. L. (1966):
Computer techniques for the analysis of gamma ray spectra obtained with NaI(Tl) and lithium ion drifted Germanium detectors. Nucl. Instr. and Meths., Vol.43, pp.209 - 229.
- Helmer, R. G., Heath, R. L., Putman, M. and Gipson, D. H. (1967):
Photopeak analysis program for photon energy and intensity determinations. Ge(Li) spectrometers. Nucl. Instr. and Meths., Vol.57, pp.46 - 57.
- Helmer, R. G., Heath, R. L., Schmittroth, L. A., Jayne, G. A. and Wagner, L. M. (1967):

Analysis of gamma ray spectra from Ge(Li) and NaI(Tl) spectrometers. Computer program. Nucl. Instr. and Meths., Vol.47, pp.305 - 319.

Helmer, R. G. and Lee, M. A. (1980):
Analytical functions for fitting peaks from Ge semiconductor detectors. Nucl. Instr. and Meths., Vol.178, pp.499 - 512.

Hilaire, M. (1973):
Treatment of errors in low-activity measurements. Nucl. Instr. and Meths., Vol.112, pp.385 - 390.

Hilchie, D. G. (1977):
Nuclear well logging for petroleum in Nuclear methods in mineral exploration and production, editor, Morse, Jerome G., Development in Economic Geology, 7. Elsevier Scientific Publishing Company, Oxford; pp.201 - 213.

International Atomic Energy Agency (IAEA) (1975):
Laboratory manual on the use of radiotracer techniques in industry and environmental pollution. Technical Reports series No.161, Vienna, 1975.

----- (1979):
Gamma ray surveys in uranium exploration. Technical Reports series No.186, Vienna, 1979.

Jackson, D. D. (1972):
Interpretation of Inaccurate, Insufficient and Inconsistent data. Geophys. Journ. Roy. Astr. Soc., Vol.28, pp.97 - 109.

----- (1973):
Marginal solutions to Quasi - Linear inverse problems in Geophysics: The Edgheog method. Geophys. Journ. Roy. Astr. Soc., Vol.35, pp.121 - 136.

Johnson, P. N. and Tolfree, D. W. L. (1976):
A blue light-emitting diode for use in calibrating and monitoring the gains of photomultipliers. Nucl. Instr. and Meths., Vol.134, pp.29 - 33.

Killeen, P. G. (1977):
Gamma ray spectrometric methods in uranium exploration - application and interpretation. in Geophysics and Geochemistry in the search for metallic ores; Peter J. Hood, editor; Geol. Surv. Can., Econ. Report 31, 1979, pp.163 - 229.

Killeen, P. G. and Carmicheal, C. M. (1970):

- Gamma ray spectrometer calibration for field analysis of thorium, uranium and potassium. *Can. Journ. Earth Sci.*, Vol.7, pp.1093 - 1098.
- Killeen, P. G., Carson, J. M. and Hunter, J. A. (1975):
Optimizing some parameters for gamma ray spectrometric survey. *Geoexpl.*, 13f, pp.1 - 12.
- Killeen, P. G., Hunter, J. A. and Carson, J. M. (1971):
Some effects of altitude and sampling rate in airborne gamma ray spectrometric surveying. *Geoexpl.*, 9, pp.231 - 234.
- Knoll, G. F. (1979):
Radiation Detection and Measurement. John Wiley and Sons, New York.
- Kokta, L. (1973):
Determination of peak area. *Nucl. Instr. and Meths.*, Vol.112, pp.245 - 251.
- Ku, H. H. (1973):
Statistical methods applicable to counting experiments and evaluation of experimental data. *Nucl. Instr. and Meths.*, Vol.112, pp.377 - 383.
- Linden, A. H. and Akerblom, G. (1976):
Method of detecting small or indistinct radioactive sources by airborne gamma ray spectrometry. in *Geology, Mining and Extractive processing of uranium*, editor, Jones, M. J., The Instit. Min. Metall., London, pp.113 - 120.
- Lovborg, L. (1972):
Assesment of uranium by gamma ray spectrometry. in *Uranium Prospecting Handbook*, edited by S. H. U. Bowie, Michael Davis and Dennis Ostle. The Inst. Min. and Metall., London; pp.157 - 173.
- Lovborg, L., Kirkegaard, P. and Christiansen, E. M. (1976):
Design of NaI(Tl) scintillation detectors for use in gamma ray surveys of geological sources in *Exploration For Uranium Ore Deposits*. Proc. Series, IAEA, Vienna, 1976; pp.127 - 148.
- Lovborg, L., Kunzendorf, H. and Hansen, J. (1968):
Use of field gamma spectrometry in the exploration of uranium and thorium deposits in South Greenland. *Nuclear Techniques and Mineral Resources*, Proc. Symp. held in Buenos Aires, 5 - 9, Nov., 1968, IAEA, Vienna, 1969; pp. - 211.
- Mariscotti, M. A. (1967):
A method for automatic identification of peaks in the

presence of background and its application to spectrum analysis. Nucl. Instr. and Meths., Vol.50, pp.309 - 320.

- Matoba, M. and Sonoda, M. (1971):
Stabilization of spectrum with no reference peaks. Nucl. Instr. and Meths., Vol.92, pp.153.
- Matolin, M. (1973):
Artificial standards for calibration of airborne, field portable and logging gamma spectrometers. in Uranium Exploration Methods, Panel proc. Series, IAEA, Vienna, 1973; pp.125 - 139.
- Milam, J. K. (1973):
Single - channel analysers. in Instrumentation in Applied Nuclear Chemistry, edited by Jan Krugers, Plenum Press, London; pp.245 - 261.
- Morris, C. L., Braithwaite, W. J. and Moore, C. F. (1976):
A stable light pulser for gain stabilizing photomultiplier tubes. Nucl. Instr. and Meths., Vol.136, pp.197 - 198.
- Moxham, R. M. (1960):
Airborne radioactivity surveys in Geologic Exploration. Geophysics, Vol.25, No.2, pp.408 - 432.
- (1963):
Natural radioactivity in Washington county, Maryland. Geophysics, Vol.28, No.2, pp.262 - 272.
- Nicholson, P. W. (1974):
Nuclear Electronics. John Wiley and Sons, London.
- Norrish, K. and Chappell, B. W. (1967):
X-ray fluorescence spectrography. in Physical methods in determinative mineralogy, edited by J. Zussmann. Academic Press, London, pp.161 - 214.
- Parasnis, D. S. (1979):
Principles of Applied Geophysics, 3rd edition. Chapman and Hall Ltd., London.
- Parr, R. M. and Lucas, Jr. H. F. (1964):
A rigorous least-squares analysis of complex gamma ray spectra with partial compensation for instrumental instability. IEEE Trans. Nucl. Sci., NS-11, No.3, pp.349 - 357.
- Parr, R. M., Houtermans, H. and Schaerf, K. (1979):
The IAEA intercomparison of methods for processing Ge(Li) gamma ray spectra: A preliminary report. in Computers in

activation analysis and gamma ray spectroscopy. Proc. Amer. Nucl. Soc. Topical Conf. at Mayaguez, Puerto Rico, April 30 - May 4, 1978; pp.544 - 562.

Pauly, J., Guzzi, G., Girardi, F. and Borella, A. (1966):
Application of gamma ray spectrometer and computer techniques to the determination of the minimum detectable content of trace elements in neutron activated materials. Nucl. Instr. and Meths., Vol.42, pp.15 - 25.

Philips (1975):
Semiconductor radiation detectors. Catalogue, Electronic components and materials.

Phillips, G. W. (1978):
Fitting peaks with very low statistics. Nucl. Instr. and Meths., Vol.153, pp.449 - 455.

----- (1979):
Automatic computer analysis of gamma ray spectra. in Computers in activation analysis and gamma ray spectroscopy. Proc. Amer. Nucl. Soc. Topical Conf. at Mayaguez, Puerto Rico, April 30 - May 4, 1978; pp.197 - 215.

Phillips, G. W. and Marlow, K. (1976):
Automatic analysis of gamma ray spectra from germanium detectors. Nucl. Instr. and Meths., Vol.137, pp.525 - 536.

----- (1977):
Peak search and analysis of gamma ray spectra with very low statistics. IEEE Trans. Nucl. Sci., NS-24, No.1, pp.154 - 157.

Pitkin, J. A. and Duval, J. S. (1980):
Design parameters for aerial gamma ray surveys. Geophysics, Vol.45, No.9, pp.1429 - 1439.

Potts, M. J. (1976):
Computer methods for geological analysis of radiometric data. in Exploration for Uranium Ore Deposits, Proc. Series, IAEA, Vienna, 1976; pp.55 - 69.

Quittner, P. (1972):
Gamma ray spectroscopy. Akademiai Kiado, Budapest.

Rama, K. and Honda, M. (1961):
Cosmic ray induced radioactivity in terrestrial materials. Journ. Geophys. Res., Vol.66, No.10, pp.3533 - 3539.

Reber, J. D. and Major, J. K. (1963):

Optimum channel width for single channel analysis. Nucl. Instr. and Meths., Vol.23, pp.162 - 164.

Reedman, J. H. (1979):
Techniques in mineral exploration. Applied Science Publishers Ltd., London.

Richards, D. J. (1977):
Extension of gamma ray spectrometer calibration of multichannel spectrometers with application to Karoo airborne Geophysical survey. Gh.2252, Geol. Surv. S. A., Pretoria.

----- (1977a):
Karoo airborne Geophysical survey: Condensation of multichannel spectrometer data to reduce computation time. Gh.2403. Map Office (PTY) Ltd, Geol. Surv. S. A., Johannesburg.

Robertson, R., Spyrou, N. M. and Kennet, T. J. (1975):
Low level gamma ray spectrometry; NaI(Tl) Vs Ge(Li). Analyt. Chem., Vol.47, No.1, pp.65 - 70.

Routti, J. T. (1968):
Graphical technique for estimating activity level produced in thermal- and fission- neutron irradiation. Analyt. Chem., Vol.40, No.3, pp.593 - 602.

Routti, J. T. and Prussin, S. G. (1969):
Photopeak method for the computer analysis of gamma ray spectra from semiconductor detectors. Nucl. Instr. and Meths., Vol.72, pp.125 - 142.

Salmon, L. (1961):
Analysis of gamma ray scintillation spectra by method of least squares. Nucl. Instr. and Meths. Vol.14, pp.193 - 199.

----- (1962):
Computer analysis of gamma ray spectra from mixtures of known nuclides by the method of least squares in Applications of computer to Nuclear and Radiochemistry, Proceedings of a Symposium, Gatlinburg, Tennessee, Oct. 17 - 19, 1962, NAS - NS 3107, pp.165 - 183.

Saunders, D. F. and Potts, M. J. (1976):
Interpretation and application of high-sensitivity airborne gamma ray spectrometer. in Exploration for Uranium Ore Deposits, Proc. Series, IAEA, Vienna, 1976; pp.107 - 125.

Savitzky, A. and Golay, M. J. E. (1964):

Smoothing and differentiation of data by simplified least-squares procedures. *Analyt. Chem.*, Vol.36, pp.1627 - 1639.

- Scharf, W. and Lisieski, W. (1980):
Amplitude distribution spectrometers. in *Fundamental studies in Engineering 3*. Elsevier Scientific Publishing Company, Oxford.
- Schonfeld, E. (1966):
ALPHA - A computer program for the determination of radioisotopes by least - squares resolution of the gamma ray spectra. *Nucl. Instr. and Meths.*, Vol.42, pp.213 - 218.
- Schonfeld, E., Kibbey, A. H. and Davis, Jr. W. (1966):
Determination of nuclide concentrations in solution containing low level radioactivity by least-square resolution of the gamma ray spectra. *Nucl. Instr. and Meths.*, Vol.45, pp.1 - 21.
- Schram, E. and Lombaert, R. (1963):
Organic scintillation detectors. Elsevier Publishing Company, London.
- Slabaugh, W. H. and Parsons, T. D. (1976):
General Chemistry. John Wiley and Sons, Inc., London.
- Spiegel, M. R. (1972):
Schaum's outline of theory and problems of statistics in SI units. McGraw-Hill International Book Company, London.
- Stephenson, G. (1973):
Mathematical methods for science students, 2nd edition. Longman Group Ltd., London.
- Steyn, J. J. and Nargolwalla, S. S. (1973):
Detectors. in *Instrumentation in Applied Nuclear Chemistry*, edited by Jan Krugers, Plenum Press, London; pp.93 - 152.
- Stromswold, D. C. and Kosanke, K. L. (1978):
Calibration and error analysis for spectral radiation detectors. *IEEE Trans. Nucl. Sci.*, NS-25, No.1, pp.782 - 785.
- Tait, W. H. (1980):
Radiation Detection. Butterworth and Co. (Publishers) Ltd., London.
- Telford, W. M., Geldart, L. P., Sherriff, R. E. and Keys, D. A. (1976):
Applied Geophysics. Cambridge University Press, London.

- Texas Instruments Incorporated, Dallas (1977):
Aerial gamma ray and magnetic surveys of The Delta Area -
Utah. Final Report, Vol.1.
- Trombka, J. I. (1962):
Least-squares analysis of gamma ray pulse-height spectra in
Applications of computer to Nuclear and Radiochemistry,
Proceedings of a symposium, Gatlinburg, Tennessee, Oct.17 -
19, 1962; NAS-NS 3107, pp.183 - 201.
- Trombka, J. I. and Schmadebeck, R. L. (1968):
A method for the analysis of pulse-height spectra containing
gain-shift and zero-drift compensation. Nucl. Instr. and
Meths., Vol.62, pp.253 - 261.
- Turner, Jr. C. E. (1970):
Numerical correction of multichannel analyzer data for
system nonlinearity. Nucl. Instr. and Meths., Vol.87,
No.1, pp.45 - 57.
- Uyttenhove, J., Segers, D., Dorikens, M. and Dorikens-Vanpraet, L.
(1977):
Electro-optical stabilization of a subnanosecond lifetime
spectrometer. Nucl. Instr. and Meths., Vol.141, pp.549 -
552.
- Velimirovich, M. (1974):
The Atomic Universe. Routledge and Kegan Paul Ltd., London.
- Watt, D. E. and Ramsden, D. (1964):
High sensitivity counting techniques. Pergamon Press Ltd.,
London.
- Wiggins, R. A. (1972):
The general linear inverse problem: Implication of surface
waves and free oscillations for earth structure. Rev.
Geophys. and Space Phys., Vol.10, No.1, pp.251 - 285.
- Wilkson, D. H. (1950):
A stable Ninety-Nine channel pulse amplitude analyser for
slow counting. Proc. Cambridge Phil. Soc., Vol.46, pp.508
- 518.
- Williams, A., Campion, P. J. and Burns, J. E. (1973):
Statement of results of experiments and their accuracy.
Nucl. Instr. and Meths., Vol.112, pp.373 - 376.
- Williams, D., Snelling, G. F. and Pickup, J. (1966):
A gamma spectrum stabiliser with compensation for the
effects of detector temperature variation. Nucl. Instr. and

Meths., Vol.39, pp.141 - 149.

Wogman, N. A. (1970):

An all sodium iodide anticoincidence shielded total absorption spectrometer for low-level radionuclide analysis. Nucl. Instr. and Meths., Vol.83, pp.277 - 282.

Wogman, N. A., Perkins, R. W. and Kaye, J. H. (1969):

An all sodium iodide anticoincidence shielded multidimensional gamma ray spectrometer for low-activity samples. Nucl. Instr. and Meths., Vol.74, pp.197 - 212.

Wogman, N. A., Robertson, D. E. and Perkins, R. W. (1967):

A large detector, anticoincidence shielded multidimensional gamma ray spectrometer. Nucl. Instr. and Meths., Vol.50, pp.1 - 10.

Wollenberg, H. A. (1977):

Nuclear techniques in evaluation of geothermal resources. in Nucl. Tech. and Min. Res., Proc. Series, IAEA, Vienna, 1977; pp.379 - 393.

----- (1977a):

Radiometric methods in Nuclear methods in mineral exploration and production, editor, Morse, Jerome G., Development in Economic Geology, 7. Elsevier Scientific Publishing Company, Oxford; pp.5 - 36.

Yamashita, M. (1974):

A pulser-controlled dual window unit for use in gain stabilization of scintillation detectors. Nucl. Instr. and Meths., Vol.114, pp.75 - 82.

Yule, H. P. (1966):

Data convolution and peak location, peak area and peak energy measurements in scintillation spectrometry. Analyt. Chem., Vol.38, pp.103 - 105.

----- (1967):

Mathematical smoothing of gamma ray spectra. Nucl. Instr. and Meths., Vol.54, pp.61 - 65.

APPENDICES

APPENDIX A - Weighting and Normalizing coefficients for least squares' fit (after Savitzky and Golay, 1964)

TABLE I

CONVOLUTES	SMOOTHING		QUADRATIC			CUBIC		A20	A30	9	7	5
	POINTS	25	23	21	19	17	15	13	11			
-12	-253											
-11	-138	-42										
-10	-33	-21	-171									
-09	62	-2	-76	-136								
-08	147	15	9	-51	-21							
-07	222	30	84	24	-6	-78						
-06	287	43	149	89	7	-13	-11					
-05	343	54	204	144	18	42	0	-36				
-04	387	63	249	189	27	87	9	9	-21			
-03	422	70	284	224	34	122	16	44	14	-2		
-02	447	75	309	249	39	147	21	69	39	3	-	
-01	462	78	324	264	42	162	24	84	54	6	12	
00	467	80.5	329	269	43	167	25	89	59	7	17	
01	462	78	324	264	42	162	24	84	54	6	12	
02	447	75	309	249	39	147	21	69	39	3	-3	
03	422	70	284	224	34	122	16	44	14	-2		
04	387	63	249	189	27	87	9	9	-21			
05	343	54	204	144	18	42	0	-36				
06	287	43	149	89	7	-13	-11					
07	222	30	84	24	-6	-78						
08	147	15	9	-51	-21							
09	62	-2	-76	-136								
10	-33	-21	-171									
11	-138	-42										
12	-253											
NORM	5175	8059	3059	2261	323	1105	143	429	231	21	35	

TABLE II

CONVOLUTES	SMOOTHING		QUARTIC		QUINTIC		A40	A50	9	7	5
	POINTS	25	23	21	19	17	15	13			
-12	1265										
-11	-345	285									
-10	-1122	-114	11628								
-09	-1255	-285	-6460	340							
-08	-915	-285	-13005	-255	195						
-07	-255	-165	-11220	-420	-195	2145					
-06	590	30	-3940	-290	-260	-2860	110				
-05	1503	261	6378	18	-117	-2937	-198	18			
-04	2385	495	17655	405	135	-165	-160	-45	15		
-03	3155	705	28190	790	415	3755	110	-10	-55	5	
-02	3750	870	36660	1110	660	7500	390	60	30	-30	
-01	4125	975	42120	1320	825	10125	600	120	135	75	
00	4253	1011	44003	1393	883	11053	677	143	177	131	
01	4125	975	42120	1320	825	10125	600	120	135	75	
02	3750	870	36660	1110	660	7500	390	60	30	-30	
03	3155	705	28190	790	415	3755	110	-10	-55	5	
04	2385	495	17655	405	135	-165	-160	-45	15		
05	1503	261	6378	18	-117	-2937	-198	18			
06	590	30	-3940	-290	-260	-2860	110				
07	-255	-165	-11220	-420	-195	2145					
08	-915	-285	-13005	-255	195						
09	-1255	-285	-6460	340							
10	-1122	-114	11628								
11	-345	285									
12	1265										
NORM	30015	6555	260015	7429	4199	46189	2431	429	429	231	

TABLE III

CONVOLUTES	1ST DERIVATIVE			QUADRATIC			A21					
	POINTS	25	23	21	19	17	15	13	11	9	7	5
-12	-12											
-11	-11	-11										
-10	-10	-10	-10									
-09	-9	-9	-9	-9								
-08	-8	-8	-8	-8	-8							
-07	-7	-7	-7	-7	-7	-7						
-06	-6	-6	-6	-6	-6	-6	-6					
-05	-5	-5	-5	-5	-5	-5	-5	-5				
-04	-4	-4	-4	-4	-4	-4	-4	-4	-4			
-03	-3	-3	-3	-3	-3	-3	-3	-3	-3	-4		
-02	-2	-2	-2	-2	-2	-2	-2	-2	-2	-3	-3	
-01	-1	-1	-1	-1	-1	-1	-1	-1	-1	-2	-2	-2
00	0	0	0	0	0	0	0	0	0	-1	-1	-1
01	1	1	1	1	1	1	1	1	1	0	0	0
02	2	2	2	2	2	2	2	2	2	1	1	1
03	3	3	3	3	3	3	3	3	3	2	2	2
04	4	4	4	4	4	4	4	4	4	3	3	3
05	5	5	5	5	5	5	5	5	5	4	4	4
06	6	6	6	6	6	6	6	6	6	5	5	5
07	7	7	7	7	7	7	7	7	7	6	6	6
08	8	8	8	8	8	8	8	8	8	7	7	7
09	9	9	9	9	9	9	9	9	9	8	8	8
10	10	10	10	10	10	10	10	10	10	9	9	9
11	11	11	11	11	11	11	11	11	11	10	10	10
12	12	12	12	12	12	12	12	12	12	11	11	11
NORM	1300	1012	770	570	408	280	182	110	60	28	10	

TABLE IV

CONVOLUTES POINTS	1ST DERIVATIVE			CUBIC	QUARTIC		A31		A41	
	25	23	21		19	17	15	13	11	9
-12	30866									
-11	8602	3938								
-10	-8525	815	84075							
-09	-20982	-1518	10032	6936						
-08	-29236	-3140	-43284	68	748					
-07	-33754	-4130	-78176	-4648	-98	12922				
-06	-35003	-4567	-96947	-7481	-643	-4121	1133			
-05	-33450	-4530	-101900	-8700	-930	-14150	-660	300		
-04	-29562	-4098	-95338	-8574	-1002	-18334	-1578	-294	85	
-03	-23806	-3350	-79564	-8179	-902	-17842	-1796	-532	-142	22
-02	-16649	-2365	-56881	-5363	-673	-13843	-1489	-503	-193	-67 1
-01	-8558	-1222	-29592	-2816	-358	-7506	-832	-296	-125	-58 -8
00	0	0	0	0	0	0	0	0	0	0 0 0
01	8558	1222	29592	2816	358	7506	832	296	125	58 8
02	16649	2365	56881	5363	673	13843	1489	503	193	67 -1
03	23806	3350	79504	8179	902	17842	1796	532	142	-22
04	29562	4098	95338	8574	1002	18334	1578	294	-85	
05	33450	4530	101900	8700	930	14150	660	-300		
06	35003	4567	96947	7481	643	4121	-1133			
07	33754	4130	78176	4648	98	-12922				
08	29236	3140	43284	-68	-748					
09	20982	1518	-10032	-6936						
10	8525	-815	84075							
11	-8602	-3938								
12	-30866									
NORM	1776060	197340	3634092	255816	23256	334152	24024	5148	1183	252 12

TABLE V

CONVOLUTES POINTS	1ST DERIVATIVE			QUINTIC	SEXIC		A51		A61	
	25	23	21		19	17	15	13	11	9
-12	-6356625									
-11	-11820675	-357045								
-10	-15593141	-654687	-15977364							
-09	-17062146	-840937	-28754154	-332684						
-08	-15896511	-878634	-35613829	-583549	-23945					
-07	-12139321	-752859	-34807914	-686099	-40483	-175125				
-06	-6301491	-478349	-26040033	-604484	-43973	-279975	-31380			
-05	544668	-106911	-10949942	-348823	-32306	-266401	-45741	-3084		
-04	6671883	265164	6402438	9473	-8671	-130506	-33511	-3776	-5758	
-03	9604353	489687	19052988	322378	16679	65229	-12	-1244	-4538	-90
-02	6024183	359157	16649358	349928	24661	169819	27093	2166	2762	18
-01	-8322182	-400653	-15033066	-255102	-14404	-78351	-14647	-573	-505	-2
00	0	0	0	0	0	0	0	0	0	0
01	8322182	400653	15033066	255102	14404	78351	14647	573	508	2
02	6024183	359157	16649358	349928	24661	169819	27093	2166	-2762	-18
03	9604353	489687	19052988	322378	16679	65229	12	1244	4538	90
04	6671883	265164	6402438	9473	8671	130506	33511	3776	5758	
05	544668	106911	10949942	348823	32306	266401	45741	3084		
06	6301491	478349	26040033	604484	43973	279975	31380			
07	12139321	752859	34807914	686099	40483	175125				
08	15896511	878634	35613829	583549	23945					
09	17062146	840937	28754154	332684						
10	15593141	654687	15977364							
11	11820675	357045								
12	6356625									
NORM	7153575	312455	5311735	81719	41990	20995	2431	143	143	1

TABLE VI

CONVOLUTES	2ND DERIVATIVE		QUADRATIC	CUBIC	A22	A32				
POINTS	25	23	21	19	17	15	13	11	9	7 8
-12	92									
-11	69	77								
-10	48	56	190							
-09	29	37	133	51						
-08	12	20	82	34	40					
-07	-3	5	37	19	25	91				
-06	-16	-8	-2	6	12	52	22			
-05	-27	-19	-35	-5	1	19	11	15		
-04	-36	-28	-62	-14	-8	-8	2	6	28	
-03	-43	-35	-83	-21	-15	-29	-5	-1	7	5
-02	-48	-40	-98	-26	-20	-48	-10	-6	-8	0 2
-01	-51	-43	-107	-29	-23	-53	-13	-9	-17	-3 -1
00	-52	-44	-110	-30	-24	-56	-14	-10	-20	-4 -2
01	-51	-43	-107	-29	-23	-53	-13	-9	-17	-3 -1
02	-48	-40	-98	-26	-20	-48	-10	-6	-8	0 -2
03	-43	-35	-83	-21	-15	-29	-5	-1	7	5
04	-36	-28	-62	-14	-8	-8	2	6	28	
05	-27	-19	-35	-5	1	19	11	15		
06	-16	-8	-2	6	12	52	22			
07	-3	5	37	19	25	91				
08	12	20	82	34	40					
09	29	37	133	51						
10	48	56	190							
11	69	77								
12	92									
NORM	26910	17710	33649	6783	3876	6188	1001	429	462	42 1

TABLE VII

CONVOLUTES	2ND DERIVATIVE		QUARTIC	QUINTIC	A42	A52				
POINTS	25	23	21	19	17	15	13	11	9	7 8
-12	-429594									
-11	31119	-346731								
-10	298155	61845	-37791							
-09	413409	281979	11628	-96084						
-08	414786	358530	38802	45084	-121524					
-07	336201	331635	41412	105444	82251	-93093				
-06	207579	236709	34353	109071	153387	88803	-72963			
-05	54855	104445	19734	76830	137085	133485	98010	-10530		
-04	-100026	-39186	1878	26376	71592	95568	115632	20358	-4158	
-03	-239109	-172935	-15678	-27846	-11799	19737	53262	17082	12243	-117
-02	-348429	-280275	-30183	-74601	-88749	-59253	-32043	117	4983	603 -3
-01	-418011	-349401	-39672	-105864	-141873	-116577	-99528	-15912	-6963	-171 44
00	-441870	-373230	-42966	-116820	-160740	-137340	-124740	-22230	-12210	-630 -44
01	-418011	-349401	-39672	-105864	-141873	-116577	-99528	-15912	-6963	-171 44
02	-348429	-280275	-30183	-74601	-88749	-59253	-32043	117	4983	603 -3
03	-239109	-172935	-15678	-27846	-11799	19737	53262	17082	12243	-117
04	-100026	-39186	1878	26376	71592	95568	115632	20358	-4158	
05	54855	104445	19734	76830	137085	133485	98010	-10530		
06	207579	236709	34353	109071	153387	88803	-72963			
07	336201	331635	41412	105444	82251	-93093				
08	414786	358530	38802	45084	121524					
09	413409	281979	11628	-96084						
10	298155	61845	-37791							
11	31119	-346731								
12	429594									
NORM	4292145	2812095	245157	490314	478686	277134	160446	16731	4719	99 3

TABLE VIII

CONVOLUTES POINTS	3RD DERIVATIVE		CUBIC		QUARTIC		A33	A43	9	7	5
	25	23	21	19	17	15	13	11			
-12	-506										
-11	-253	-77									
-10	-55	-35	-285								
-09	93	-3	-114	-204							
-08	196	20	12	-68	-28						
-07	259	35	98	28	-7	-91					
-06	287	43	149	89	7	-13	-11				
-05	285	45	170	120	15	35	0	-30			
-04	258	42	166	126	18	58	6	6	-14		
-03	211	35	142	112	17	61	8	22	7	-1	
-02	145	25	103	83	13	49	7	23	13	1	-1
-01	77	13	54	44	7	27	4	14	9	1	2
00	0	0	0	0	0	0	0	0	0	0	0
01	-77	-13	-54	-44	7	-27	-4	-14	-9	-1	-2
02	-149	-25	-103	-83	13	-49	-7	-23	-13	-1	1
03	-211	-35	-142	-112	17	-61	-8	-22	-7	1	
04	-258	-42	-166	-126	18	-58	-6	-6	14		
05	-285	-45	-170	-120	15	-35	0	30			
06	-287	-43	-149	-89	7	13	11				
07	-259	-35	-98	-28	-7	91					
08	-196	-20	-12	68	28						
09	-93	3	114	204							
10	55	35	285								
11	253	77									
12	506										
SUM	296010	32890	86526	42636	3876	7956	572	858	198	6	2

TABLE IX

CONVOLUTES POINTS	3RD DERIVATIVE		QUINTIC		SEXIC		A53	A63	9	7	5
	25	23	21	19	17	15	13	11			
-12	118745										
-11	217640	23699									
-10	279101	42704	425412								
-09	290076	52959	749372	317655							
-08	244311	51684	887137	1113240	4915						
-07	144616	38013	787382	1231500	8020	93135					
-06	5131	13632	448909	932760	7975	141320	11260				
-05	-146408	-16583	-62644	259740	4380	113065	15250	1580			
-04	-266403	-43928	-598094	-589080	-1755	3800	8165	1700	2295		
-03	-293128	-55233	-908004	-1220520	-7540	-150665	-6870	-55	1280	65	
-02	-144463	-32224	-625974	-1007760	-7735	-260680	-16335	-2010	-2285	-40	
-01	284372	49115	748068	940600	5720	-169295	7150	645	500	5	
00	0	0	0	0	0	0	0	0	0	0	0
01	-284372	-49115	-748068	-948600	-5720	-169295	-7150	-645	-500	-5	
02	144463	32224	625974	1007760	7735	260680	16335	2010	2285	40	
03	293128	55233	908004	1220520	7540	150665	6870	55	-1280	-65	
04	266403	43928	598094	589080	1755	-3800	-8165	-1700	-2295		
05	146408	16583	62644	-259740	-4380	-113065	-15250	-1580			
06	-5131	-13632	-448909	-932760	-7975	-141320	-11260				
07	-144616	-38013	-787382	-1231500	-8020	-93135					
08	-244311	-51684	-887137	-1113240	-4915						
09	-290076	-52959	-749372	-317655							
10	-279101	-42704	-425412								
11	-217640	-23699									
12	-118745										
SUM	5722860	749892	4249388	4247012	16796	2144809	9724	572	286	2	

TABLE X

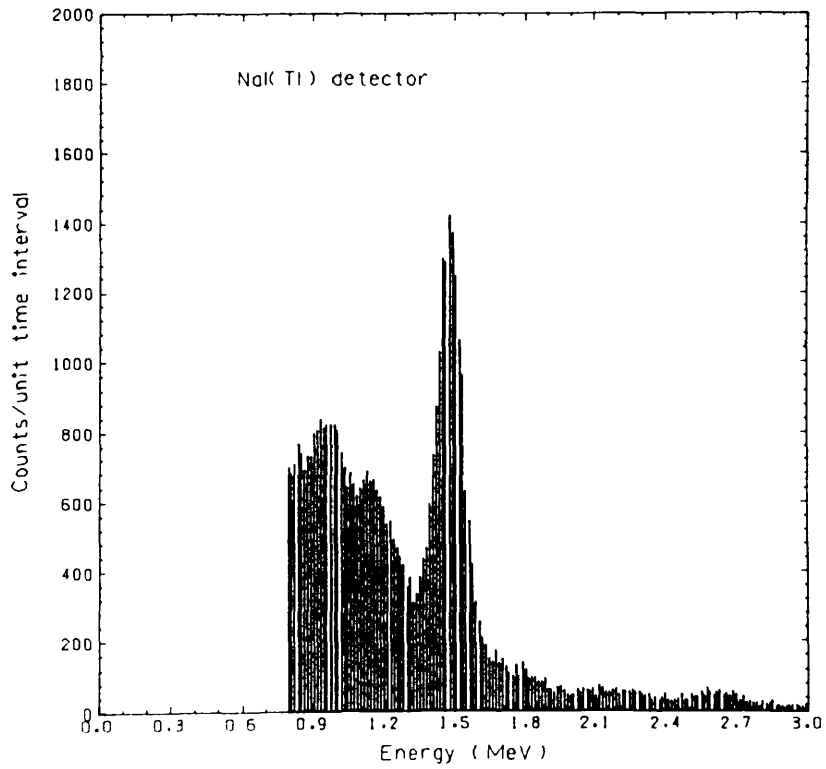
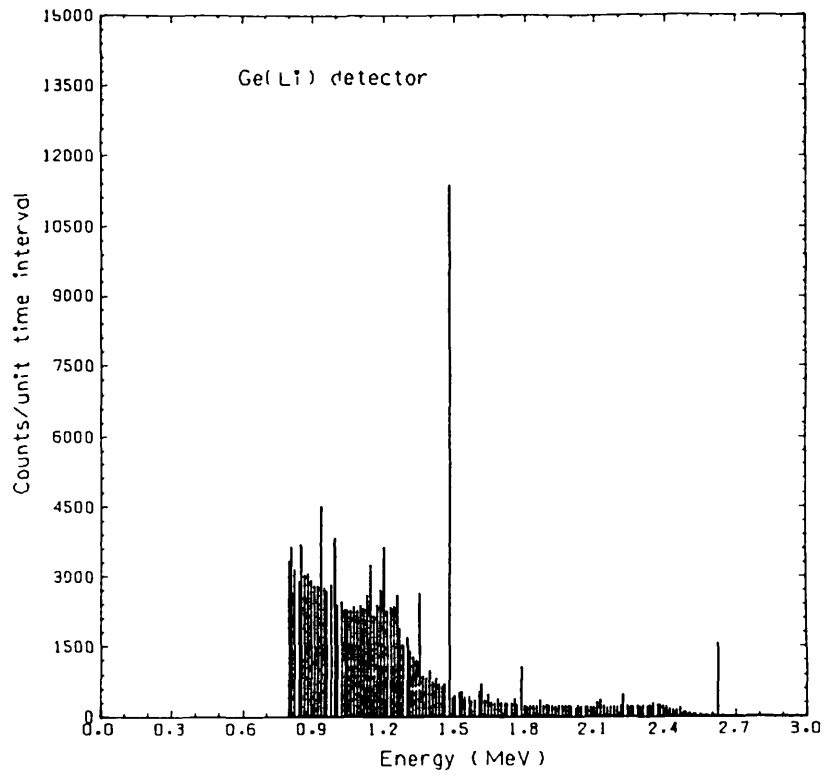
CONVOLUTES	4TH DERIVATIVE			QUARTIC		QUINTIC		A44	A54	9	7	5
	POINTS	25	23	21	19	17	15	13	11			
-12	858											
-11	803	858										
-10	643	793	594									
-09	393	605	540	396								
-08	78	315	385	352	36							
-07	-267	-42	150	227	31							
-06	-597	-417	-130	42	17	621	84					
-05	-857	-747	-406	-168	-3	251	64	6				
-04	-982	-955	-615	-354	-24	-249	11	4	18			
-03	-897	-950	-680	-453	-39	-704	-54	-1	9	6		
-02	-517	-627	-510	-388	-39	-869	-96	-6	-11	1		
-01	253	133	0	-68	-13	-429	-66	-6	-21	-7		
00	1518	1463	969	612	52	1001	99	6	14	-3		
01	253	133	0	-68	-13	-429	-66	-6	-21	-7		
02	-517	-627	-510	-388	-39	-869	-96	-6	-11	1		
03	-897	-950	-680	-453	-39	-704	-54	-1	9	6		
04	-982	-955	-615	-354	-24	-249	11	4	18			
05	-857	-747	-406	-168	-3	251	64	6				
06	-597	-417	-130	42	17	621	84					
07	-267	-42	150	227	31	756						
08	78	315	385	352	36							
09	393	605	540	396								
10	643	793	594									
11	803	858										
12	858											
NORM	1430715	937365	408595	163438	8398	92378	4862	143	143	11		

TABLE XI

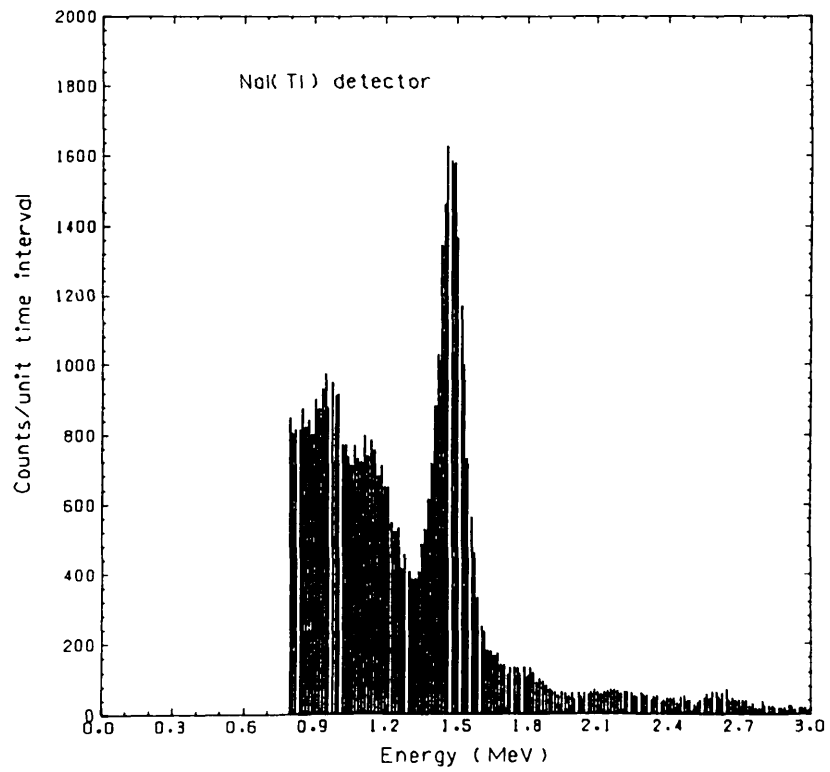
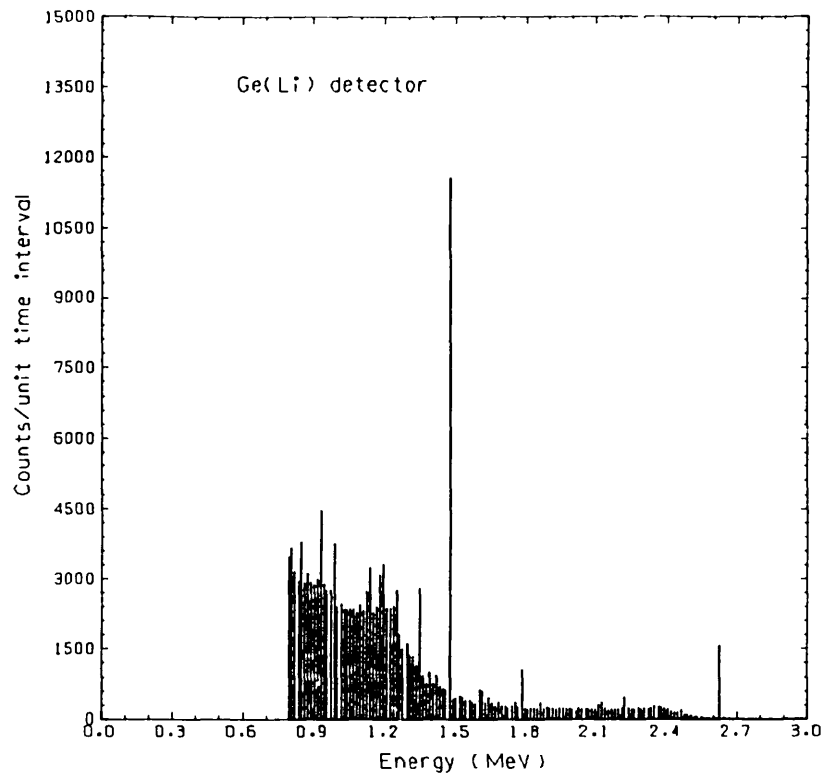
CONVOLUTES	5TH DERIVATIVE			QUINTIC		SEXIC		A55	A65	9	7	5
	POINTS	25	23	21	19	17	15	13	11			
-12	-275											
-11	-500	-65										
-10	-631	-116	-1404									
-09	-636	-141	-2444	-44								
-08	-501	-132	-2819	-74	-55							
-07	-236	-87	-2354	-79	-88	-675						
-06	119	-12	-1063	-54	-83	-1000	-20					
-05	488	77	788	-3	-36	-751	-26	-4				
-04	753	152	2618	58	39	44	-11	-4	-9			
-03	748	171	3468	98	104	979	18	1	-4	-5		
-02	253	76	1938	68	91	1144	33	6	11	4		
-01	-1012	-209	-3876	-102	-104	-1001	-22	-3	-4	-1		
00	0	0	0	0	0	0	0	0	0	0		
01	1012	209	3876	102	104	1001	22	3	4	1		
02	-253	-76	-1938	-68	-91	-1144	-33	-6	-11	-4		
03	-748	-171	-3468	-98	-104	-979	-18	-1	4	5		
04	-753	-152	-2618	-58	-39	-44	11	4	9			
05	-488	-77	-788	3	36	751	26	4				
06	-119	12	1063	54	83	1000	20					
07	236	87	2354	79	88	675						
08	501	132	2819	74	55							
09	636	141	2444	44								
10	631	116	1404									
11	500	65										
12	275											
NORM	1300650	170430	1931540	29716	16796	83980	884	52	26	2		

APPENDIX B - SPECTRA

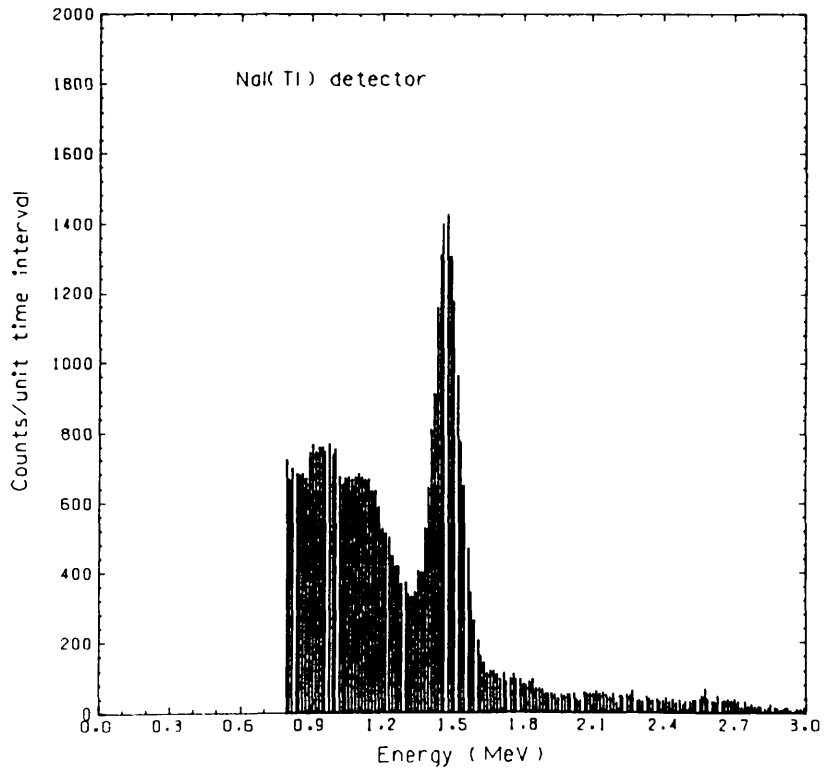
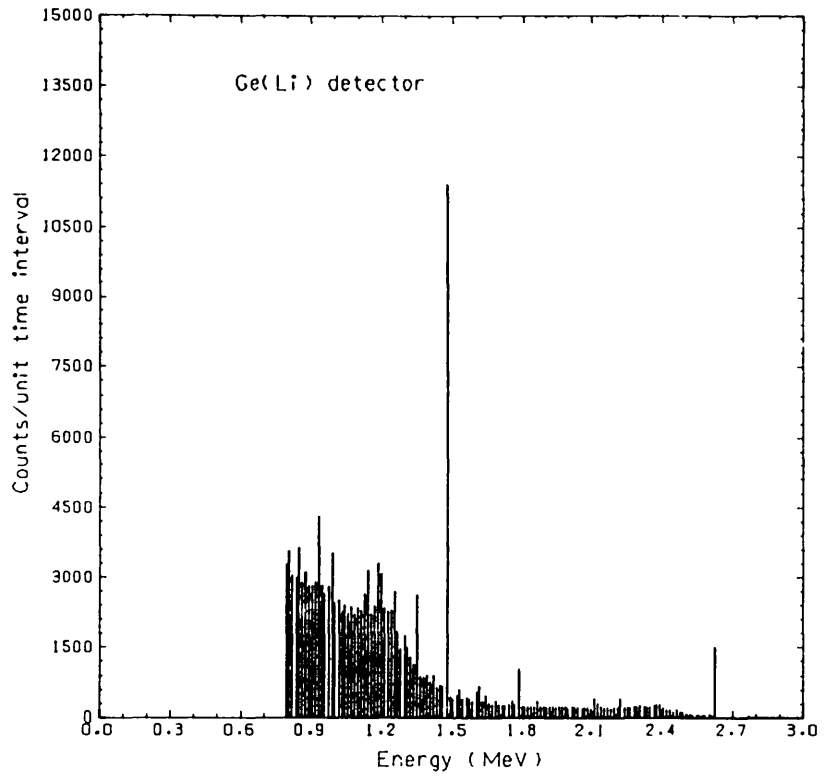
B1 - Laboratory sample spectra



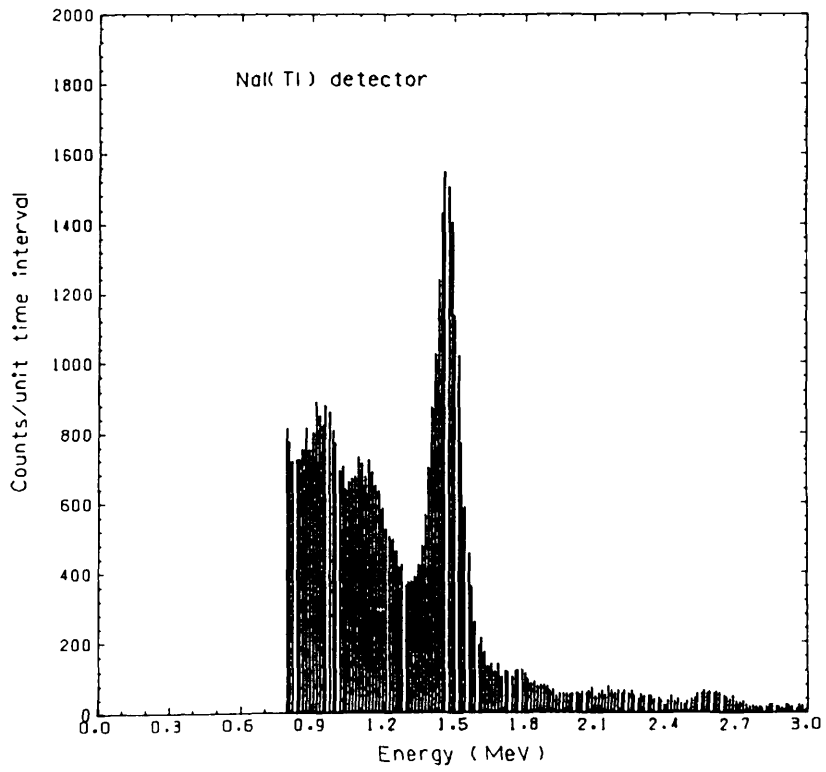
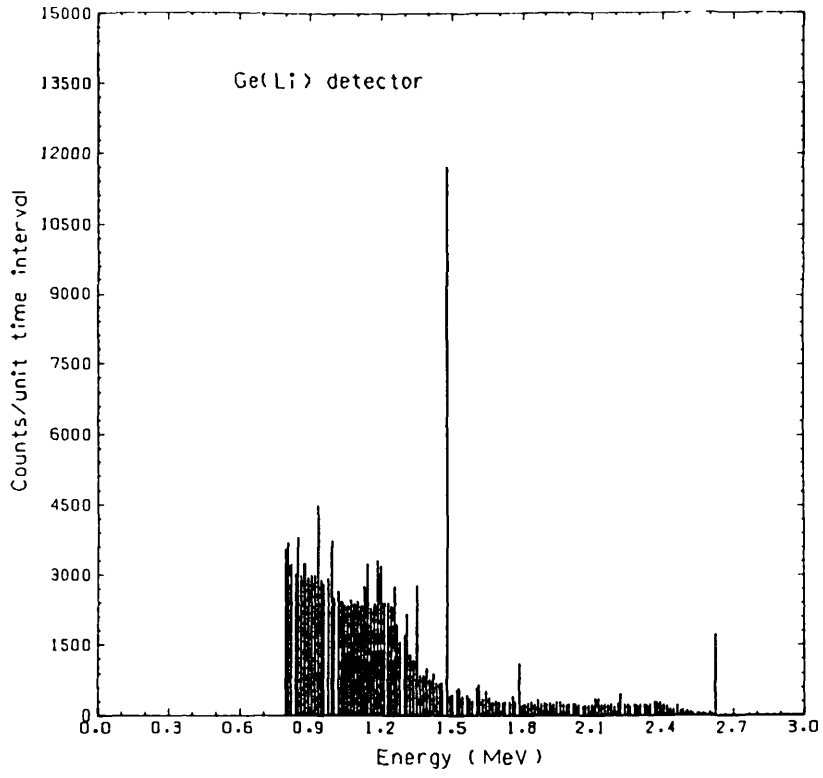
Sample 0000 spectrum



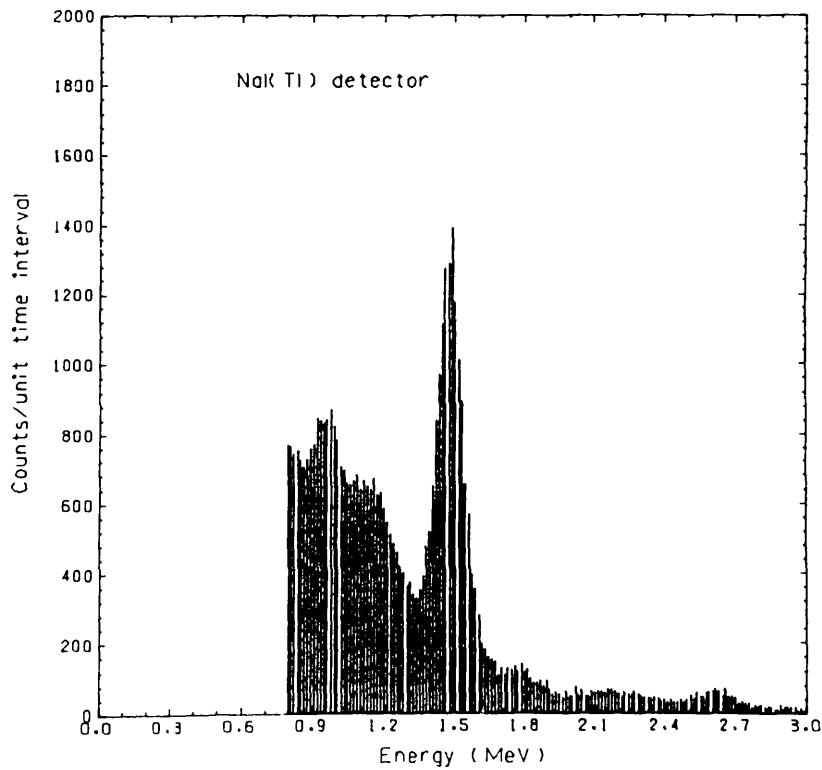
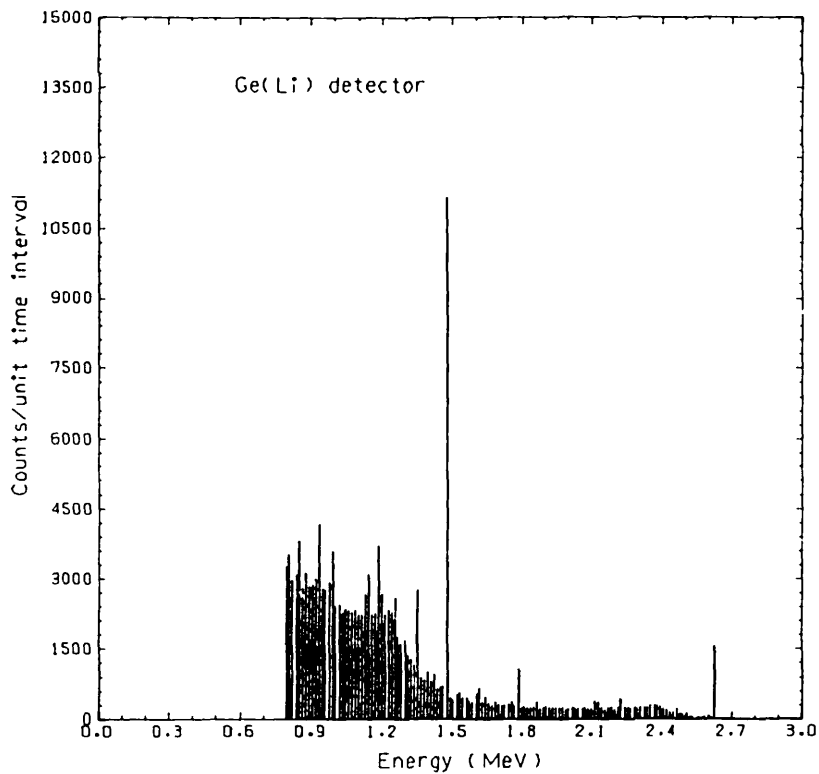
Sample 0060 spectrum



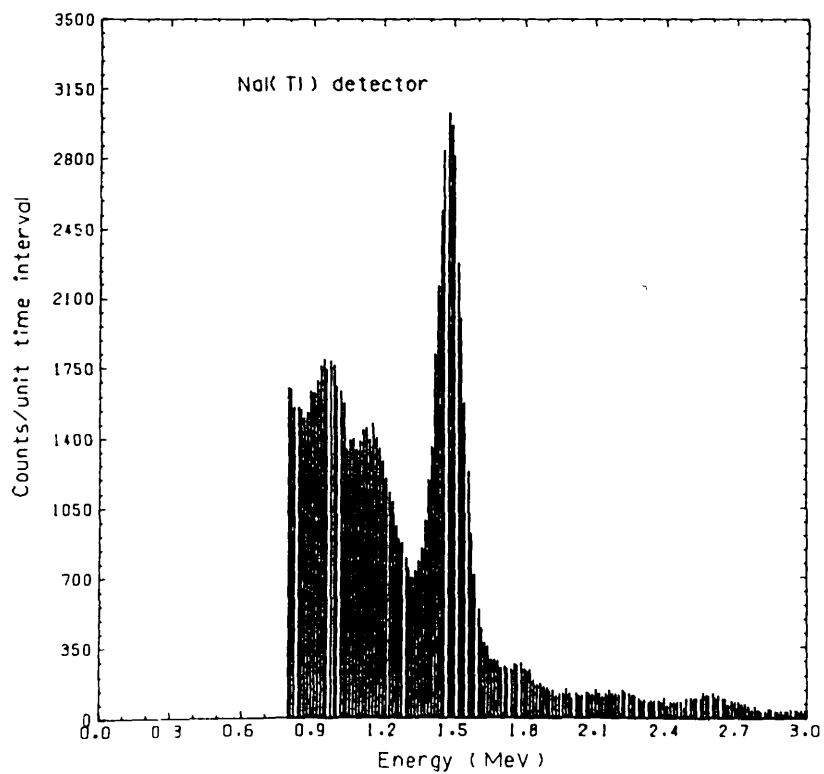
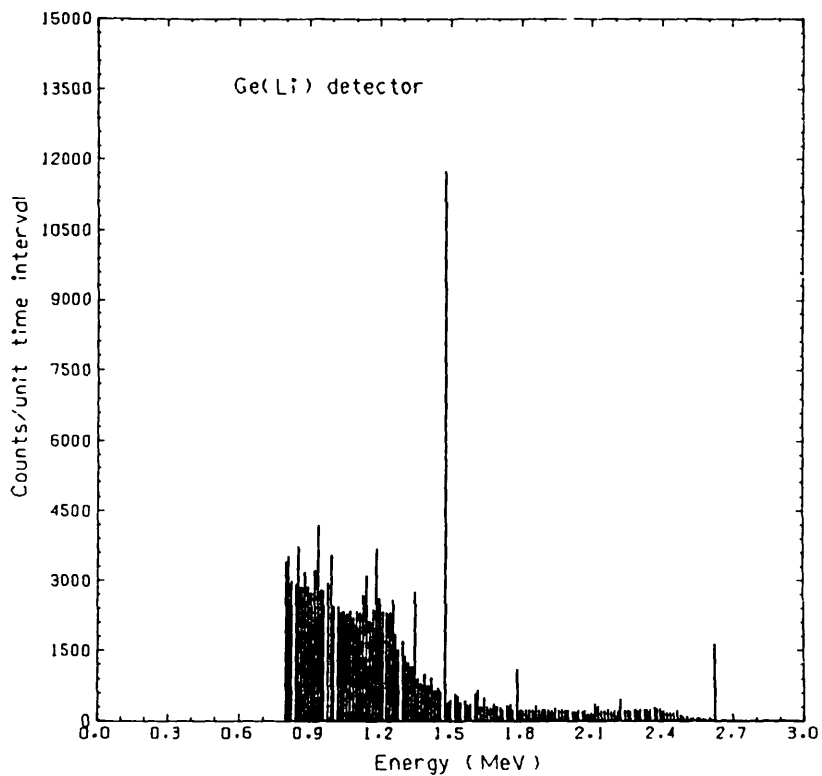
Sample 0120 spectrum



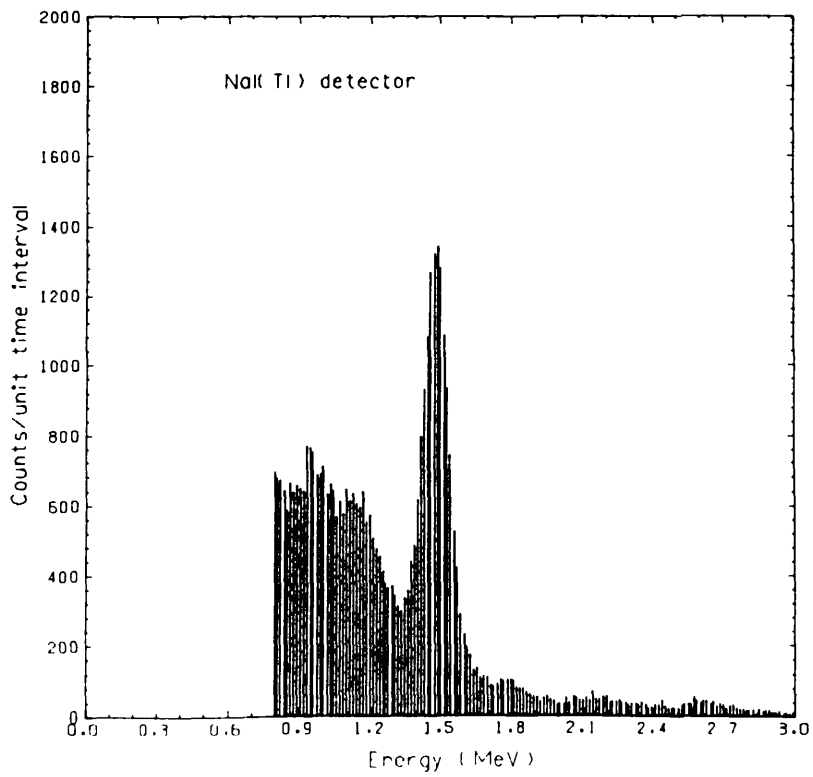
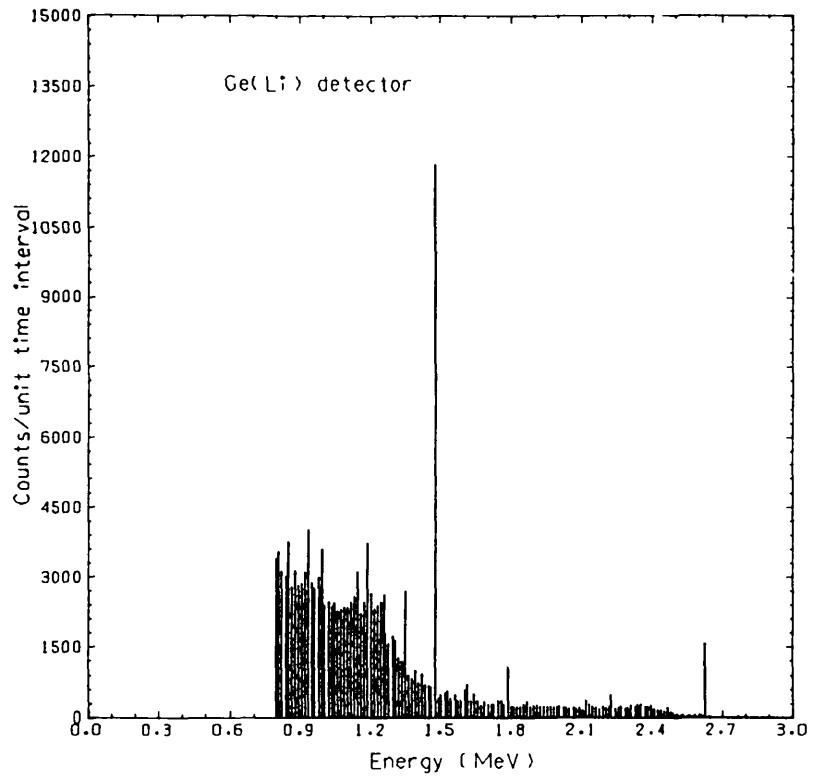
Sample 0180 spectrum



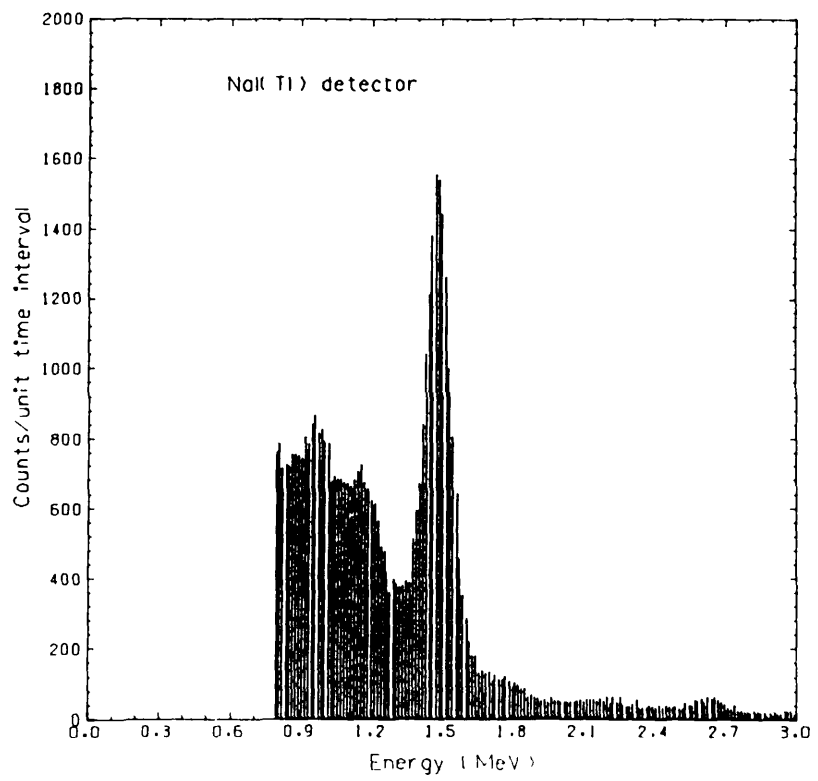
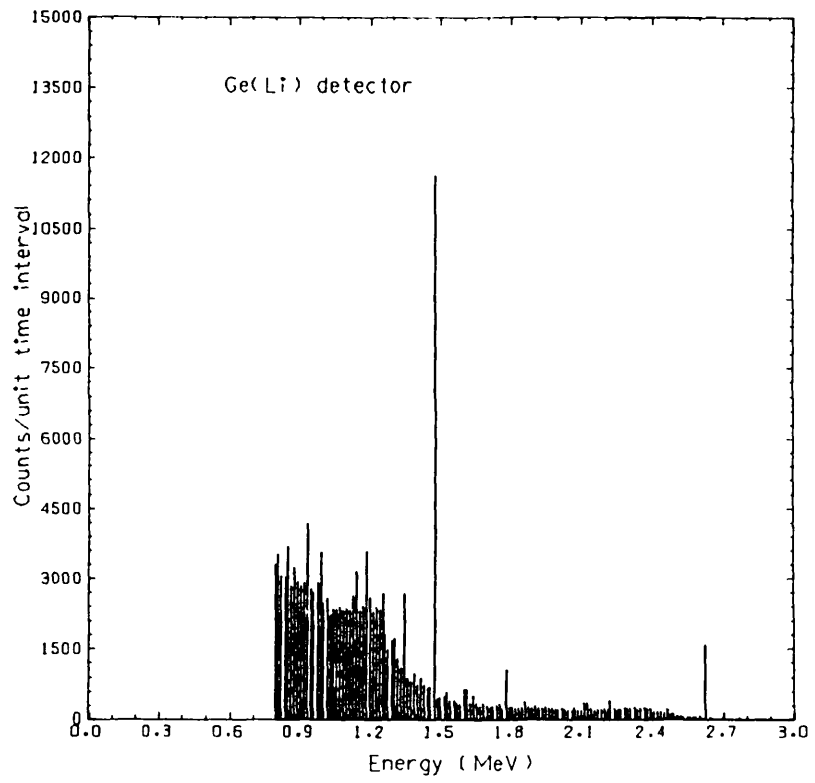
Sample 0240 spectrum



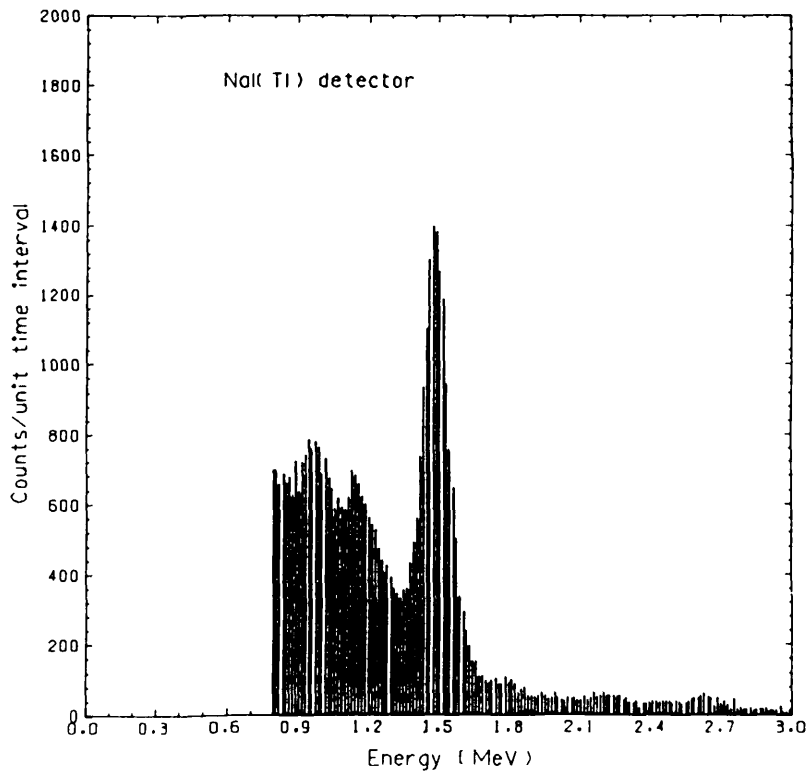
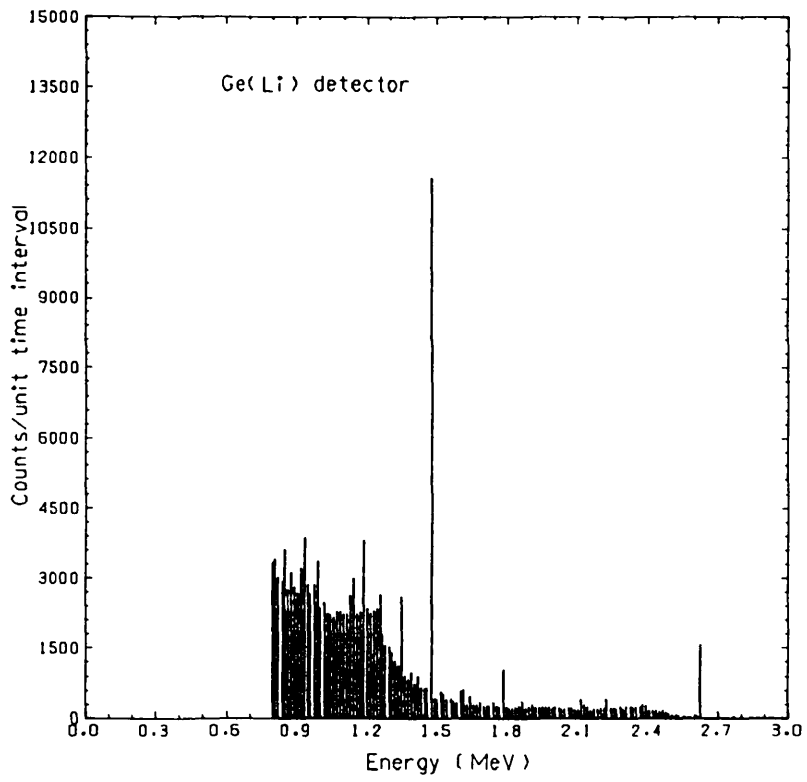
Sample 0300 spectrum



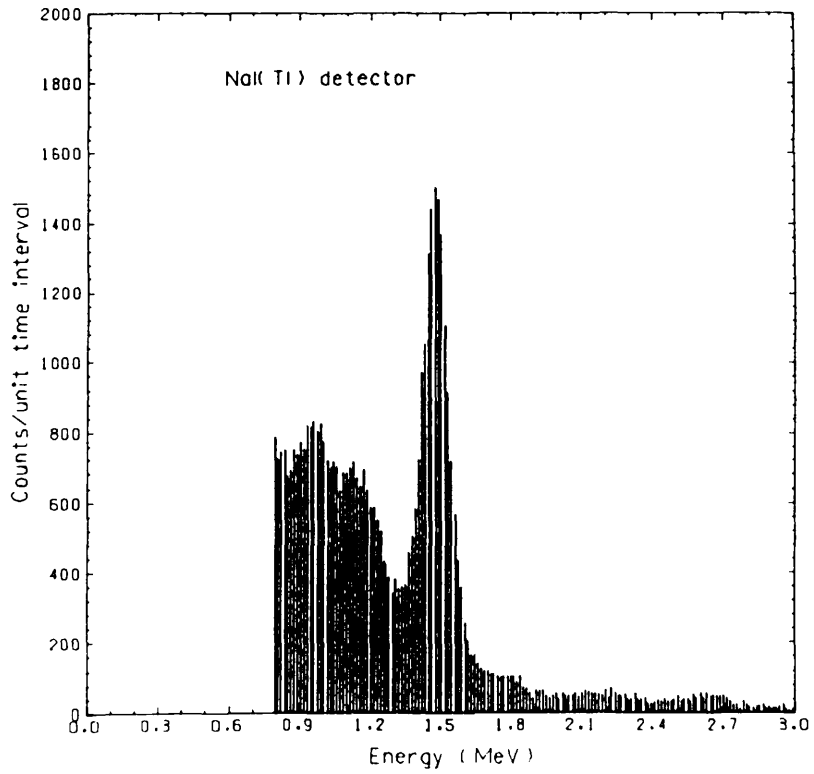
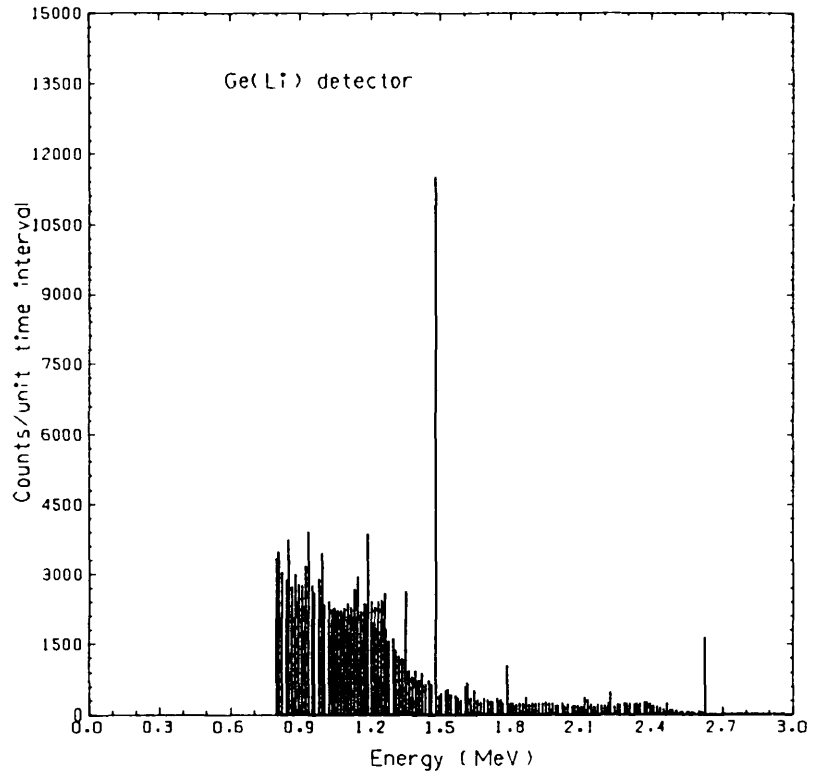
Sample 0360 spectrum



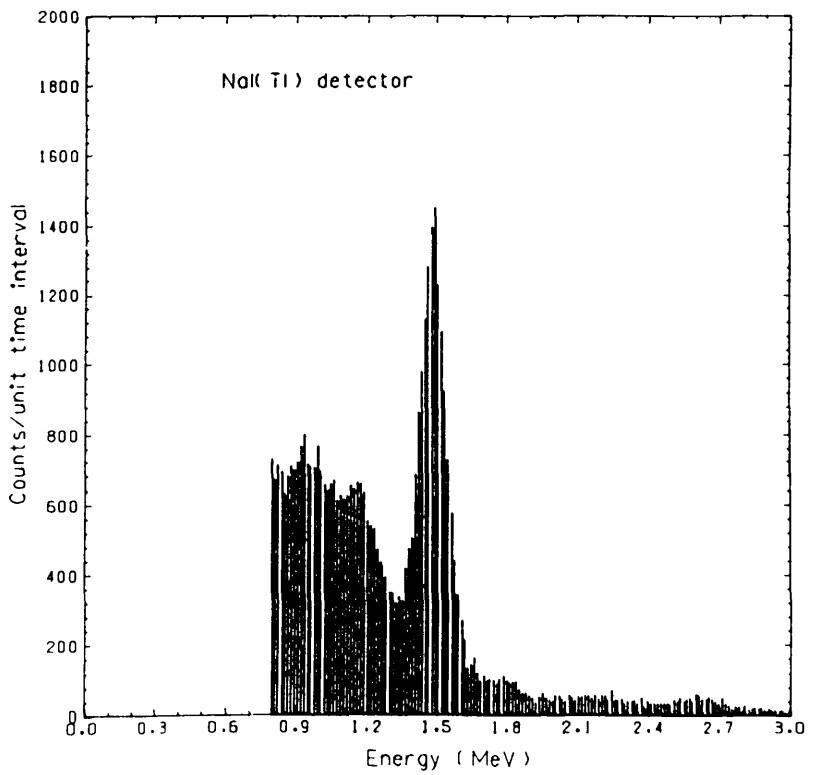
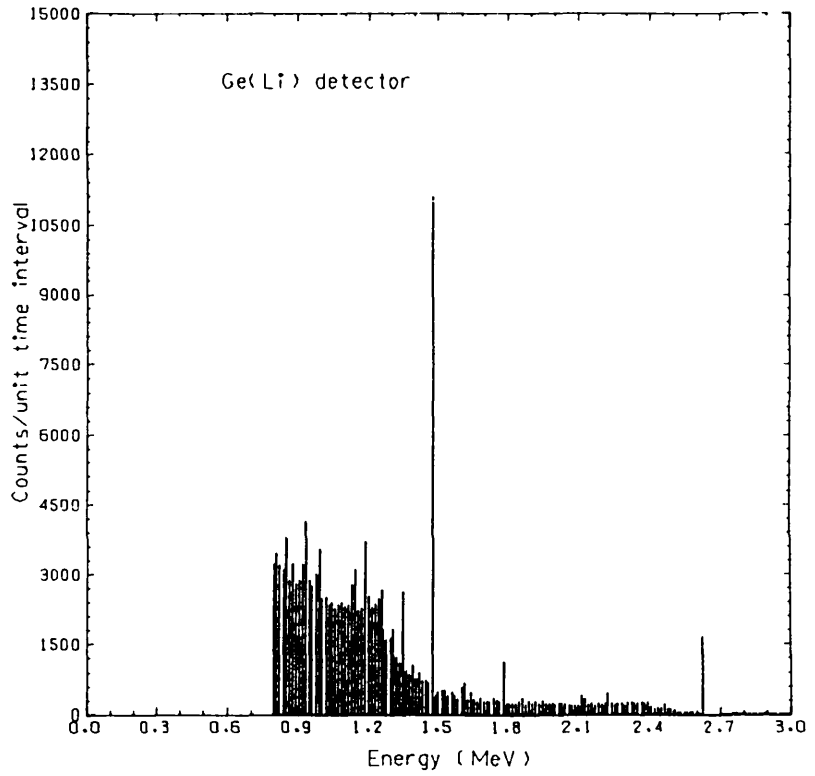
Sample 0420 spectrum



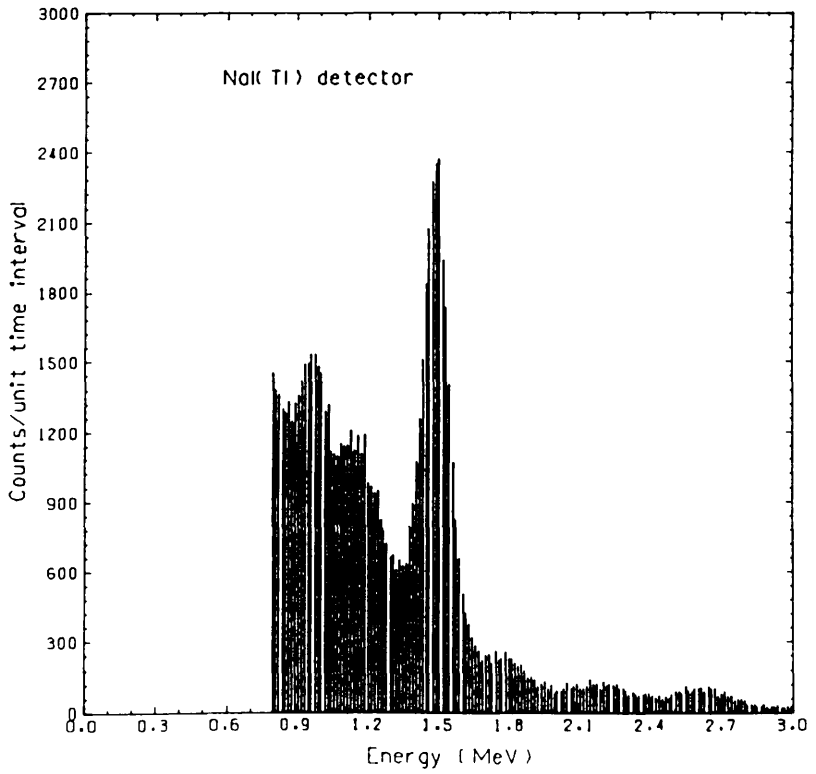
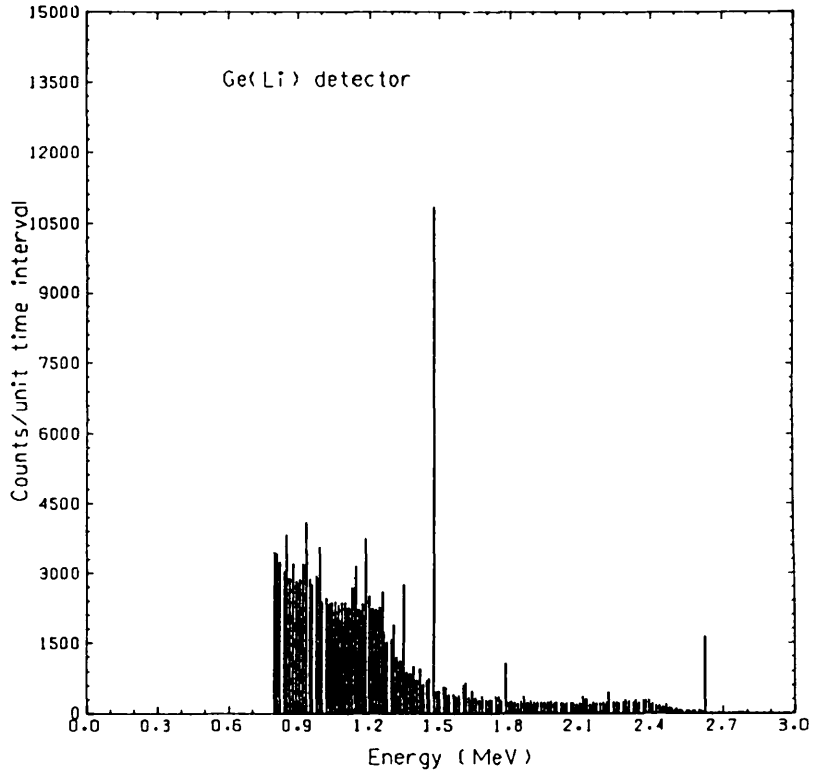
Sample 0480 spectrum



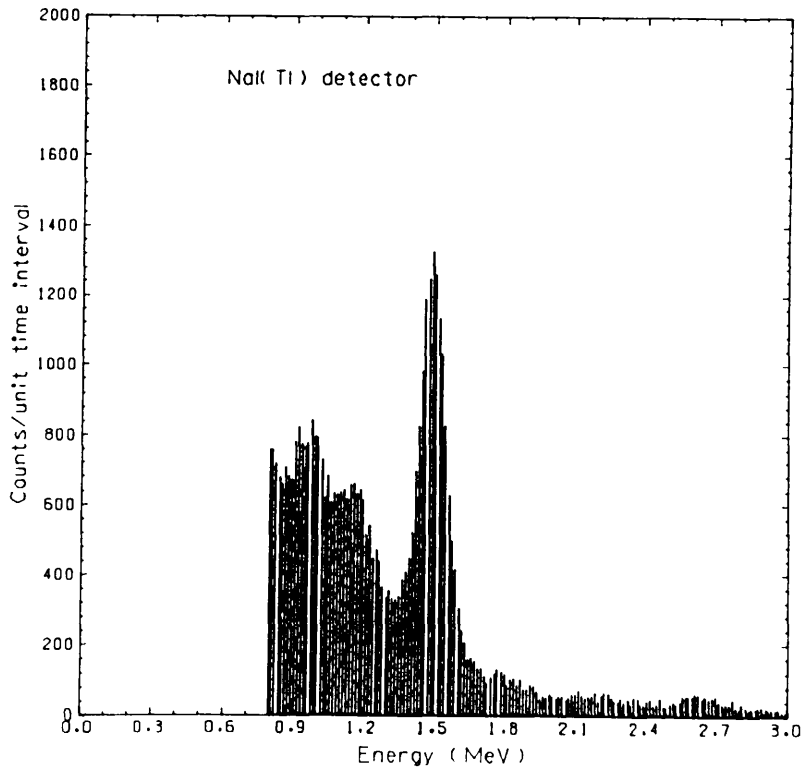
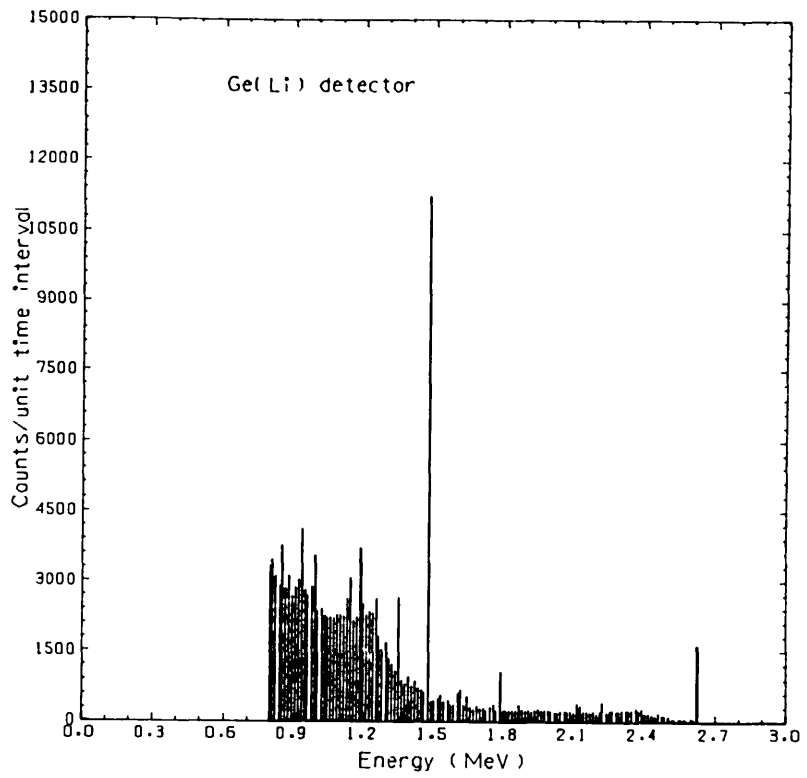
Sample 0540 spectrum



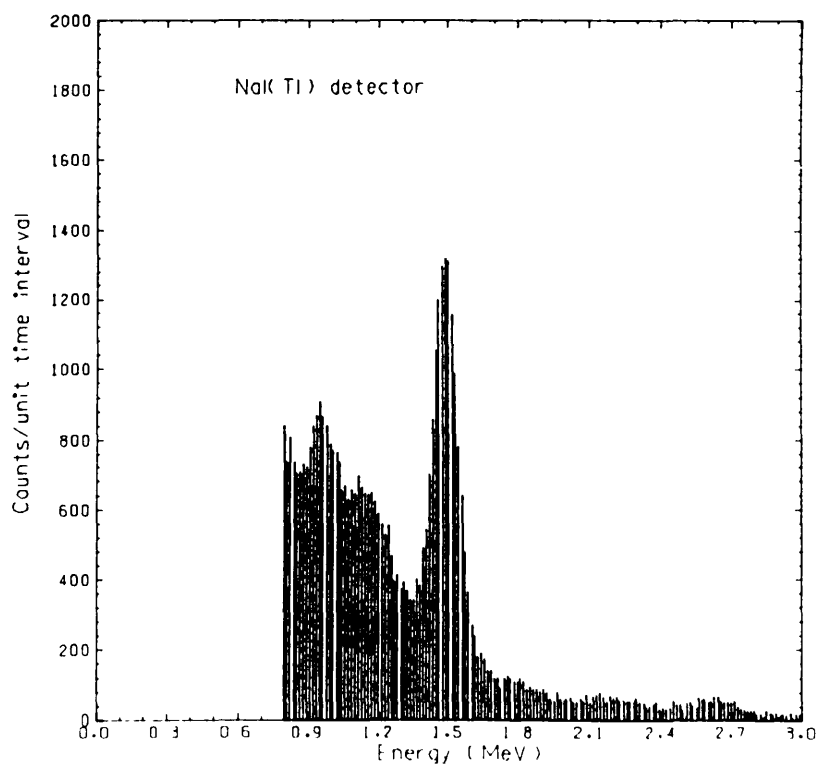
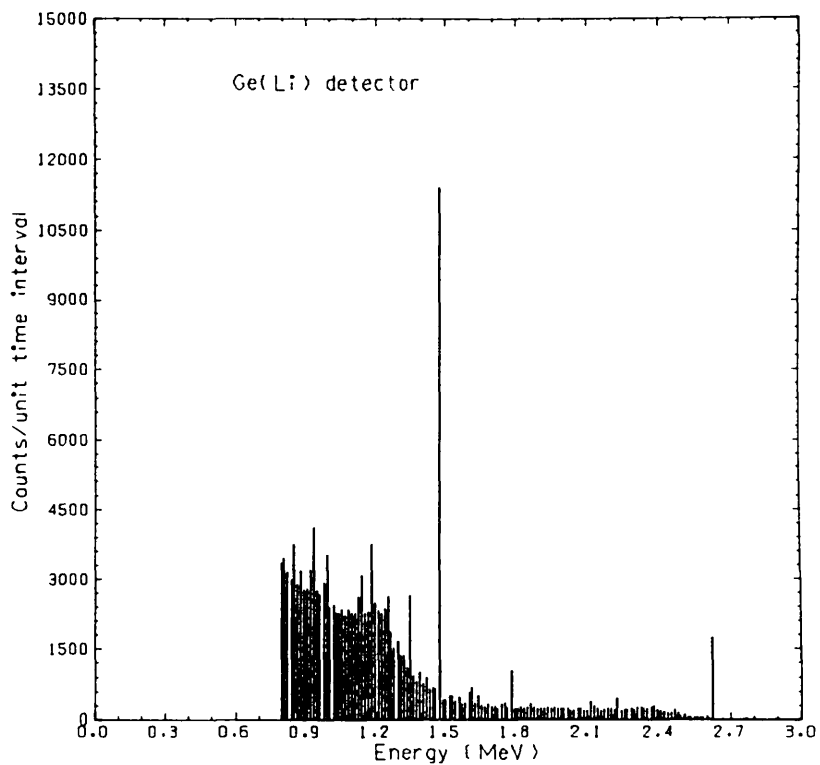
Sample 0600 spectrum



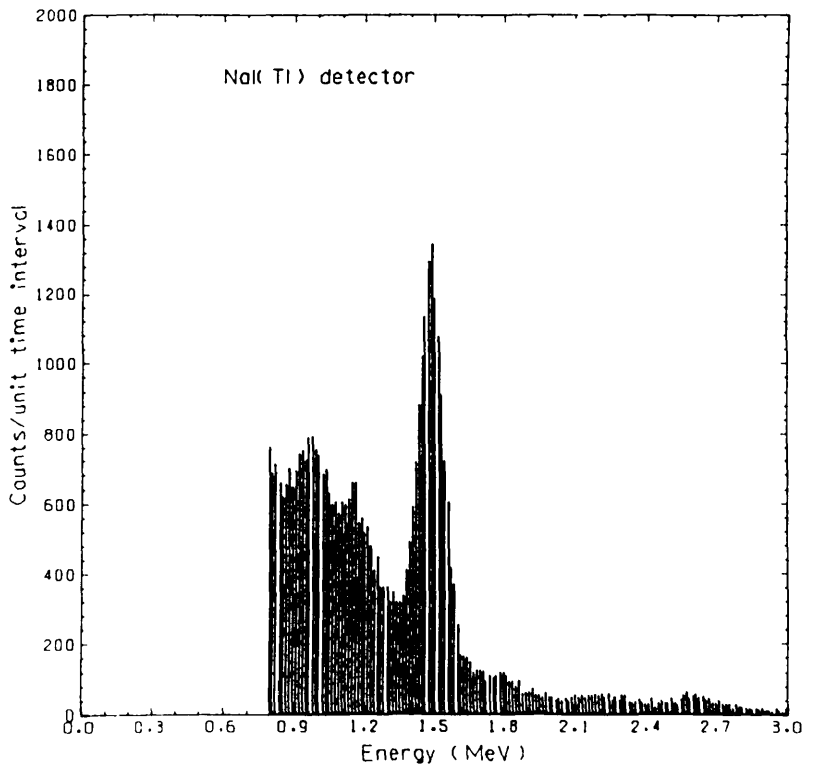
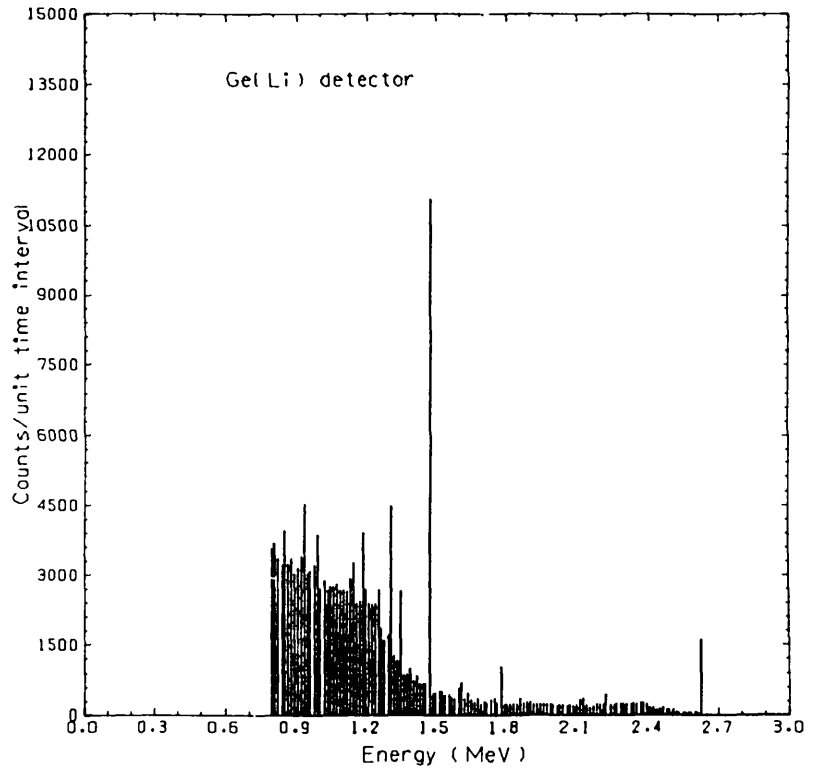
Sample 0660 spectrum



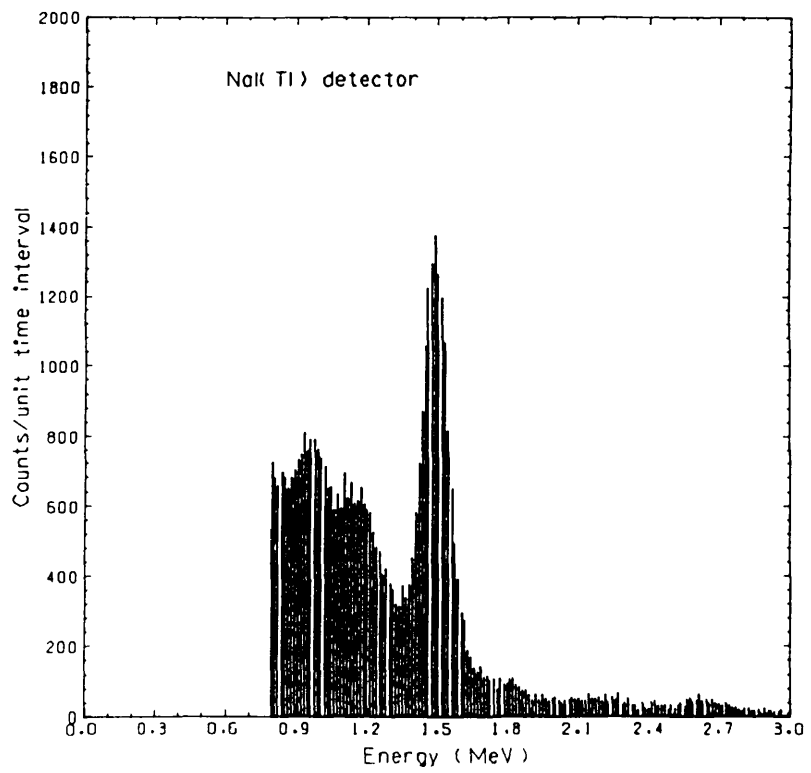
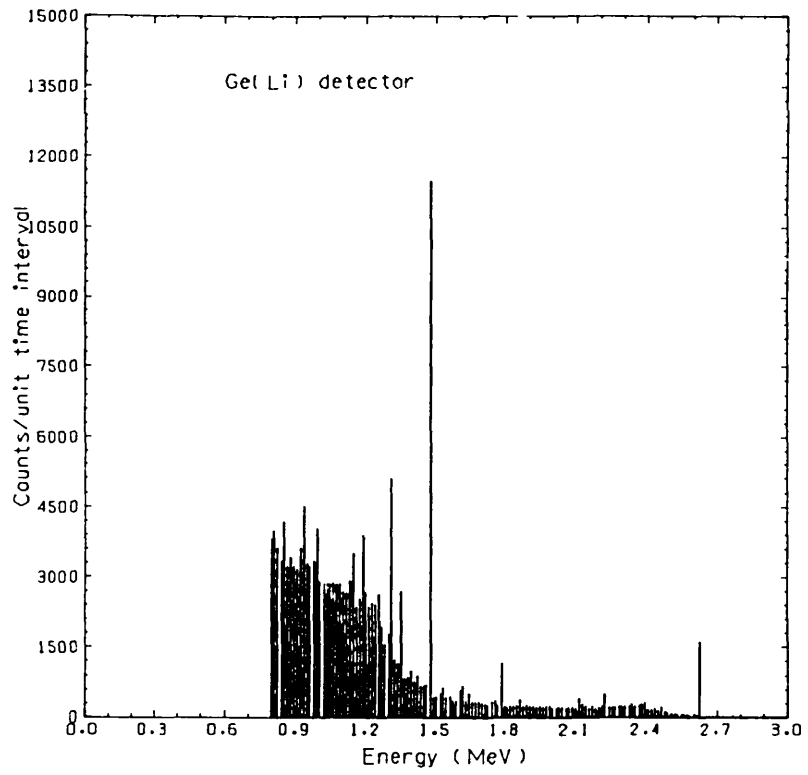
Sample 0720 spectrum



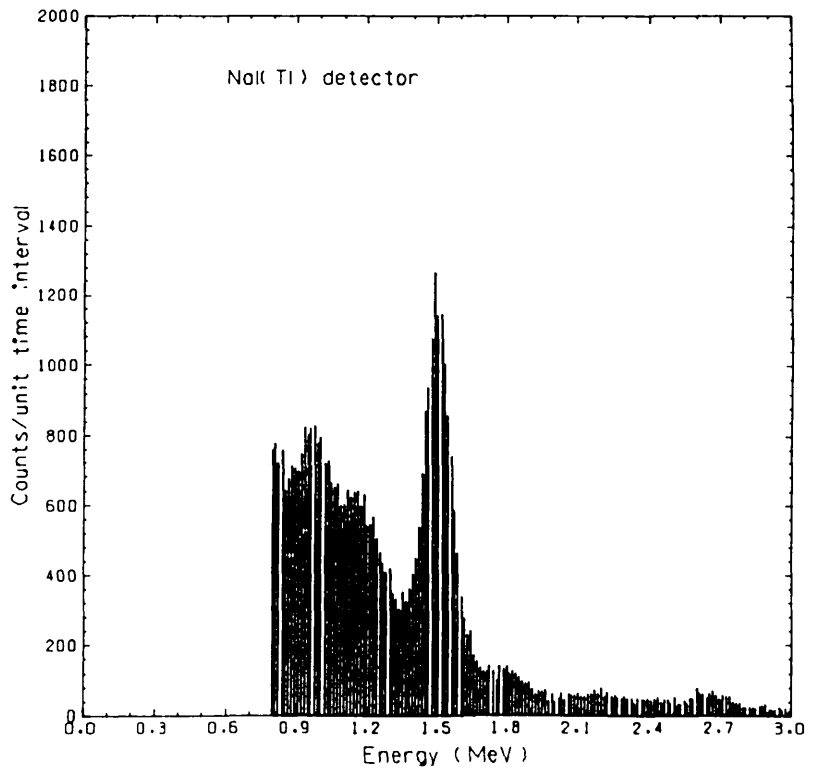
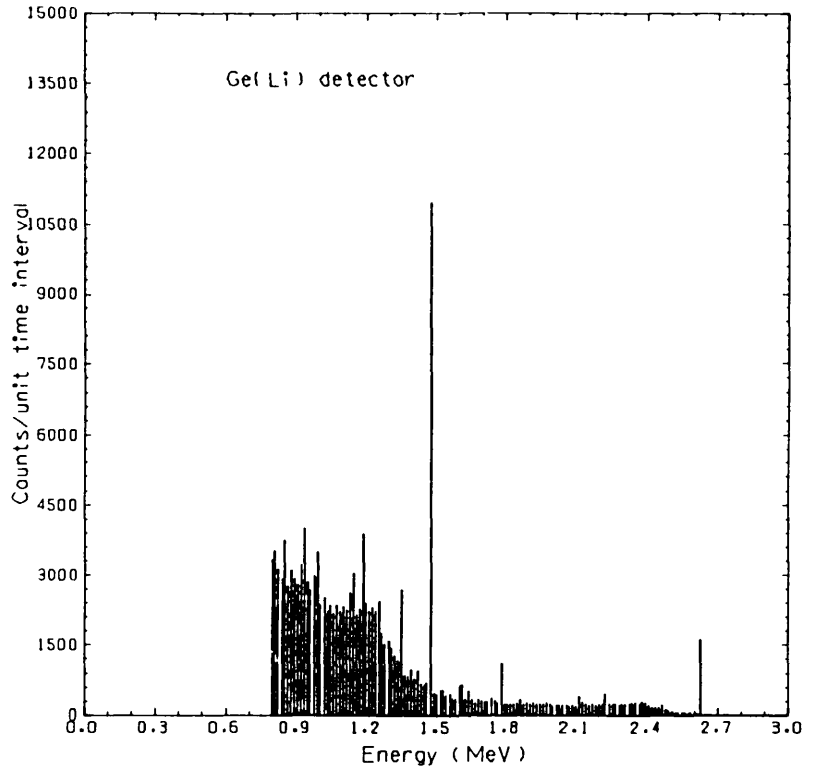
Sample 0/80 spectrum



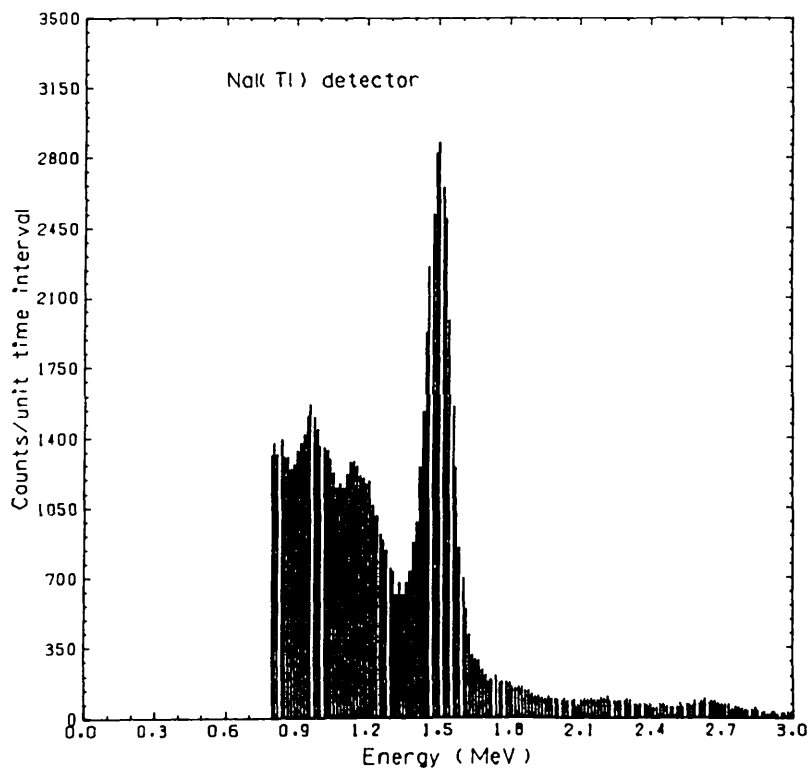
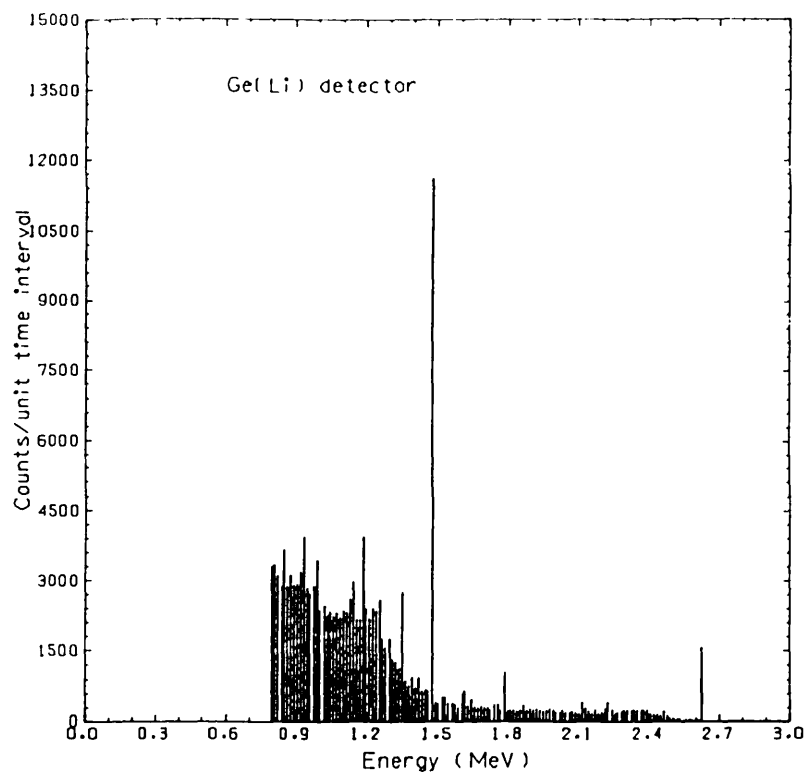
Sample Q840 spectrum



Sample 0900 spectrum

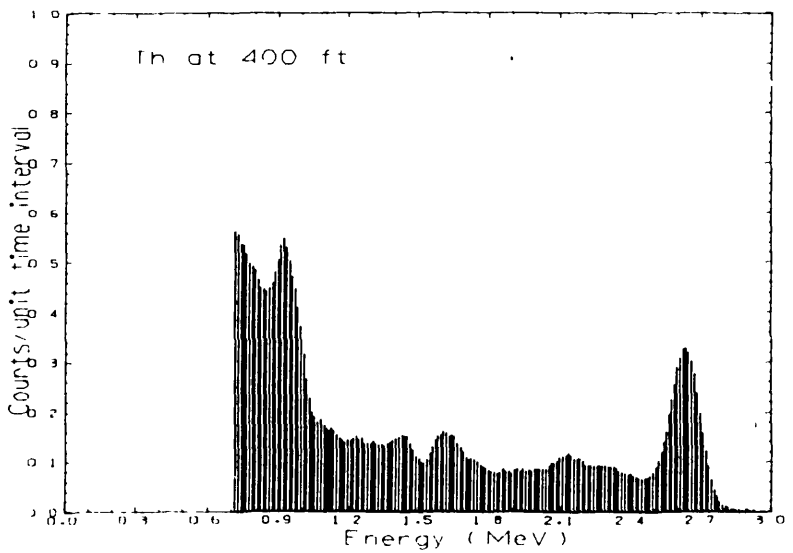
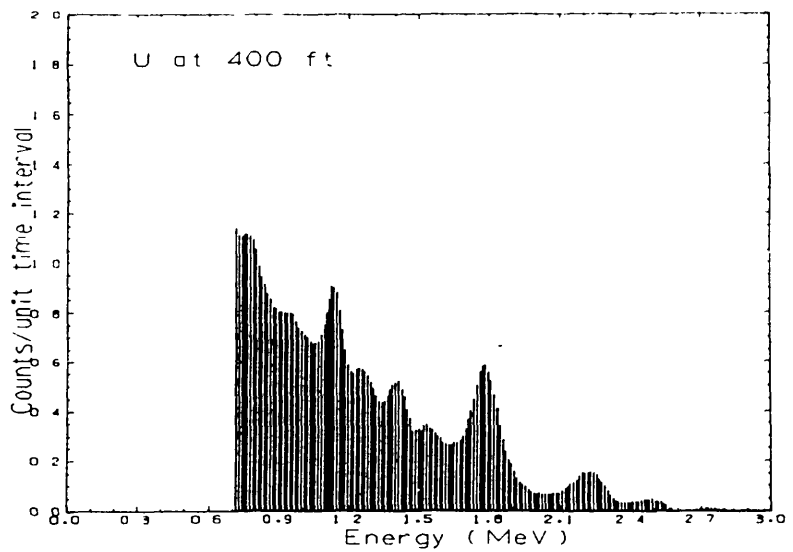
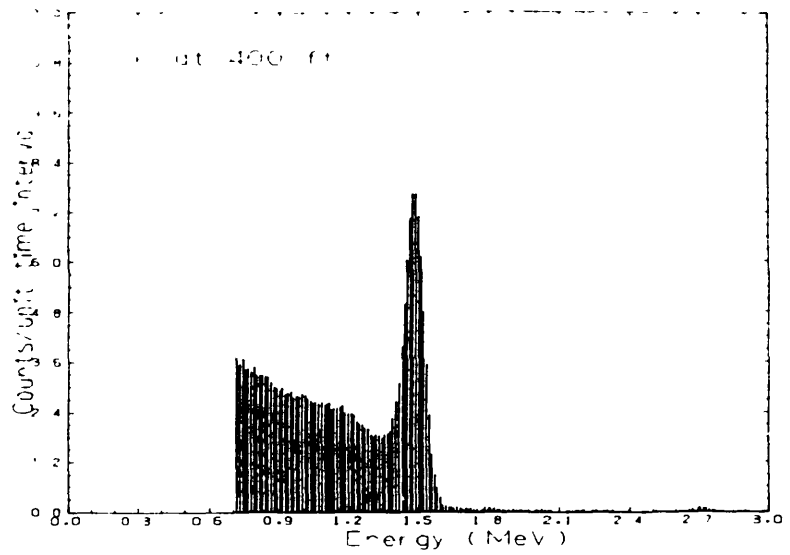


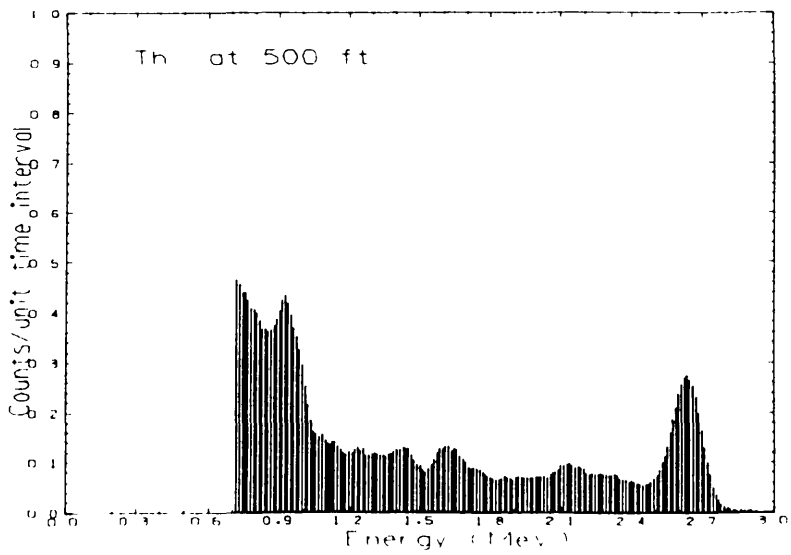
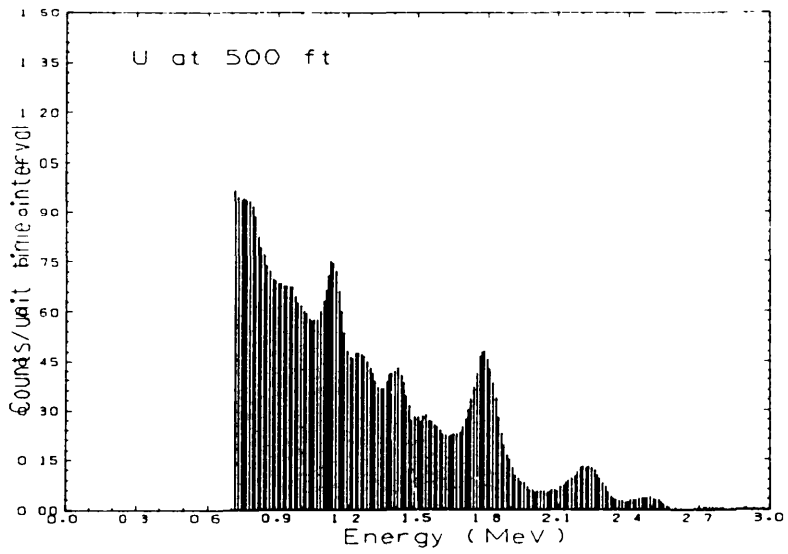
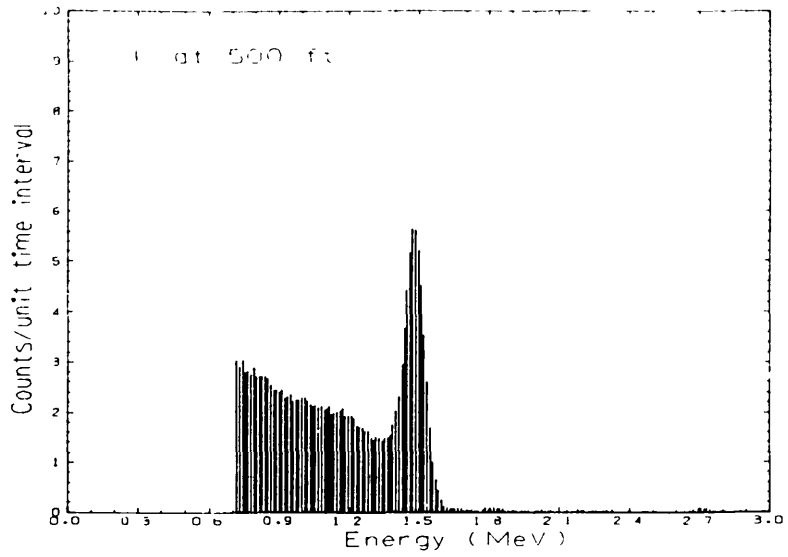
Sample 0960 spectrum

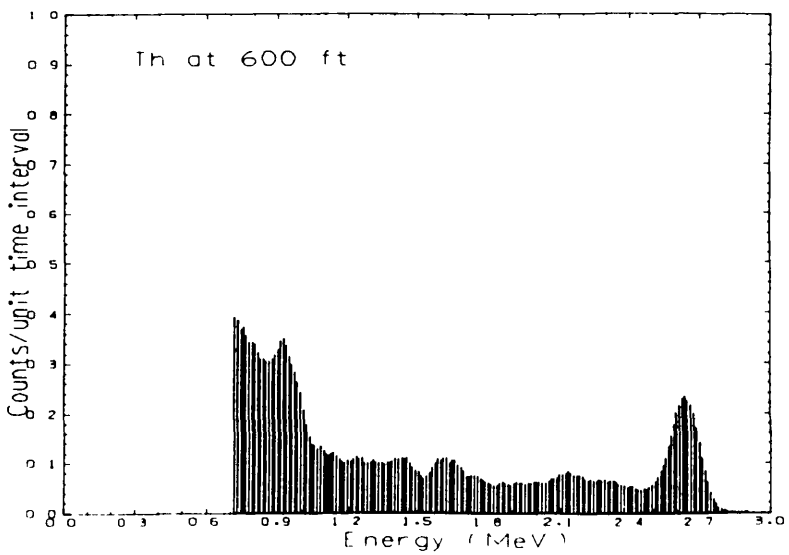
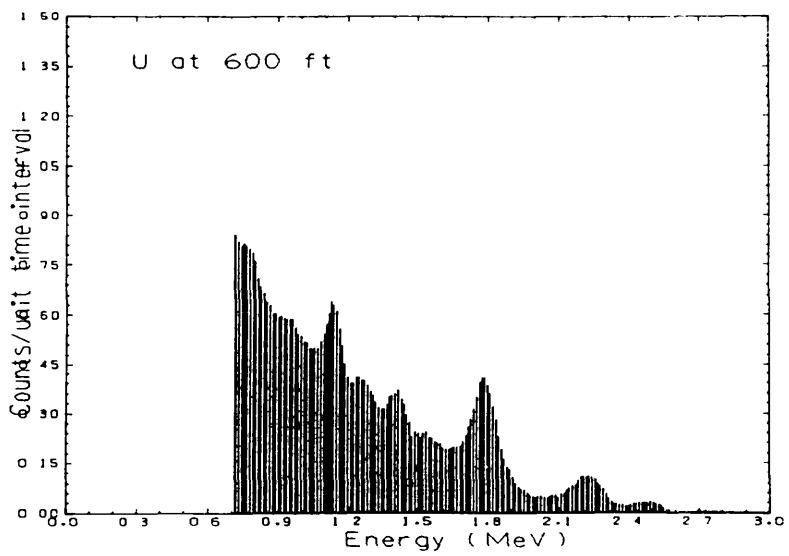
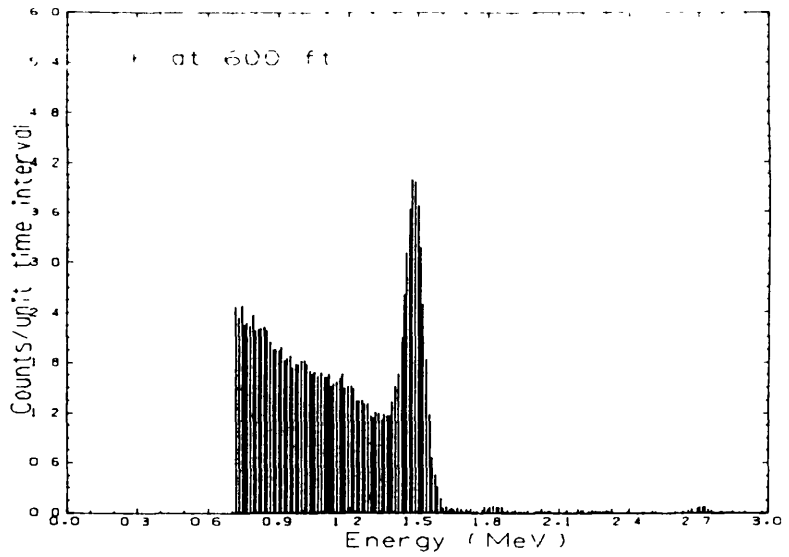


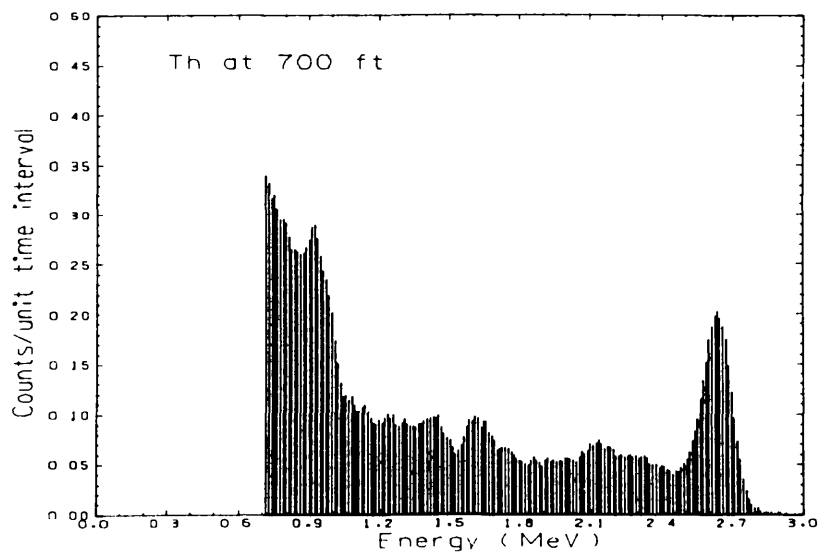
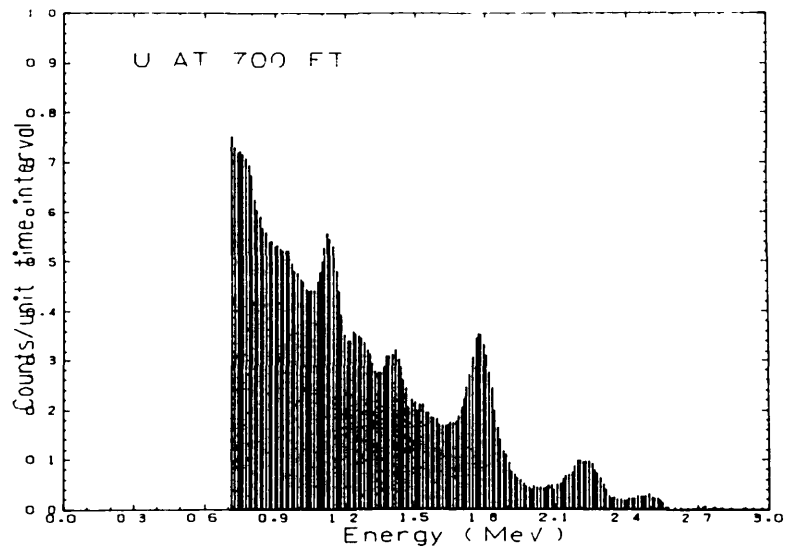
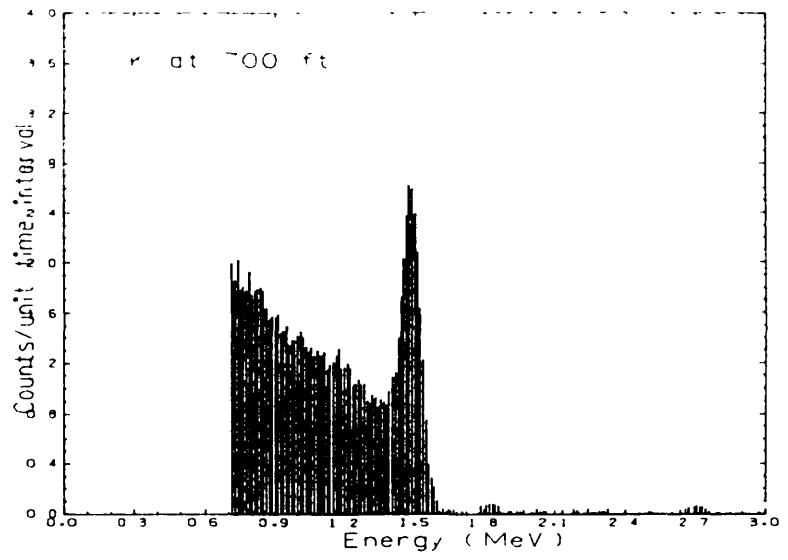
Sample 1000 spectrum

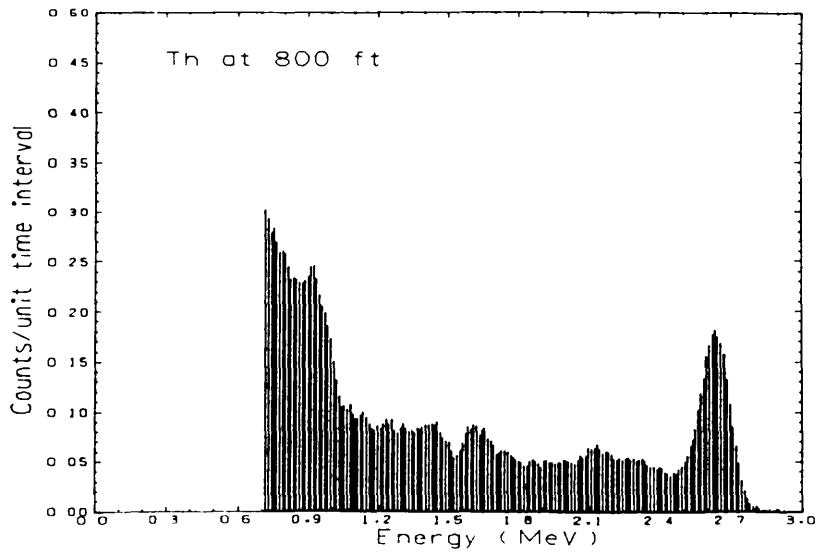
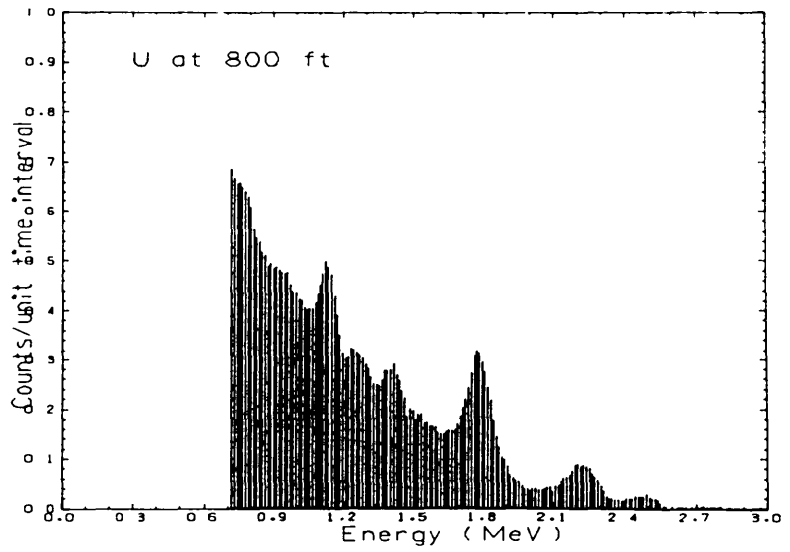
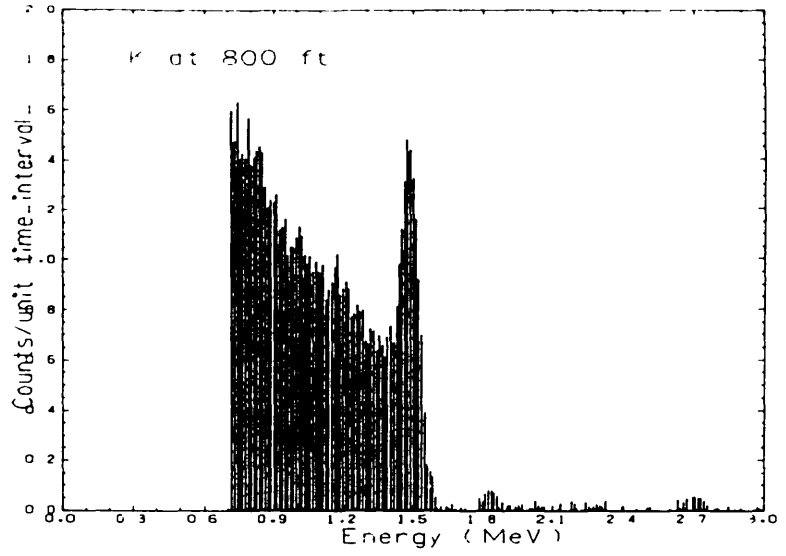
B2 - Calibration spectra at various heights

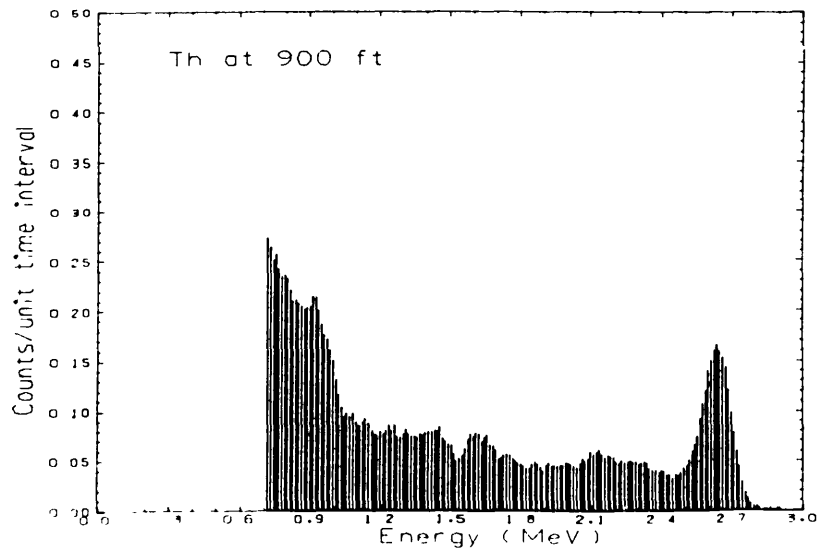
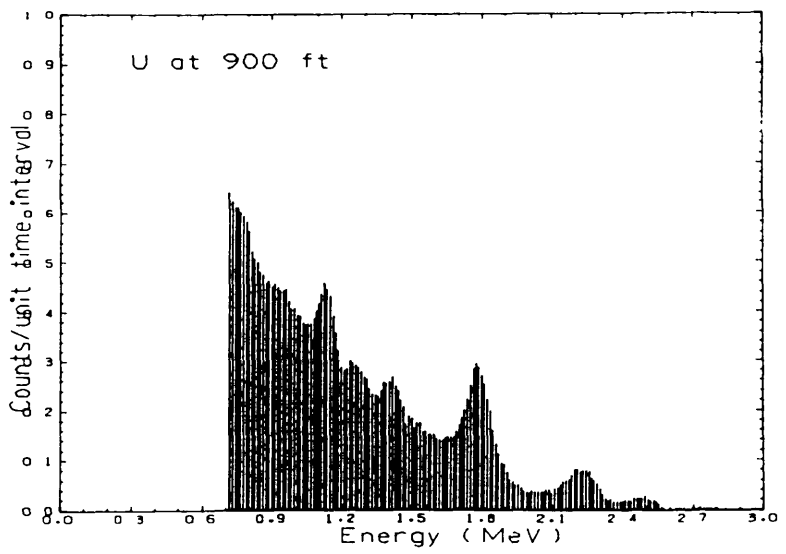
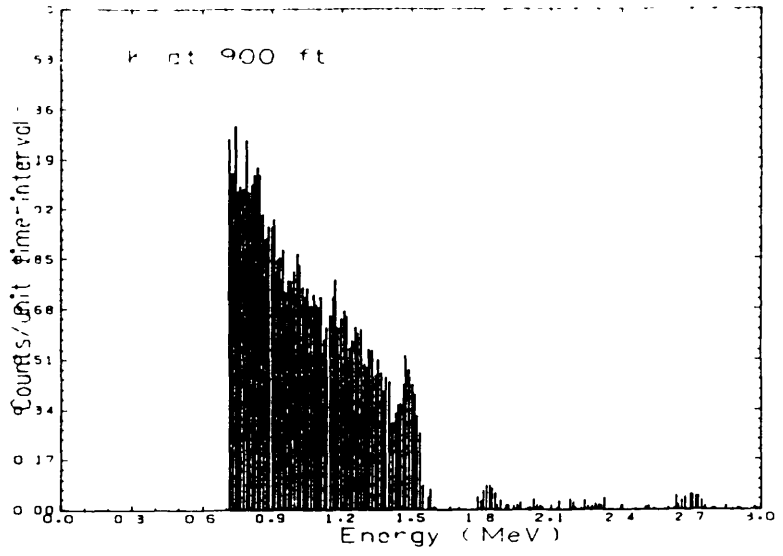


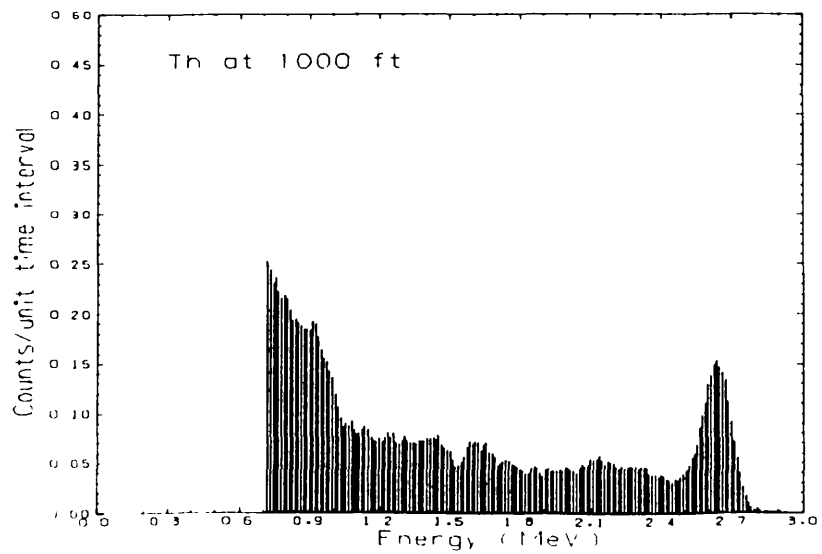
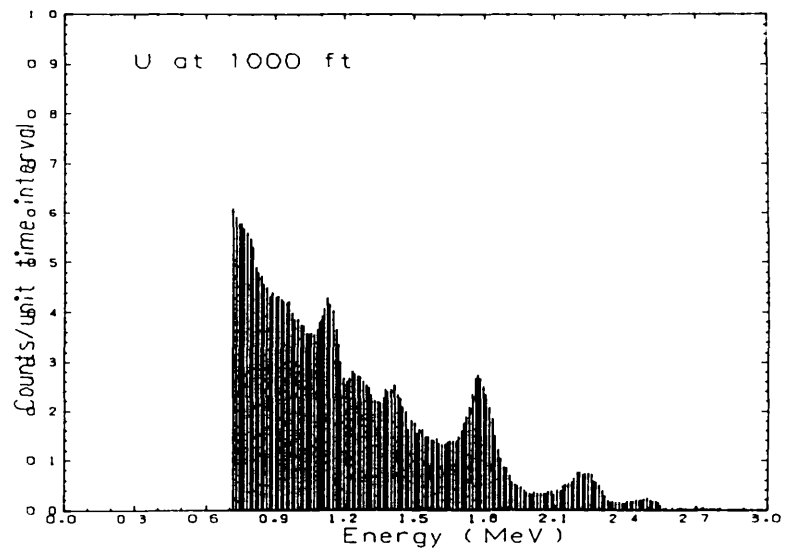
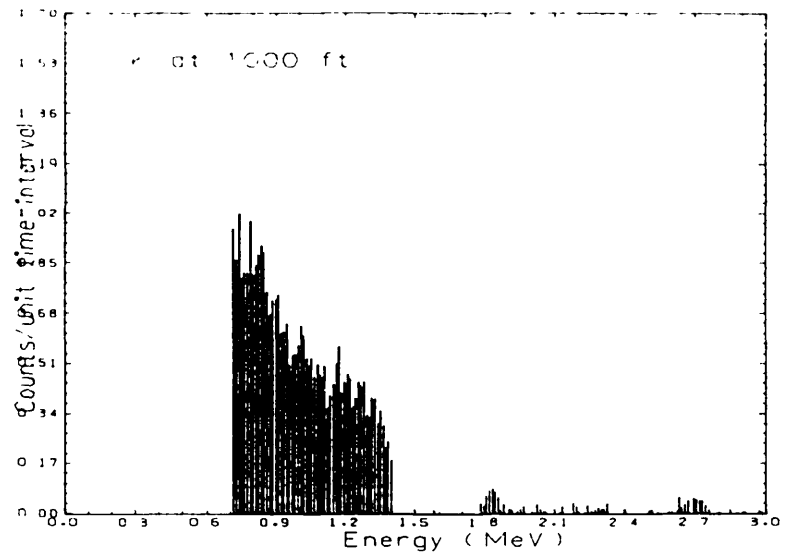


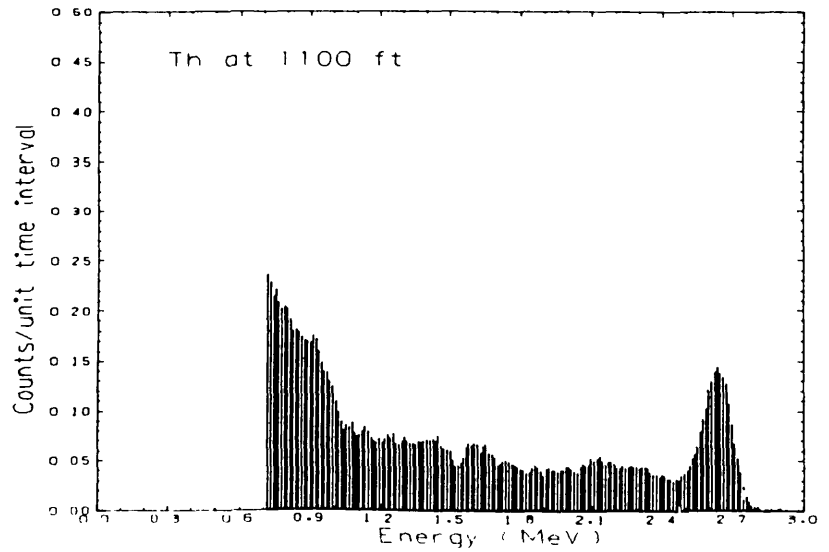
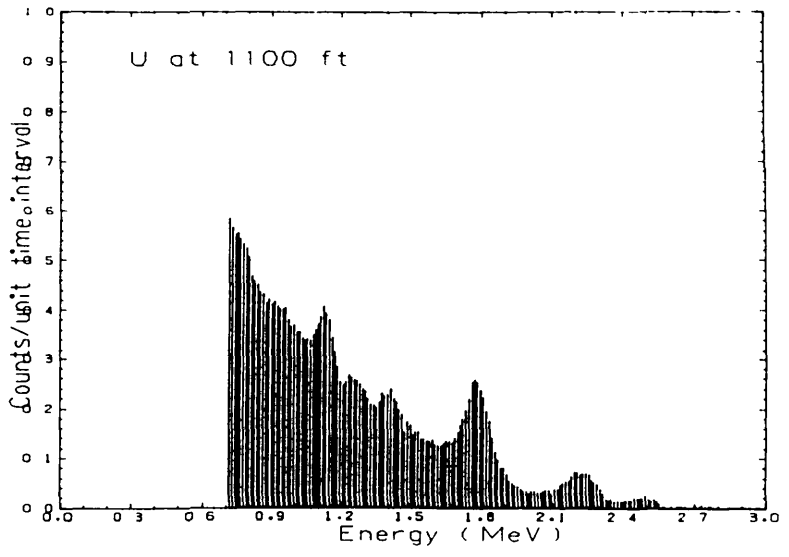
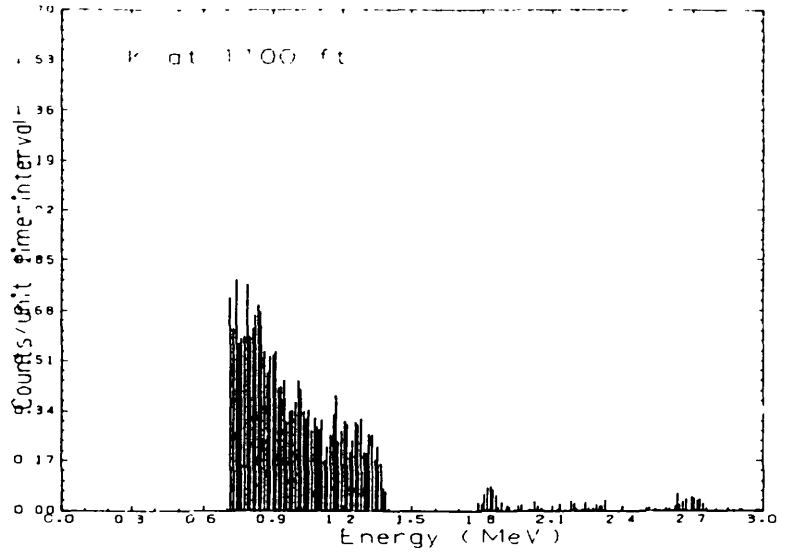












B3 - Survey and background spectra

